CRANFIELD UNIVERSITY

I A F DAS

THE CHARACTERISTICS AND FORCES DUE TO SLUGS IN AN 'S' SHAPED RISER

SCHOOL OF ENGINEERING

PhD THESIS

CRANFIELD UNIVERSITY

SCHOOL OF ENGINEERING

PhD THESIS

Academic Year 2002-2003

I A F DAS

The Characteristics and Forces due to Slugs in an 'S' Shaped Riser

Supervisor: Professor C Thompson

July 2003

This thesis is submitted in partial fulfilment of the requirements for the degree of Doctor of Philosophy

ABSTRACT

The characteristics and forces due to slugs in an 'S' shaped riser have been investigated.

A series of experiments were carried out using the Cranfield University Riser Test Facility, using a 9.9m high riser. Single phase (water) and two phase (air and water) tests were conducted at a system pressure of 2 bara. The two phase tests covered a range of flow regimes: severe slugging, transitional severe slugging, oscillation and normal slug flow.

The two phase data was used to investigate the characteristics of severe slugging, to determine the liquid inventory in the riser downward limb and, to model the forces on a bend during the slug build-up, production and bubble penetration and gas blowdown stages of the severe slugging cycle.

During the bubble penetration and gas blowdown stage, high velocities and large fluctuations in the force were observed. The resultant dynamic forces on the bend during the slug build-up and production stages were small compared to the bubble penetration and gas blowdown stage, and dominated by the hydrostatic forces due to liquid in the riser. Normal slug flow is potentially more problematic in terms of fatigue damage than severe slug flow, due to the higher velocity of the slugs coupled with large dynamic forces.

ACKNOWLEDGEMENTS

I would like to thank the following people who have contributed to the completion of this thesis.

Firstly I would like to thank my supervisor, Professor Chris Thompson, for his advice at the onset of this research, with a special thanks to Dr Hoi Yeung, who has provided much guidance and support.

I would like to thank my mentor, Dr Carl Wordsworth at BHR Group Limited. Also, a thank you to Stan Collins, John Knopp and Ron Chapman at BHR Group for their help in the setting up and running of the riser test facility.

Thank you to Paul Fairhurst at BP for the useful discussions on slug loading and for inviting me to visit the experimental facility at Sunbury.

Finally to my family and friends, thank you for all your love and encouragement. A special thanks to my Mother, who has always supported the decisions I've made. To Peter, thank you for your advice and patience.

LIST OF FIGURES

CHAPTER 1- OVERVIEW OF DEEPWATER OFFSHORE PRODUCTION

1.1 Examples of flexible riser configurations
1.2 Structural damage due to slug loading

CHAPTER 2- LITERATURE REVIEW OF THE HYDRAULICS OF SLUG FLOW

2.1 Stages of the severe slugging cycle
2.2 Pressure-time trace during the severe slugging cycle
2.3 Free hanging catenary riser flow pattern map
2.4 Lazy 'S' riser flow pattern map
2.5 Free hanging catenary riser, SS1 trace
2.6 Lazy 'S' riser, SS1t trace
2.7 Lazy 'S' riser, SS1b trace
2.8 Lazy 'S' riser, SS1i trace
2.9 Lazy 'S' riser, SS2 trace
2.10 Lazy 'S' riser, SS3 trace
2.11 Lazy 'S' riser, SS4 trace
2.12 Lazy 'S' riser, oscillation trace
2.13 The hydrodynamic model for severe slugging
2.14 Measured versus calculated slug length
2.15 Process of slug formation
2.16 Schematic diagram of the apparatus to measure slug forces at a bend
2.17 Force-time and pressure-time traces as a slug passes around a bend
2.18 Normalized force at a bend with dispersion distance
2.19 Experimental pressure-time trace at an elbow, $L_s = 1.52m$
2.20 Experimental pressure-time trace at an elbow, $L_s = 3.35m$
2.21 Normalized force at an elbow versus dispersion distance
2.22 Control volume analysis around an elbow
2.23 Schematic of the apparatus to measure slug forces at an elbow
2.24 Experimental slug velocity before and after an elbow
2.25 Comparison of calculated force with experimental data
2.26 Schematic diagram of the apparatus to measure slug forces at a bend
2.27 Relationship between average and maximum peak force with mixture velocity
2.28 Schematic diagram of the forces on a bend
2.29 Schematic diagram of a force-time trace
2.30 Graph of impulse peak force versus mixture velocity
2.31 Maximum impact pressures on orifices, by slugs of different lengths
2.32 Model of transient slug flow

CHAPTER 3- LAZY 'S' RISER TEST FACILITY

3.1 P and ID of riser test facility
3.2 Photograph of isolation joint
3.3 Diagram showing instrumentation on pipeline-riser
3.4 Photograph of strain-gauged strut
3.5 Diagram of bend
3.6 Diagram of conductance probe
3.7 Diagram of the separator at the top of the riser
3.8 Liquid mass balance validation
3.9 LabVIEW calibration screen- process instrumentation
3.10 LabVIEW data file control screen
3.11 LabVIEW meters screen
3.12 LabVIEW pipeline-riser screen
3.13 LabVIEW force monitor screen

CHAPTER 4- CALIBRATION OF STRAIN-GAUGED STRUTS

4.1 Free-hanging strain-gauged strut calibration
4.2 Isolation joint and cross-talk tests
4.3 Isolation joint test 1: applied (spring-balance) force in vertical direction, vertical strut in compression
4.4 Isolation joint test 2: applied (spring-balance) force in vertical direction, vertical strut in tension
4.5 Isolation joint test 3: applied (spring-balance) force in horizontal direction, horizontal strut in compression
4.6 Isolation joint test 4: applied (spring-balance) force in horizontal direction, horizontal strut in tension
4.7 Example of isolation joint test data analysis procedure
4.8 Determination of isolation joint calibration coefficient (vertical strut)
4.9 Determination of isolation joint calibration coefficient (horizontal strut)
4.10 Example of cross-talk (vertical strut to horizontal strut)
4.11 Determination of cross-talk calibration coefficient (horizontal strut to vertical strut)
4.12 Determination of cross-talk calibration coefficient (vertical strut to horizontal strut)
4.13 Polarity of force traces

CHAPTER 5- LAZY 'S' RISER SINGLE PHASE AND TWO PHASE TESTS

5.1 Flow pattern map showing test points and observed flow regimes
5.2 Typical trace for severe slugging 1 (SS1)
5.3 Typical trace for severe slugging 1b (SS1b)
5.4 Typical trace for severe slugging 2 (SS2)
5.5 Typical trace for severe slugging 2 with intermediate cycles on the lower limb (SS2i)
5.6 Typical trace for oscillation flow
5.7 Typical trace for slug flow

5.8 Pressure over the riser and resultant force versus time traces
5.9 Extrapolation technique used to determine the resultant dynamic force on the bend during slug build-up
5.10 Typical resultant force during the bubble penetration and gas blowdown stage, of a severe slugging cycle
5.11 Close-up of the resultant force during the bubble penetration and gas blowdown stage, of a severe slugging cycle
5.12 Flow pattern map showing cycle times
5.13 Flow pattern map showing slug build-up times
5.14 Flow pattern map showing slug production times
5.15 Flow pattern map showing bubble penetration and gas blowdown times
5.16 Flow pattern map showing slug lengths
5.17 Cranfield University lazy 'S' riser flow pattern map, 4 bara
5.18 Cranfield University lazy 'S' riser flow pattern map, 7 bara
5.19 Comparison between free-hanging catenary riser and lazy 'S' riser severe slugging boundaries
5.20 Results for the liquid inventory in riser downward section investigations
5.21 Liquid inventory in riser downward section during severe slugging versus liquid velocity
5.22 Liquid inventory in riser downward section during severe slugging versus mixture velocity
5.23 Effect of trapped gas on slug length and cycle time
5.24 Build-up stage simulation test: pressure over riser, P4-P9
5.25 Build-up stage simulation test: pressure over lower limb, P4-P5, and upper limb, P6-P9, as riser filled with liquid
5.26 Build-up stage simulation test: vertical force on a bend
5.27 Build-up stage simulation test: horizontal force on a bend
5.28 Vertical 'zero' offset under the condition of no gas or liquid in the flow loop
5.29 Build-up stage simulation test: resultant dynamic and hydrostatic force on a bend compared to theory, $FR = 2^{0.5} \rho_L A v_L^2$
5.30 Production stage simulation test: resultant dynamic force on a bend compared to theory, $FR = 2^{0.5} \rho_L A v_L^2$
5.31 Typical traces during the build-up and production stage of the severe slugging 1 cycle
5.32 Resultant dynamic force on a bend during slug build-up
5.33 Comparison of resultant dynamic force on a bend with slug build-up time
5.34 Flow pattern map showing resultant dynamic force on a bend during slug build-up and cycle times
5.35 Theoretical resultant dynamic force on a bend during slug build-up and production
5.36 Liquid velocity at riser outlet
5.37 Resultant force and liquid velocity during bubble penetration and gas blowdown
5.38 Conductance probe and liquid velocity trace during bubble penetration and gas blowdown
5.39 Resultant dynamic force on a bend during bubble penetration and gas blowdown
5.40 Measured and predicted resultant dynamic force during bubble penetration and gas blowdown

5.41 Resultant force and liquid velocity during bubble penetration and gas blowdown, worse case
5.42 Resultant force and liquid production during normal slug flow- insert

Appendices

Appendix E

E1.1 Severe slugging 1 traces [v_{SG}=0.11m/s, v_{SL}=0.14m/s]
E1.2 Severe slugging 1 traces [v_{SG}=0.28m/s, v_{SL}=0.20m/s]
E1.3 Severe slugging 1 traces [v_{SG}=0.17m/s, v_{SL}=0.09m/s]
E1.4 Severe slugging 1 traces [v_{SG}=0.14m/s, v_{SL}=0.28m/s]
E1.5 Severe slugging 1b traces [v_{SG}=0.35m/s, v_{SL}=0.11m/s]
E1.6 Severe slugging 1 traces [v_{SG}=0.32m/s, v_{SL}=0.19m/s]
E1.7 Severe slugging 1 traces [v_{SG}=0.07m/s, v_{SL}=0.10m/s]
E1.8 Severe slugging 1 traces [v_{SG}=0.26m/s, v_{SL}=0.06m/s]
E1.9 Severe slugging 1 traces [v_{SG}=0.18m/s, v_{SL}=0.19m/s]
E1.10 Severe slugging 1 traces [v_{SG}=0.31m/s, v_{SL}=0.31m/s]

LIST OF CONTENTS

CHAPTER 1- OVERVIEW OF DEEPWATER OFFSHORE PRODUCTION		**1**
1.1	Introduction	1
1.2	Deepwater Developments	1
1.2.1	Affect of Economic Climate on Deepwater Exploration and Production	2
1.3	Floating Production Systems	2
1.4	Riser Systems	3
1.5	Multiphase Transportation	3
1.5.1	Severe Slugging	4
1.5.1.1	Issues Associated With Severe Slugging	4
1.5.2	Integrity Related Issues	5
1.6	Research Objectives	6
1.7	Outline of Thesis	6
	Figures	8
CHAPTER 2- LITERATURE REVIEW OF THE HYDRAULICS OF NORMAL AND SEVERE SLUG FLOW		**9**
2.1	Introduction	9
2.2	Severe Slugging	9
2.2.1	Occurrence of Severe Slugging	9
2.2.2	Description of the Severe Slugging Cycle	10
2.2.3	Investigation into Severe Slugging in Flexible Risers	10
2.2.3.1	Severe Slugging 1 (SS1) in a Catenary Riser	11
2.2.3.2	Severe Slugging in a Lazy 'S' Riser	11
2.3	Severe Slugging Models	13
2.3.1	Schmidt et al (1979)	13
2.3.2	Bøe (1981)	14
2.3.3	Pots et al (1985)	15
2.3.4	Goldzberg and McKee (1985)	15
2.3.5	Fabre et al (1987)	16
2.3.6	Tin et al	16
2.4	Normal Slug Flow	17
2.5	Investigation of the Forces Due to Normal Slug Flow	18
2.5.1	Slug Forces on a Pipe Bend/Elbow	18
2.5.2	Slug Forces on an Orifice Plate	24
2.5.3	Slug Forces on a Structure Located Outside a Horizontal Pipe	25
2.5.4	Alleviation of Slug Force Effects	27
2.6	Summary	28
2.6.1	Severe Slugging Models	28
2.6.2	Investigation of the Forces Due to Normal Slug Flow	28
Figures		30

CHAPTER 3- LAZY 'S' RISER TEST FACILITY **48**

3.1 Introduction 48
3.2 Flow Loop 48
3.3 Instrumentation 49
3.3.1 Strain Gauges 50
3.3.1.1 Strain Gauged Strut Calibration 50
3.3.2 Conductance Probes 51
3.3.3 Gamma Densitometer 51
3.3.3.1 Calibration of Gamma Densitometer 52
3.3.4 Pressure Transducers 52
3.3.4.1 Calibration of Pressure Transducers 53
3.3.5 Thermocouples 53
3.3.6 Liquid Flowmeters 53
3.3.6.1 Liquid Flowmeter Commissioning Tests 53
3.3.6.2 Liquid Mass Balance on Separator 54
3.3.6.2.1 Liquid Mass Balance Validation 55
3.3.6.3 Slug Length 55
3.3.7 Gas Flowmeters 56
3.3.7.1 Gas Flowmeter Commissioning Tests 56
3.3.7.2 Gas Mass Balance on Separator 57
3.4 Liquid Level Control 59
3.5 Data Acquisition System (DAS) 59
3.5.1 LabVIEW Screens 60
3.5.2 Sampling Rates 60
3.6 Summary 61
Figures 62

CHAPTER 4- CALIBRATION OF STRAIN GAUGED STRUTS **70**

4.1 Introduction 70
4.2 Free-Hanging Strain Gauged Strut Calibration 70
4.2.1 Free-Hanging Strain Gauged Strut Tests 70
4.2.2 Determination of Free-Hanging Calibration Factors 71
4.2.3 Polarity of Free-Hanging Calibration Factors 71
4.3 Isolation Joint and Cross-Talk Effects 72
4.3.1 Isolation Joint and Cross-Talk Tests 72
4.3.2 Data Analysis Procedures 73
4.3.2.1 Isolation Joint Tests 73
4.3.2.2 Cross-Talk Tests 74
4.3.3 Polarity of Force Traces 74
4.4 Calculation of Isolation Joint and Cross-Talk Calibration Coefficients 74
4.5 Discussion 76
4.5.1 Isolation Joint Tests 76
4.5.2 Cross-Talk Tests 77
4.6 Summary 77
Figures 78

CHAPTER 5- LAZY 'S' RISER SINGLE PHASE AND TWO PHASE TESTS 86

5.1	Introduction	86
5.2	Test Programme	86
5.2.1	Single Phase Tests	86
5.2.1.1	Test Matrix	86
5.2.1.2	Build-Up Stage Simulation Test Procedure	87
5.2.1.3	Production Stage Simulation Test Procedure	87
5.2.2	Two Phase Tests	88
5.2.2.1	Test Matrix	88
5.2.2.2	Test Procedure	88
5.3	Description of Observed Flow Regimes	88
5.3.1	Severe Slugging	88
5.3.1.1	Severe Slugging 1 (SS1)	89
5.3.1.2	Severe Slugging 1b (SS1b)	89
5.3.2	Transitional Severe Slugging	89
5.3.2.1	Severe Slugging 2	89
5.3.3	Oscillation Flow and Normal Slug Flow	90
5.4	Data Analysis Procedures	90
5.4.1	Analysis of Force Data- Single Phase Tests	90
5.4.1.1	Slug Build-Up and Production Simulations	90
5.4.2	Analysis of Force Data- Two Phase Tests	91
5.4.2.1	Slug Build-Up Stage	91
5.4.2.2	Bubble Penetration and Gas Blowdown Stage	92
5.5	The Effect of Trapped Gas in Riser Downward Limb	93
5.5.1	Determination of Liquid Inventory in Riser Downward Limb	94
5.6	Discussion of Results	95
5.6.1	Severe Slugging Characteristics	95
5.6.1.1	Cycle Time	95
5.6.1.2	Slug Build-Up Time	95
5.6.1.3	Slug Production Time	96
5.6.1.4	Bubble Penetration Time and Gas Blowdown Time	96
5.6.1.5	Slug Length	97
5.6.1.6	Comparisons to Previous Work	97
5.6.1.6.1	Flow Pattern Maps	97
5.6.1.6.2	Severe Slugging Characteristics	99
5.6.2	Liquid Inventory in Riser Downward Limb	99
5.6.3	Forces on a Bend during the Build-Up and Production Stages of the Severe Slugging Cycle	101
5.6.3.1	Single Phase Simulations	101
5.6.3.1.1	Description of Pressure-Time Traces	101
5.6.3.1.2	Description of Force-Time Traces	102
5.6.3.1.3	Results and Comparisons to Theory	104
5.6.3.2	Two Phase Tests	105
5.6.3.2.1	Slug Build-Up Stage	105
5.6.3.2.2	Slug Production Stage	107
5.6.3.2.3	Theoretical Force-Time Traces	107

5.6.4 Forces on a Bend during the Bubble Penetration Time and Gas Blowdown Stages of the Severe Slugging Cycle 107
5.7 Forces on a Bend during Normal Slug Flow 110
5.8 Summary 111
Figures 114

CHAPTER 6- CONCLUSIONS AND FURTHER WORK 139

6.1 Research Summary 139
6.2 Conclusions 140
6.2.1 Severe Slugging Characteristics 140
6.2.2 Liquid Inventory in Riser Downward Limb 140
6.2.3 Forces on a Bend during the Severe Slugging Cycle 141
6.3 Suggestions for Further Work 143

REFERENCES 145

PUBLICATIONS 149

Appendix A- Derivation of the Resultant Force on a Bend
Appendix B- Operating Procedures for the Lazy 'S' Riser Test Facility
Appendix C- Strain Gauged Strut Design Calculations
Appendix D- Derivation of Screen Force to Actual Force
Appendix E- Severe Slugging Force Traces

NOTATION

A	cross-sectional area
B	spring-back factor
C	calibration coefficient
C_{HV}	cross-talk calibration coefficient (horizontal to vertical gauge)
C_{VH}	cross-talk calibration coefficient (vertical to horizontal gauge)
c_2	no slip liquid hold-up
D^*	dispersion distance
D	diameter
D_{LIF}	Dynamic Load and Inertia Factor
E	isolation joint calibration coefficient
F^*	normalised force
F	force
F'bg	force during bubble penetration and gas blowdown stage
F'bu	force during build-up stage
F'off	offset force
F'p	force during production stage
FB_L	liquid fall-back
FH	applied spring-balance horizontal force
FV	applied spring-balance vertical force
FR	resultant force
Fs	DAS screen force
F_{free}	free-hanging force
F_m	measured peak force
$F_{plateau}$	measured plateau force
F_{static}	static force
g	acceleration due to gravity
H_L	liquid hold-up
h	height of limb
$h_{d'}$	liquid inventory in downward limb
L	length
L_G	equivalent length of gas volume
M_G	molecular weight of gas phase
M_I	total momentum
m	mass
ΔP_{TP}	two phase pressure drop
P	pressure
P_a	atmospheric pressure
P_m	measured peak pressure
Q_T	total volume of liquid during slug cycle
q	volumetric flowrate
R	gas constant
S	separator liquid level
T	temperature
t	time
t_b	bubble transit time

$t_{build\text{-}up}$	slug build-up time
t_{cycle}	severe slugging period
u_b	bubble buoyancy effect
V	volume
V_{out}	output voltage
v	velocity
v_{Gf}	final gas velocity
v_{Gi}	initial gas velocity
v_{mix}	mixture velocity
v_{mo}	model velocity
v_t	Taylor bubble velocity
x	x-direction
x	gas quality
y	y-direction
Z	liquid level
z	gas compressibility factor
Π_{SS}	severe slugging group
α	pipeline inclination from horizontal
α_P"	average void fraction
β	riser deviation from vertical
λ	velocity distribution profile factor
ρ	density
τ	acting period of impact force
SS1	severe slugging 1
SS2	severe slugging 2
SS3	severe slugging 3
SS4	severe slugging 4
OSC	oscillation
SS1p	severe slugging with pipeline gas penetration
SS1t	severe slugging with trapped gas penetration
SS1b	severe slugging with bubble penetration
SS1i	severe slugging with intermediate cycle on lower limb

Subscripts

G	gas
H	horizontal
L	liquid
V	vertical
d	downward limb
f	frictional losses
l	lower limb
p	pipeline
r	riser
S	superficial
s	slug
u	upper limb
dy	dynamic

hy	hydrostatic
max	maximum
min	minimum
mix	mixture
nom	nominal
off	offset
sep	separator

Superscripts

'	actual

Definitions

Superficial gas/liquid velocity- The velocity that the gas/liquid would have if it occupied the whole cross section of the pipe.

CHAPTER 1- OVERVIEW OF DEEPWATER OFFSHORE PRODUCTION

1.1 Introduction

In 2000, the world consumed an estimated 70 million barrels of oil per day (bpd)[1]. Therefore, with the depletion of offshore oil and gas fields, there is an urgent need for an economic solution to recover the hydrocarbon reserves from marginal and in particular, deepwater environments. Instead of the construction of separate oil and gas pipelines, hydrocarbon fluids are transported as a multiphase flow via a pipeline-riser to a floating production system (refer to Section 1.3). The multiphase flow comprises all the material produced from the reservoir; hydrocarbon gas mixtures (sometimes with CO_2, N_2, H_2S), hydrocarbon liquid mixtures ('black' oil, heavy oil, condensate), water (from formation, or from injection for pressure maintenance) and solids (reservoir sand)[2].

Future offshore oil production from deepwater developments, will lead to an increase in the use of floating production systems and hence, flexible risers. Flexible risers are used to connect the subsea pipelines to the topsides processing equipment. These flexible risers are suited to the use of floating production systems and offer many benefits over rigid risers (discussed in Section 1.4). However, when operating under multiphase conditions, the geometry of the pipeline-riser system coupled with particular flow conditions can lead to a condition called severe slugging (rigid risers can also experience severe slugging). Some of the issues associated with severe slugging are; large gas and liquid flowrate variations, high average back-pressure at wellhead and high physical loadings on equipment, which may lead to fatigue damage.

1.2 Deepwater Developments

A large proportion of future offshore oil production is likely to be centred around deepwater developments. In 1997, industry classed a water depth of 450m as deepwater[3], now this number is seen around the 750m mark; with the ultradeepwater threshold defined as greater than 1525m of water[4]. At present, of the world's current offshore reserves of 191 billion barrels of oil equivalent (boe), 14% is in deepwater[5].

For deepwater fields to be economical, reserves must be large and flowrates high, as investments in these fields are very large, \$1.5-\$3 billion[6], with similar large amounts spent on operations over the field life. These deepwater fields can require between 25 to 50 wells, with production facilities of 150 -250,000 bpd[6].

Most major deepwater explorations are concentrated in the Gulf of Mexico, West Africa and in the Campos Basin off Southern Brazil. Other offshore projects include Norway and the West of Shetland, UK, with future deepwater developments in areas such as the Black Sea and the Caspian Sea.

In recent years there have been very large deepwater discoveries in West Africa, where water depths range from 300-1500m. In 1998, 12 finds were made off the coast of Angola, with expected reserves of 5-6 billion boe[6]. BP expect their Gulf of Mexico fields (in water depths ranging from 1300-1800m), which have reserves of 2.5 billion boe, to increase output to 300,000 bpd by 2003 and 800,000 bpd in 2009[7].

One of the deepest fields is Petrobras's Roncador field, which is currently producing from a water depth of 1853m[3] but, it is expected that future production will be possible from water depths of 2500m, with a global deepfield development CAPEX of $76 billion[3].

1.2.1 Affect of Economic Climate on Deepwater Exploration and Production

In the last twenty years there has been a large fluctuation in the price of oil, ranging from around $40 a barrel in 1981 to $10 in 1998[6]. In February 1999, the complete cost of a North Sea barrel was $12, this included exploration, development, operations and overheads[8]. When oil sells for as low as $10 per barrel, this results in a loss, therefore no investment in deepwater exploration and production can be undertaken. These low oil prices demand breakthroughs in cost reduction by pushing the boundaries of deepwater technology. Hence, BP set a total cost target for finding, developing and operating a deepwater field in the Gulf of Mexico of $5-$6 a barrel[7]. This was to be achieved with new drilling technologies and improvements in flow assurance. By June 2001, the price of oil was around $34 a barrel[9], therefore, exploration budgets are spent on drilling, bringing as much production on line as possible, while prices remain high.

1.3 Floating Production Systems

Deepwater environments are associated with problems due to wave action and currents. High pressures also create severe problems for anchoring and mooring systems and risers, which connect surface vessels to the seabed. Hence, conventional steel or cement platforms with foundations sunk into the seabed, are no longer economic or feasible for use in deepwater developments. Therefore, floating platforms or vessels that are moored, but not rigidly fixed, to the seabed and can cope with strong currents and severe weather are required.

Floating production systems that are suitable for deepwater include: tension leg platforms, spars, FPSO's (floating production storage and offloading vessel) and semi-submersibles. In a typical large deepwater development the costs are divided as follows; 31% floating production vessels, 38% subsea systems (16% on risers and pipelines) and 31% on wells[6].

Investment in the floating production systems sector, is set to increase to more than $32 billion in the next five years. That figure compares with $20 billion invested in worldwide floating production in the previous five years[9]. There are currently 62 FPSO's under construction and planned, with the largest proportion (27%) of these projects in Latin America[10]. From these figures it can be seen that the present and the future reliance on floating production systems is tremendous.

1.4 Riser Systems

Predicting the effects of the riser, on the production of a multiphase mixture, is important, as this is potentially the weak link between the subsea pipeline and the topside processing equipment. There are two main types of riser- rigid, which are usually steel pipes and flexible, usually steel polymer composite pipes[11]. Rigid risers are either vertical or hung in a catenary shape, and flexible risers are usually hung in a catenary or 'S' shape, Figure 1.1. Rigid risers are only satisfactory where the motions of the platform are relatively small, which makes them unsuitable for use with floating production systems. Flexible risers can provide the necessary compliance to accommodate large relative motions. Other benefits offered by flexible risers include:

- They can remain connected and in operation in more severe environments
- They are insensitive to permanent misalignments where precise location/orientation may be difficult to guarantee
- Low cost of installation
- The ability to be recovered and readapted, in case of a change in system configuration.

A disadvantage of flexible riser systems is that they become very expensive as water depth increases, due to the cost of the flexible riser pipe. In the North Sea, a flexible riser system, for depths of 350-500m, costs approximately £25 million[11]. With future offshore oil production at depths of up to 2500m, the cost could be nearly 5 times this. To reduce the cost, the flexible riser is replaced with steel pipe where possible. For example, hybrid risers are vertical bundled steel riser pipes that ascend from the riser base to about 50-100m below sea level. Flexible jumpers are then used to connect the top of the riser to the floating production facility[11]. Advantages are low cost installation methods and high levels of thermal insulation, therefore preventing the formation of wax and hydrates[12].

1.5 Multiphase Transportation

The pipeline-riser system provides a major challenge for operation under multiphase conditions, therefore a good understanding of the basic design needs for sizing the pipeline-riser system is required. However, predicting the problems associated with multiphase transportation needs to be advanced, particularly when flexible and longer risers are to be used. This is because one of the major problems is due to liquid slugs, which can be formed either hydrodynamically, as a direct result of the relative velocities of liquid and gas in the pipeline, or can be induced by the terrain, where liquid accumulates in dips and are eventually generated as long infrequent slugs. In the latter case, the shape of the pipeline-riser in particular flow conditions, can significantly influence the distribution of the multiphase fluids and how they are delivered to the topsides processing equipment.

1.5.1 Severe Slugging

A special case of terrain induced slugging is severe slugging, which if encountered, will adversely affect downstream process operation, and has therefore to be avoided or mitigated if possible. Classical severe slugging, described by Schmidt[13] (this is detailed in Chapter 2, Section 2.3.2) results in the cyclical production of long liquid slugs (often several times longer than the length of the riser) followed by a sharp gas blowdown phase. In this case, the liquid slug builds up at the base of the riser and blocks off the flow of gas until the pressure is high enough to drive the liquid out of the riser.

1.5.1.1 Issues Associated With Severe Slugging

Severe slugging is a complex transient phenomena generating tremendous concerns from both operational and safety viewpoints. Some of the problems resulting from severe slugging are:

- High instantaneous flowrates[14]

Severe slugging causes gas and liquid flowrate variations which lead to periods of no gas or liquid production (up to 6 hours for a deep water field) followed by large liquid production rates (up to 4 times the volume of the riser) and high gas velocities (up to five times higher than the velocity prior to blowdown).

Near the end of slug production the liquid flowrate can be 15 times higher than the average flowrate. This generates great instability in the liquid control system of the separation equipment, sometimes resulting in the operator manually choking the well because of the high liquid loading.

Sometimes the compressor system cannot cope with the high gas velocities during blowdown, causing safety pressure valves to vent the gas to the flare, to keep the process pressure in the operational range.

- High average back-pressure at wellhead[14]

Assuming stable flow, the back-pressure at the wellhead would be less than the actual average pressure under severe slugging conditions. The average back-pressure of a typical offshore low flow rate well (2400 bpd) is 700 psi but, under severe slugging, this average could be 900 psi. For a high productivity index well this can mean production losses of 800 bpd.

- Slug loading and fatigue

The formation of liquid slugs during slugging, may lead to fatigue damage of equipment. Figure 1.2 shows structural damage due to slug loading on the BP expansion loop in Alaska. The expansion loop, on the left, moved as a result of slug loading and damaged the instrument trunking on the right. Slug loading and fatigue will be even more important in

deepwater operations, where large, high momentum slugs can be expected. For example, in severe slugging conditions, a 1000m high riser can lead to 100 tonne slugs travelling at speeds in excess of 10m/s[15]. This could result in high physical loadings on equipment and large pressure variations. Due to the cyclical nature of severe slugging and the size and energy of these slugs, the capability of conventional handling facilities may well be exceeded, leading to structural and fatigue damage.

Methods used to overcome severe slugging include; riser base gas lift, foams and design tools to predict the occurrence of severe slugging, e.g. OLGA, PROFES. Comparisons of OLGA predictions against catenary and lazy 'S' riser data showed reasonable success in predicting flow regimes in the pipeline-riser, but severe slugging characteristics were not correctly predicted by the code. Predicting the occurrence and characteristics of slugs, is an essential element in the design of offshore pipelines and separation equipment. By not accurately predicting the size and frequency of slugs, may lead to the over-design of a system (resulting in increased CAPEX and possibly making a development uneconomic) or, if the system is under-designed, to operational problems with a resulting reduction in production

1.5.2 Integrity Related Issues

Other problems associated with deepwater developments include:

- Low operating temperatures due to lower ambient temperatures and increased heat loss

This can lead to hydrate and wax formation, which can result in pipeline blockages. The colder temperatures can also cause emulsion formation, which prevents water accumulation, but impedes the flow due to the high viscosity and results in separation problems.

These problems can be overcome by insulating pipelines, chemical or electrical heating, pigging of pipelines and using inhibitors.

- Pipelines operating at higher pressures and lower velocities

This can allow water to build-up and sand to accumulate, which results in corrosion (where corrosion rates are increased due to the higher pressures).

Pigging and inhibiting corrosion can surmount these problems.

- Pressure drop increases with water depth

This can result in insufficient wellhead flowing pressure.

The pipeline inlet pressure can be boosted using down hole electrical submersible pumps (ESP's).

1.6 Research Objectives

The main objectives of this research are to improve understanding of the characteristics of severe slug flow and to develop models that predict the forces on a bend, during each stage of the severe slugging cycle, using experimental data from a lazy 'S' riser test facility.

1.7 Outline of Thesis

Chapter 2 is a literature review of the hydraulics of normal and severe slug flow. The review describes normal slug flow and discusses the experimental and theoretical studies of severe slug flow, in pipeline-riser systems. In particular, the review highlights previous investigations into the forces on bends due to normal slug flow.

Chapter 3 describes the lazy 'S' riser test facility used to determine severe slugging flow characteristics and to investigate the forces on a bend during each stage of the severe slugging cycle. The Chapter describes the flow loop, instrumentation and the procedures used to calibrate and commission the instrumentation, and the data acquisition system. The liquid and gas mass balances on the separator are also detailed.

Chapter 4 details the procedures used to calibrate the strain-gauged struts, which measured the vertical and horizontal forces on the bend, at the top of the lazy 'S' riser.

Chapter 5 describes the lazy 'S' riser single phase and two phase tests. Single phase tests are carried out to simulate slug build-up (as the slug front impacts upon the bend) and slug production (as the liquid passes around the bend). The results of the investigations into severe slugging flow characteristics are discussed and comparisons are made to previous work. The Chapter also describes the analysis procedures used to determine the forces on the bend during each stage of the severe slugging cycle. From the experimental data, models are developed to predict the slug forces on a bend.

Finally, in Chapter 6 conclusions from the research are made and recommendations are given on further work.

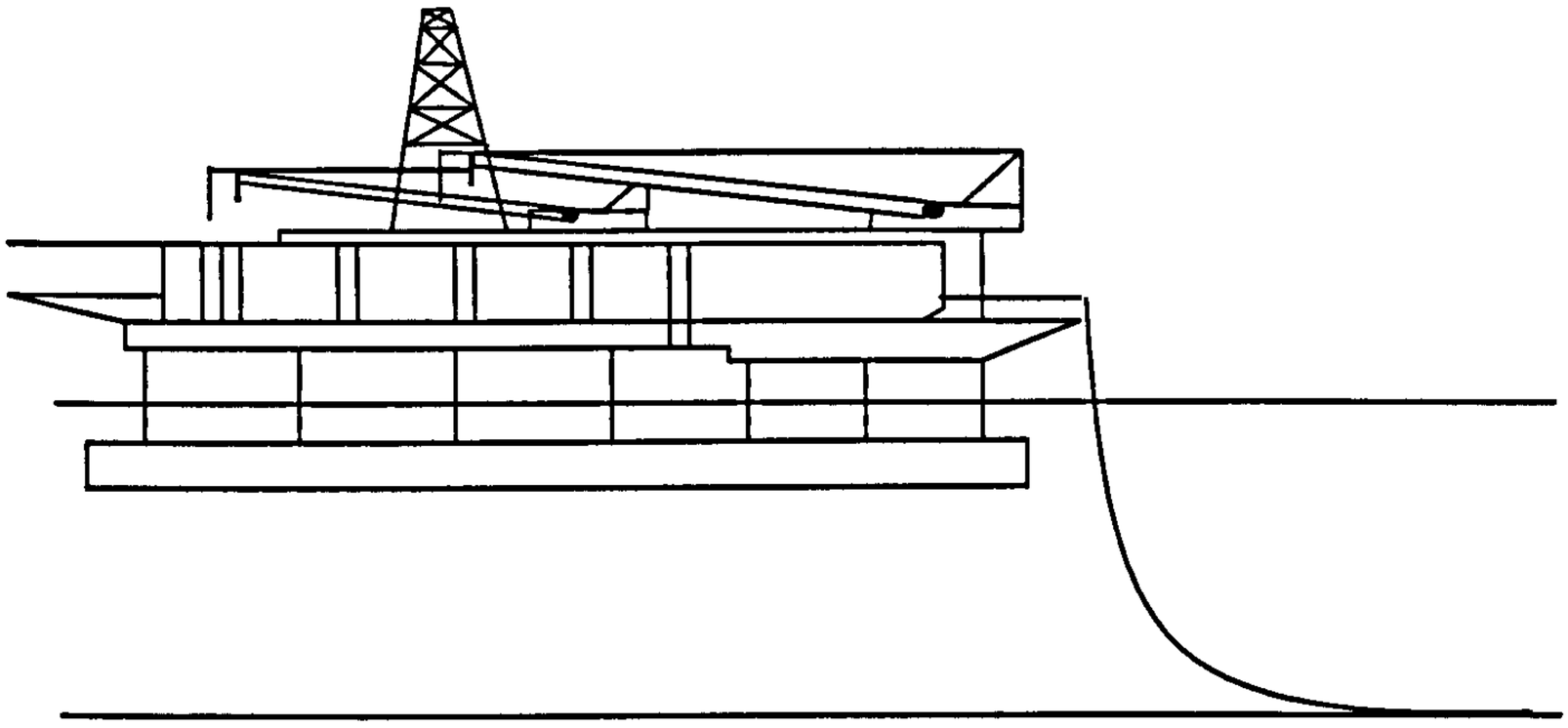

Free hanging catenary

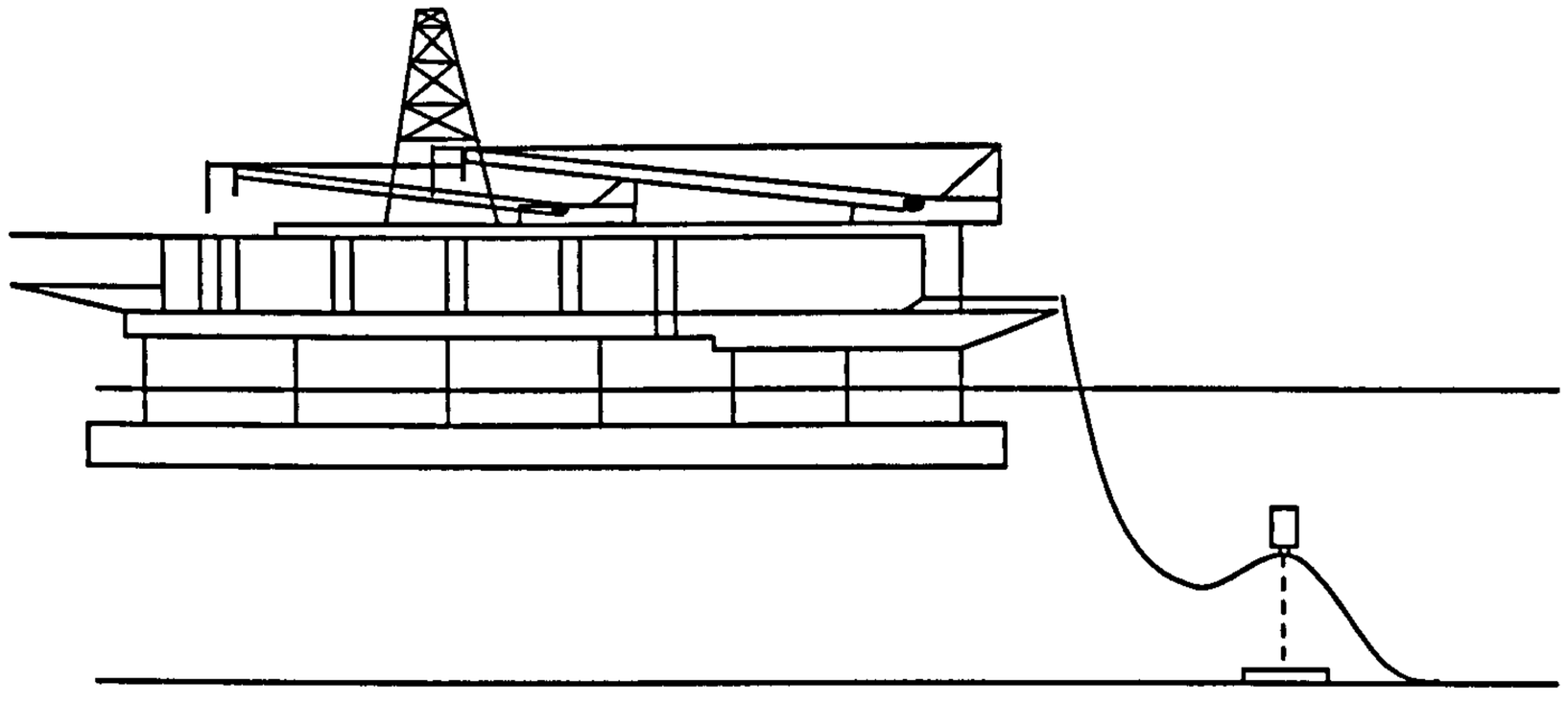

Lazy 'S'

Figure 1.1 Examples of flexible riser configurations

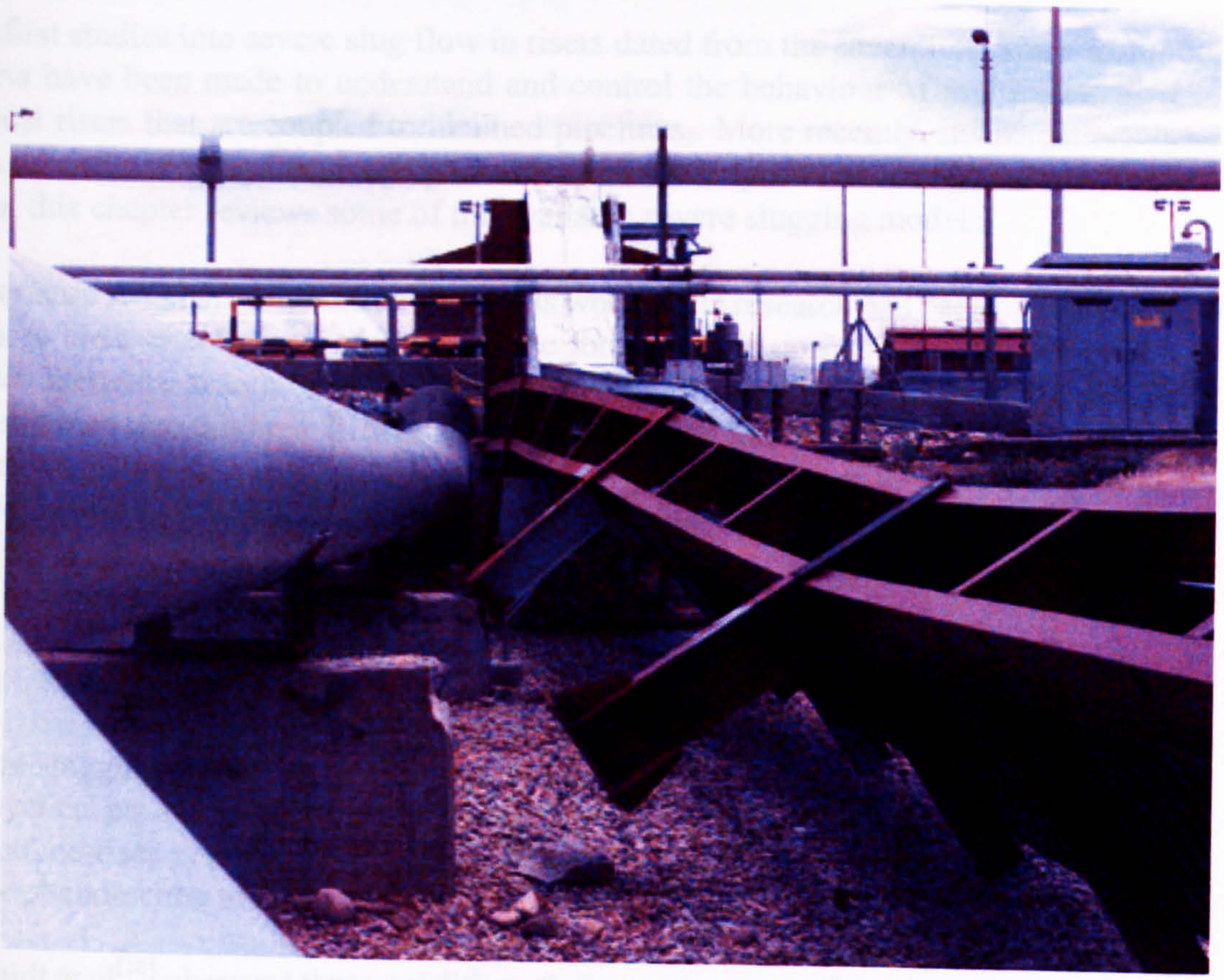

Figure 1.2 Structural damage due to slug loading

CHAPTER 2 - LITERATURE REVIEW OF THE HYDRAULICS OF NORMAL AND SEVERE SLUG FLOW

2.1 Introduction

The initial aim of this literature review is to bring together and assess the information on the experimental and theoretical studies of the hydraulics of severe slug flow, in pipeline-riser systems. The review concluded that from the large number of papers published, it was apparent that a great deal of work had been carried out to help understand the fundamental hydrodynamics of pipeline-riser systems.

The first studies into severe slug flow in risers dated from the seventies. Since that time, efforts have been made to understand and control the behaviour of multiphase flow in vertical risers that are coupled to inclined pipelines. More recently, investigations have been carried out using free hanging catenary and 'S' shaped riser configurations. Section 2.4 of this chapter reviews some of the available severe slugging models.

A literature search highlighted subject areas where little research had been carried out. One of these areas was the investigation of the forces due to normal or severe slug flow. A further literature search on this subject, reviewed in Section 2.5, confirmed the limited investigation into this area. In fact, no papers have been found that look at the forces due to severe slug flow. This review led to the decision that research into the severe slug forces in a pipeline-riser system was required.

2.2 Severe Slugging

2.2.1 Occurrence of Severe Slugging

Severe slugging is a terrain dominated phenomenon that is characterised by the formation and cyclical production of long liquid slugs and fast gas blowdown. Severe slugging occurs in pipeline-riser systems, where the riser base represents the low point necessary for this cyclic phenomenon to occur.

Schmidt et al[16] observed three conditions that were necessary for severe slugging to exist in a pipeline-riser system:

(i) The pipeline must be at a negative inclination.

(ii) Low gas and liquid flowrates; as severe slug flow is dependent on there being insufficient energy in the gas to unblock the pipeline when it fills up with liquid at the low point.

(iii) Stratified flow must exist in the pipeline.

2.2.2 Description of the Severe Slugging Cycle

Classical severe slugging in a vertical riser was described by Schmidt[16] and is recounted here.

Referring to Figure 2.1, a liquid slug has just passed from the riser into the separator. Some liquid from the tail of the slug and the film from the riser wall, falls back down the riser and accumulates at the base of the riser. At the same time liquid is continually flowing into the base of the riser along the pipeline. Whether or not the severe slugging cycle occurs is then governed by the flowrates of the incoming liquid and compressibility of the gas.

If the increase in gas pressure in the pipeline per unit time is less than the hydrostatic pressure gain per unit time (due to the incoming and fallback liquid) then liquid will continue to accumulate at the base of the riser. The base of the riser will become blocked cutting off the gas passage, causing the riser and pipeline to start to fill with liquid, Stage 1. When the liquid slug completely fills the riser, the pressure in the pipeline has almost reached its maximum.

When the gas pressure has sufficiently overcome the hydrostatic head of liquid in the riser, the slug production stage begins with the passing of the slug tail moving along the pipeline and into the riser, Stage 2. When the slug has passed completely out of the pipeline and into the riser, the bubble penetration stage begins, Stage 3. This stage is characterised by a rapidly expanding gas bubble penetrating the liquid slug that it is pushing up the riser, leaving a thin film on the riser pipe walls. This stage continues until the slug is fully delivered into the separator and the gas bubble enters the separator.

At this point the gas blowdown stage begins, Stage 4. The pipeline is in stratified flow and the gas has an unblocked path from the pipeline, up the riser and into the separator. This allows the gas that follows the slug to expand rapidly and results in high flowrates of gas into the separator. The gas flowrate into the separator is far greater than that into the pipeline and so the pipeline rapidly depressurises. The gas velocity in the riser quickly drops off and becomes insufficient to support the film on the riser wall, consequently liquid falls back down the riser and the next cycle begins.

Figure 2.2 shows the pressure at the base of the 9.9m lazy 'S' riser, during the severe slugging cycle.

2.2.3 Investigation into Severe Slugging in Flexible Risers

Tin[17] carried out extensive work to investigate the transportation of multiphase fluids (gas/liquid) along pipeline-riser systems using flexible risers. The main aspect of the work was to investigate severe slugging within a catenary shaped riser, however work was also completed on investigating severe slugging in a lazy 'S' shaped riser, refer to Figure 1.1.

This resulted in the development of a flow pattern map and defined the location of the severe slugging, oscillation, transitional and steady flow regions, in both a catenary and a 'S' shaped riser, Figures 2.3 and 2.4.

Experimental studies were carried out on a Flexible Riser Facility. The simulated pipeline-riser system consisted of a 60m long, 50mm i.d. pipeline that entered the base of the riser at an angle of –2° from the horizontal. Each riser was 33m high. Tests were performed with a two phase mixture of air and water. Data obtained included flowrates, pressure, liquid hold-up, slug length, slug velocity and visual flow pattern observations.

2.2.3.1 Severe Slugging 1 (SS1) in a Catenary Riser

Tin[17] described SS1 as being similar to severe slugging in a vertical riser, as explained above, but the riser base bubble penetration was in the form of a series of bubbles rather than a single gas cap. SS1 was defined as follows, refer to Figure 2.5:

- Slug length was greater to or equal to one riser height.
- No air penetrated the riser during the slug build-up stage.
- Maximum pipeline pressure was equal to the hydrostatic head of the riser.
- The increase in pressure per unit time was less than the increase in the hydrostatic pressure due to the slug build-up in the riser.

2.2.3.2 Severe Slugging in a Lazy 'S' Riser

With reference to Figure 2.4, Tin[17] defined the flow regimes in a lazy 'S' riser as follows:

Severe Slugging 1, SS1:

The severe slugging 1 cycle, observed in the 'S' shaped riser, was sub-divided into four different categories, described below:

Severe Slugging 1p (pipeline gas penetration), SS1p:

The 1p cycle was considered to be similar to severe slugging 1 cycles in a catenary riser and vertical riser, Schmidt[16]. The only difference in the 1p cycle was that the gas trapped in the downward limb was compressed as the hydrostatic head built in the upper limb. Therefore, the long liquid slugs produced were separated by trapped gas.

Severe Slugging 1t (trapped gas penetration), SS1t, (Figure 2.6):

The 1t cycle was characterised by the trapped gas in the downward limb, penetrating the upper limb, before the pipeline gas penetrates the bottom of the riser during the bubble penetration stage. The 1t cycle occurred at relatively high liquid flowrates.

Severe Slugging 1b (bubble penetration), SS1b, (Figure 2.7):

The 1b cycle was a variation on the 1p cycle. There was no slug production stage in this cycle and no liquid built up in the pipeline during the slug build-up stage.

Severe Slugging 1, (with intermediate cycle on the lower limb), SS1i, (Figure 2.8)

The 'S' shaped riser was considered to be two free hanging catenary risers connected together, which could result in each riser having independent effects on the cycle. After blowdown, the liquid accumulated in the lower limb of the riser. Before the lower limb filled with liquid, it was periodically moved into the upper limb by the pipeline gas. This process continued until the riser was filled with liquid and a severe slug was formed.

Transitional Severe Slugging:

Three types of transitional severe slugging were observed, they are described below:

Severe Slugging 2, SS2, (Figure 2.9):

Characterised by no back-up of liquid in the pipeline and slug lengths less than one riser height. Severe slugging 2 occurred at higher flowrates compared to severe slugging 1.

Severe Slugging 3, (with intermediate cycle on the lower limb), SS3i, (Figure 2.10):

This flow regime was identified by pressure signals from the base of the downward limb. Liquid accumulation was initiated by periodic blowdown of the lower limb, moving liquid into the upper limb.

Severe Slugging 4, SS4, (Figure 2.11):

Due to high gas flowrates, gas penetrated the lower limb of the riser and accumulated in the downward limb of the riser. When the downward limb was filled with gas, penetration of the upper limb was initiated and gas blowdown began.

Oscillation, OSC, (Figure 2.12):

Oscillation flow was identified by a sinusoidal fluctuation in the riser base pressure reading. Tin[17] described oscillation flow as resembling the severe slugging cyclic process, but without the spontaneous vigorous blowdown.

2.3 Severe Slugging Models

2.3.1 Schmidt et al (1979)

Schmidt et al[13] suggested that three conditions were required for severe slugging to occur:

- A negatively inclined pipeline
- Stratified flow in the pipeline
- The rate of hydrostatic head accumulation at the riser base is greater than the rate of pipeline gas increase.

Schmidt et al[13] carried out work on a 30m long, 50mm diameter, negatively inclined pipeline, connected to a 15m high vertical riser. The test fluids used were air and kerosene and the separator pressure was kept approximately at atmospheric pressure. A simple hydrodynamic model was developed for severe slug flow. The assumptions made were:

(i) Input liquid and gas mass flow rates remain constant during the period of severe slugging, t_{cycle}.

(ii) Separator pressure, P_{sep}, is a constant.

(iii) Liquid slugs formed in the riser pipe and in the pipeline do not contain entrained bubbles.

Basic equations were developed and 6 unknowns were present. Empirical correlations were presented for 2 of these unknowns, liquid hold-up in the pipeline, H_L and liquid fall-back, FB_L.

Liquid hold-up was described as the ratio of the area of the pipeline occupied by liquid, A_L, to the total area of the pipeline, A_P.

Liquid fall-back was defined as the liquid that had fallen down the riser, after the tail of the main liquid slug had passed into the separator.

The dimension dependent expression for FB_L was based on the liquid fall-back experimental data collected, to give, in feet:

$$FB_L = -7.71 + 5.8(v_{SL} + \frac{1}{v_{SG}}) \qquad (2.a)$$

The correlation to predict fall-back was limited to the severe slugging 1 region, it was acknowledged that applicability of Equation (2.a) to pipe sizes other than 50mm was questionable.

Schmidt et al[13] compared the experimental build-up times, $t_{build\text{-}up}$, against the mathematical model and found that the build-up times compared to within 2%. The build-up times also agreed with field data. The pipeline pressure, P_p, and liquid levels in the pipeline and riser, Z_{Lp} and Z_{Lr} (refer to Figure 2.13), tended to be slightly under-predicted, but compared well to the values when the riser was full of liquid.

2.3.2 Bøe (1981)

The aim of the work carried out by Bøe[18] was to develop simple analytical expressions to define the flow conditions under which severe slugging could occur.

Two formulae were developed for the onset of severe slugging. The first was based on the model developed by Schmidt et al[13]. The following formula described the condition for which severe slugging would occur:

$$v_{SL} \geq \frac{P_P}{\sin\beta \rho_L g L_G (1 - H_L)} v_{SG} \qquad (2.b)$$

where,

β riser deviation from vertical
L_G equivalent length of gas volume

Bøe noted that the above onset criteria assumed no upper limitations on the velocities, i.e. that severe slugging could occur for any superficial liquid velocity, v_{SL}, or superficial gas velocity, v_{SG}, as long as the equation was satisfied. Therefore, Equation (2.b) gave a 'low-flow' boundary below which severe slugging could not occur.

Based on the stability of the stratified flow in the pipeline, a 'high-flow' boundary was determined. The stratified flow would become unstable if:

$$v_{SG} \leq c_2 (1 - H_L)^{3/2} \left(\frac{\rho_L - \rho_G}{\rho_G} g D \cos\alpha \right)^{1/2} \qquad (2.c)$$

where,

D pipe diameter
α pipe inclination from horizontal
c_2 no slip liquid hold-up, $c_2 = (1\text{-}H_L) = \frac{v_{SG}}{v_{SG} + v_{SL}}$

2.3.3 Pots et al (1985)

Pots et al[19] carried out experiments on a 50mm diameter, 30m long pipeline connected to a 15m high vertical riser, to predict the onset of severe slugging. The fluids used were air and water.

The formulation for the onset of severe slugging was derived as:

$$\Pi_{SS} = \frac{(zRT)/M_G}{gL_P\alpha_P''}\frac{\dot{m}_G}{\dot{m}_L} \qquad (2.d)$$

where,

L_p	pipeline length
$\dot{m}_G$	mass gas flowrate
$\dot{m}_L$	mass liquid flowrate
α_P''	average void fraction in the pipeline

When $\Pi_{SS}<1$, severe slugging occurred.

A simple hydrodynamic computer code, SLUGFLOW, was developed that was similar to that presented by Schmidt[13]. The model on which the code was based simulated the complete severe slugging cycle in a pipeline-riser system. It described the onset of severe slugging, liquid slug build-up, production and blowdown. Mass and momentum conservation were applied to the riser to determine slug acceleration up the riser, maximum slug velocity in the riser, slug length and slug frequency.

When experimental data was compared to SLUGFLOW, the model was found to over-predict slugging periods and under-predict maximum slug velocities. Comparisons between the slug lengths predicted by Pots[19] and the slug lengths predicted by Schmidt[13], showed that both models over-predicted slug lengths. With the model developed by Schmidt predicting slug lengths more accurately (10% compared to 43%).

The problem with the Pots[19] model was that it did not take into account the two phase flow in the upstream pipeline, this could explain the differences between experimental and model values.

The model was still useful for obtaining worse case predictions in pipeline-riser design.

2.3.4 Goldzberg and McKee (1985)

The mathematical model presented by Goldzberg and McKee[20] was used for predicting liquid accumulation and terrain-induced slugging occurrence, in low liquid/gas ratio pipelines.

The model's calculations for liquid accumulation and the prediction of severe slugging were based on simple mechanistic concepts similar to those used in the theory of irregular motion of liquid in open channels.

The model could be used in the design and operation of two phase pipelines, but was developed primarily for systems with low liquid loading, e.g. gas transmission lines.

2.3.5 Fabre et al (1987)

Fabre et al[21] performed experiments on a 50mm diameter, 25m long pipeline that was connected to a 13.5m high vertical riser. The fluids used were air and water.

A severe slugging model was developed for the riser by expressing the local conservation of mass and momentum as a set of partial differential equations for position, x, and time, t. For the pipeline, mass conservation for gas and liquid was used to develop differential equations in respect to time only. The method of characteristics was used to solve the partial differential equations to give riser base pressure, void fraction, liquid and gas velocity into the riser and liquid height in the riser.

The numerical solutions were compared to experimental results and were found to be in good agreement, as shown by the riser base pressure results in Table 2.1, below.

	Model (bar)	Experimental (bar)
Minimum Riser Base Pressure	0.72	0.68
Maximum Riser Base Pressure	1.4	1.4

Table 2.1 Comparison between Experimental and Numerical Results

2.3.6 Tin et al (1993)

Tin et al[22] developed a model that could be used for predicting slug length during the severe slugging 1 cycle, in a free hanging catenary and lazy 'S' riser. To calculate the slug length, the analysis was based on time-dependent pressure balance, and liquid and gas mass balance equations.

The analytical results were compared to experimental results, as shown in Figure 2.14. Experimental results were obtained from the test rig described in Section 2.3.3. Results showed that predicted values were generally in good agreement with the experimental data, with the catenary riser slugs lengths tending to be under-predicted by 18% and the lazy 'S' riser slugs lengths over-predicted by 26%.

The disadvantage of the model was that it used a number of simplifying assumptions, for example, it assumed a constant liquid hold-up for different mixture flowrates, where as experimental results showed that the pipeline liquid hold-up fluctuates during the cycle.

2.4 Normal Slug Flow

Dukler and Hubbard[23,24] developed a model for the slug flow in horizontal and near horizontal pipes. The model defined the different interactions found in slug flow and allowed slug velocity and pressure drop to be calculated. Referring to Figure 2.15, the mechanism of the slug flow model was described as:

"If gas and liquid are entering a pipe, at low gas velocities, the liquid flows as a stratified phase, with the gas passing above at a higher velocity. At gas and liquid velocities where slug flow takes place, the gas velocity is sufficient to generate waves on the surface of the liquid. These waves grow in amplitude as they travel along the pipe and in a short distance they bridge the pipe, blocking the gas flow.

As soon as the bridging occurs, the liquid in the bridge is accelerated. The liquid acts as a scoop, picking up all the slow moving liquid in the film ahead of it. By this mechanism, the wave grows and becomes a liquid slug.

As the slug is formed and moves down the pipe, liquid is shed from its trailing edge and falls, under the influence of gravity, to the bottom of the pipe reforming the stratified film.

Shortly after a slug is formed it sweeps up all the excess liquid that had entered the pipe since the last slug was formed. At this time, the liquid film, which is about to be picked up by the slug, is only that liquid which has been shed from the previous slug. Since the slug is picking up liquid at the same rate that it is shedding it, the length of the slug stabilises.

Since the slug has a higher kinetic energy than the liquid film, the film penetrates a distance into the slug before it is finally assimilated at the slug velocity. This overrunning phenomenon creates an eddy at the front of the slug, which is essentially a mixing vortex and, therefore, exists without a pressure gradient. The distance of penetration constitutes the length of the mixing eddy. Gas is entrapped in this mixing zone. This gas migrates to the top of the pipe due to gravity forces and is subsequently trailed off the end of the slug with its neighbouring liquid.

As the gas rate and, consequently, the slug velocity increase, the degree of aeration of the slug increases. Ultimately the gas forms a continuous phase along the top of the slug. When this occurs, the slug begins bypassing some of the gas. At this point, the slug no longer maintains a competent bridge to block the gas flow and the character of the flow changes.

This point is referred to as the beginning of blow-through. In the blow-through regime the slug velocity begins to fall below that of the gas phase due to the bypassing of the slug.

As blow-through becomes more pronounced, with increasing gas rate, the slug begins to dissipate due to the entrainment of the liquid in the high velocity gas phase. This entrainment process begins the transition to annular-mist flow."

2.5 Investigation of the Forces Due to Normal Slug Flow

2.5.1 Slug Forces on a Pipe Bend/Elbow

Fenton et al[25] investigated the forces experienced by a pipe bend, when a trapped upstream liquid slug was cleared from a pipe, by a high velocity gas flow. Two models were proposed- a simple model and an advanced model. Both models were based on the fact that the force on a bend resulted from the momentum transfer, in changing the fluid flow direction around the bend. The simple model was based on the assumption that a coherent liquid slug, instantaneously accelerated to the nominal velocity of the gas driving the slug. The advanced model took into account factors such as gas compressibility and fluid emptying from the pipe.

Figure 2.16 shows a schematic diagram of the experimental apparatus. The apparatus consisted of a 1" (25mm) horizontal plexiglass pipe section, which had a slight dip to retain the liquid slug. The pipe then continued straight and horizontal until reaching a 90° downward bend. A reservoir tank was filled with air to a given pressure, with the ball valve closed. A known volume of water was introduced into the dip of the 1" pipe and allowed to settle. The ball valve was suddenly opened and the slug was cleared from the dip by the high velocity gas flow. Measurements of the pressure downstream of an orifice and the horizontal force at the bend (measured using load cells), were recorded at a sampling rate of 500 Hz. Any remaining fluid in the pipe was drained. The ball valve was then closed and the experiment repeated. Experiments were carried out by varying the volume of the water trapped in the dip, the distance of the trapped water to the 90° bend, 8, 11ft (2.4, 3.4m), and the driving pressure in the reservoir tank, 60, 80, 100 psig (414, 552, 690kPa), which corresponded to nominal gas velocities, v_{nomG}, of 58.4, 74.8, 92f/s (18, 23, 28m/s) respectively.

A simple analysis of the problem was made, which resulted in the force on the bend being calculated based on momentum transfer only. The nominal peak force, in the horizontal direction, was given by:

$$F_{nom} = \rho_L v_{nomG}^2 A \qquad (2.e)$$

Figure 2.17 shows typical force-time and pressure-time traces. The force remained zero until a point at which the force increased sharply for up to 0.15s, and then diminished. The pressure rose smoothly to a point where it remained constant and then decreased to atmospheric pressure.

The sharp increase in force was due to the impact of the slug as it passed around the bend. The lower force readings were due to the sweep out of the fluid, which was left behind by the slug, or because the slug was not 100% liquid, due to gas entrainment.

The pressure rise was due to the accumulation of air, between the orifice and slug, when the valve was opened. The pressure then reached a point where it could force the slug from the dip, causing the slug to accelerate. The pressure decreased as the gas passage became clear.

To compare Equation (2.e), the proposed estimate of the peak force, to the measured peak force, F_m, a graph was plotted of normalised force, F^* (measured peak force divided by the nominal peak force) versus dispersion distance, D^*. A horizontal line at $F^* = 1$, was ideal, as at this point the estimated peak force was equal to the actual measured peak force. Results showed that for $D^* < 4$, the actual measured peak force was under-estimated by the nominal peak force, in the worst case, by 2 ½ times. For $D^* > 4$, the measured peak force was over-estimated.

Changes were made to the assumptions of the original model to improve the accuracy between the model and the actual measured force. The assumptions made included:

(i) The driving gas was ideal and the compression of the gas was isothermal.

(ii) Fluid emptying out of the pipe bend caused the mass of the slug to diminish.

(iii) The force at the pipe bend was still assumed to be dominated by momentum transfer, but fluid velocity, v_{mo}, was that resulting from the acceleration calculated with this model, not the nominal gas velocity. Therefore force at the bend, F_{mo}, is estimated by:

$$F_{mo} = \rho_L v_{mo}^2 A \qquad (2.f)$$

With these new assumptions, the agreement between the actual measured peak force and the nominal peak force, using the new model, was improved. Figure 2.18 shows the graph of normalised force versus dispersion distance. For $3.5 < D^* < 4.5$, the model tended to underestimate the forces, as slug erosion, due to shedding, may have left a filament of liquid which accelerated to a velocity greater than that of the model. For $D^* > 5$, the measured forces were greatly over-estimated, as the model assumed that the fluid remained a solid slug of liquid, therefore gas penetration of the slug was not accounted for. This became more dominant at higher dispersion distances.

Neumann et al[26] investigated the effect of section change on the forces experienced by a bend, during pipe clearing. This work was based on a similar set up to that described by Fenton et al[25]. In this work, the 1" (25mm) pipe was replaced by a 0.75" (19mm) pipe, which was connected to a 1.75" (44mm) pipe and bend.

F^* was calculated using the following equation:

$$F^* = \frac{F_m}{\rho_L v_{nomG}^2 A} \qquad (2.g)$$

Data from the 1.75" pipe and the 0.75" pipe was used to calculate F^*. From the data obtained from these experiments, the maximum normalised force (where A is the cross-sectional area of the 0.75" pipe) and the distance travelled by the slug, before the force dropped to negligible values, were similar to those of the constant diameter pipe[25]. This suggested that the section decrease before the bend did not have much effect on the forces experienced by the bend.

Bozkus et al[27] investigated the impact on an elbow, by a liquid slug travelling along a horizontal pipeline. The work looked at three aspects of the slug motion: 1) evolution of the slug, 2) time history of the slug up to the point of break-up, and 3) resultant forces on the elbow due to slug impact. A simplified analytical model was developed to predict these slug dynamics.

A pressurised air tank was used to propel the slug along a 9.45m long, 51mm diameter clear PVC pipe, which contained a fast acting ball valve and a 90° elbow, at the end of the pipe. This was followed by a short vertical open-ended pipe section. Slugs were formed using a variable length pipe section upstream of the valve. Two pressure transducers were installed at the elbow, to record pressure-time histories of the impacting slugs.

Various slug lengths, 1.22 to 3.35m, were propelled into the pipeline under various reservoir pressures, 70 to 275kPa. The data from the horizontal transducer was used in the analysis, as the slug impact at the elbow was greatest in this direction.

Figures 2.19 and 2.20 show the pressure-time histories for the shorter and longer length slugs. The short slugs (1.22 to 1.52m) showed a single peak followed by a rapid depressurisation and the longer slugs (2.1 to 3.35m) showed a double peaked response followed by the depressurisation. The double peak was explained by the observation that the longer slugs broke into two distinct masses, before they impacted upon the elbow.

The slug motion was simulated numerically by assuming, one-dimensional, incompressible motion of the slug, with no entrainment taking place. A hold-up parameter was introduced to account for the continuous loss of liquid mass from the slug. This parameter was the percentage of the pipe area for which the liquid at the trailing edge of the moving slug remained behind. The flow of pressurised air in the pipe behind the slug was assumed to be compressible, one-dimensional and adiabatic.

The normalised force at the elbow was defined as:

$$F^* = \frac{P_m}{P_{nom} + \rho_L v_{nom}^2} \qquad (2.h)$$

where,

P_m magnitude of peak pressure at elbow (For the double peak phenomenon, the first peak was chosen as P_m)
P_{nom} nominal pressure at elbow
v_{nom} nominal velocity of slug at instant of impact

Figure 2.21 is a graph of normalised force, F^*, versus dispersion distance, D^* (length travelled by slug divided by the slug length). The graph shows two sets of data, the solid lines were those of Fenton et al[25] assuming $P_{nom} = 0$ and no hold-up (as a coherent slug was assumed), and the dashed lines, the Bozkus et al data with $P_{nom} \neq 0$ and 5% hold-up (as this data matched the estimated data most closely). The Fenton et al[25] data showed that for $D^* < 5$, the estimated and measured forces compared well. For $D^* > 6$, the actual force tended to be over-estimated, due to gas entrainment not being considered. The Bozkus et al[27] data showed a similar trend, but with a greater range of normalised force.

Overall the Fenton et al[25] and Bozkus et al[27] models were better at predicting the forces due to longer slugs, with the Fenton et al[25] model predicting the forces at the elbow most closely.

Sánchez et al[28] carried out a theoretical and experimental study to determine the forces exerted on an elbow by a two phase slug flow.

Based on the momentum transfer in changing the slug direction around the elbow, Figure 2.22, the slug force could be determined. A control volume analysis around the elbow gave the forces in the x and y directions:

$$F_x = -[v_x^2 \rho A + (P_x - P_a)A] \qquad (2.i)$$

$$F_y = [v_y^2 \rho A + (P_y - P_a)A] \qquad (2.j)$$

where

P_a atmospheric pressure
P_x pressure in x-direction
P_y pressure in y-direction

therefore, the resultant force was,

$$FR = (F_x^2 + F_y^2)^{1/2} \qquad (2.k)$$

Due to the alternative occurrence of liquid slugs and Taylor bubbles, it was suggested that the maximum force was applied during the slug transit time, t_s and the minimum force during the bubble transit time, t_b.

The experimental rig, shown in Figure 2.23, consisted of a 41mm diameter, 33m long pipeline, at the end of which was a 90° elbow. Air velocities, between 7.4 and 15.2m/s and water velocities, between 0.6 and 1.6m/s, entered the horizontal pipeline through a mixing chamber and then passed through an elbow and into a separator. Pressure transducers were used to obtain pressure loss and slug velocity, by cross correlating two signals, and conductance probes determined slug frequency, length and hold-up. The forces exerted on the elbow were measured using two strain gauges.

From the hydrodynamic model proposed by Dukler and Hubbard[23], the slug velocity was given by:

$$v_s = \lambda v_{mix} + u_b \qquad (2.1)$$

where,

λ velocity distribution profile factor, ~ 1.2
v_{mix} mixture velocity
u_b bubble buoyancy effect. $u_b = 0$ for horizontal flows

From Figure 2.24, (where x is the gas quality, which is the ratio of the mass of gas, to total mass), it can be seen that the experimental slug velocity, before the slug reached the elbow, compared well to Equation (2.1), as the ratio of slug velocity to mixture velocity was approximately 1.2. With the less aerated slugs (lower values of x) the velocity before the elbow was less than the velocity after the elbow, as the slugs accelerated as they passed around the elbow, due to gas expansion. As the slugs became more aerated (as x increased), the velocity before the elbow was approximately equal to the velocity after the elbow, with the liquid hold-up decreasing after the elbow.

Figure 2.25 shows the comparison between the measured data and the estimated force. The model tended to overestimate the forces and was less accurate at higher forces i.e. at higher slug velocities. Overall the model compared quite well to the actual slug forces on the elbow.

BP[29] carried out experiments to investigate the forces on a 90° bend due to slug flow. Figure 2.26 shows the experimental rig, which consisted of a horizontal, 50mm diameter pipeline and a 90° steel bend. The bend lay on a table where it was supported by two arms, holding the bend at 45°. Strain gauges were placed on these arms to measure the resultant forces. Air velocities, up to 4.2m/s, and water velocities, up to 1.4m/s, were used as the test fluids. The rig was operated at a pressure of 6 bar and data was sampled at 10 Hz. The bend was isolated from the surrounding pipework, by installing rubber isolation joints on either side of the bend.

The slug forces on the bend were recorded at different flowrate conditions. In total 44 samples were taken for 19 different flowrates.

For each force trace, the static, F_{static}, (due to film flow), average, F_{mav}, and maximum peak, F_m, forces were determined. The nominal peak force on the bend, F_{nom}, was calculated using:

$$F_{nom} = \sqrt{2}\rho_L v_{mix}^2 A \qquad (2.m)$$

NB Please refer to Appendix A for the derivation of Equation (2.m)

Figure 2.27 shows a graph of average and maximum peak force versus mixture velocity. As the mixture velocity increased, there was an increase in the average and maximum forces. For $v_{mix} < 1$, the slugs almost disappeared. The maximum force could be seen to grow at a faster rate than the average force. Comparing this graph to Equation (2.m), the measured force showed a linear relation of slug force with mixture velocity, where as Equation (2.m) shows a parabolic relation.

Hargreaves[30] carried out experiments to investigate the forces on a 90° bend due to slug flow.

The rig consisted of a 45mm diameter, 12m long horizontal perspex pipe, with a stainless steel bend at the end. Forces were measured using a strain gauge load cell, which was clamped below the bend and supported at its base by a stiff board. To mechanically isolate the bend, isolation joints were installed on each side of the bend. Air and water were supplied to the test rig at a range of flowrates of, 0.36 to 0.56m/s and 0.13 to 0.23m/s, respectively. Flowrates were measured using rotameters.

The forces on the bend were calculated based on Newton's second law, referring to Figure 2.28:

$$F_x = P_1 A + v_{mix}^2 \rho_L A \qquad (2.n)$$

$$F_y = (P_1 + \Delta P_{TP})A + v_{mix}^2 \rho_L A \qquad (2.o)$$

where,

ΔP_{TP} two phase pressure drop

the resultant force was,

$$FR = (F_x^2 + F_y^2)^{1/2} \qquad (2.p)$$

Before any experimental work took place, calibration tests were carried out to ensure that the forces obtained could be quantified and were due to the slug flow around the bend only. These tests involved subjecting the load cell to known forces and measuring the resulting output. Vertical and horizontal forces were applied to the load cell, before installation on the bend, and with the load cell in place on the bend, at atmospheric and test (0.5 barg)

pressure. Calibration plots from the tests before installation on the bend, showed linearity between force applied and corresponding output. With the load cell installed, at atmospheric pressure, the plots were again linear, but with lower readings than the initial calibration. This was due to the isolation joints exerting elastic forces on the load cell. At the test pressure, the readings were slightly lower than at atmospheric pressure, as the joints expanded under pressure, therefore having more of a damping effect. The plots obtained from this calibration were used to process the experimental force data, as they were obtained under actual test conditions.

The force traces observed were divided into three regions; (i) an impulse peak due to the slug front impacting upon the bend, (ii) a sharp drop off as the slug passed around the bend and (iii) a decaying increase due to the slug having passed through the bend and the next slug approached, as shown in Figure 2.29.

Hargreaves[30] calculated values for the impulse peak, $F_{impulse}$, and drop off, F_{drop}, regions:

$$F_{impulse} = F_m - F_{plateau} \qquad (2.q)$$

$$F_{drop} = F_{plateau} - F_{min} \qquad (2.r)$$

Assuming a constant slug density of 1000kg/m^3, the impact force was seen to decrease with an increase in mixture velocity ($v_{SG} + v_{SL}$), Figure 2.30.

2.5.2 Slug Forces on an Orifice Plate

Owen et al[31] investigated the force exerted on an orifice plate by a liquid slug being propelled along a pipeline by a high pressure gas.

A relationship was developed for the impact of a slug with an orifice plate. Assumptions were made that the slug behaved as a solid and remained intact upon impact. Considering the variables, force on plate (F), slug velocity (v_s), cross-sectional area of the pipe (A), area of orifice (A_o), slug length (L_s), diameter of the pipe (D) and slug density (ρ_L), the relationship became:

$$\frac{F}{\rho_L v_s A} = \text{function}\left\{\frac{A_o}{A}, \frac{L_s}{D}\right\} \qquad (2.s)$$

Air, at a pressure of up to 11 bar, was used to propel a water slug along a 50mm diameter steel pipe. Slug lengths were generated by filling pipe lengths of 0.99, 2.16 and 3.15m with water. At this point, the slug was enclosed by the closed valve and a thin polythene sheet. The valve was then quickly opened and the slug was propelled, by the high pressure air, through the polythene sheet along the pipe. The slug travelled a distance of 13m before it impacted upon the orifice plate. This method was repeated using different pressures to propel the slugs. The impact on the orifice plate was measured using a piezo-electric pressure transducer. Conductivity probes, 0.215m apart, were used to measure the velocity.

During the experiments, it was noted that the 0.99m slug had disintegrated before it had reached the end of the pipe. This showed that a single slug travelling along an empty pipeline, would reach a certain velocity or travel a certain distance and then disintegrate; due to shedding at the rear of the slug and gas entrainment.

Figure 2.31 shows the impact pressures generated by the different slug lengths impacting on orifice plates of different area ratios, with different tank pressures. Figure 2.31(i) shows that the shorter slug produced a higher impact pressure at the orifice plate, at a given tank pressure. The shorter slug had an impact pressure of 105 bar at an area ratio of 0.375 and air pressure of 4 bar. At the same conditions the impact pressure of the longer slug was 75 bar, nearly 1 ½ times smaller, Figure 2.31(ii). These results were due to the fact that the smaller slug had a higher velocity, due to its reduced frictional surface area and that it had travelled further.

The results from these experiments showed that slugs could generate large forces on an orifice plate, leading to considerable damage. For these experiments, the worst case applies at higher tank pressures and shorter slugs, as the velocities under these conditions are higher, and smaller orifice area ratios.

2.5.3 Slug Forces on a Structure Located Outside of a Horizontal Pipe

Sakaguchi et al[32] investigated the impact force on a structure, located outside of a pipe, by a liquid slug travelling along a horizontal pipe.

The apparatus consisted of a water supply system, an air supply system and a transparent horizontal pipe, 8m in length. The pipe diameters used were 30 and 40mm. Gas velocities were split into initial and final velocities. With an initial gas velocity, v_{Gi}, of 0.5m/s, the flow regime in the pipe was either stratified or wavy flow. Increasing the velocity to a final gas velocity, v_{Gf}, in the range 1.6-2.6m/s, resulted in slug flow. The liquid velocity range was v_L = 0.04-0.08m/s. Measurements of slug position, slug length, liquid hold-up, pressure and impact force were recorded. The structure on which the slug impacted was a 176 x 225mm rectangular plate that was supported vertically by a cantilever. Strain gauges were attached to the cantilever to measure the force on the plate.

The flow model, see Figure 2.32, consisted of five parts: the liquid slug (B-C-C*-B*), the large bubble (A-B-A**), the liquid film (A**-B-B*-A*), under the large bubble, the liquid layer (D*-C*-C**-D**) and the gas layer (D**-C**-C-D).

The model was based on the scooping-shedding mechanism proposed by Dukler and Hubbard[23]. The following assumptions were made:

(i) The shape of the large bubble did not change whilst the slug was flowing along and out of the pipe, therefore, the minimum liquid hold-up, H_{Lmin} = constant.

(ii) The air was not absorbed by scooping at the nose of the slug and there was no bubble in the slug.

(iii) The pressure distribution was uniform in the large bubble and in the gas layer downstream of the liquid slug.

(iv) The air was regarded as a perfect gas.

The impact force of the slug acting on the plate was assumed to be given by the following equation:

$$F_{nom} = \rho_L A v_{mix}^2 \qquad (2.t)$$

From graphs of impact force of the slug, F, as it acts on the plate, versus time, t, it could be seen that the graphs behaved in one of three ways; (i) after an increase in impact force at the initial stage, the force remained approximately constant, (ii) the impact force increased linearly then decreased near the end or (iii) the force increased linearly with an increase near the end. The calculated force results were deduced by substituting experimental values of slug velocity, v_s, into Equation (2.t). These calculated results seemed to slightly overestimate the impact force, but otherwise they compared well to the experimental values.

Sakaguchi et al[32] suggested that the characteristic quantities of the impact force were:

(i) The acting period of the impact force, defined as the time from the initial increase to the initiation of the rapid decrease, τ

(ii) The initial value of the impact force, F_i

(iii) The maximum force, F_m

(iv) Total momentum, M_I, which is defined by the following equation:

$$M_I = \int_0^{\tau} F dt \qquad (2.u)$$

From the graphs, F_m, F_i and M_I increased with increasing final gas velocity, v_{Gf}, but τ tended to decrease. With an increase in liquid velocity, v_L, F_m and F_i decreased and τ increased.

The results suggested that pipe diameter did have an effect on maximum impact force, initial impact force and acting period. For the conditions of $v_{Gi} = 0.5$m/s, $v_L = 0.06$m/s and $v_{Gf} = 2.2$m/s, for D = 40mm, the maximum impact force, initial impact force and acting period were 9.5N, 5.5N and 0.6s respectively, for D = 30mm, 6.5N, 3.0N and 1.1s respectively. Therefore, under the same velocity conditions, but different pipe diameters,

the slug in the larger pipe exerted a larger initial and maximum impact force, but for a shorter amount of time.

Calculated results compared well to experimental results. Therefore, the model and method of calculation were applicable to estimating the forces exerted by slug flow from a pipe. Improvements could be made to the model, as it assumed that the amount of liquid picked up at the front of the slug was equal to the amount of liquid shed at the tail, therefore slug growth or slug erosion was not considered. It also assumed that the slug was 100% liquid.

2.5.4 Alleviation of Slug Force Effects

The ARCO Kuparuk River Unit was located in North Slope, Alaska. Problems arose at this unit due to the forces generated by slug flow. This resulted in excessive movement of partially restrained piping, causing fatigue cracking in piping branch connections and pressure vessel nozzles. Santana et al[33] described a program that was implemented at the production facility, to improve slug force resistance, by modifying existing inlet systems.

The program consisted of a unique design sequence that began with a definition of the design loads, then proceeded to analysis and was completed after several iterations of analysis and design. The program used real-time pressure and strain data to quantify and confirm design loads. Therefore, changes to design could then be made.

As there was little data available on two phase flow slug forces in large diameter pipes, a concept of slug equivalent static loads (SESLs) was developed. The size of the slug load, F, was proportional to the slug's mass density, ρ, and the square of its velocity, v_s. To consider factors such as, hydrodynamic properties of the fluid stream, a coefficient was incorporated into the slug equivalent static load. This dimensionless coefficient was known as the Dynamic Load and Inertia Factor (D_{LIF}) and was thought to range between 0.5 and 2.0. Therefore, the slug load can be described by:

$$F = D_{(LIF)} \sqrt{2} (\rho_L - \rho_G) v_s^2 A \qquad (2.v)$$

The inlet systems that were investigated consisted of flowlines from the drill sites varying from 12 to 24 inches (0.3 to 0.6m) in diameter. These were attached to 36" (0.9m) inlet lines, between 100 to 300 feet (30.5 to 91.4m) in length. An inlet line was connected to the inlet nozzle of a 15 foot (4.6m) diameter separator vessel, designed for an internal operating pressure of 150 psig (103kPa). The flowlines were supported by pipe rack structures and the inlet line by a inlet module structure, which was a flexible steel support.

Real-time data was used to confirm design load assumptions, based on Equation (2.v), then ways in which to improve the slug force resistance of this facility could be considered. This resulted in the installation of a structure to reduce the large forces in the inlet line. The structure had two legs made from 4 foot (1.2m) diameter, concrete-filled steel pipes. This was classed as an intermediate term modification i.e. it would increase slug force resistance for a few years and operational shutdown was likely during installation.

Real-time data was collected using a Slug Force Monitoring System (SFMS). This was a PC-based system, monitoring 28 to 30 channels of dynamic pressure and strain gauge information, at a sampling rate of 100Hz. The monitor displayed current and historical statistics for each data channel. Comparing these statistics showed if the slug force resistance of the modified inlet system had improved.

The statistics showed that the maximum amplitude of the forces in 1991 was greater than that in 1992, hence the slug force resistance of the inlet system had been increased by the bipod structure. Therefore, due to the implemented program, the final slug force resistance method was successful.

2.6 Summary

2.6.1 Severe Slugging Models

In Section 2.3 the severe slugging models described were developed with a varying degree of complexity, ranging from the prediction of the onset of severe slugging (Boe[18], Pots[19], Goldzberg and McKee[20]) to the attempted modelling of the complete severe slugging cycle (Schmidt[13], Pots[19]). The majority of the experimental investigations into severe slugging, were carried out using vertical risers, Schmidt[13], Pots[19], Fabre[21]. Tin[22] developed a model that could be used for predicting slug length, during the severe slugging cycle, in a free hanging catenary and lazy 'S' riser.

2.6.2 Investigation of the Forces Due to Normal Slug Flow

Section 2.5 presented an overview of the major investigations into the forces due to normal slug flow. The investigations consisted of three types of experimental and theoretical studies; slug forces on a pipe bend/elbow, slug forces on an orifice plate and slug forces on a structure located outside of a horizontal pipe.

The experiments of Fenton[25], Neumann[26], Bozkus[27] and Owen[31] simulated slug flow, by clearing a single trapped liquid slug in a pipe, by a high velocity gas flow. Sanchez[28], BP[29], Hargreaves[30] and Sakaguchi[32] carried out two phase slug flow tests. All tests were carried out using horizontal pipelines, with pipe diameters of 19 to 51mm.

All the slug force models were based on the fact that the force on a bend resulted from the momentum transfer, in changing the slug direction around the bend. The force on a bend in a x- or y- direction is given by:

$$F = \rho_L A v^2 \qquad (2.w)$$

With the resultant force on the bend given by:

$$FR = (F_x^{\,2} + F_y^{\,2})^{1/2} \qquad (2.x)$$

$$FR = \sqrt{2}\rho_L A v^2 \qquad (2.y)$$

Various methods were used to calculate the slug velocity. Fenton[25] and Neumann[26] assumed that the slug instantaneously accelerated to the nominal velocity of the gas driving the slug, i.e. $v_s = v_{Gnom}$. Sanchez[28] determined slug velocity, based on the hydrodynamic model proposed by Dukler and Hubbard[23]; where $v_s = 1.2v_{mix}$ and for BP[29], Hargreaves[30] and Sakaguchi[32], $v_s = v_{SG} + v_{SL} = v_{mix}$.

Fenton[25], Neumann[26] and Bozkus[27] measured or considered the horizontal forces on the bend only. Sanchez[28] and Hargreaves[30] measured the vertical and horizontal forces on the bend, with BP[29] measuring the resultant force at 45°. Various techniques were used to measure the slug forces; pressure transducers (Bozkus[27]), strain gauges (Sanchez[28], BP[29] Sakaguchi[32]) and load cells (Fenton[25], Neumann[26], Hargreaves[30]).

BP[29] and Hargreaves[30] mechanically isolated the bend using rubber isolation joints. Hargreaves[30] discussed the affect of these isolation joints on the load cell and quantified these effects, by carrying out a sequence of calibration tests. BP[29] found a linear relationship between force and mixture velocity and Hargreaves[30], a increase in force with mixture velocity, but in both cases, force was not proportional to the velocity squared, as expected.

Discrepancies between the calculated forces and the actual measured forces, were due to the assumption of a 100% liquid slug ($\rho = \rho_L = 1000 kg/m^3$). The models of Fenton[25], Neumann[26], Bozkus[27], Sanchez[28], BP[29], Owen[31] and Sakaguchi[32] over-estimated the slug density, as gas entrainment was not accounted for. This led to the models overestimating the actual measured forces of the shorter slugs, as gas penetration of the liquid slugs became more dominant at higher dispersion distances (number of times a slug travelled its own length).

The work of Neumann[26] was based on the work of Fenton[25] and investigated the effect of an upstream expansion (bend diameter > pipe diameter) on the force experienced by the bend. This did not have a significant affect and similar trends were seen to the constant diameter work of Fenton[25].

Investigations to determine the forces on pipe bends concentrated on the forces due to normal slug flow in horizontal pipelines. The literature review highlighted that no previous research into the normal and severe slug flow forces in a pipeline-riser system had been performed, therefore research into this area was required.

The following Chapters describe the lazy 'S' riser test facility, the calibration of the strain-gauged struts and the lazy 'S' riser single phase and two phase tests.

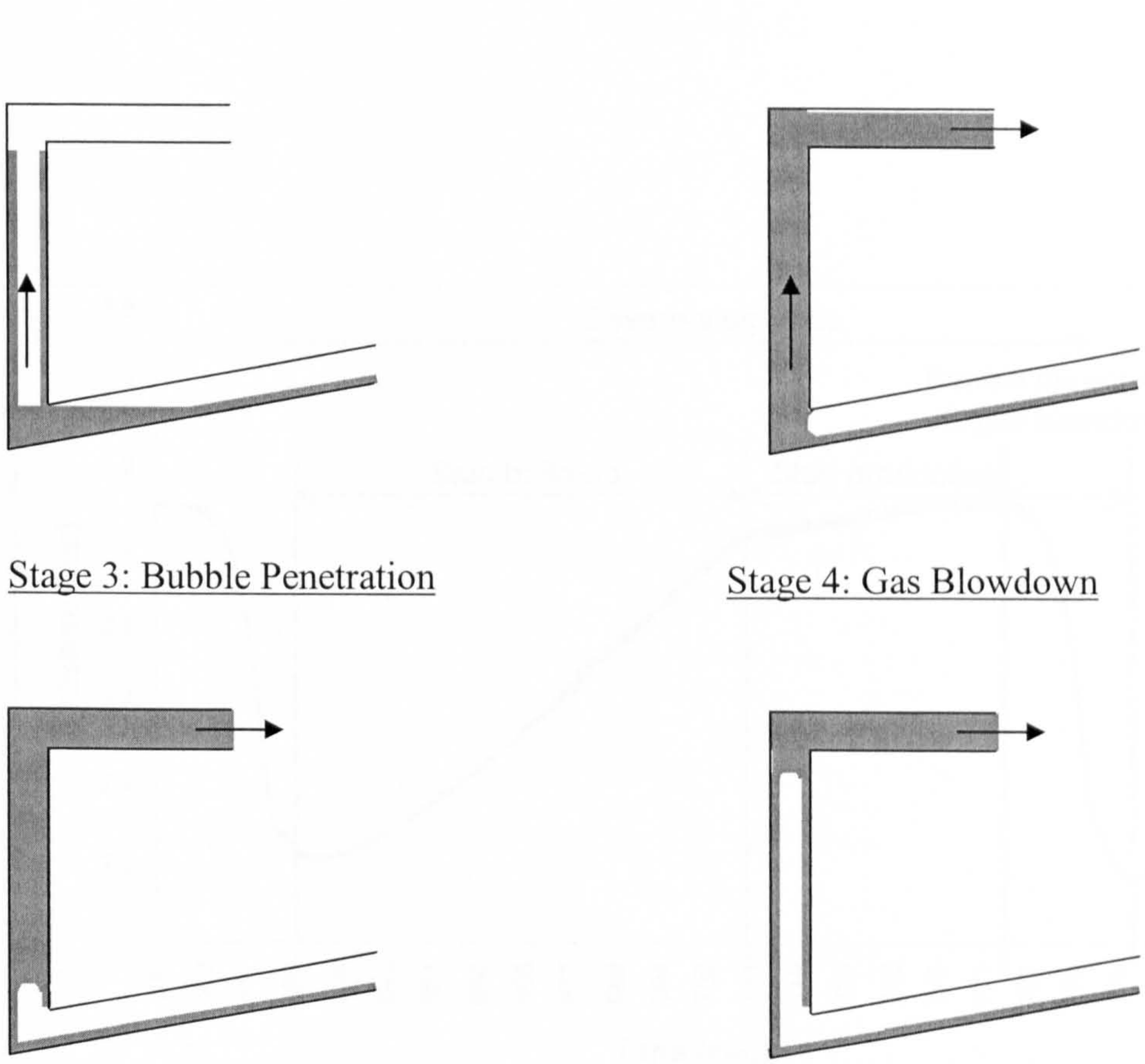

Figure 2.1 Stages of the severe slugging cycle

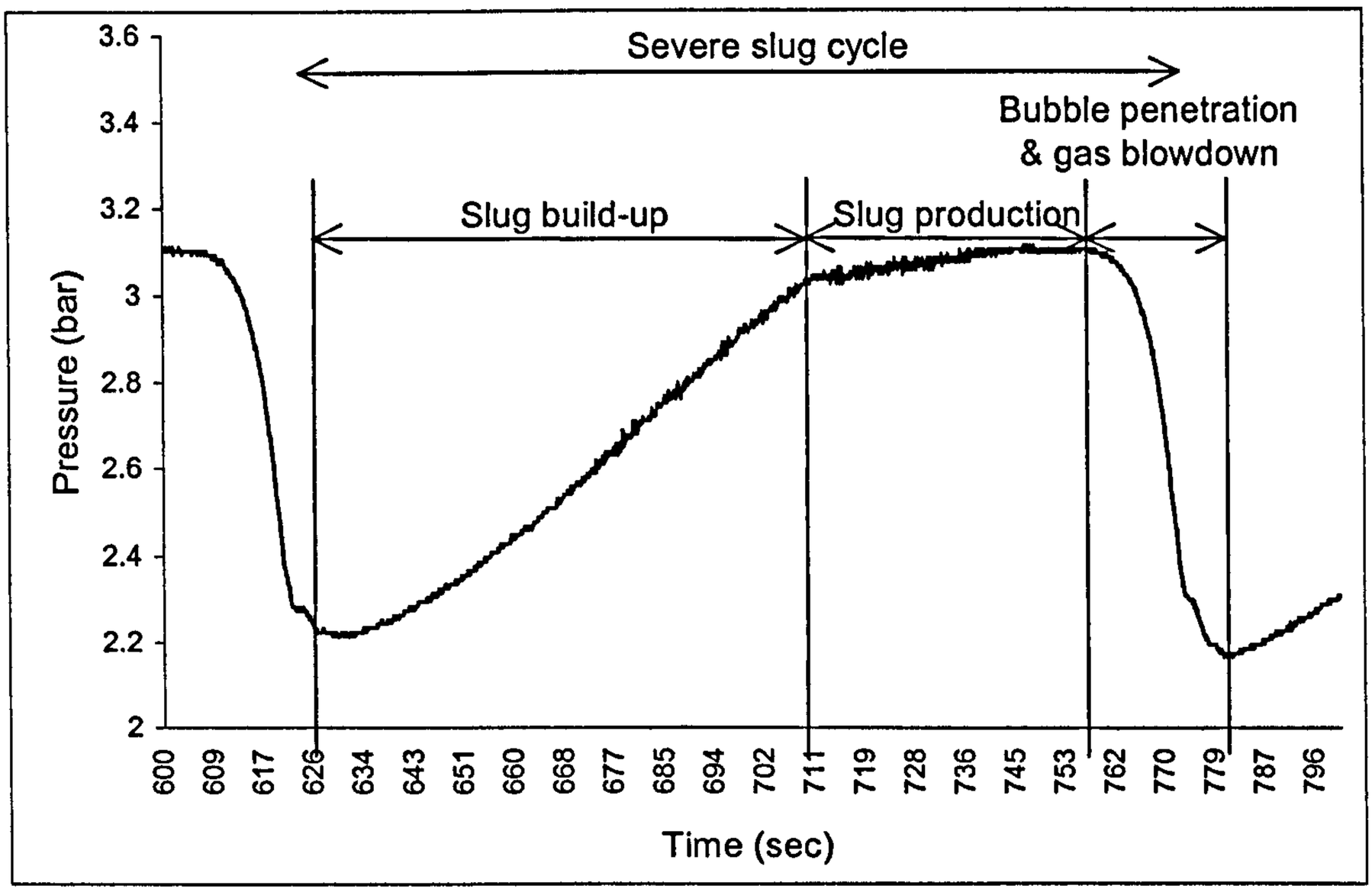

Figure 2.2 Pressure-time trace during the severe slugging cycle

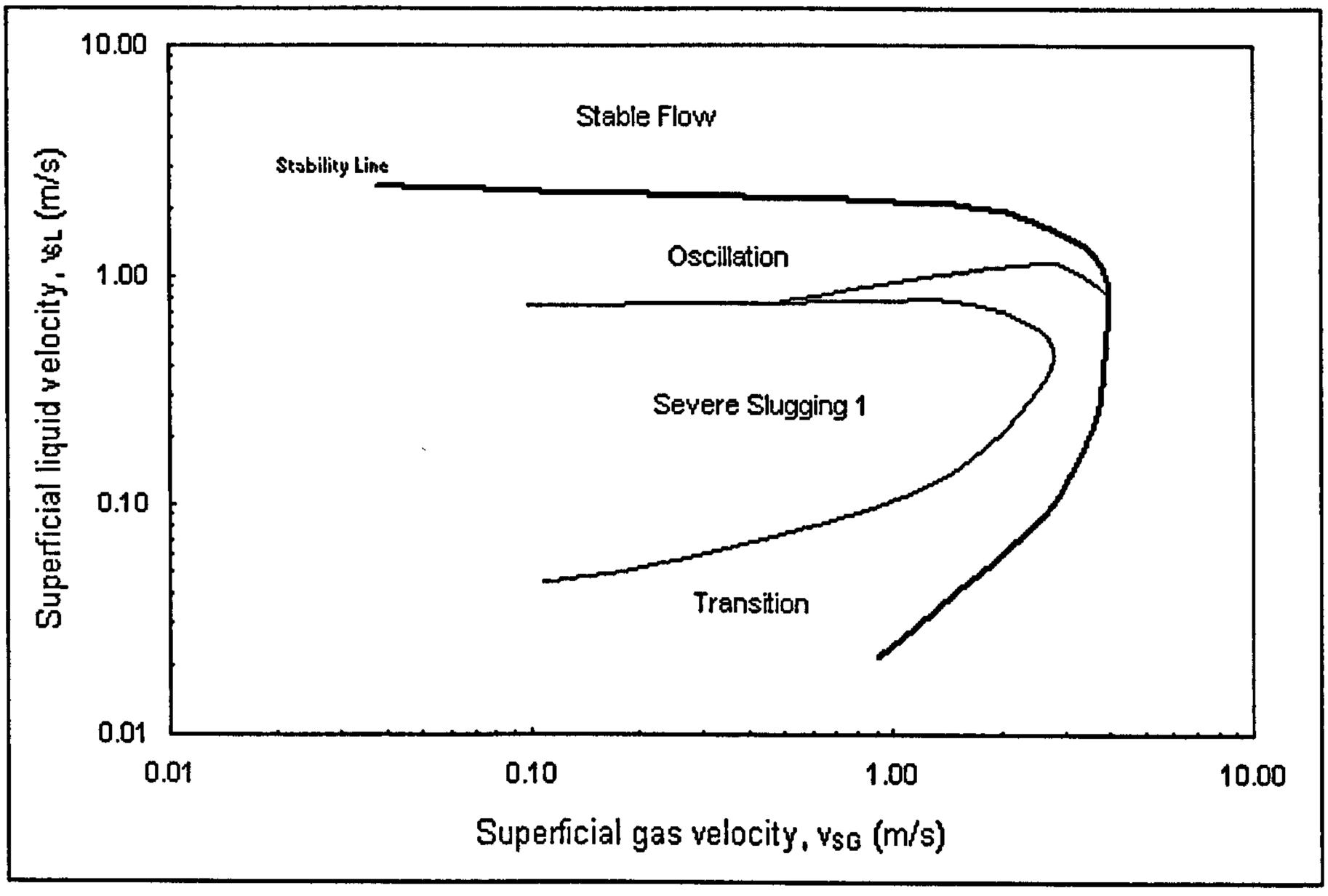

Figure 2.3 Free hanging catenary riser flow pattern map[17]

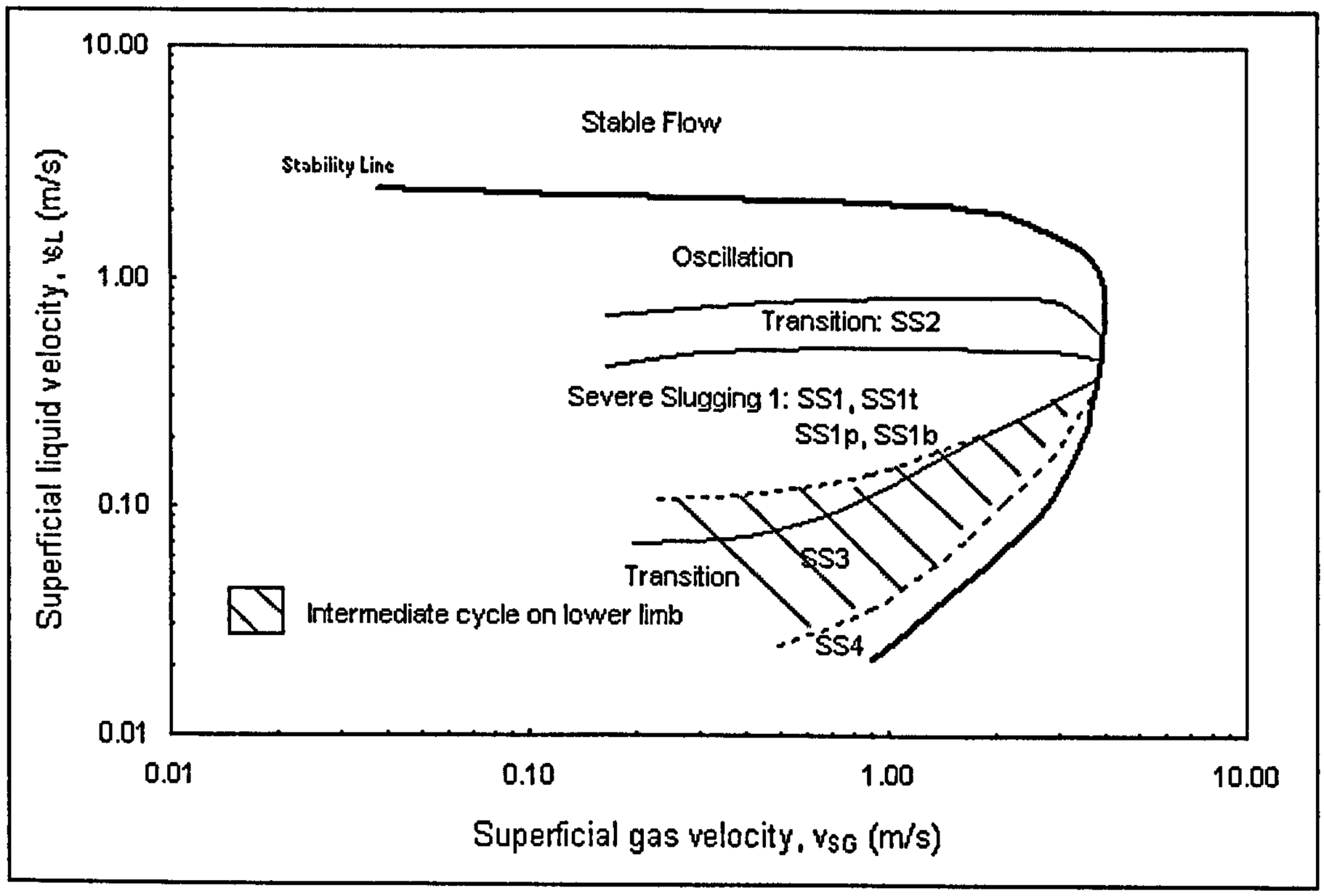

Figure 2.4 Lazy 'S' riser flow pattern map[17]

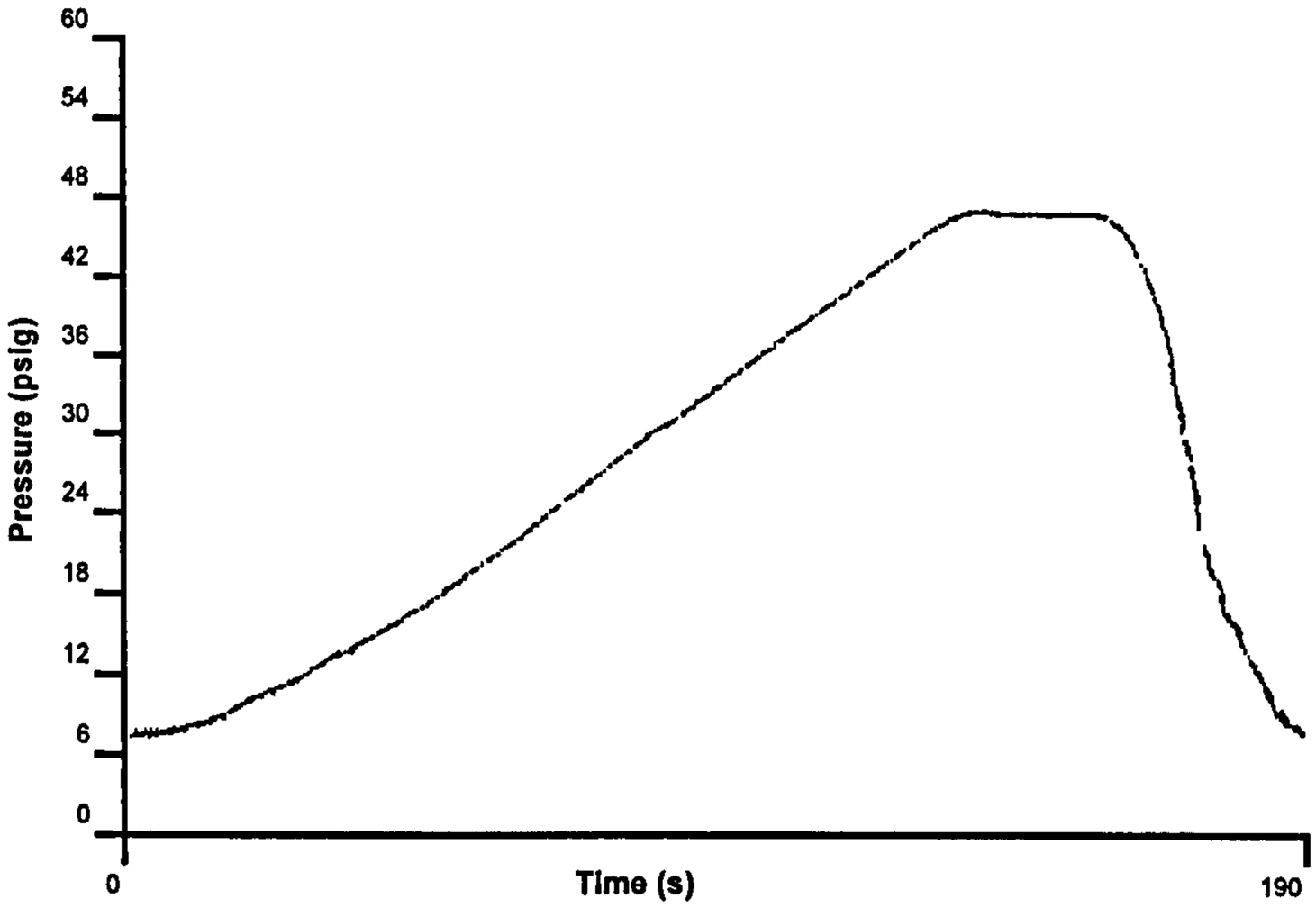

Figure 2.5 Free hanging catenary riser, SS1 trace[17]

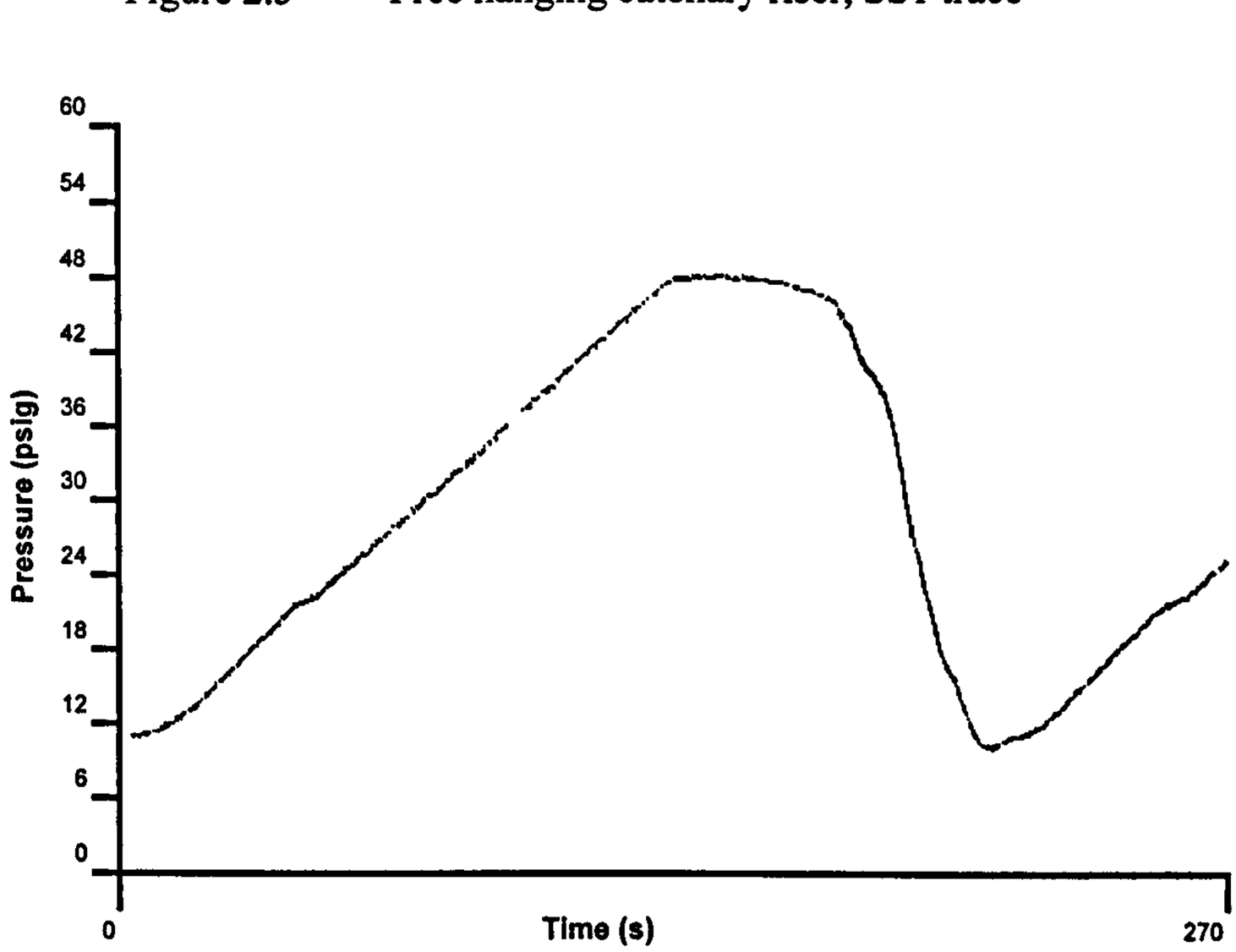

Figure 2.6 Lazy 'S' riser, SS1t trace[17]

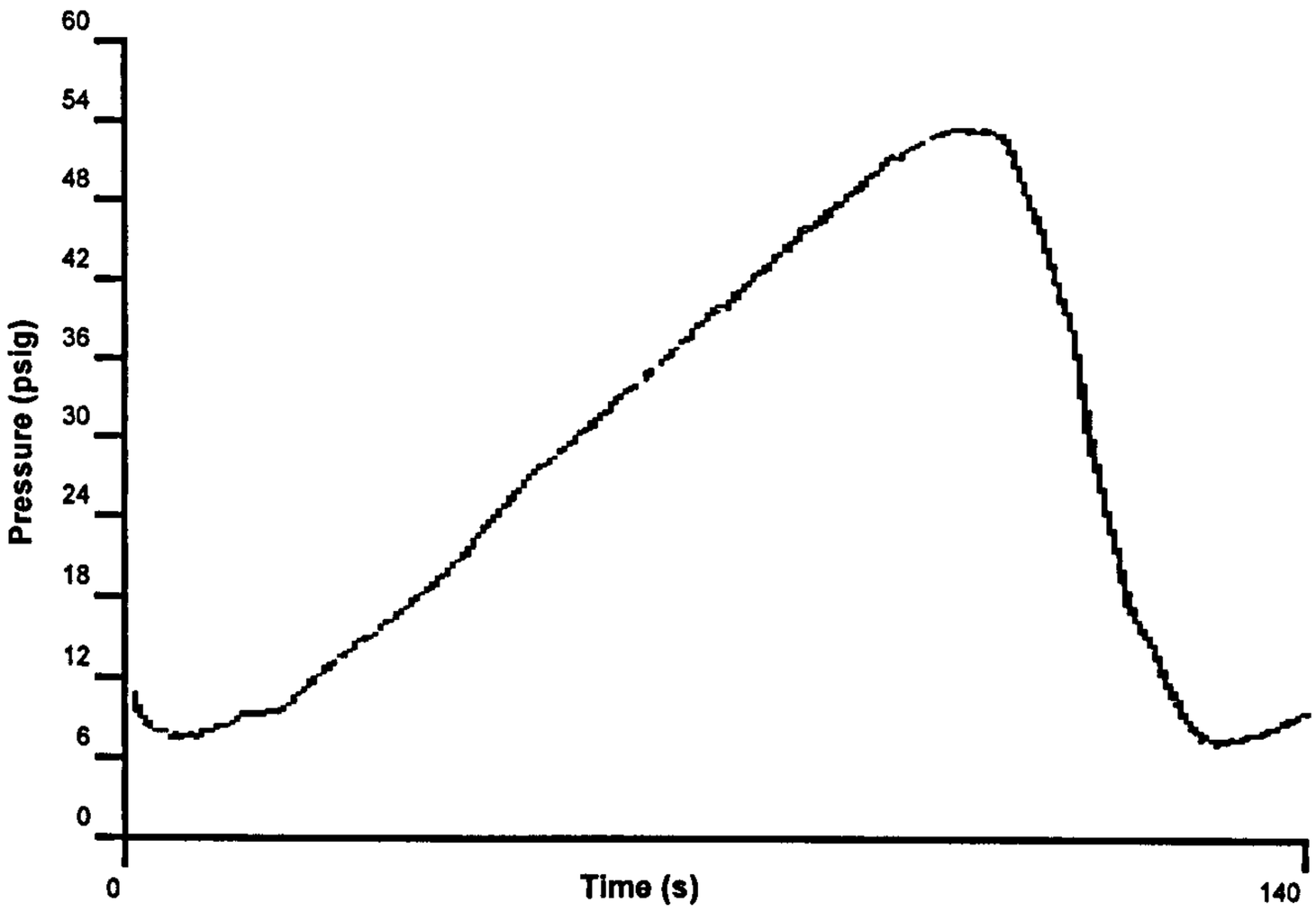

Figure 2.7 Lazy 'S' riser, SS1b trace[17]

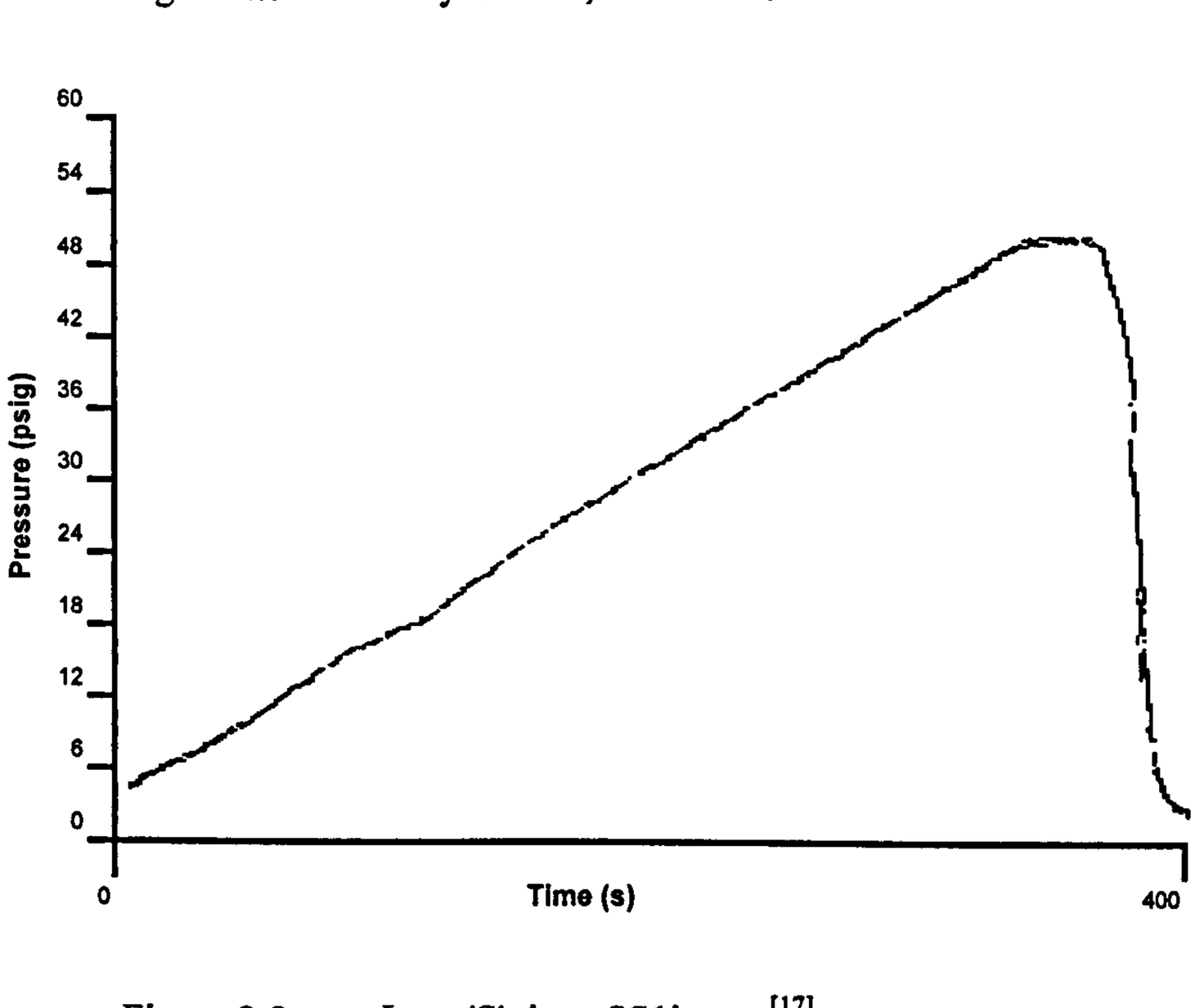

Figure 2.8 Lazy 'S' riser, SS1i trace[17]

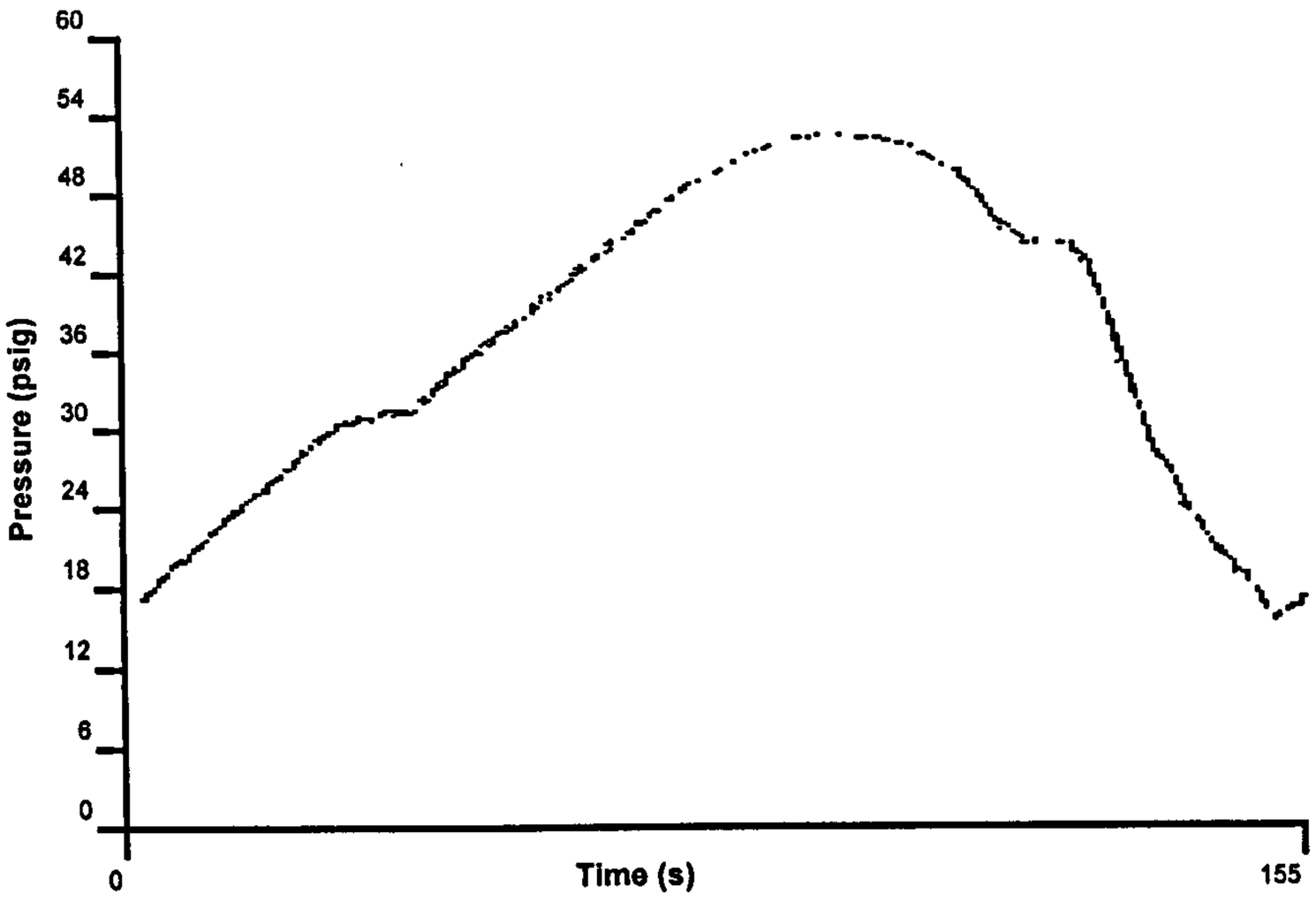

Figure 2.9 Lazy 'S' riser, SS2 trace[17]

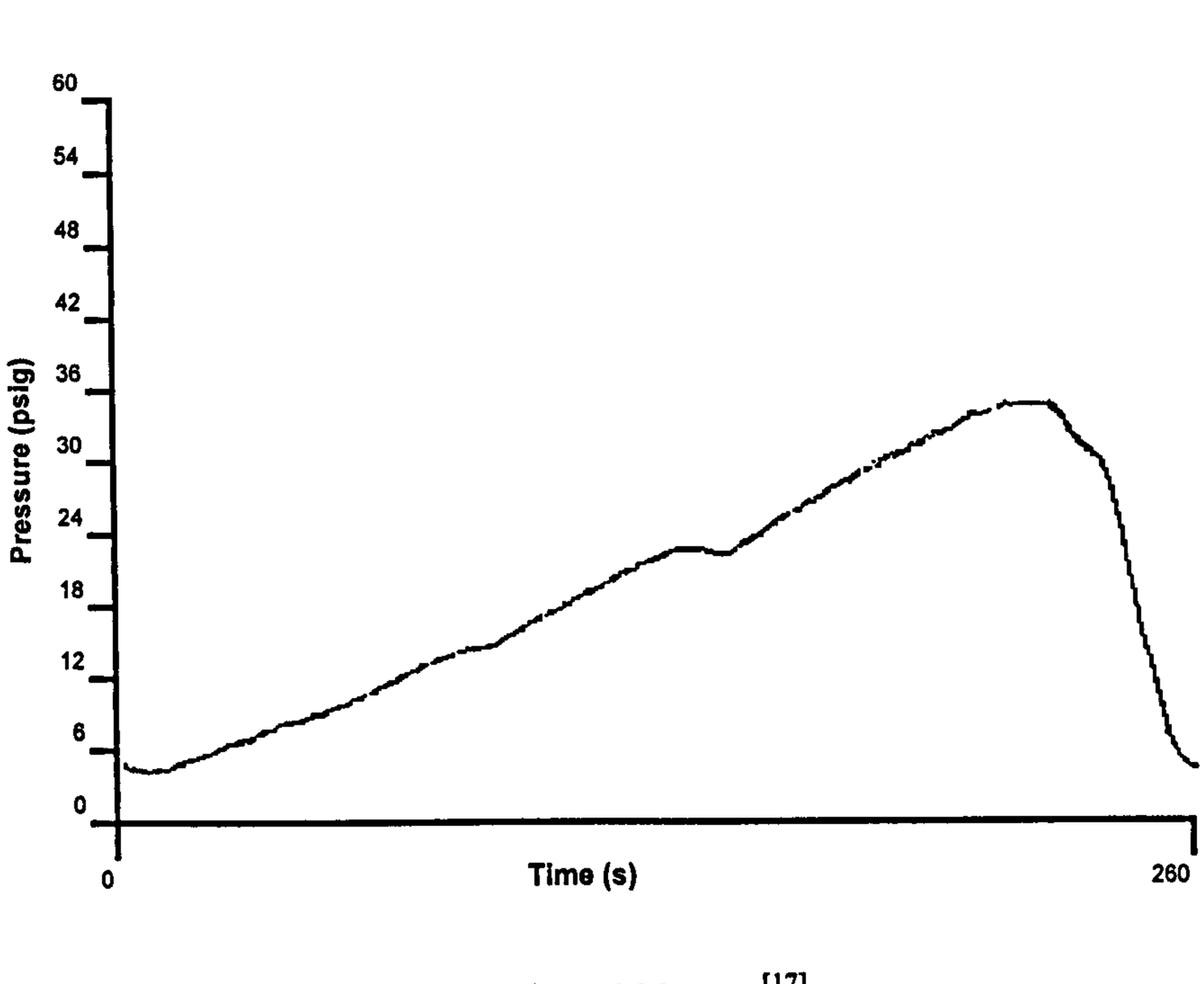

Figure 2.10 Lazy 'S' riser, SS3 trace[17]

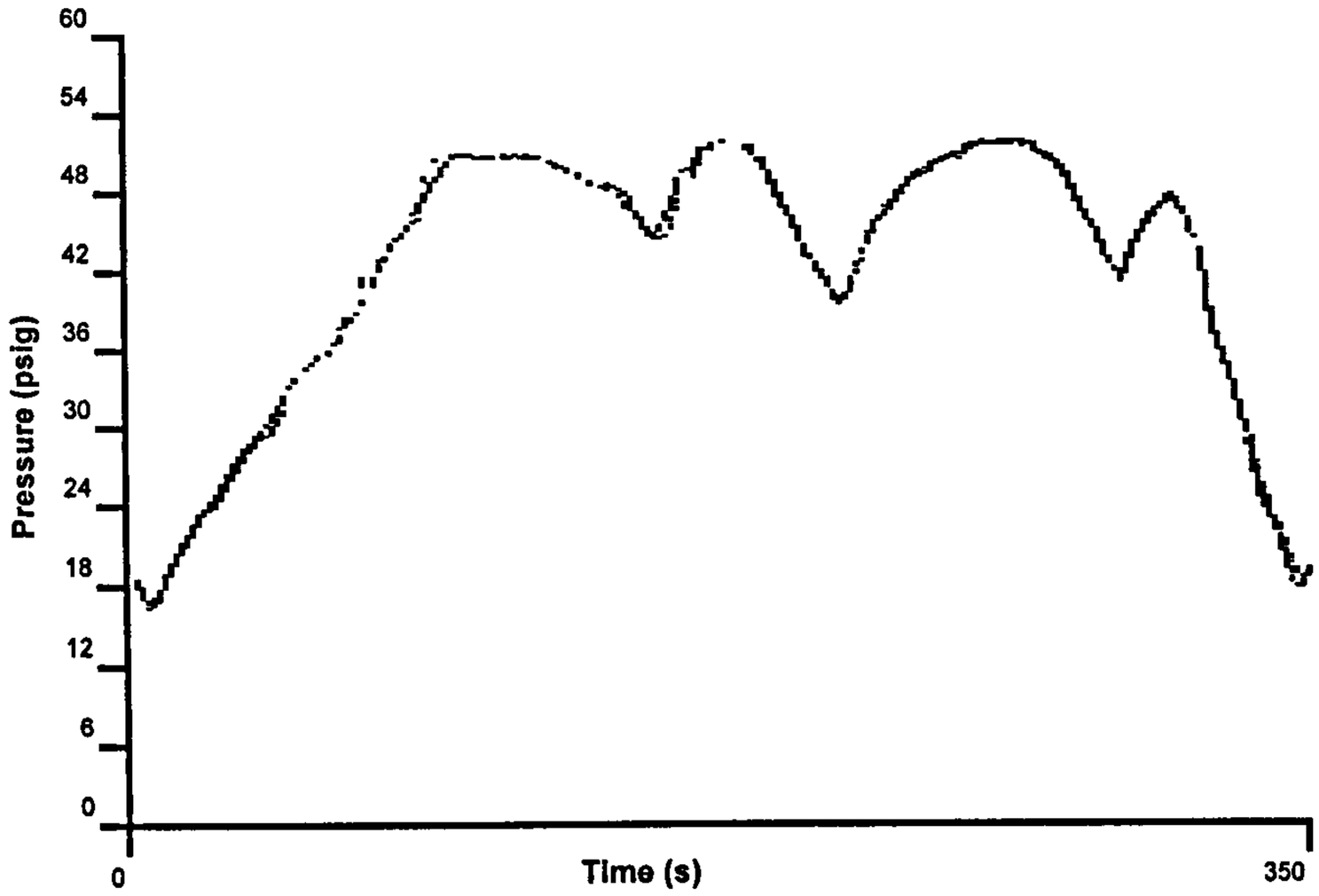

Figure 2.11 Lazy 'S' riser, SS4 trace[17]

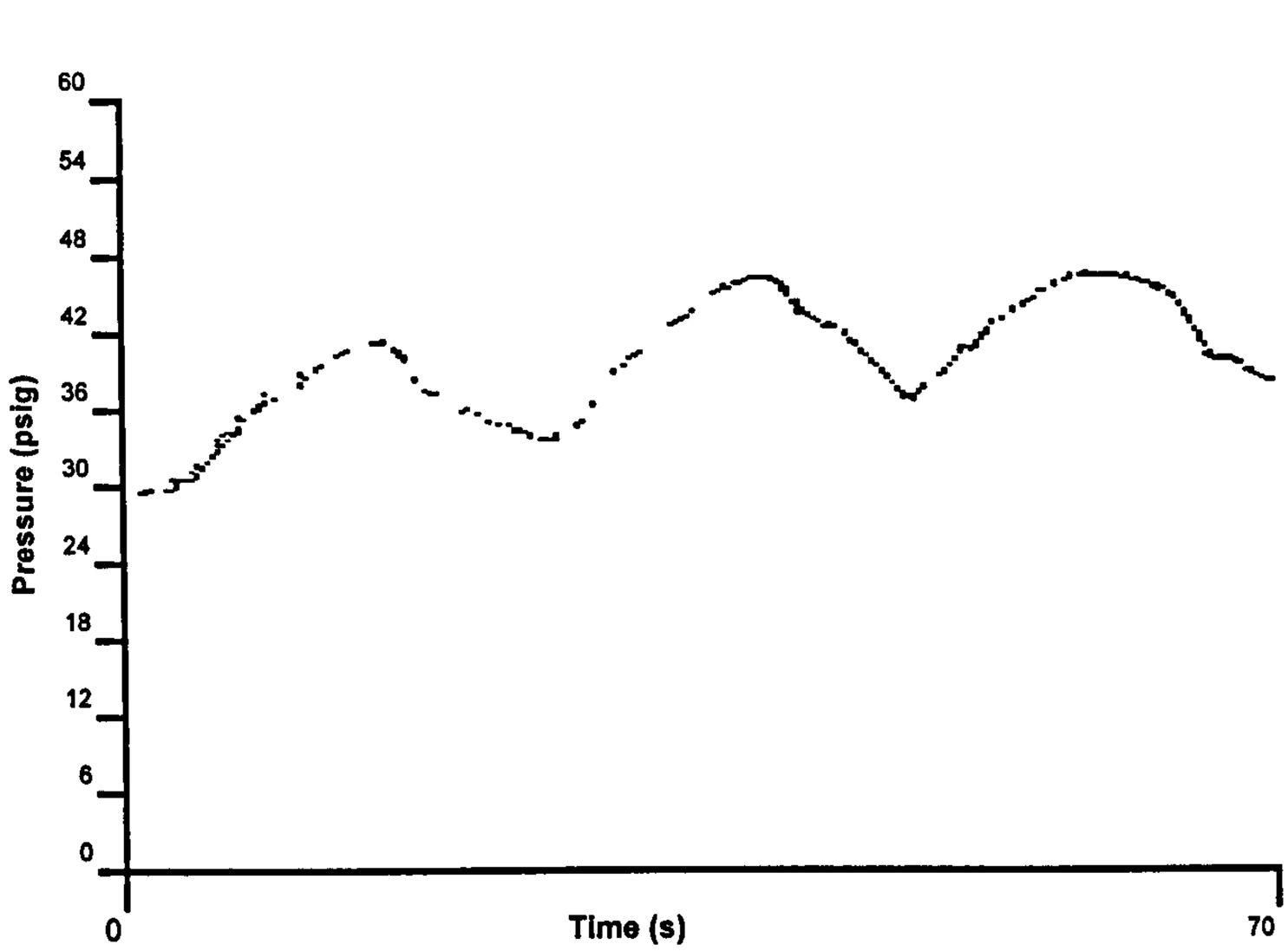

Figure 2.12 Lazy 'S' riser, OSC trace[17]

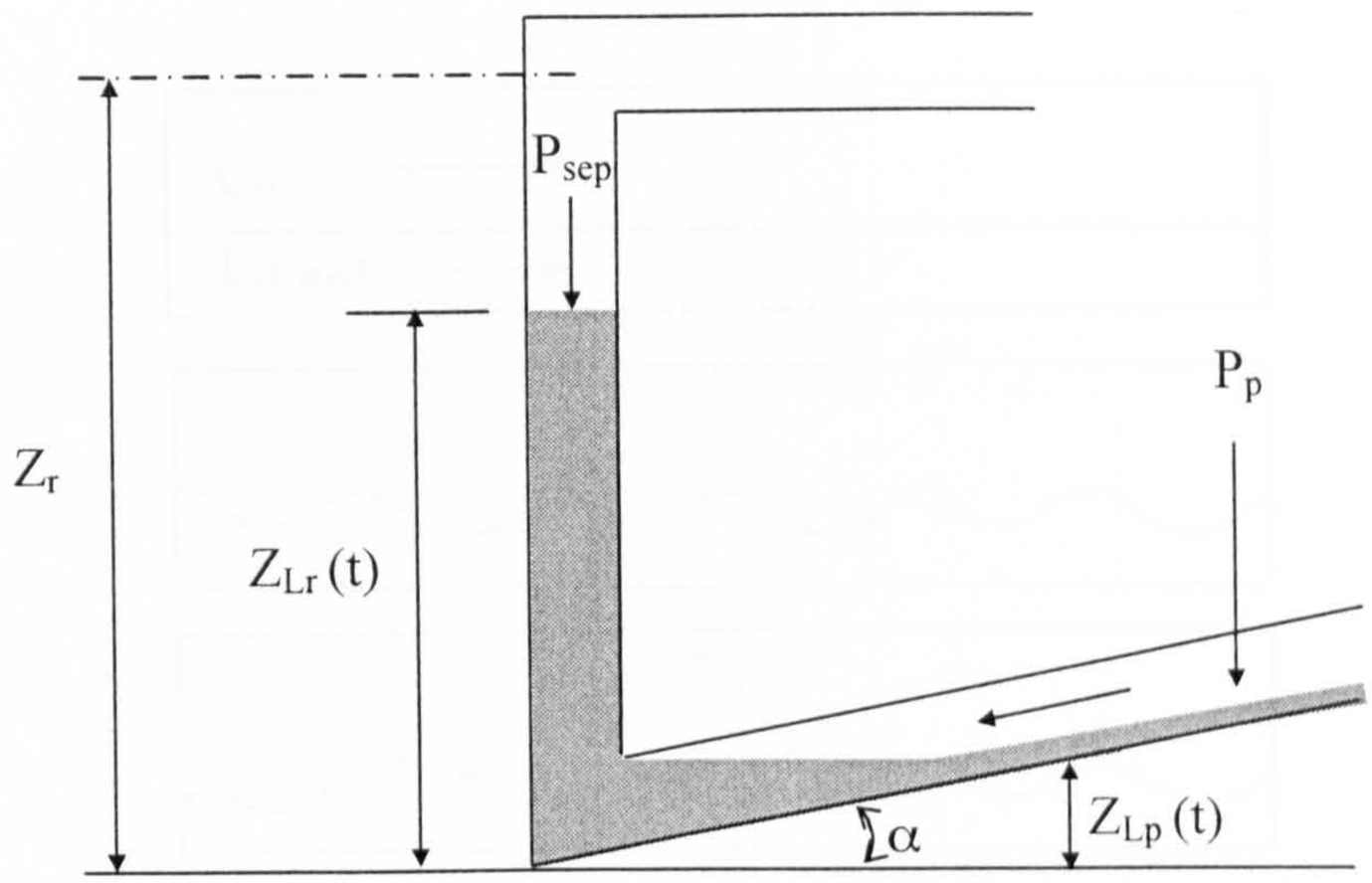

Figure 2.13 The hydrodynamic model for severe slugging[13]

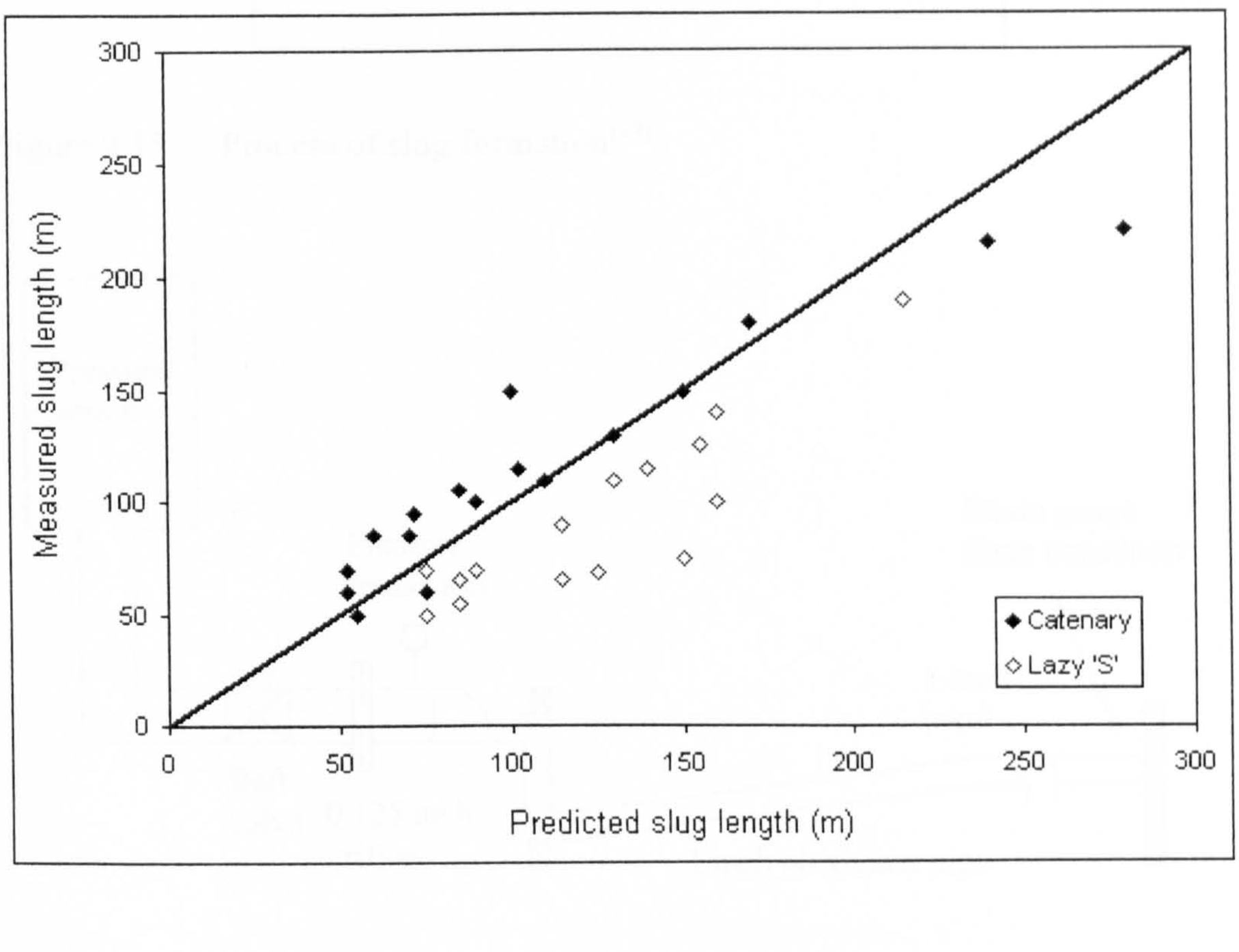

Figure 2.14 Measured versus calculated slug length[22]

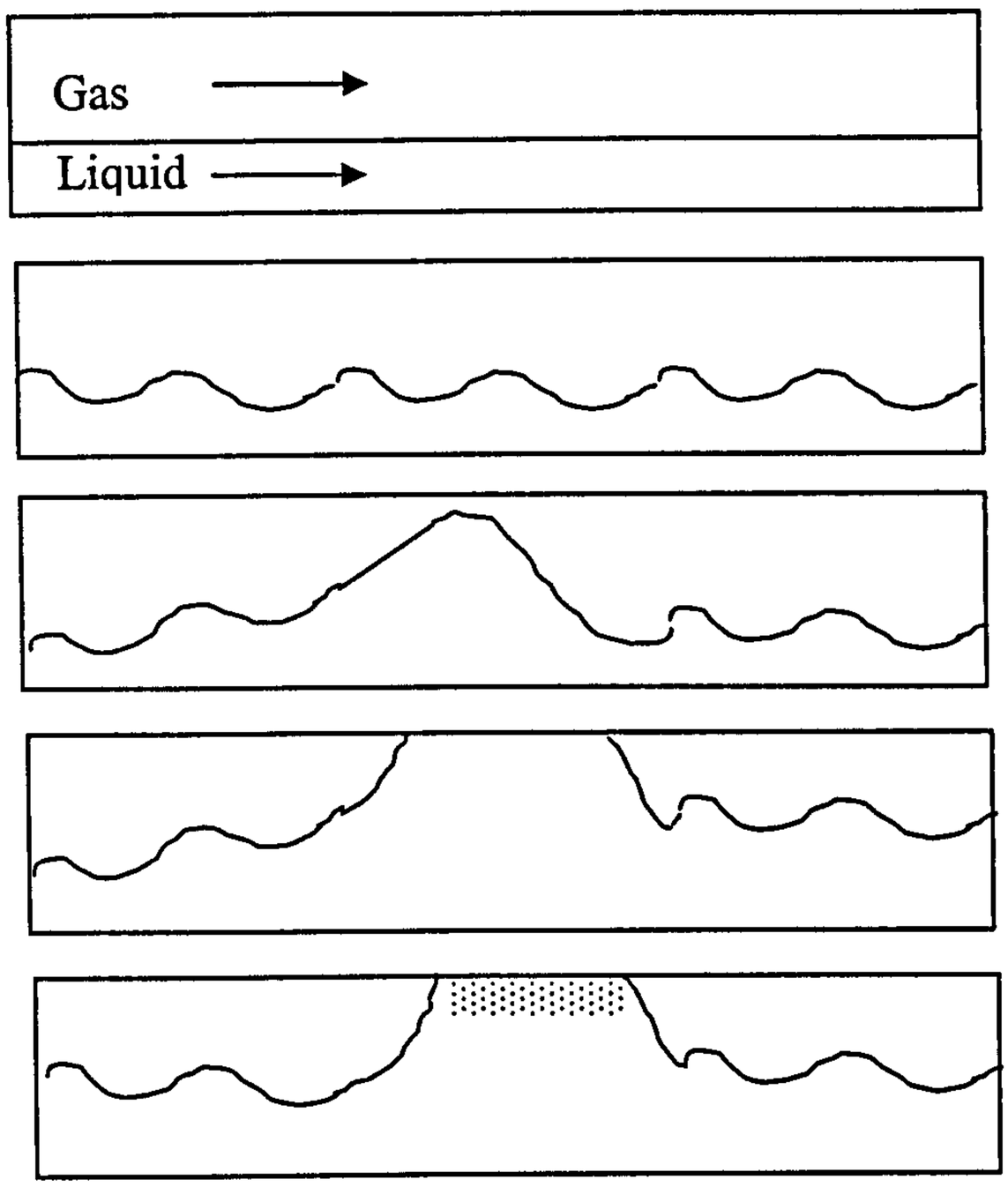

Figure 2.15 Process of slug formation[24]

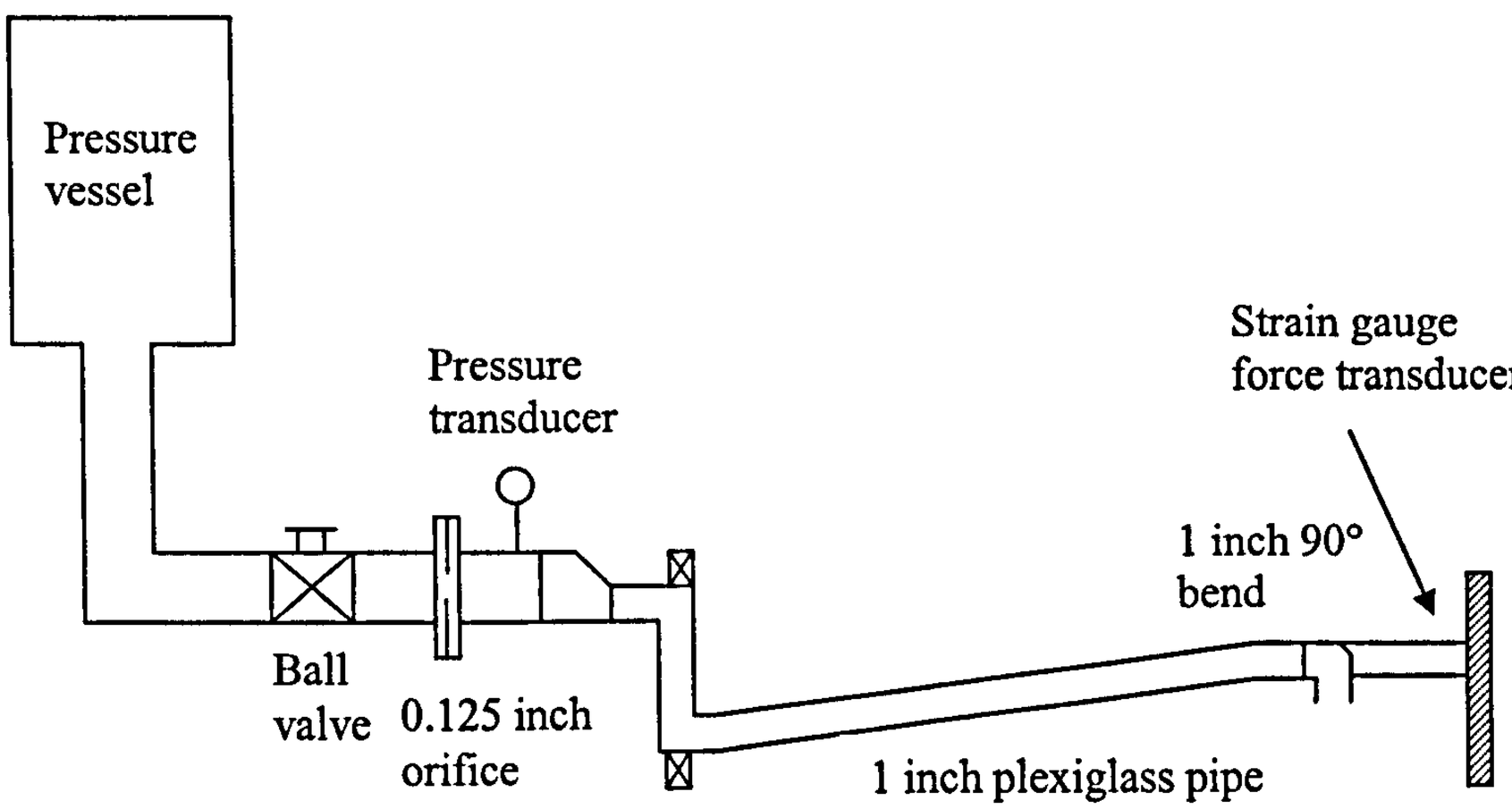

Figure 2.16 Schematic diagram of the apparatus to measure slug forces at a bend[25]

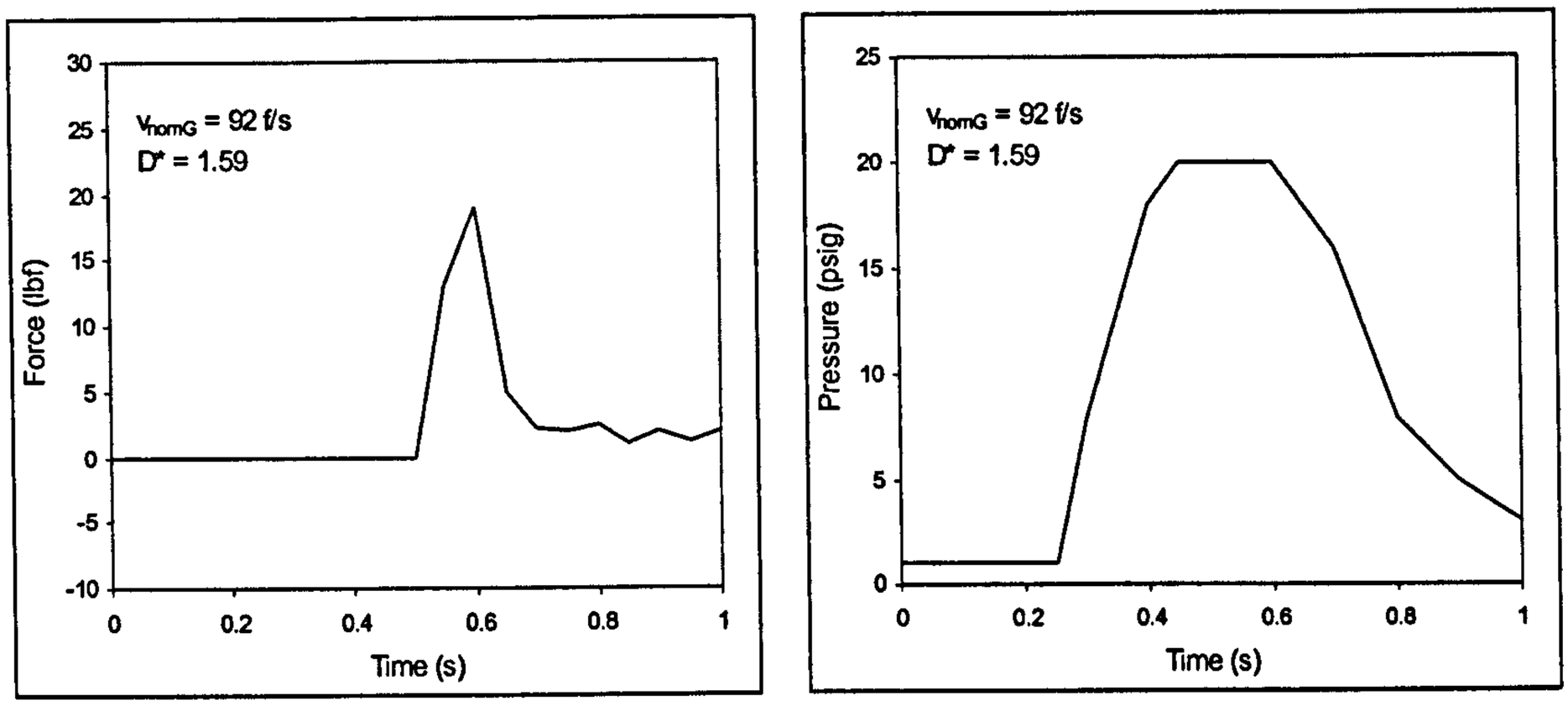

Figure 2.17 Force-time and pressure-time traces as a slug passes around a bend[25]

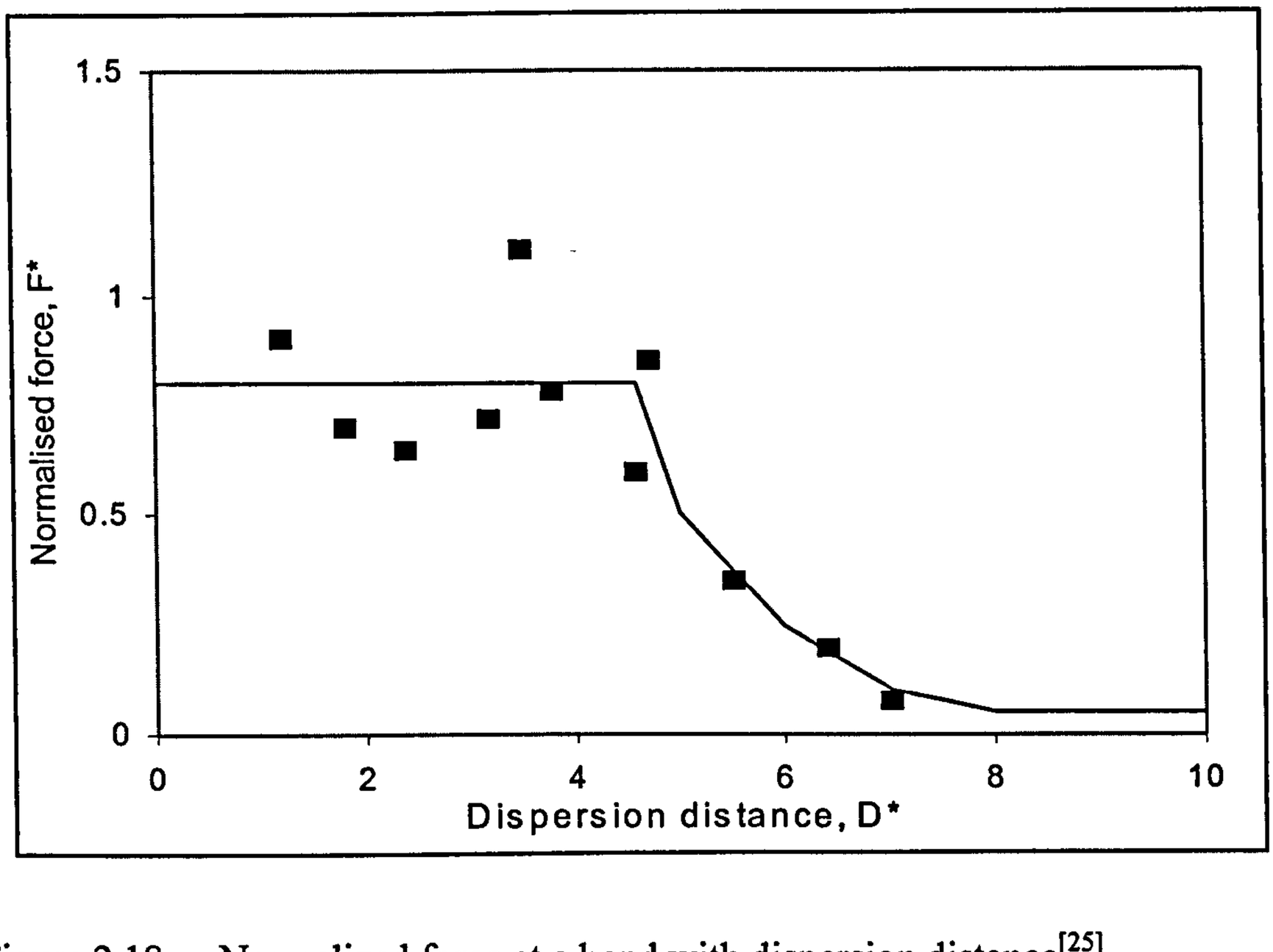

Figure 2.18 Normalized force at a bend with dispersion distance[25]

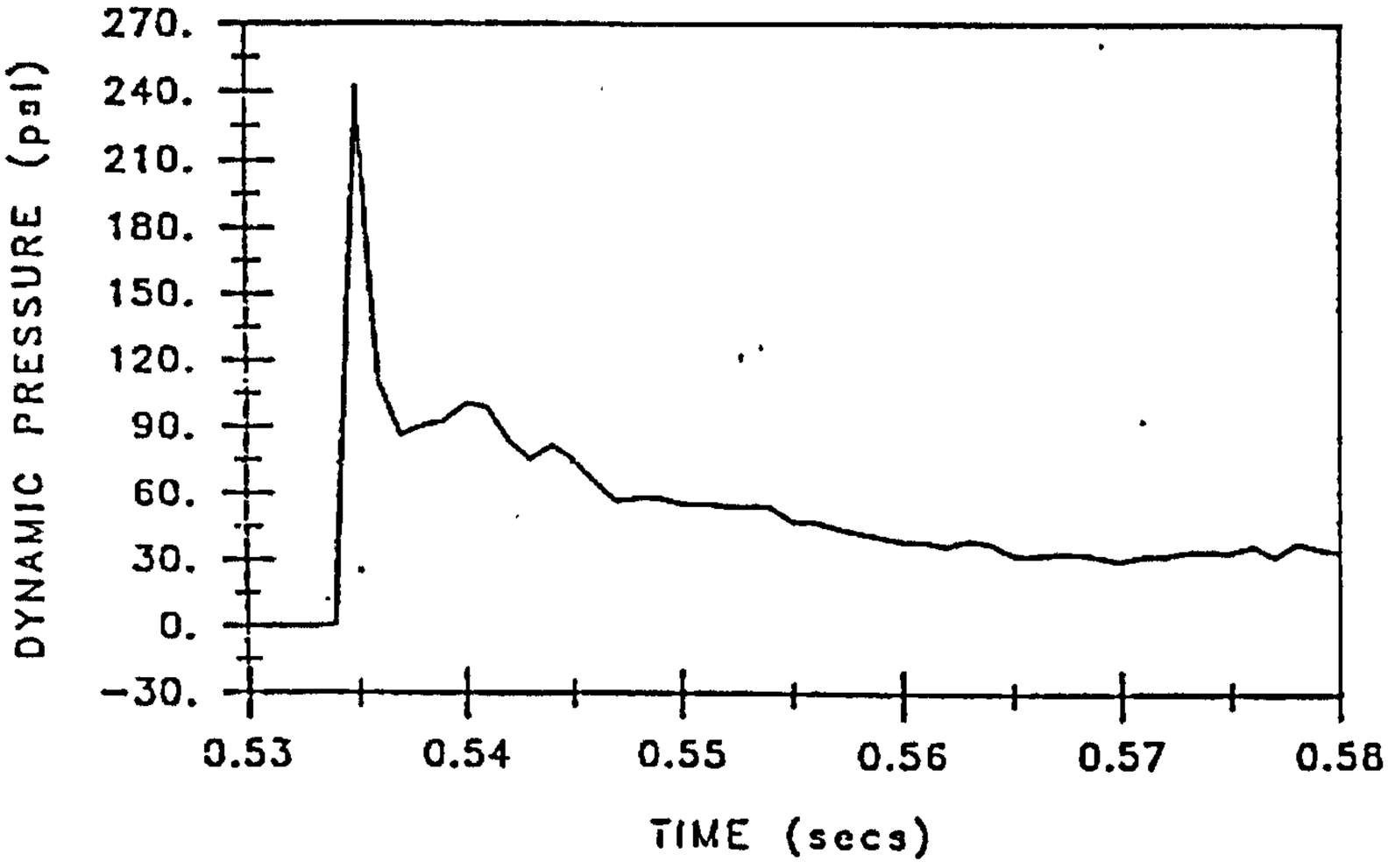

Figure 2.19 Experimental pressure-time trace at an elbow, L_s=1.52m[27]

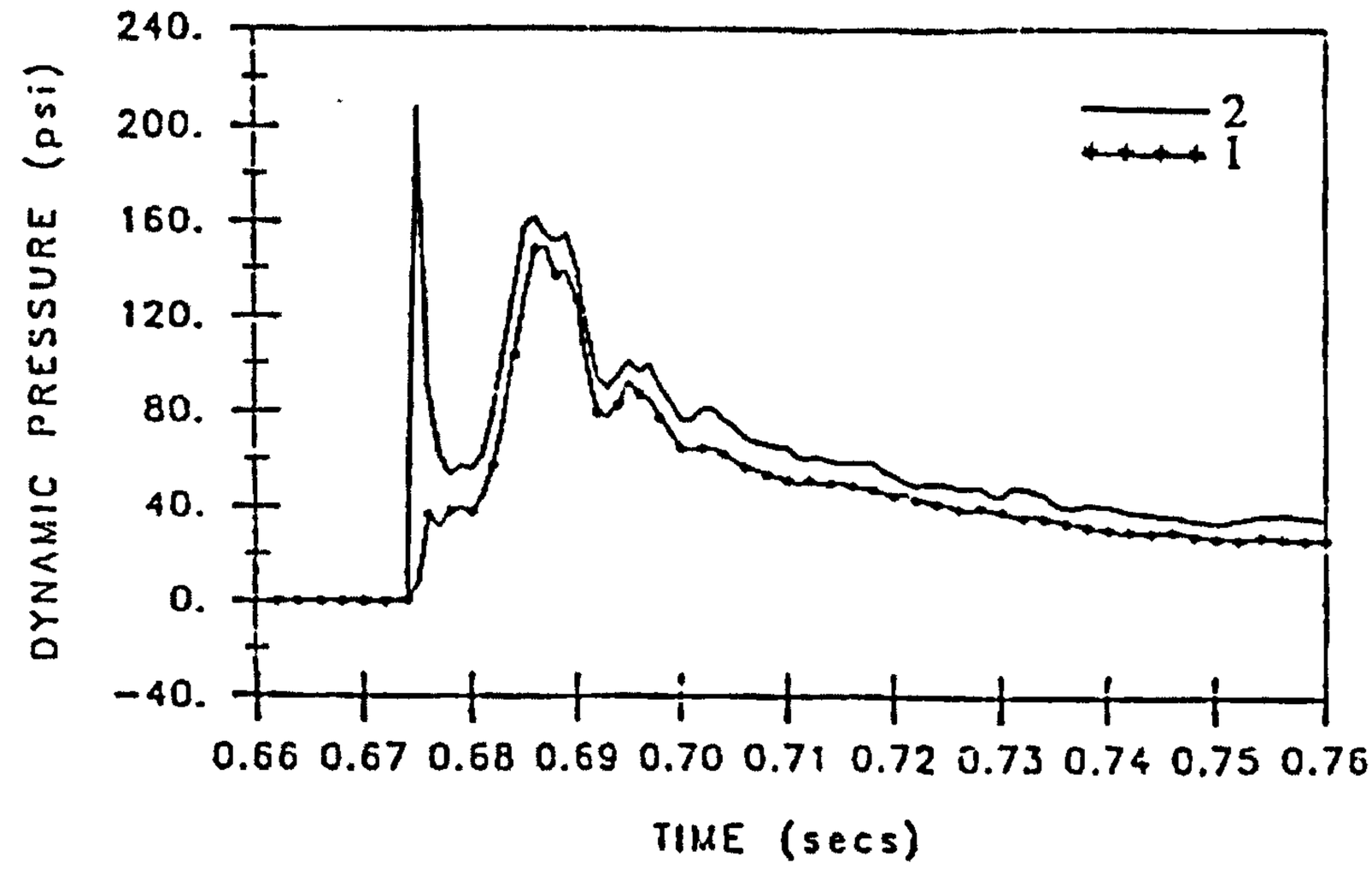

Figure 2.20 Experimental pressure-time trace at an elbow, L_s=3.35m[27]

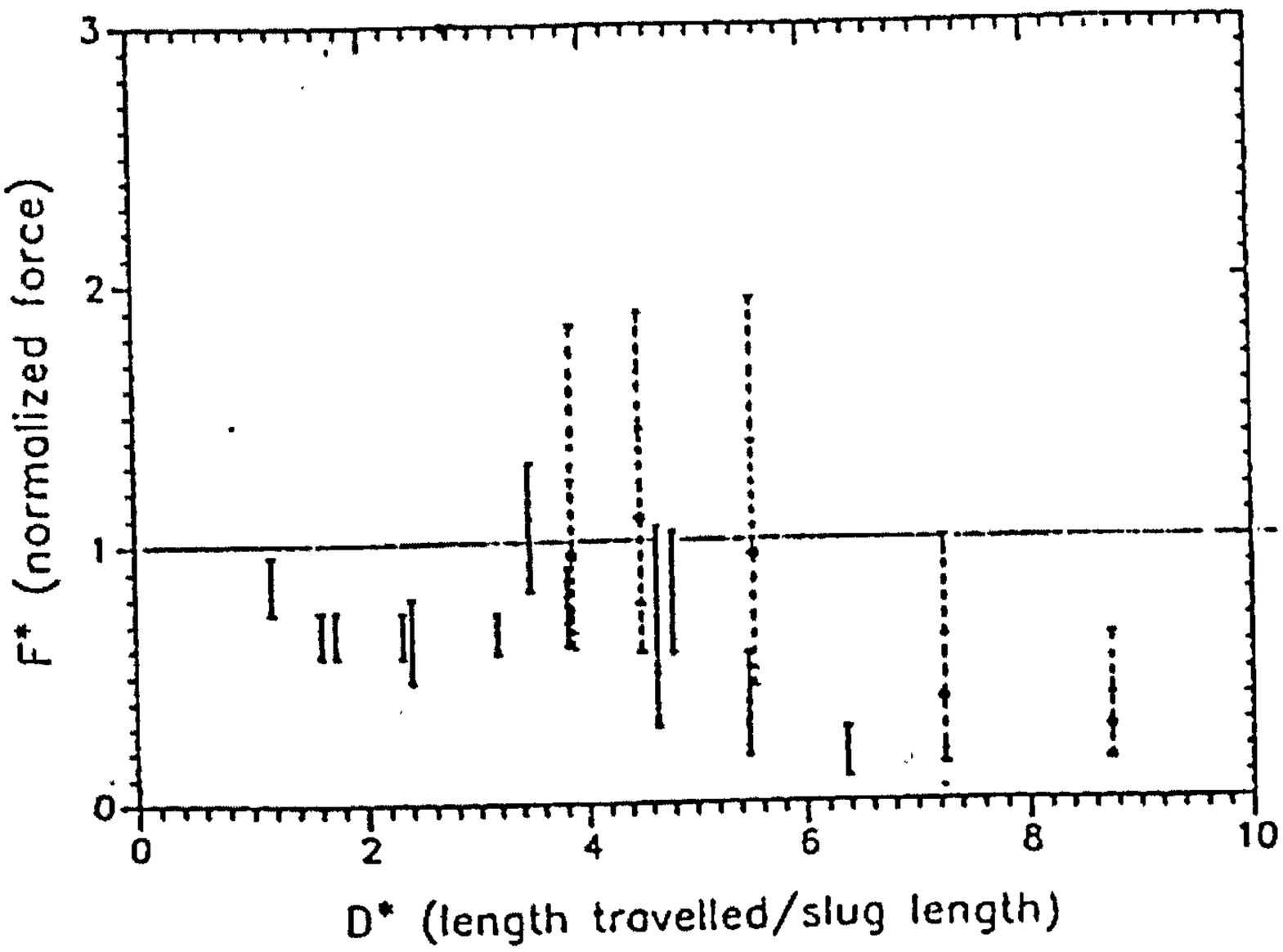

Figure 2.21 Normalized force at an elbow versus dispersion distance[27]

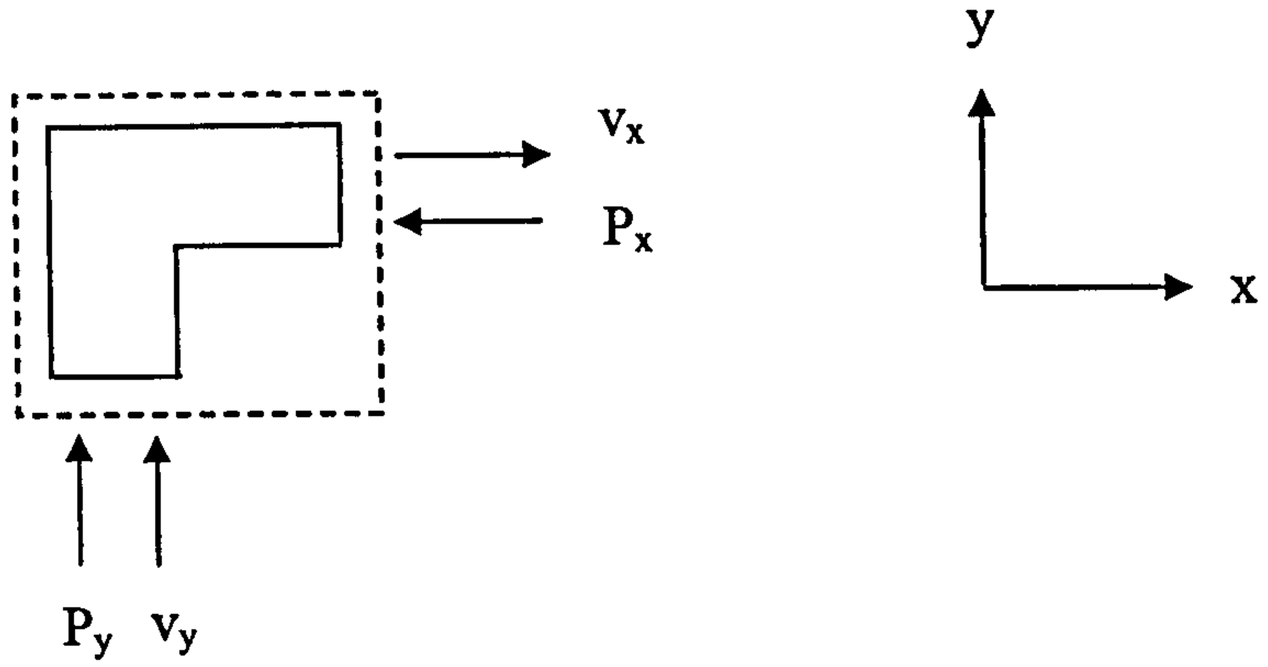

Figure 2.22 Control volume analysis around an elbow[28]

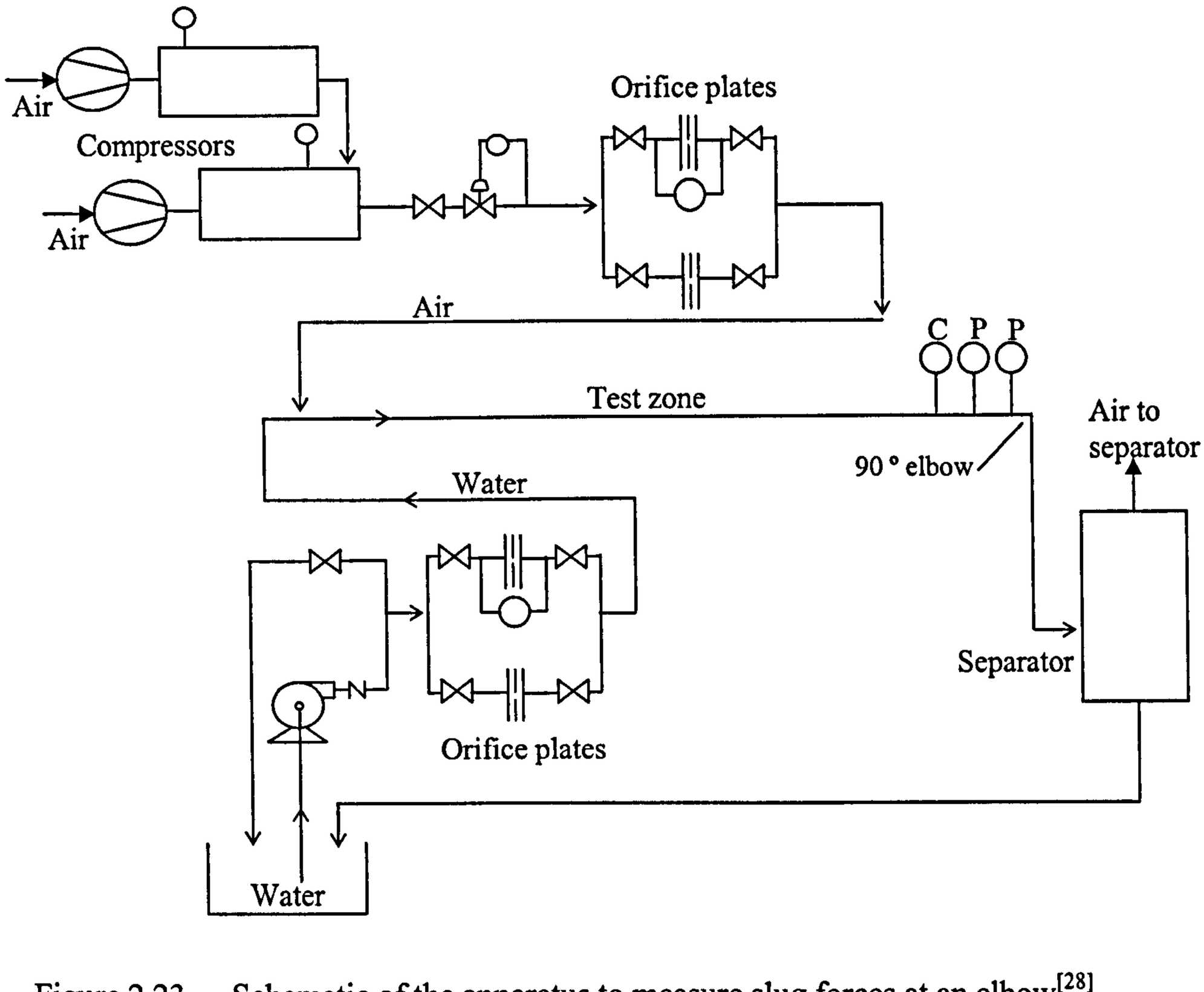

Figure 2.23 Schematic of the apparatus to measure slug forces at an elbow[28]

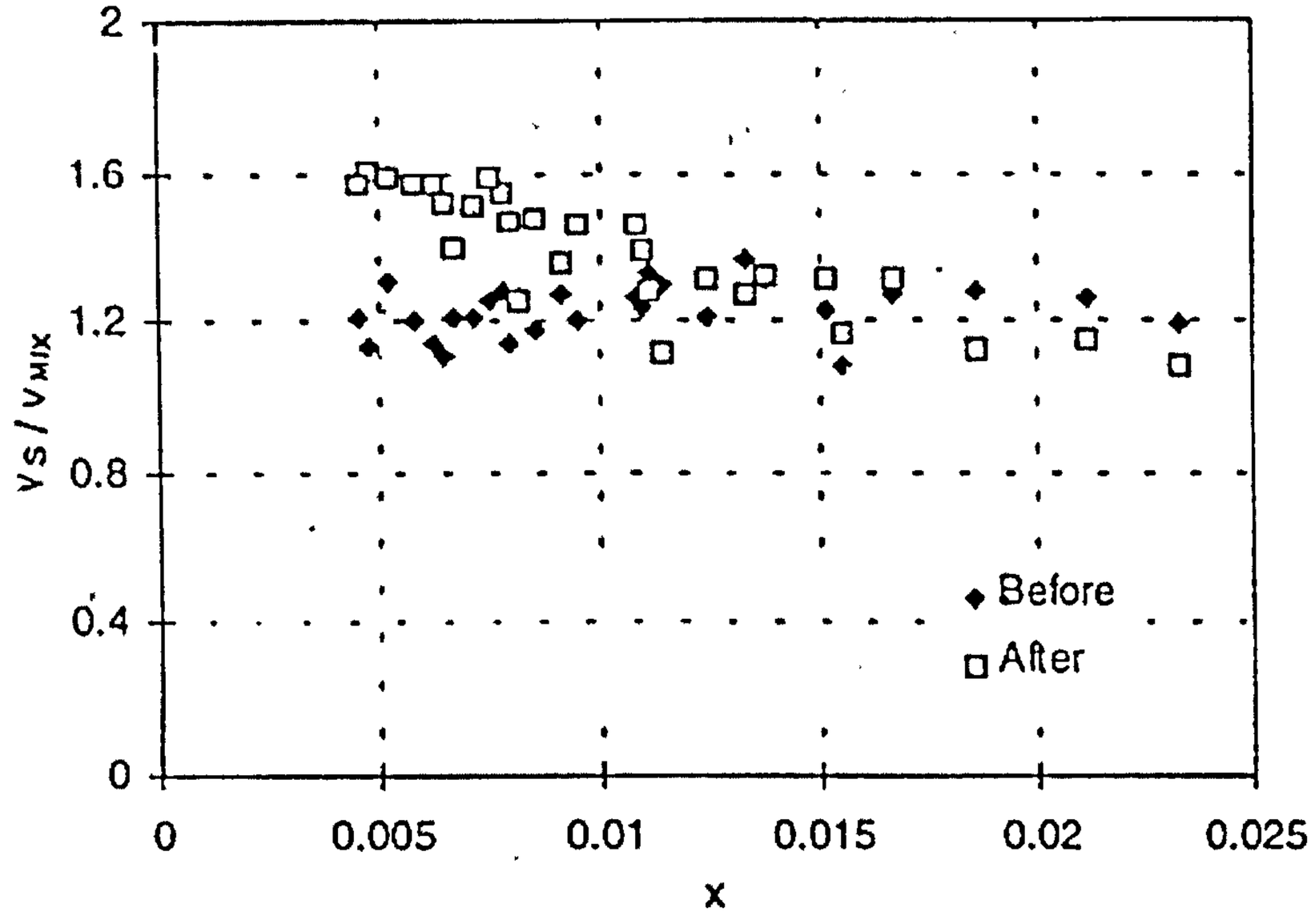

Figure 2.24 Experimental slug velocity before and after elbow[28]

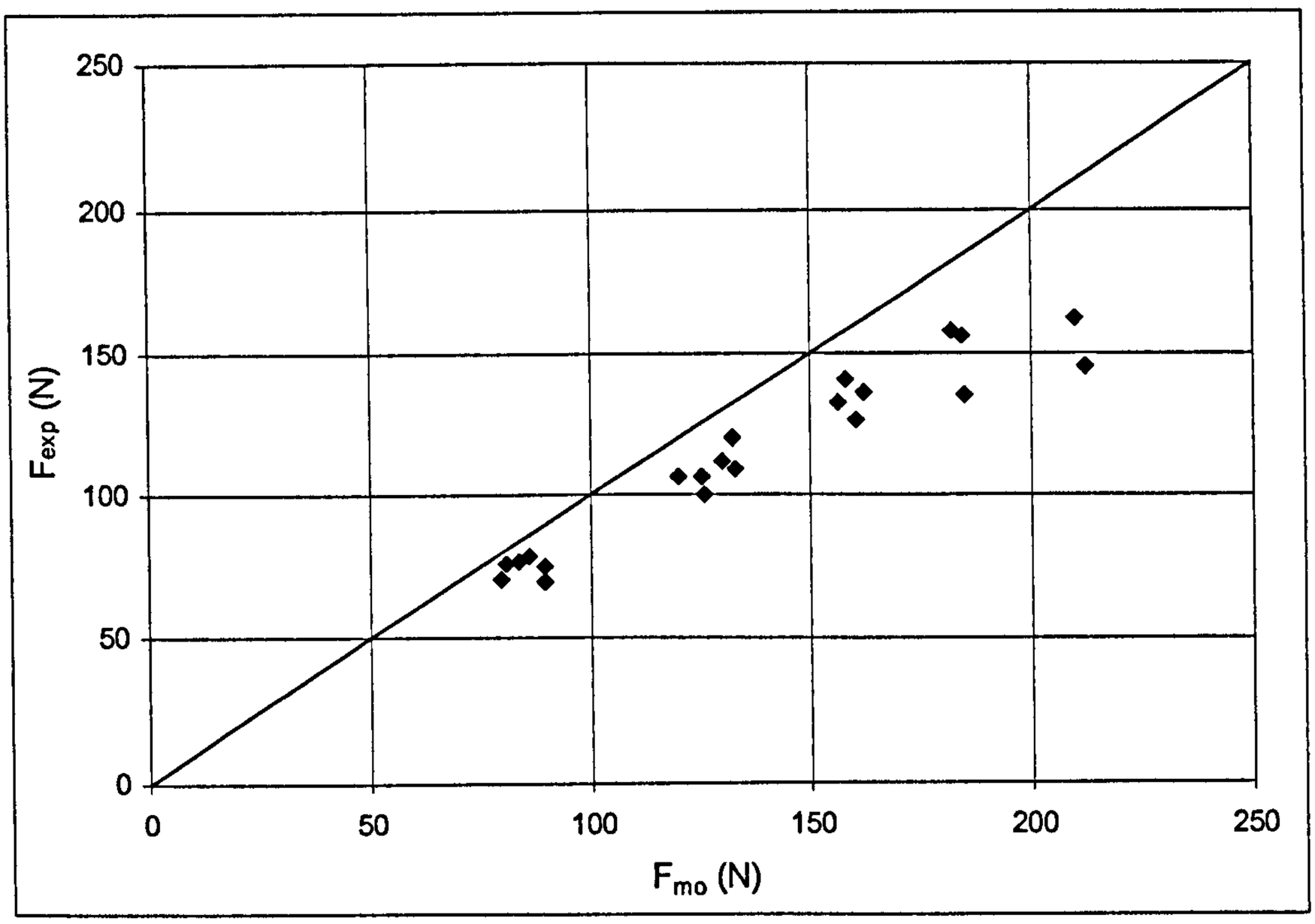

Figure 2.25 Comparison of calculated force with experimental data[28]

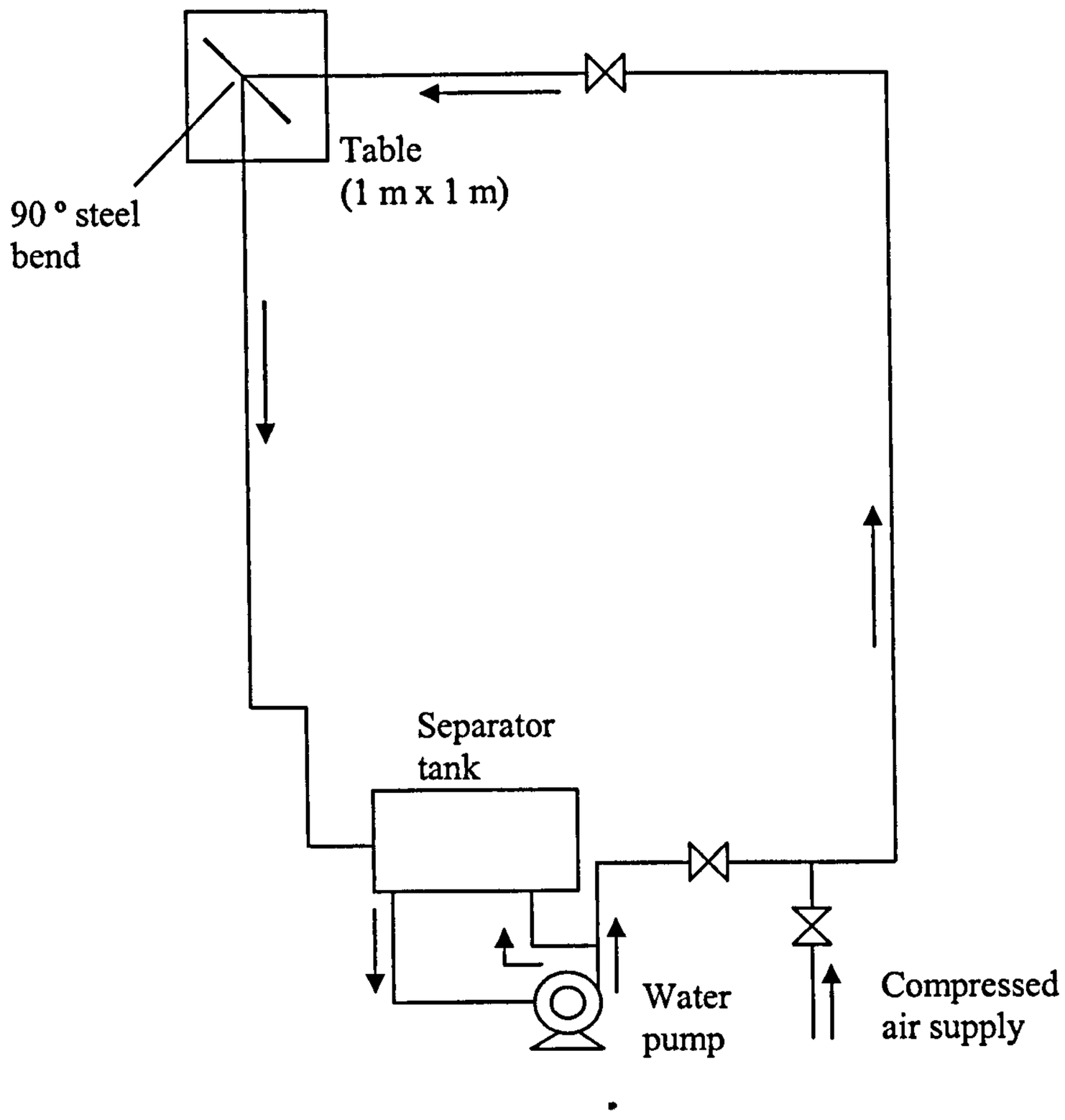

Figure 2.26 Schematic diagram of the apparatus to measure slug forces at a bend[29]

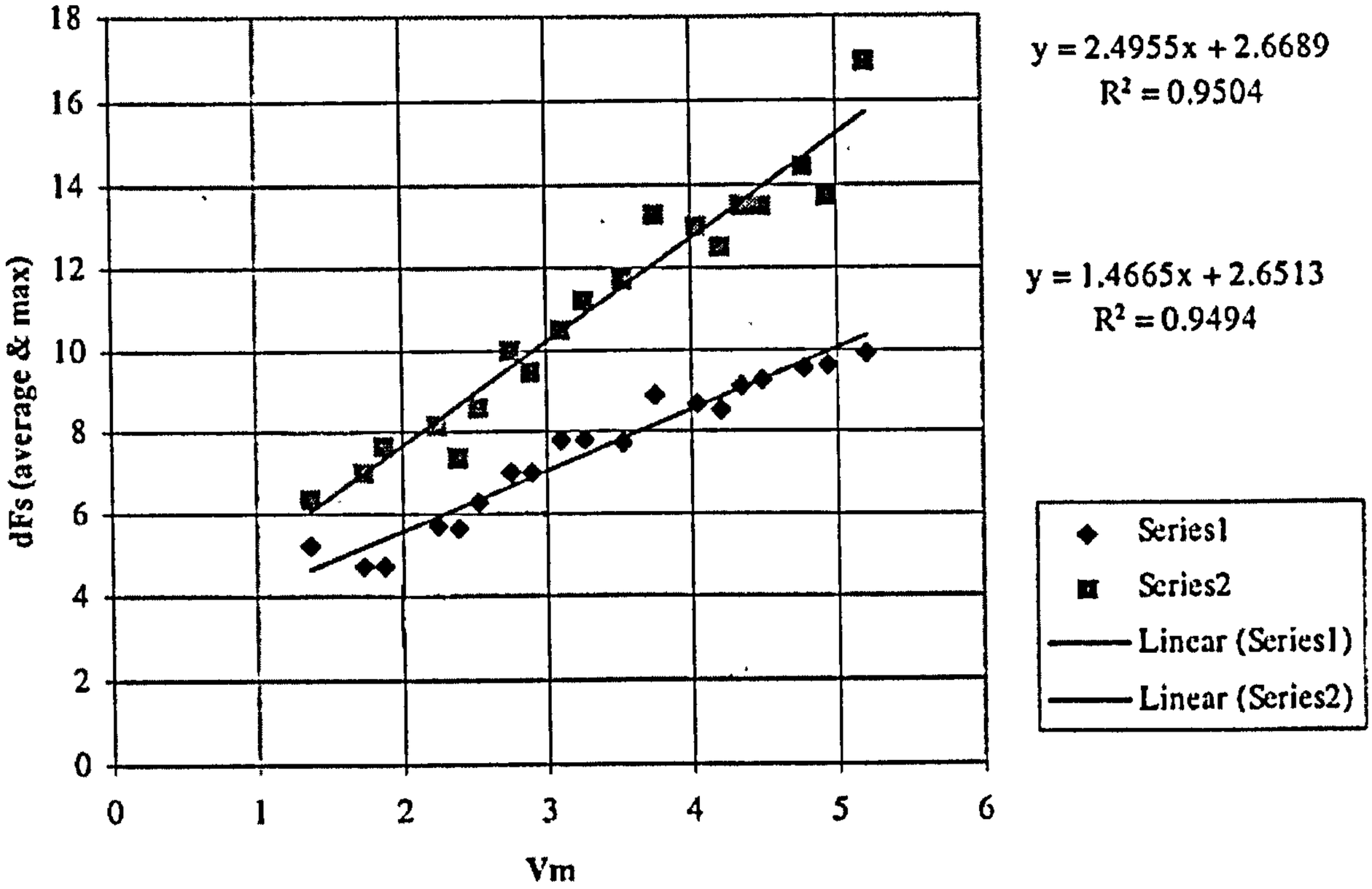

Figure 2.27 Relationship between average and maximum peak force with mixture velocity[29]

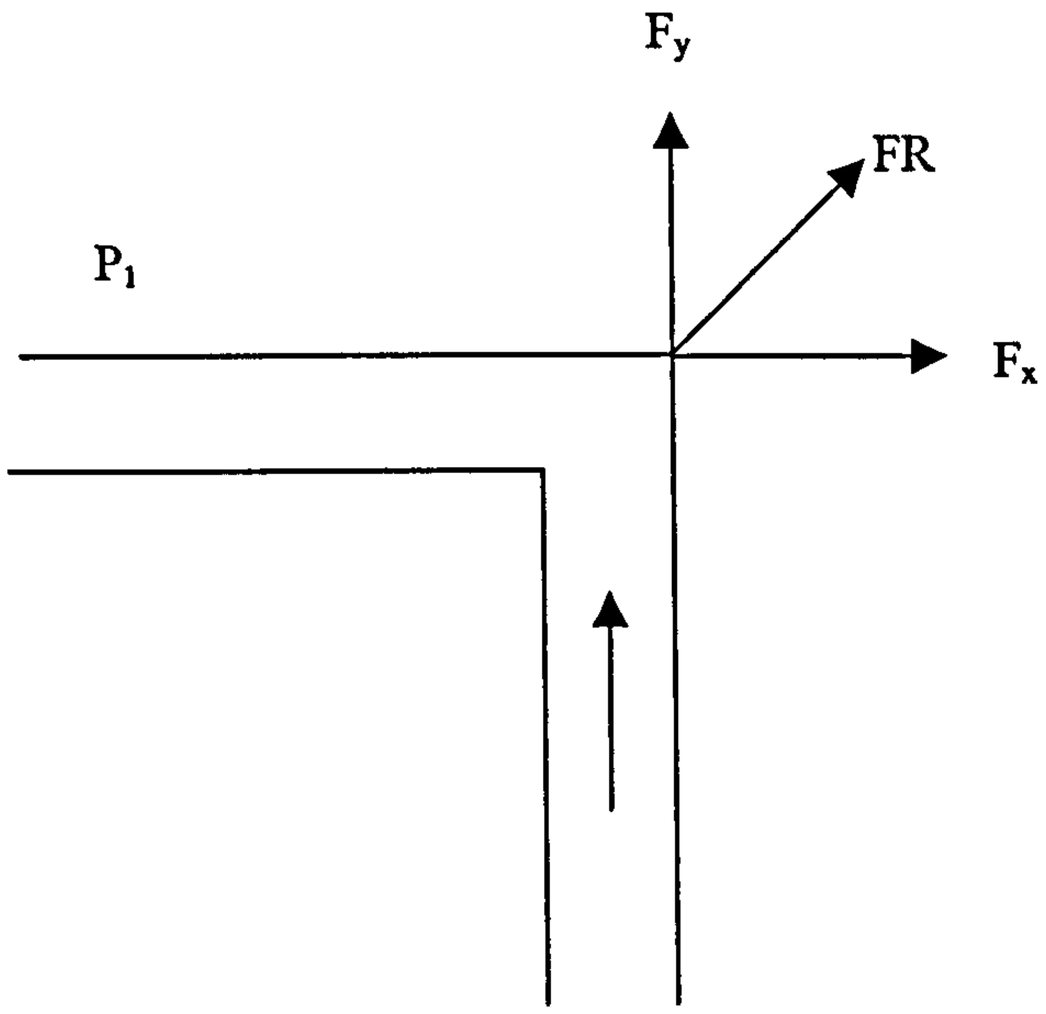

Figure 2.28 Schematic diagram of the forces on a bend[30]

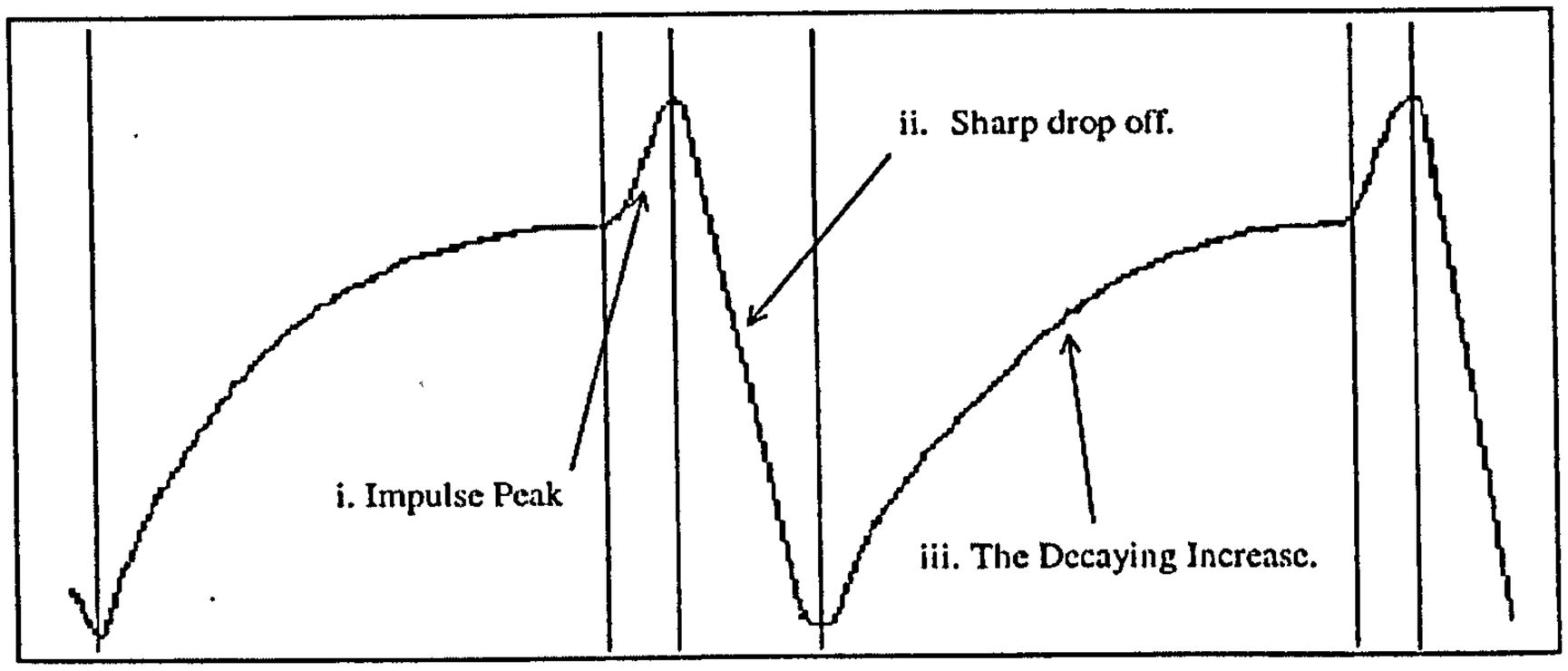

Figure 2.29 Schematic diagram of force-time trace[30]

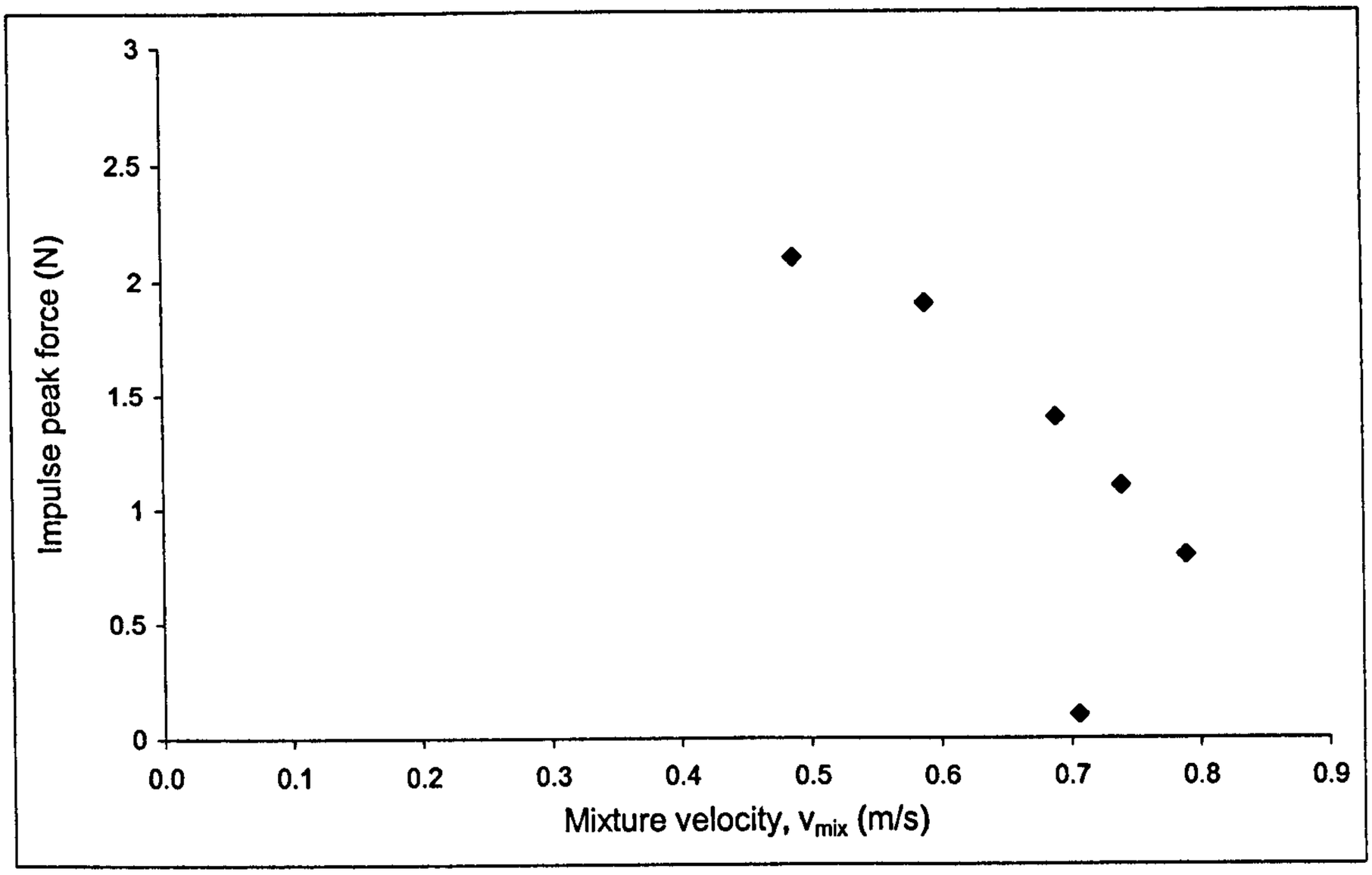

Figure 2.30 Graph of impulse peak force versus mixture velocity[30]

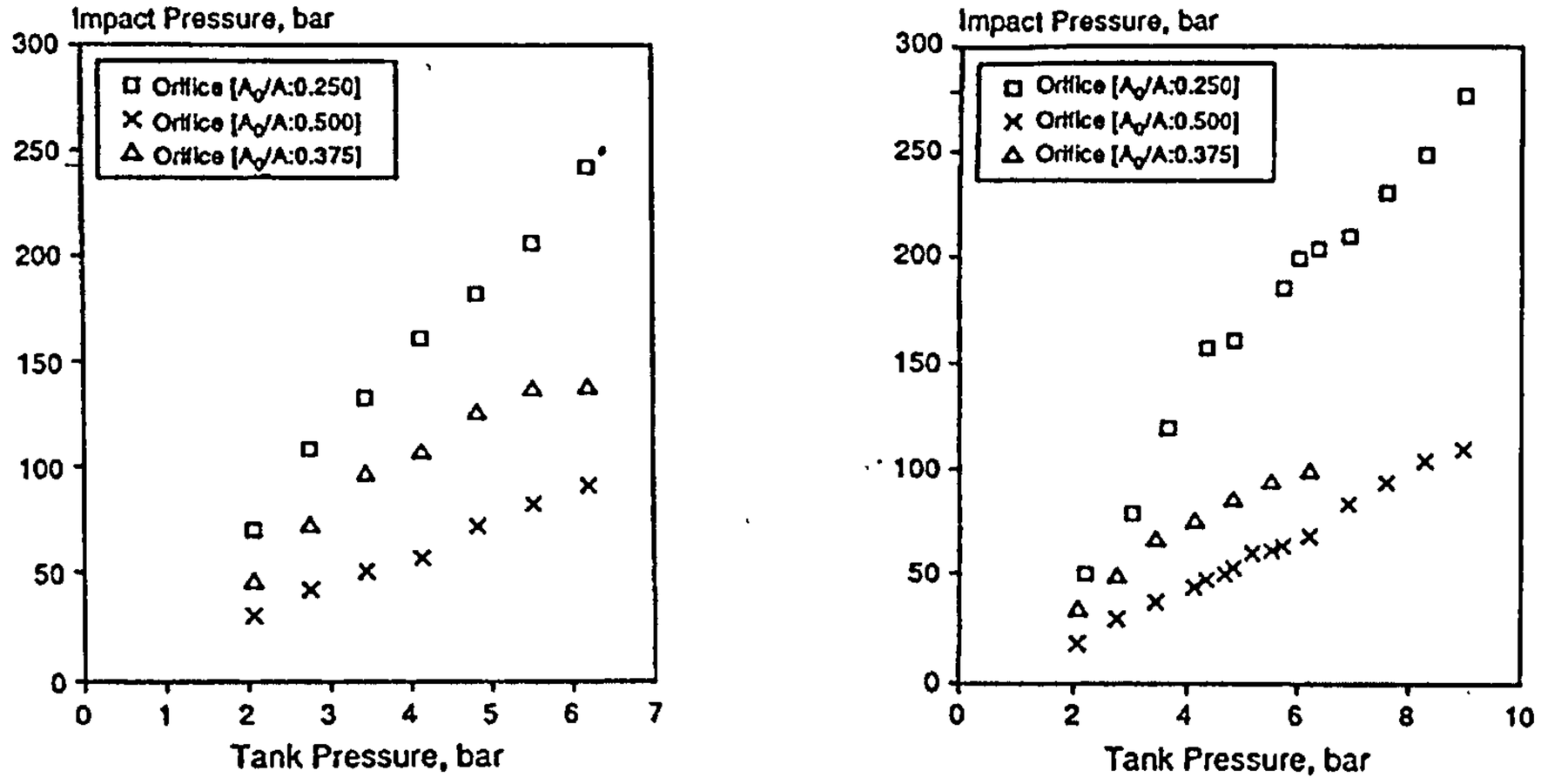

(i) 2.16m slug (ii) 3.15m slug

Figure 2.31 Maximum impact pressures on orifices by slugs of different lengths[31]

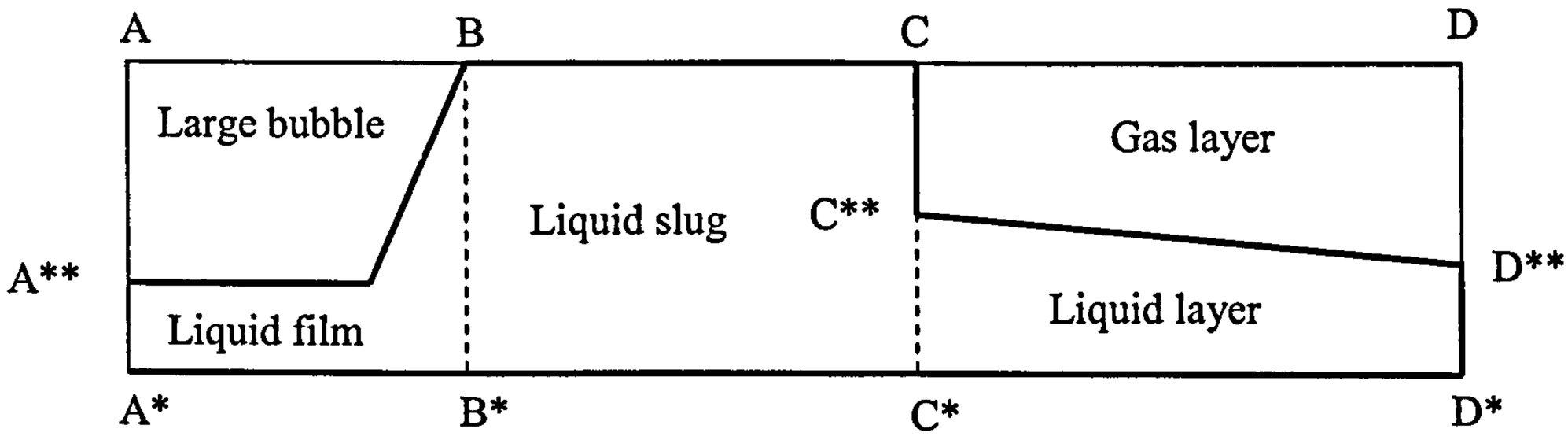

Figure 2.32 Model of transient slug flow[32]

CHAPTER 3 – LAZY 'S' RISER TEST FACILITY

3.1 Introduction

This Chapter describes the lazy 'S' riser test facility used to determine severe slugging flow characteristics and to investigate the forces on a bend during each stage of the severe slugging cycle. The Chapter describes the flow loop, instrumentation and the procedures used to calibrate and commission the instrumentation, and the data acquisition system. Also detailed, are liquid and gas mass balances on the separator.

The literature review in Chapter 2, highlighted that the majority of the previous slug loading work, investigated the resultant force on a bend, in a horizontal pipeline. For this test work, it was decided to look at the vertical and horizontal forces on the bend, as well as the resultant force. Based on the design of the instrumentation used in the slug loading investigations by BP[29], these horizontal and vertical forces on the bend were measured using a strain-gauged strut arrangement (this is described in Section 3.3.1)

All the single phase and two phase test work was carried out using this test facility. The test fluids used were air and water, but the test facility was capable of delivering a three phase mixture, of air, water and oil, into the flow loop.

3.2 Flow Loop

Referring to Figure 3.1, a schematic of the process equipment and pipeline-riser used in the test work, water was supplied from an $8m^3$ storage tank, which also acted as a receiver for the water returning from the flow loop. Water was delivered into the flow loop using a positive displacement pump, P3 (Worthington Simpson, Serial No. F9889T), which had a $35m^3/hr$ capacity and a maximum discharge pressure of 7 bar. The water was then metered using one of two electromagnetic flowmeters; FL1 (Altometer, Serial No. 881916A2), which had a range of 0-1.67l/s and FL2 (Magflo, Plant No. 10437), which had a range of 0-12.5l/s.

Air was supplied from a reciprocating compressor that had a maximum delivery capacity of $595m^3/hr$. The compressor supplied air into a $2.57m^3$ buffer vessel, which acted as an air receiver and smoothed out any pressure fluctuations from the compressor. Gas flowrates were controlled using a needle valve, VI21, downstream of the buffer vessel. The air then passed into the metering section, where the flowrate was measured using one of two turbine flowmeters; FG1 (Quadrina, Serial No. 11977) and FG2 (Meterflow, Serial No. 21374/79) which had ranges of 0.28-2.22l/s and 2.4-25l/s, respectively.

After the metering sections, the water and air were combined and the two phase flow entered the pipeline.

The pipeline-riser test facility consisted of a 69m long, 50.8mm i.d. pipeline that entered the base of the riser at an angle of –2 ° from the horizontal. The lazy 'S' shaped riser was 9.9m high. At the top of the riser was a 90 ° bend, with a radius of 1½D. To isolate the bend from the surrounding pipework, two rubber isolation joints were installed on either side of the bend. The isolation joints, as shown in Figure 3.2, consisted of rubber bellows with steel flanges. These joints were pressure rated to 15.5 bar at 77°C. To increase the mechanical isolation of the bend, the surrounding pipework was supported by metal scaffolds, which in turn, were bolted to the laboratory walls. The 50.8mm i.d. pipeline, bend and riser were fabricated from carbon steel flanged sections and were rated to schedule 40, with flanges rated to class 300.

After the bend, at the top of the riser, the two phase mixture flowed along a horizontal section of pipework, into a separator, which was mounted on a tower. The separator separated the mixture into a liquid and gas line. The gas exited the top of the separator, where it was metered by a turbine flowmeter, FG3 (Quadrina, Serial No. 7475), that had a range of 1.67-16.67l/s. The liquid exited through an actuated valve, VA6, at the base of the separator, where it was metered by an electromagnetic flowmeter, FL4 (Altometer, Serial No. V/0009072/1), that had a range of 0-6l/s. The water level in the separator was controlled with the use of a differential pressure cell, DP, the output of which was supplied to a digital controller, which controlled the operation of valve, VA6. The calibration of the DP cell is described in Section 3.4.1.

The liquid flowmeter, FL4, and the gas flowmeter, FG3, were used to obtain a mass balance on the separator, so that the liquid and gas production out of the riser could be calculated, this is detailed in Sections 3.3.6 and 3.3.7.

The liquid and gas lines were then recombined and the two phase mixture entered a 3-phase separator. Pressure is regulated in the 3-phase separator by a pressure controller and a camflex valve. This combination acts on the outlet air flow to maintain the set-point pressure (system) pressure and in effect controls the pressure in the test facility as a whole. The liquid level was controlled in the 3-phase separator using a liquid level interface controller, which operated the actuated valve, VA3. Hence, a constant liquid level was maintained. The liquid was then sent through a water coalescer and finally back to the storage tank.

(Please refer to Appendix B for the operating procedures for the riser test facility)

3.3 Instrumentation

Figure 3.3 shows a schematic of the test loop showing the location and actual co-ordinates of all of the instrumentation described below.

3.3.1 Strain Gauges

The forces on the bend at the top of the riser were measured using a strain-gauged strut arrangement, shown in Figure 3.4. The struts were made of mild steel, onto which the strain gauges were bonded. The struts were designed to be 10mm wide and 1mm thick, with a length of 25mm (refer to Appendix C for the strut design calculations). Each strain-gauged strut was attached to the bend, at one end, by pipe a clamp. The other end of the strut was attached to a support, which was bolted to a metal scaffold, which was then bolted to the laboratory wall, Figure 3.5. The clamps and supports were designed so that there was no slip between the clamp and the bend, and the support and the scaffold; therefore, the forces seen by the strain-gauged struts were due to the movement of the bend only. Before installation on the bend, the struts were checked that they read 0N when no force was applied, to ensure that there was no pre-strain on the struts. When the struts were installed, checks were again made to ensure there was no pre-strain. The struts were attached to the clamp and supported by a pin joint. The dimensions of the pin joint allowed the strut to rotate about the pin, to minimise bending in the strut. The struts were raised from the surface of the pipe clamp and support using washers. By installing the struts at 90° to each other, the horizontal and vertical forces on the bend were measured and the resultant force could be determined. The struts were installed as close to the centre-lines of the bend as possible. The installation of the struts was restricted by the space needed by the strut supports and the existing scaffolding.

The strain gauges (Measurements Group UK, Model No. CEA-06-250uw-350) used were a single foil type gauge, consisting of a copper nickel alloy, with a polyamide backing. The gauges had a gauge length of 5mm and were temperature compensated for the use with the mild steel. Each vertical and horizontal strut had 4 strain gauges; 2 active gauges and 2 dummy gauges.

The electrical resistance of a strain gauge changes in direct proportion to the applied force[30]. This change in resistance was measured using a Wheatstone Bridge circuit. In fact, two Wheatstone Bridge circuits were used, one for the forces in the vertical direction and one for the forces in the horizontal direction. Each of the four gauges, on a strut, formed an arm in a Wheatstone bridge circuit. When no force was applied to the strut, the bridge was balanced, i.e the output voltage, V_{out} = 0V. When a force was applied to the bend, the strut experienced tension or compression. This resulted in a change in resistance and the bridge became unbalanced. The corresponding V_{out} was measured and sent to the data acquisition system, via a signal conditioning unit. The unit was fitted with a low pass filter, to reduce electrical noise.

3.3.1.1 Strain-Gauged Strut Calibration

For the calibration of the strain-gauged struts please refer to Chapter 4.

3.3.2 Conductance Probes

Conductance probes were used to monitor slug progression in the pipeline-riser.

The conductance probes were made-up of a 1mm diameter insulated wire, within a 6mm o.d. stainless steel tube, see Figure 3.6.

The conductance probe signal was recorded as an analogue signal, not a digital signal. This was because the probes produced a voltage of 0V (gas at a particular pipeline-riser point) or 5V (liquid at a particular pipeline-riser point), the data acquisition system then converted the voltage to 0 (off) or 1 (on), respectively.

In total, 14 conductance probes were used to monitor slug progression, in the pipeline-riser; 4 positioned along the pipeline, 7 along the riser and 3 probes along the horizontal section into the separator.

The probes located on the pipeline were inserted a quarter of the way in through the top of the pipe and were used to detect how far the liquid backed-up the pipeline, during the slug build-up stage, of the severe slugging cycle. If the probes were inserted through the bottom of the pipe, then at higher liquid flowrates, as liquid entered the flow loop, the probes would be continuously on. Therefore, liquid back-up would be undetected. The probes on the horizontal section were inserted half-way through the bottom of the pipe, as this section was not always full of liquid.

Conductance probes L9 and L10 (refer to Figure 3.3), were used to estimate the time the slug arrived at the bend during the build-up stage of the severe slugging cycle, this is described in more detail in Chapter 5, Section 5.4.2.1.

Probes L8, L9 and L10 were inserted into the riser in a stepped arrangement, i.e. inserted a quarter of the way, half way and three quarters of the way, into the riser, for probes L8, L9 and L10 respectively. This stepped probe arrangement, gave an indication of the composition and distribution of gas and liquid, within the slug. During severe slugging, when a slug passed from the riser into the separator, a film of liquid was left upon the riser walls[13]. Therefore, ensuring that probes L8 and L10 were not too close to the riser walls, prevented the probes from continuously detecting liquid during severe slugging.

3.3.3 Gamma Densitometer

The gamma densitometer was used to measure the liquid hold-up, at the base of the riser, and to determine the flow pattern entering the riser.

The densitometer worked on the principle that radiation emitted from a radioactive source (Caesium 137), was attenuated as it passed through the test fluid and pipe walls, before reaching a detector (GammaTrol, type PRI116), where the radiation was then measured by a control unit.

3.3.3.1 Calibration of Gamma Densitometer[34]

For the gamma densitometer to give accurate readings it had to be calibrated under three different conditions[35]:

Pipeline empty and open to the atmosphere with the gamma source veiled.
Pipeline empty and open to the atmosphere with the gamma source unveiled.
Pipeline full of water with the gamma source unveiled.

The calibration procedure for the densitometer was as follows:

(i) A plug at the base of the riser was removed; this allowed the riser to be open to atmosphere and to check that the pipeline was empty.
(ii) With the gamma source veiled, a background radiation count was initiated on the densitometer control box.
(iii) The gamma source was unveiled and a radiation count was obtained using the control box. This gave the I_o count.
(iv) The plug at the riser base was replaced and the pipeline was filled with water.
(v) The values for the background count rate and the I_o count rate were inputted into the densitometer control box.
(vi) The units for density were set at kg/m^3.
(vii) The calibration constant, K, was calculated:

$$K=\frac{(\rho_{ref}-\rho_o)}{(\rho_{ind}-\rho_o)} \qquad (3.a)$$

where,

ρ_{ref} density of water
ρ_{ind} indicated density with pipe filled with water
ρ_o density of air

NB During the calibration of the densitometer the calibration constant was initially set to 1.

(viii) The calibration constant was inputted into the densitometer.
(vix) To ensure that the calibration settings for the gamma densitometer were accurate, it was checked that for a pipeline full of water, the density reading was $1000kg/m^3$.

3.3.4 Pressure Transducers

Pressure transducers (Control Transducers, Model No. SA200 and SA300) were used to measure the pressure at particular points on the pipeline-riser. Referring to Figure 3.3, the pressure data from the transducer at the base of the riser, P4, was used to determine the cycle times for the severe slugging data. Using transducers P4 and P9, the pressure difference over the riser was used to help identify the flow patterns in the riser.

Transducers P4 and P5, P6 and P9, and P5 and P6 were used to measure the pressure difference, and hence the liquid inventory, in the lower limb, upper limb and downward section respectively, see Chapter 5, Section 5.5 for details.

The flow loop contained 9 pressure transducers, 2 in the air metering section, 2 in the pipeline, 4 in the riser and 1 at the outlet of the separator.

3.3.4.1 Calibration of Pressure Transducers[34]

To ensure that all the pressure transducer readings were consistent, the transducers were calibrated to read 1.013 bar (atmospheric pressure) when the pipeline-riser was empty.

The commissioning procedure for the pressure transducers was as follows:

(i) A plug at the base of the riser was removed, this ensured that the riser was at atmospheric pressure and to check that the pipeline was empty.
(ii) The data acquisition system was turned on and the 'analogue meters' screen was observed.
(iii) The pressure readings were then zeroed to read 1.013 bar, using the zero screw on the signal conditioning unit and observing the readings on the data acquisition screen.

3.3.5 Thermocouples

The type 'T' thermocouples monitored the temperature at 4 positions; 2 in the gas metering lines, 1 in the pipeline and 1 located at the outlet of the separator. These temperature measurements were used to correct the measured gas flows to standard conditions, see Section 3.3.6.1.

3.3.6 Liquid Flowmeters

Liquid flowrates were measured using electromagnetic flowmeters. Two flowmeters, FL1 (0-1.67l/s) and FL2 (0-12.5l/s), measured the inlet liquid flowrate to the pipeline-riser. Flowmeter FL4 (0-6l/s) was installed at the exit of the separator vessel on the tower and was used to obtain a liquid mass balance on the separator, so that liquid production out of the riser could be calculated, see Section 3.3.6.2.1 below. For remaining liquid flowmeter makes and serial numbers, refer to Section 3.2.

3.3.6.1 Liquid Flowmeter Commissioning Tests

Manufacturers calibrated all the liquid flowmeters used on the riser test facility. To ensure that the flowmeters were reading correctly, a "back to back" check was performed to check the flowmeter readings. The checks were carried out between FL1 and FL4 and between FL2 and FL4, for a range of liquid flowrates.

The "back to back" tests showed that the flowmeters agreed to within 3%, which was considered to be an acceptable error, with the exception of tests where the flowmeters were outside of their reliable range.

3.3.6.2 Liquid Mass Balance on Separator[34, 36]

The flowmeter FL4, on the outlet line of the separator vessel on the tower, refer to Figure 3.3, and the separator internal conditions, see Figure 3.7, allowed the balance to be performed, using the basic relation:

IN - OUT = Accumulation

The total inflowing liquid mass, into the separator, over a given time step, Δt, was:

$$m_{L,in} = q_{L,in} \rho_L \Delta t \qquad (3.b)$$

The exiting total liquid mass from the separator, $m_{L,out}$, was equal to the volumetric flowrate (measured using flowmeter FL4) times the liquid density, assuming a constant flow over each time step. This was consistent with the discrete sensor signal for the measurements.

$$m_{L,out} = q_{L,out} \rho_L \Delta t \qquad (3.c)$$

The accumulation of mass in the separator, Δm_{sep}, was equal to the volume change of liquid in the separator, times the liquid density.

$$\Delta m_{sep} = \frac{dV_{sep}}{dt} \rho_L \Delta t \qquad (3.d)$$

Where the volume change was given by:

$$\frac{dV_{sep}}{dt} = \frac{\Delta V_{sep}}{\Delta t} = \frac{A_{sep} \Delta S}{\Delta t} \qquad (3.e)$$

In order to prevent noise from the liquid level measurement in the separator, S, giving excessive fluctuations in the Δm_{sep} term in the mass balance, a ten-point moving average smoothing was carried out on the level signal:

$$S_n = \frac{1}{10} \sum_{i=n-10}^{i=n-1} S_i \qquad (3.f)$$

Combining into the basic relation:

$$q_{L,in} \rho_L \Delta t - q_{L,out} \rho_L \Delta t = A_{sep} \frac{\Delta S}{\Delta t} \rho_L \Delta t \qquad (3.g)$$

gave:

$$\dot{m}_{L,in} = q_{L,in}\rho_L = \{q_{L,out} + A_{sep}\frac{\Delta S}{\Delta t}\}\rho_L \qquad (3.h)$$

For the discrete time signal of the sensors, the liquid level change was:

$$\frac{\Delta S}{\Delta t} = \frac{(S_{,n} - S_{,n-1})}{\Delta t} \qquad (3.i)$$

Hence, the mass flowrate of liquid into the separator was given by:

$$\dot{m}_{L,in} = \{q_{L,out} + A_{sep}\frac{(S_{,n} - S_{,n-1})}{\Delta t}\}\rho_L \qquad (3.j)$$

where,

Δt time step, for sampling rate of 10 Hz, $\Delta t = 0.1s$
A_{sep} cross sectional area of separator, $A_{sep} = 0.19635m^2$

3.3.6.2.1 Liquid Mass Balance Validation

The liquid mass balance was validated using the results from the single phase and two phase tests, described in Chapter 5.

To validate the liquid mass balance, the liquid entering the flow loop (using the readings from the liquid flowmeters, FL1 and FL2) was compared to the liquid entering the separator (based on the liquid mass balance). Figure 3.8 shows the comparison between the flowmeter and the mass balance readings. The liquid mass balance compared to within 10% of the flowmeter readings.

3.3.6.3 Slug Length[34]

Slug lengths were calculated to enable severe slugging flow regimes to be categorised.

To calculate the slug length, time references for the start and end of each severe slugging cycle were determined. These time references were used as the limits to calculate the total volume of liquid, which exited from the riser, using the liquid mass balance described in Section 3.3.6.2, during the severe slugging cycle.

The total volume of liquid, Q_T, based on a continuous measurement of flow q(t) over the timescale t_1 to t_2 is:

$$Q_T = \int_{t_1}^{t_2} q(t)dt \qquad (3.k)$$

For a discrete time signal, $q_i(t)$, the total volume between timesteps n and n+k (corresponding to t_1 and t_2 respectively) is:

$$Q_T = \sum_{i=n}^{i=n+k} q_i(t)\Delta t \qquad (3.l)$$

The slug volume, $V_s = Q_T$, giving the slug length, L_s, as:

$$L_S = \frac{V_s}{A} = \frac{\sum_{i=n}^{i=n+k} q_i(t)\Delta t}{A} \qquad (3.m)$$

where,

A cross-sectional area of pipe
t_1 start of severe slugging cycle
t_2 end of severe slugging cycle
q volumetric liquid flowrate from the riser, $q = q_{L,\,in}$

3.3.7 Gas Flowmeters

Gas flowrates were measured using turbine flowmeters. Two flowmeters, FG1 (0.28-2.22l/s) and FG2 (2.4-25l/s), measured the inlet gas flowrate to the pipeline-riser. Flowmeter FG3 (1.67-16.67l/s) was installed at the exit of the separator vessel on the tower and was used to obtain a gas mass balance on the separator, so that gas production out of the riser could be calculated, see Section 3.3.7.2 below. For gas flowmeter makes and serial numbers, refer to Section 3.2.

3.3.7.1 Gas Flowmeter Commissioning Tests

The manufacturers calibrated all the gas flowmeters used on the riser test facility. As with the liquid flowmeters, a "back to back" check was carried out between flowmeters FG1 and FG3 and between FG2 and FG3. The commissioning tests were performed in single phase gas, therefore, any gas entering the test loop through either FG1 or FG2, should equal that leaving the test loop through FG3 (only if the actuated valve, VA6, on the liquid line at the base of the separator, was closed). For all these tests, gas entered the flow loop at the required flowrate, where it was allowed to stabilise, before recording the flowmeter readings for 2 minutes.

The gas flowmeters measured the volumetric flowrates at local pressure, therefore, for a "back to back" check between two flowmeters at different locations and being subjected to different local temperatures, the flows had to be converted to standard conditions before they were compared. The flowrates were converted using:

$$\frac{Pq}{T} = \frac{P_{std}q_{std}}{T_{std}} \qquad (3.n)$$

Therefore, the standard flowrate was given by:

$$q_{std} = \frac{Pq}{T}\frac{T_{std}}{P_{std}} \qquad (3.o)$$

where,

P_{std} standard pressure (101325 Pa)
T_{std} standard temperature (293K)
P local pressure (Pa)
T local temperature (K)
q flowmeter reading (l/s)

As with the liquid flowmeter commissioning tests, the "back to back" tests showed that the gas flowmeters agreed to within 3%, with the exception of tests where the flowmeters were outside of their reliable range.

3.3.7.2 Gas Mass Balance on the Separator

A gas mass balance was developed, to calculate the gas flowrate out of the riser and into the separator. Flowmeter FG3, installed at the exit of the separator vessel on the tower, refer to Figure 3.3, was used to obtain the mass balance. As with the liquid mass balance, the gas mass balance was based on the relation:

IN – OUT = Accumulation

The total inflowing gas mass, into the separator, over a given time step, Δt, was:

$$m_{G,in} = q_{G,in}\rho_G \Delta t \qquad (3.p)$$

Similarly, for the gas mass out of the separator, $m_{G,out}$, was equal to the volumetric flowrate (measured using flowmeter FG3) times the gas density:

$$m_{G,out} = q_{G,out}\rho_G \Delta t \qquad (3.q)$$

where,

$$\rho_G = \frac{P_{sep}M}{RT_{sep}} \qquad (3.r)$$

(R, gas constant = 8314KJK^{-1}mol^{-1} and M, molecular weight = 28.84)

The mass of gas in the separator, was given by:

$$m_{G,sep} = V_{G,sep}\rho_G \qquad (3.s)$$

Where, volume of gas in the separator,

$$V_{G,sep} = V_{sep} - V_{L,sep} \tag{3.t}$$

Volume of liquid in the separator, $V_{L,sep}$, was given by:

$$V_{L,sep} = A_{sep} S \tag{3.u}$$

NB Liquid level in the separator, S, was measured in % height, where 0% ht = 0m and 100 % ht = 0.5m, see Figure 3.7. Therefore:

$$S(m) = S(\%\ ht)\frac{0.5}{100} \tag{3.v}$$

hence,

$$V_{sep} = 0.5A_{sep} + V_{head} \tag{3.w}$$

Where V_{head} was the header volume i.e. volume in a semi-ellipsoid head:

$$V_{head} = \frac{\pi}{6} D_{sep}{}^2 h \tag{3.x}$$

Substituting Equations (3.w) and (3.u) into Equation (3.t), the volume of gas in the separator was given by:

$$V_{G,sep} = A_{sep}[0.5 - S] + V_{head} \tag{3.y}$$

Hence, the mass of gas in the separator became:

$$m_{G,sep} = V_{G,sep}\rho_G = A_{sep}[0.5 - S] + V_{head}\frac{P_{sep}M}{RT_{sep}} \tag{3.z}$$

The mass change of gas in the separator was:

$$\frac{dm_{Gsep}}{dt} = \frac{\Delta m_{Gsep}}{\Delta t} = \frac{(m_{Gsep,n} - m_{Gsep,n-1})}{\Delta t} \tag{3.aa}$$

Combining into the basic relation, the mass flowrate of gas into the separator was given by:

$$\dot{m}_{G,in} = q_{G,in}\rho_G = q_{G,out}\frac{P_{sep}M}{RT_{sep}} + \frac{(m_{Gsep,n} - m_{Gsep,n-1})}{\Delta t} \tag{3.ab}$$

3.4 Liquid Level Control

There were two types of liquid level controller used on the riser test facility:

(i) A DP (Differential Pressure) cell transmitter- this was used to control the level of water within the separator mounted on the tower. The DP cell sends a signal, via a digital controller, to an I/P (current to pressure) converter. The digital controller controls a pneumatically actuated valve, VA6, which determines the liquid level in the separator, refer to Figure 3.1.

The DP cell transmitter was calibrated using the electronic display on the cell and two known conditions; a lower range value and an upper range value, this referred to the separator vessel being empty and full respectively. Further information can be found in the manufacturer handbook[37].

(ii) A liquid level interface controller- this was used to control the level of the water within the 3-phase separator, by operating a pneumatically actuated valve, VA3, refer to Figure 3.1.

3.5 Data Acquisition System (DAS)

The programme used for the DAS was written in LabVIEW 4.0. The software ran on a Pentium P166 computer with 1.2GB HDD and 32MB of RAM. The operating system was Windows 3.11.

The responses from the various instrumentation were either 4-20mA or 0-5V signals. In an attempt to remain consistent, all the signals were converted to a 0-5V output signal, before being sent to the data acquisition system.

A total of 38 analogue signals were captured by the data acquisition system, comprising:

2 Strain Gauges- Horizontal and Vertical
14 Conductance Probes
1 Gamma Densitometer
9 Pressure Transducers
4 Thermocouples
3 Turbine Flowmeters (Air)
4 Electromagnetic Flowmeters (Water)
1 Differential Pressure Cell Transmitter

The output signals were captured using two sets of hardware. An ATMIO16E-10 data acquisition card, mounted inside the computer, captured outputs from the conductance probes. The remaining signals were sampled using a SCXI (Signal Conditioning Extensions for Instrumentation) and passed to the parallel port of the computer.

3.5.1 LabVIEW Screens

Within LabVIEW, several screens were designed to help set-up the required flow conditions (flowrate, pressure) and to check the conditions in the pipeline-riser, during testing.

The calibration screens allowed access to the instrumentation calibration data, the process instrumentation calibration screen is shown in Figure 3.9. The calibration data, was entered prior to any test work and recording of measurements taking place.

Figure 3.10 shows the 'data file control' screen. Using this screen, data was recorded by pressing 'start/stop.' In this screen, the test filename was entered and the recording sampling rate and recording duration were changed.

The 'meters' screen in Figure 3.11 was used when setting up the initial gas and liquid flowrate/velocity conditions.

In the 'pipeline-riser' screen in Figure 3.12, the slug progression could be monitored, as the conductance probes turned on as liquid was detected. The liquid hold-up readings taken from the densitometer were also displayed on this screen, along with the riser and separator inlet pressures. This screen was used to identify the flow regime within the riser.

Figure 3.13 shows the 'force monitor' screen, this displayed the horizontal and vertical force readings from the strain-gauged struts. The screen also displayed the pressure at the base and top of the riser.

The 'analogue meters' screen, showed the data from all the analogue meters. This screen was checked to ensure that there were no problems with the pressure within the pipeline.

3.5.2 Sampling Rates[34]

The conductance probe data was used to give an indication of the composition of a slug therefore, the higher the sampling rate, the higher the resolution. For the conductance probe data, a sampling rate of 100Hz was used, e.g. for a slug travelling at 2m/s, at 100Hz, the slug would have travelled 0.02m between each scan. This sampling rate caused problems in trying to read the very large data files that were produced (approximately 35MB for 25 minutes recording). As only the conductance probe data was sampled at 100Hz, the remaining process data was then collected at a much lower sampling rate of 10Hz.

10Hz was used as the sampling rate for the process data, as the gamma densitometer was limited to a signaller rate of 10Hz. The DAS system was modified so that the data was sampled at two different rates, 10Hz for the process data and 100Hz for the conductance probe data. The two data acquisition cards were initially tested and calibrated and then synchronised, so that when data recording began, the two cards

started together. This resulted in two files being produced for each test condition, one with the suffix .PRC, for the process data, and a second file with the suffix .CON, for the conductance probe data.

3.6 Summary

This Chapter described the data acquisition system, flow loop, instrumentation and the procedures used to calibrate and commission the instrumentation, which were used to determine severe slugging flow characteristics and the forces on a bend, at the top of a lazy 'S' riser.

Test work commenced, when the calibration and commissioning of all the instrumentation was complete and there was confidence that the instrumentation was working correctly. During testing, daily checks were made to the instrumentation, by using an instrumentation checklist (Refer to Appendix B- operating procedures for the riser test facility).

The following Chapter describes the procedures used to calibrate the strain-gauged struts, which measured the vertical and horizontal forces on the bend. It was necessary that the strain-gauged struts were calibrated prior to any test work, so that the readings from the struts could be quantified.

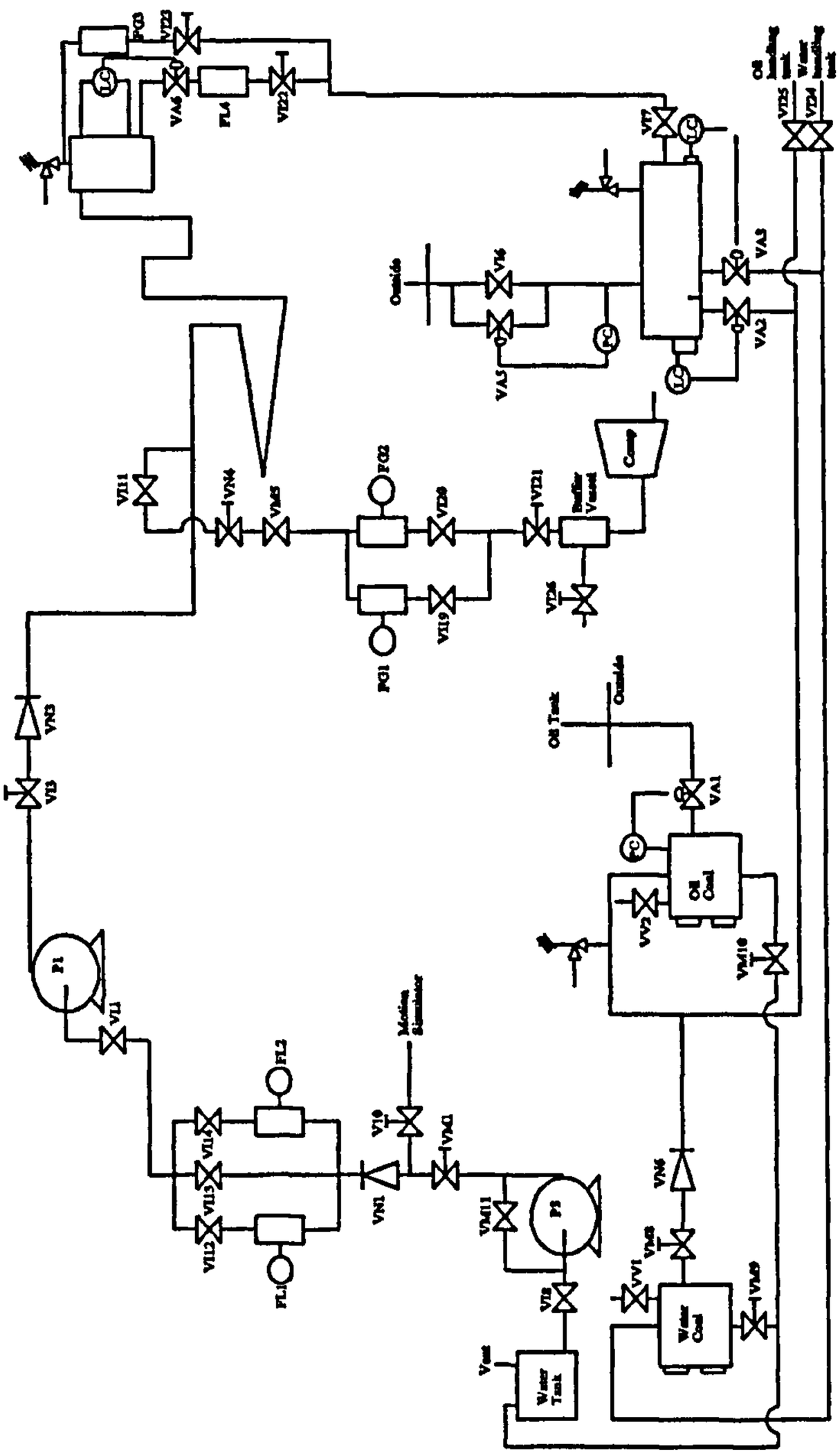

Figure 3.1 P and ID of riser test facility

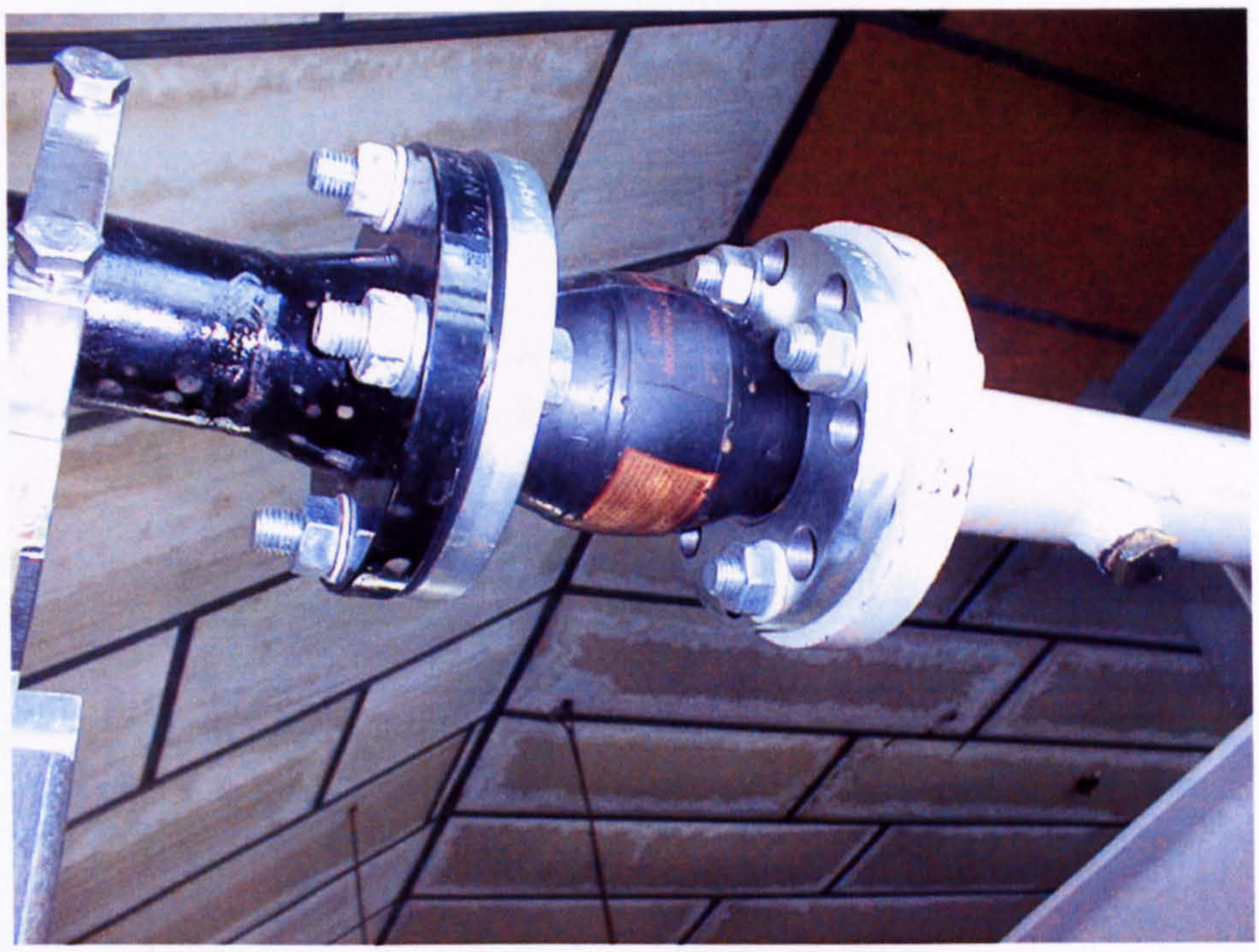

Figure 3.2 Photograph of isolation joint

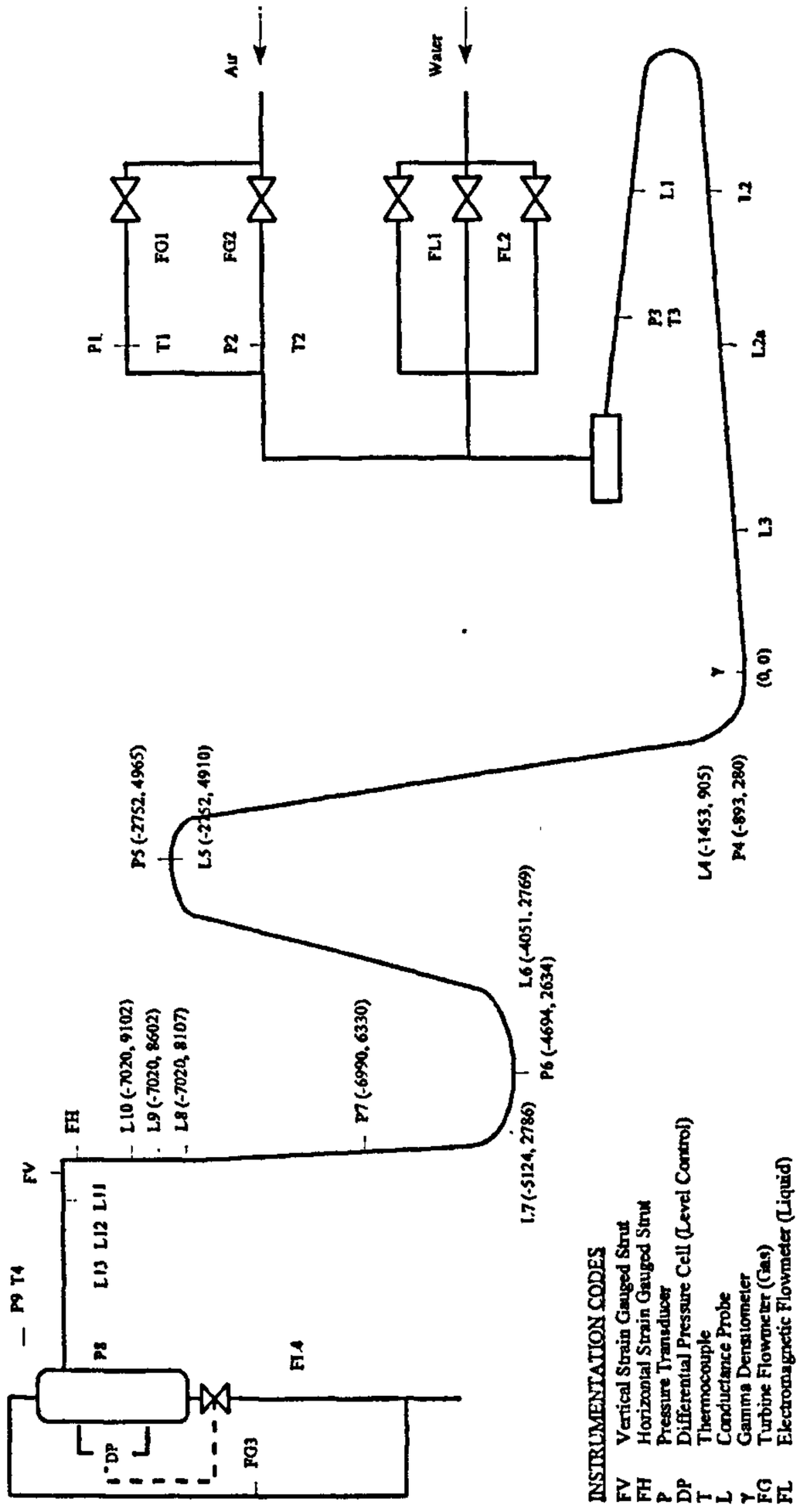

Figure 3.3 Diagram showing instrumentation on pipeline-riser

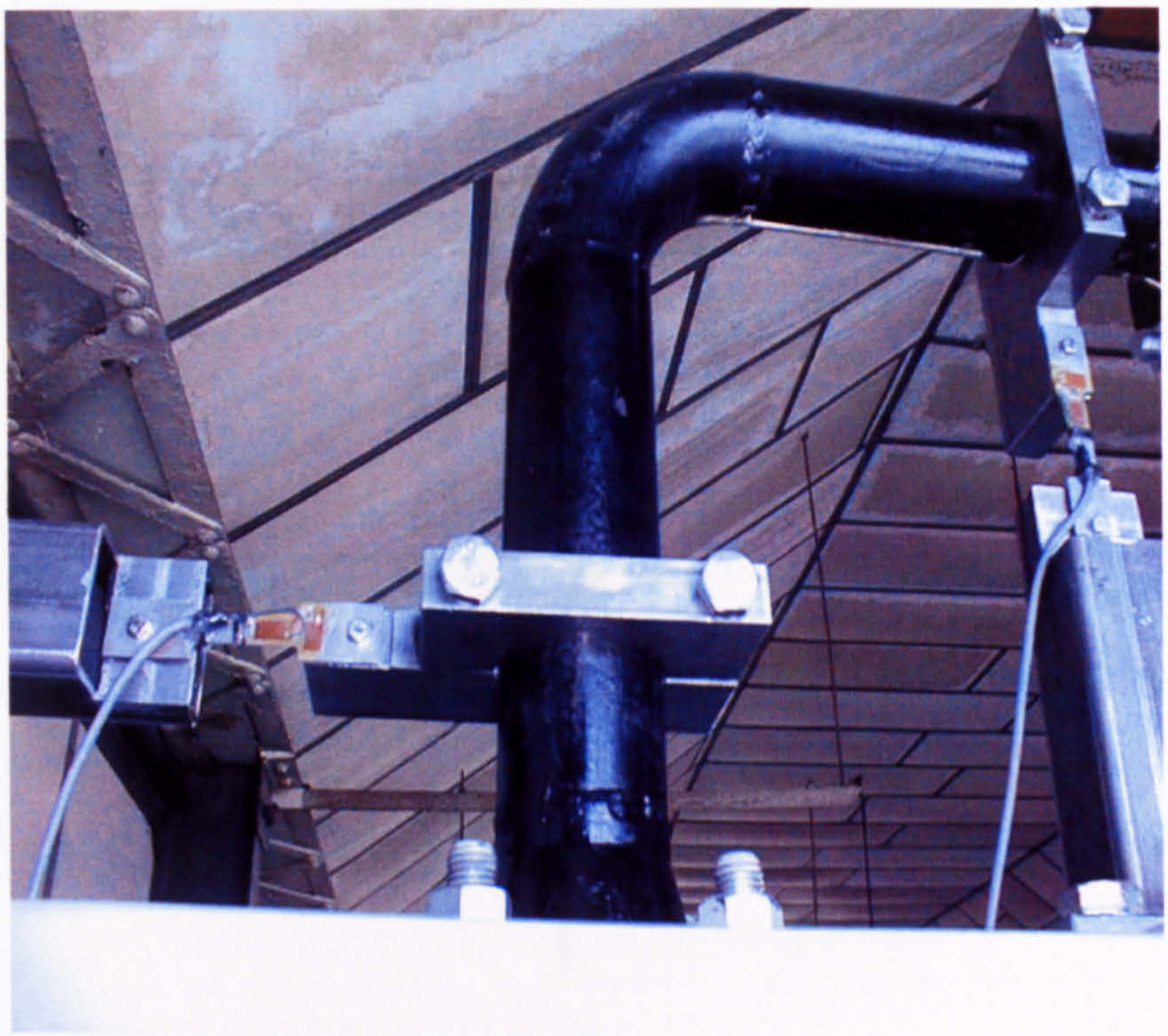

Figure 3.4 Photograph of strain-gauged strut

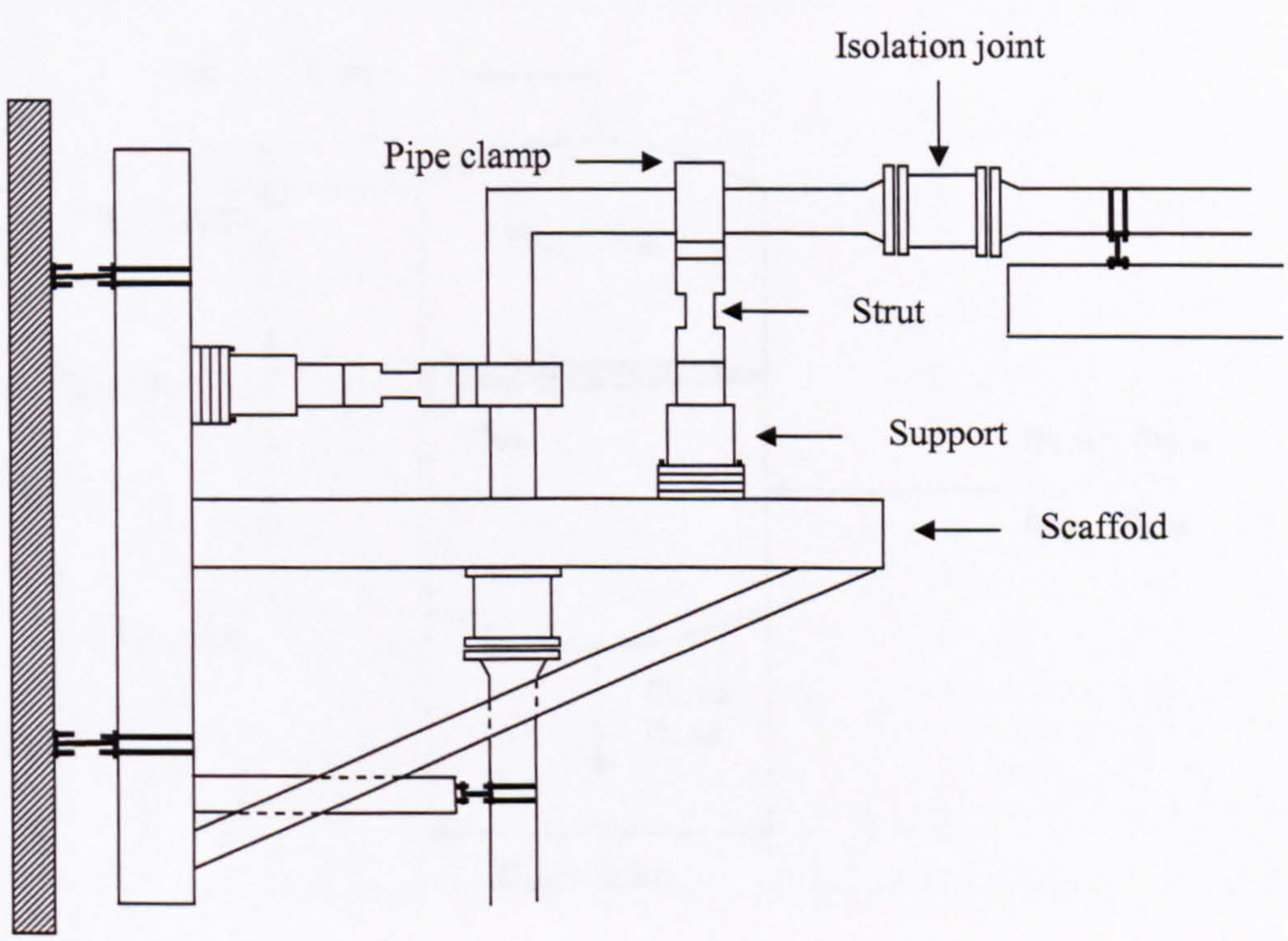

Figure 3.5 Diagram of bend

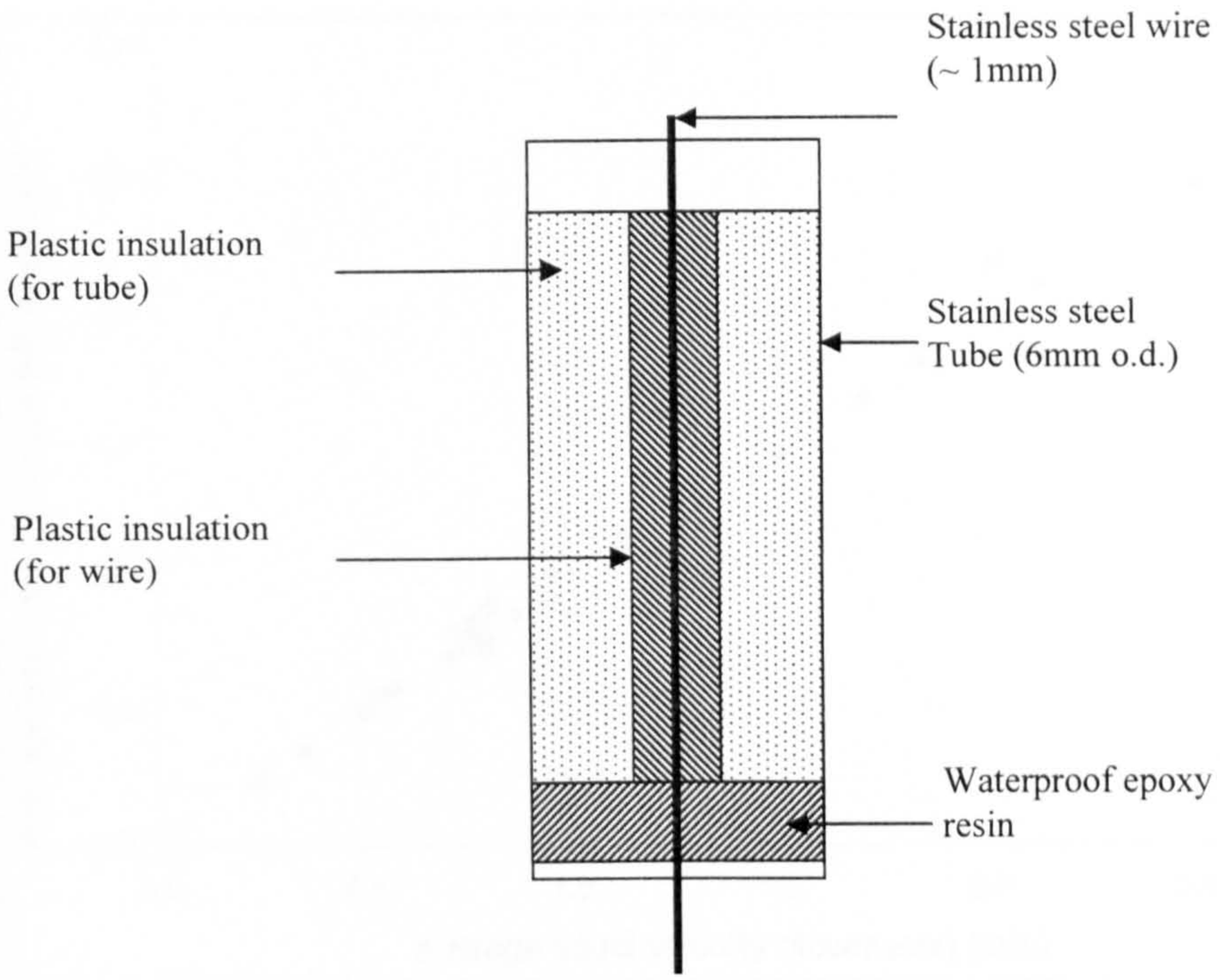

Figure 3.6 Diagram of conductance probe

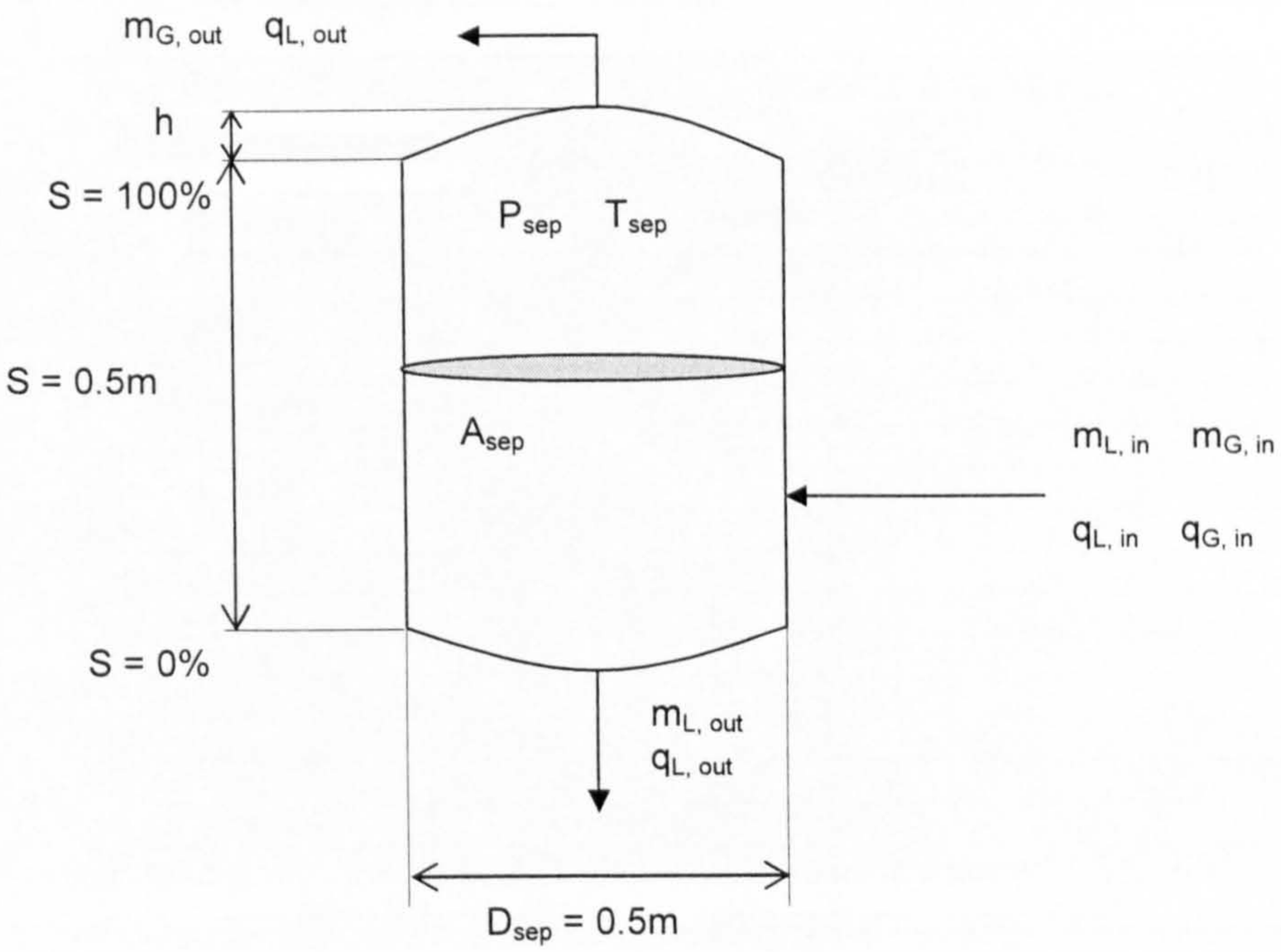

Figure 3.7 Diagram of the separator at the top of the riser

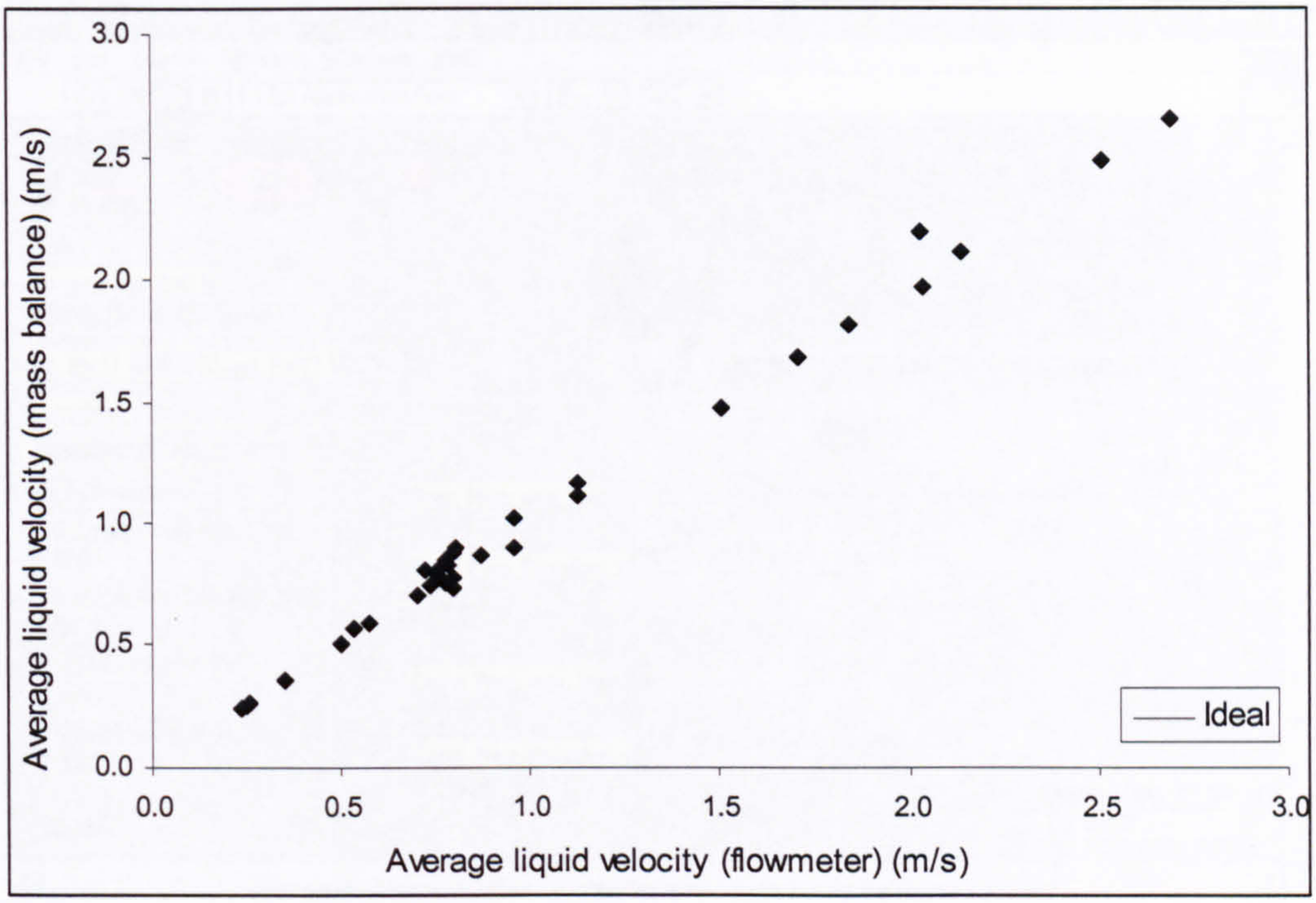

Figure 3.8 Liquid mass balance validation

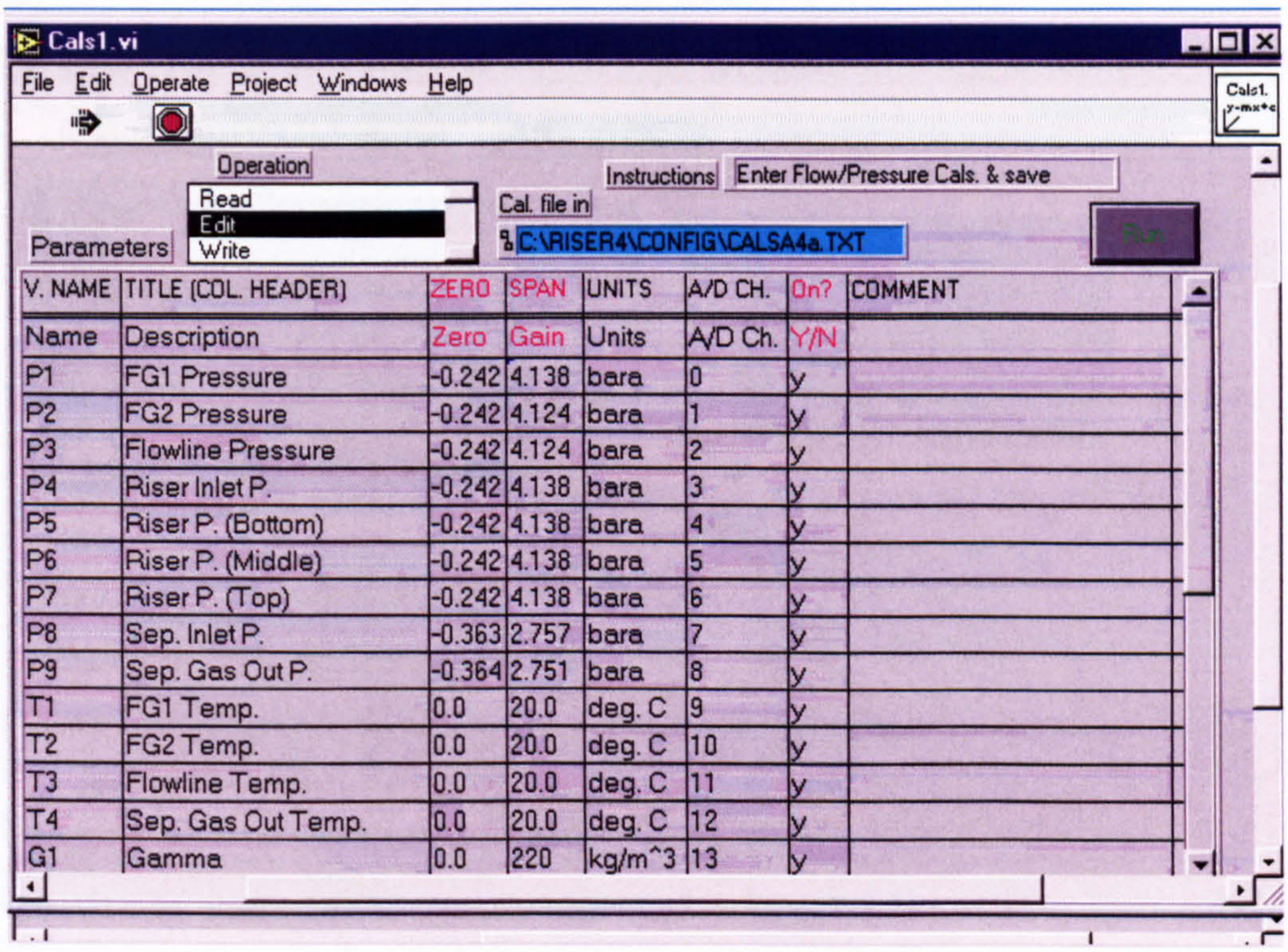

V. NAME	TITLE (COL. HEADER)	ZERO	SPAN	UNITS	A/D CH.	On?	COMMENT
Name	Description	Zero	Gain	Units	A/D Ch.	Y/N	
P1	FG1 Pressure	-0.242	4.138	bara	0	y	
P2	FG2 Pressure	-0.242	4.124	bara	1	y	
P3	Flowline Pressure	-0.242	4.124	bara	2	y	
P4	Riser Inlet P.	-0.242	4.138	bara	3	y	
P5	Riser P. (Bottom)	-0.242	4.138	bara	4	y	
P6	Riser P. (Middle)	-0.242	4.138	bara	5	y	
P7	Riser P. (Top)	-0.242	4.138	bara	6	y	
P8	Sep. Inlet P.	-0.363	2.757	bara	7	y	
P9	Sep. Gas Out P.	-0.364	2.751	bara	8	y	
T1	FG1 Temp.	0.0	20.0	deg. C	9	y	
T2	FG2 Temp.	0.0	20.0	deg. C	10	y	
T3	Flowline Temp.	0.0	20.0	deg. C	11	y	
T4	Sep. Gas Out Temp.	0.0	20.0	deg. C	12	y	
G1	Gamma	0.0	220	kg/m^3	13	y	

Figure 3.9 LabVIEW calibration screen- Process Instrumentation

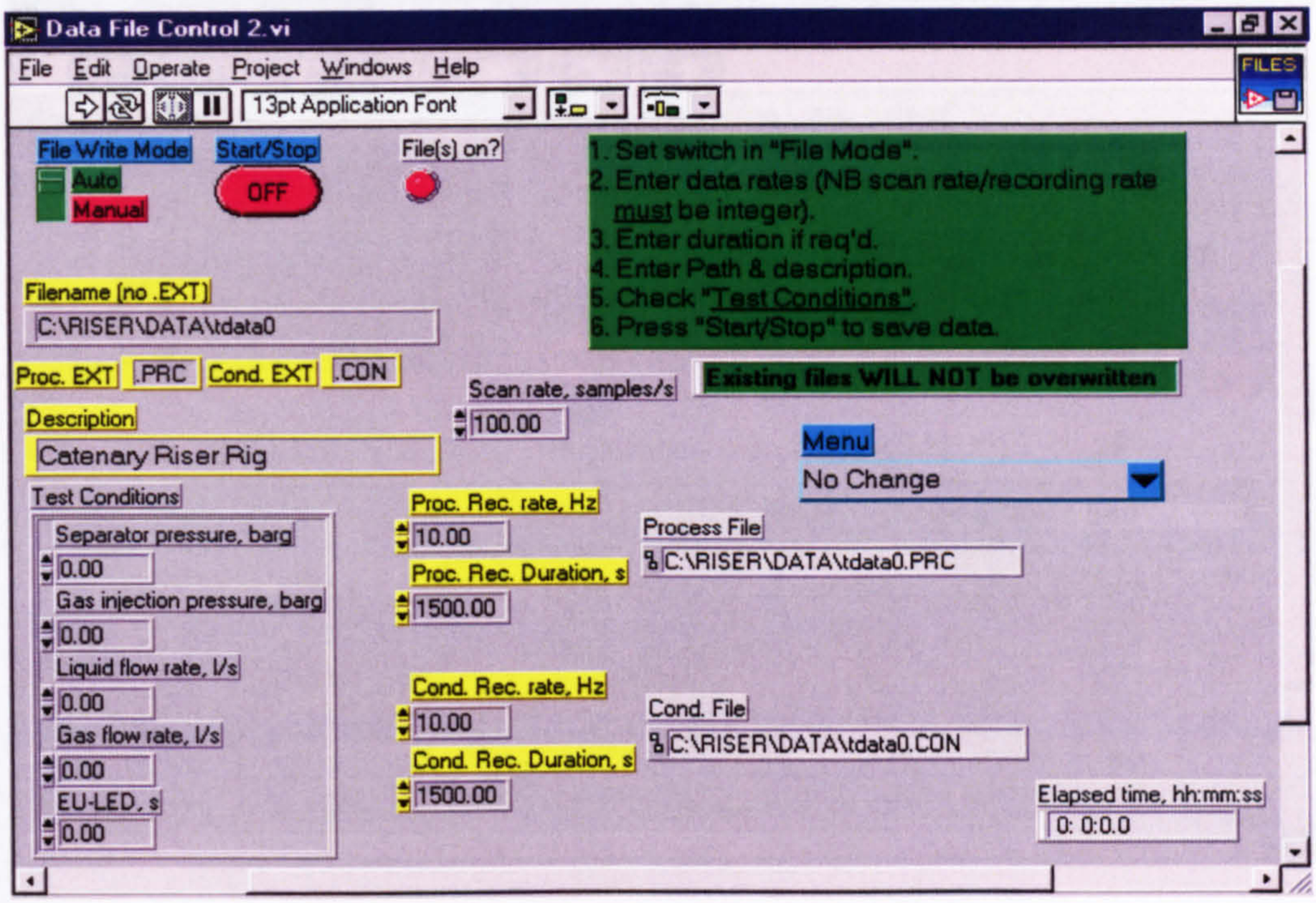

Figure 3.10 LabVIEW data file control screen

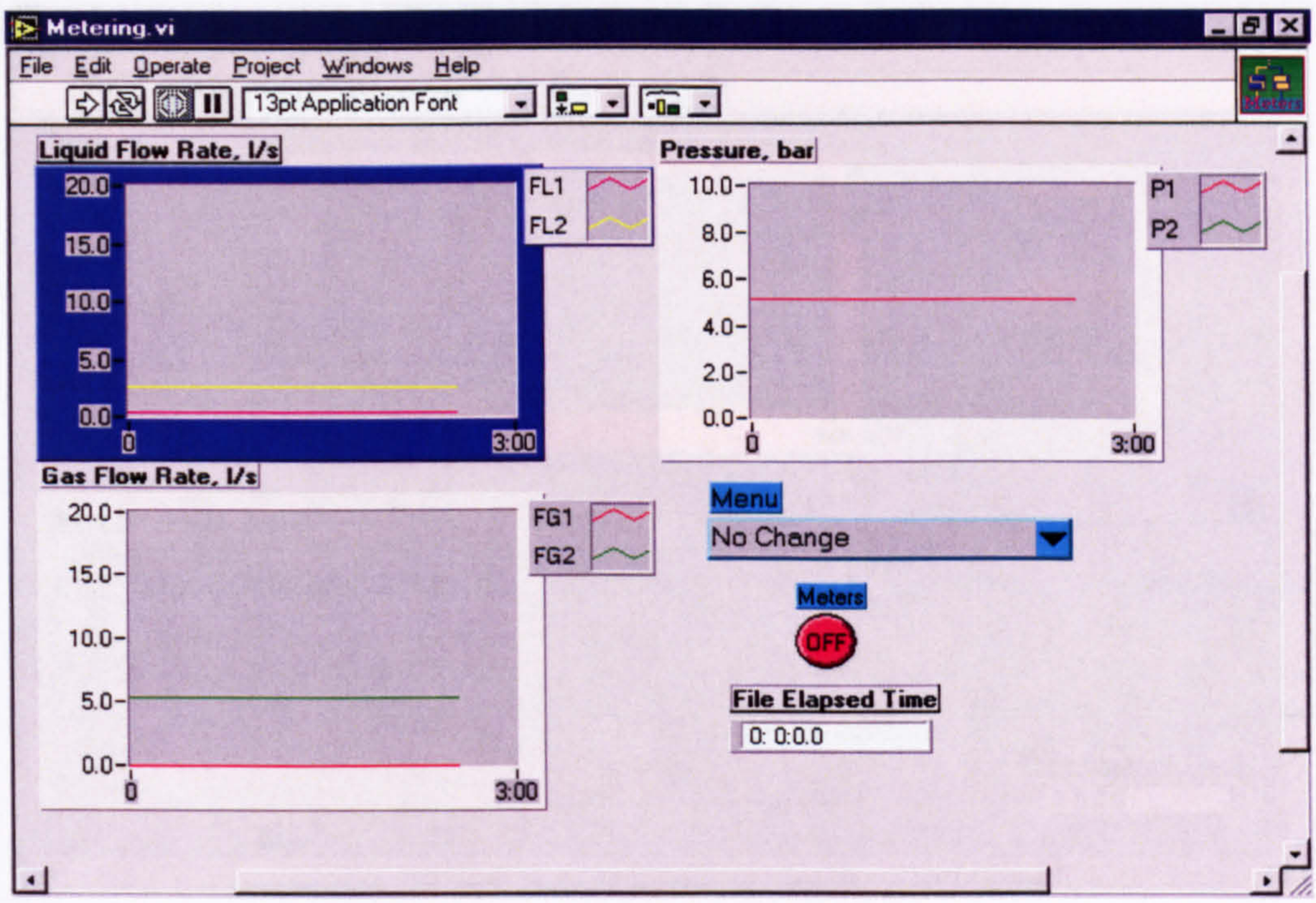

Figure 3.11 LabVIEW meters screen

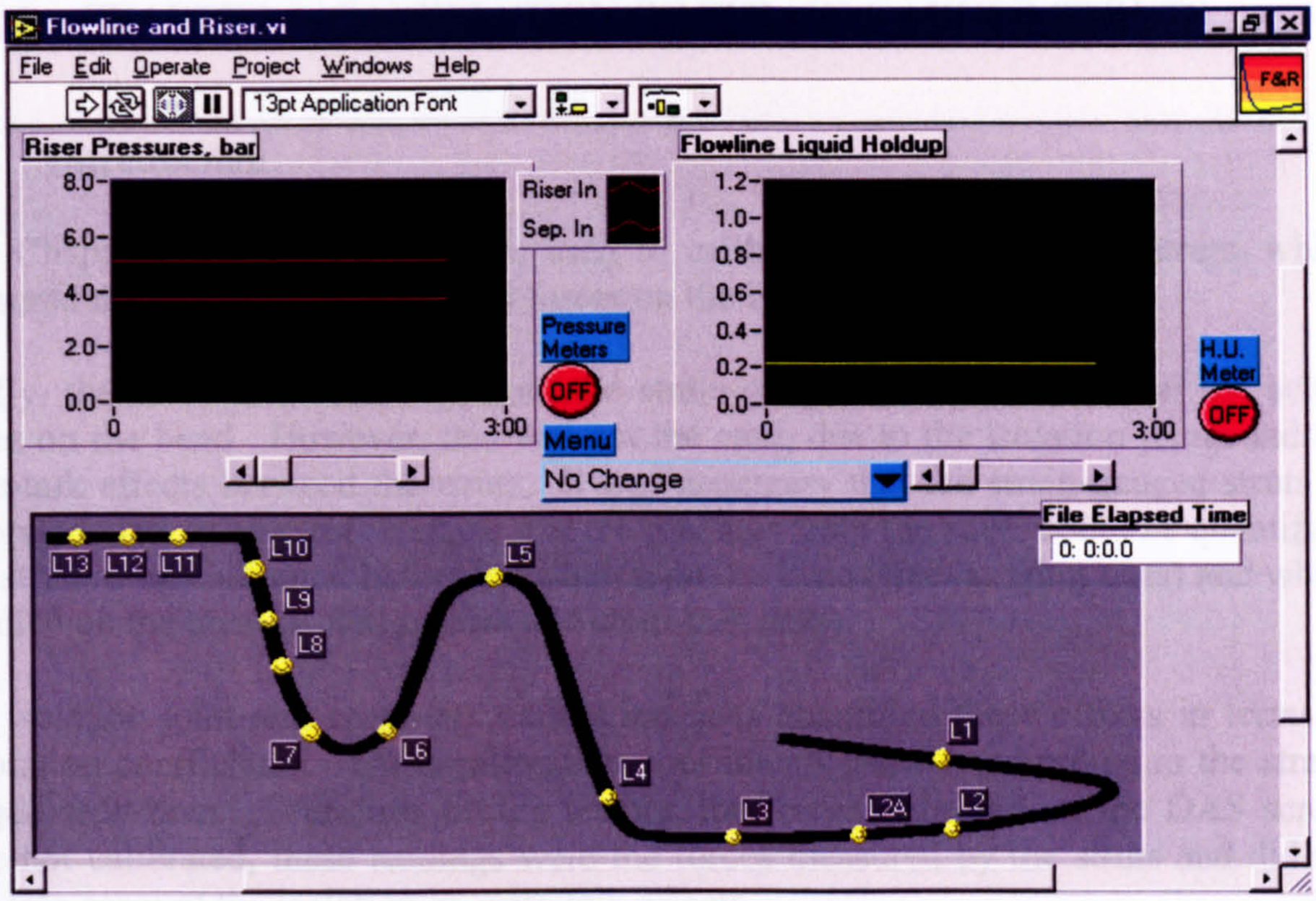

Figure 3.12 LabVIEW pipeline-riser screen

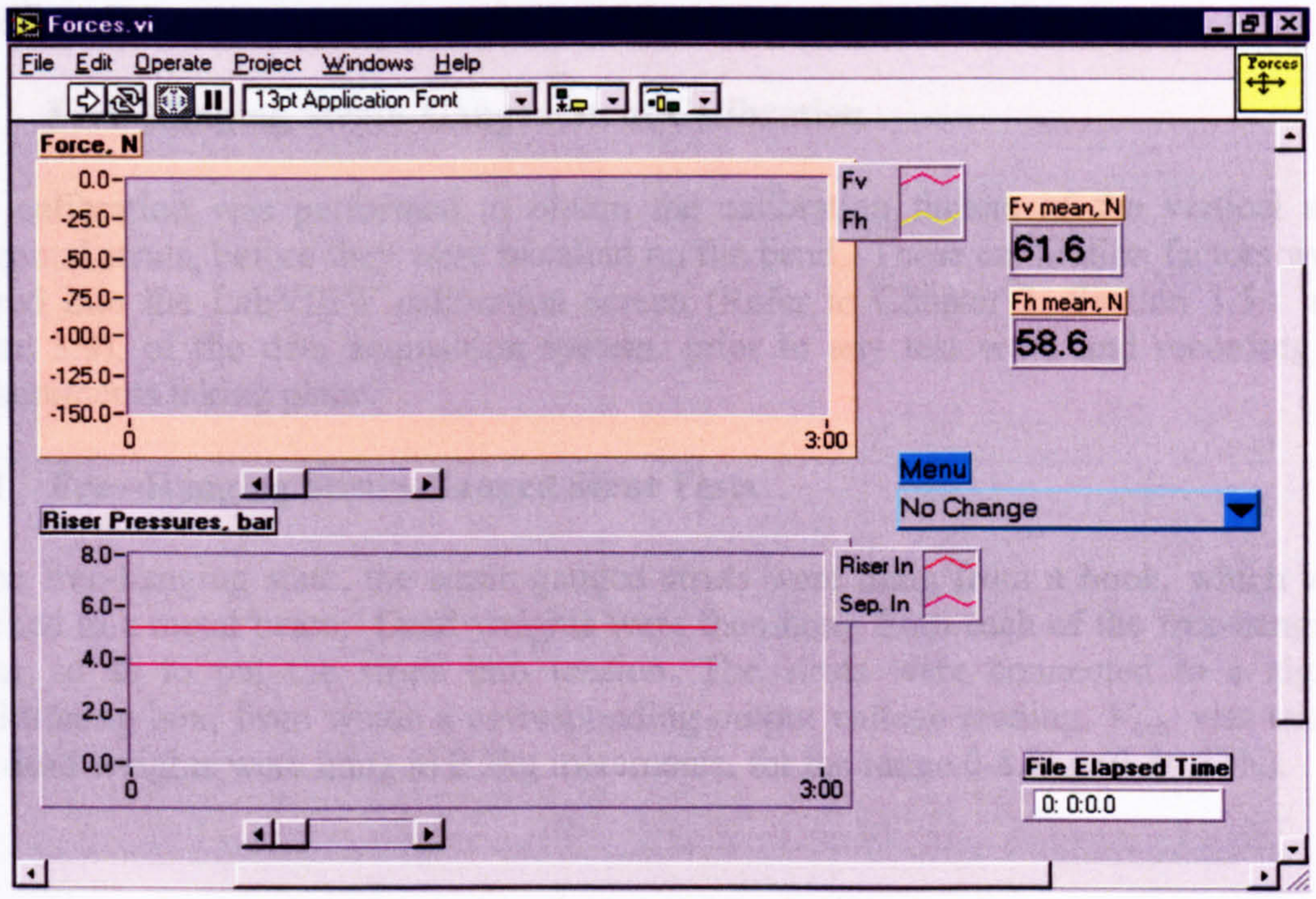

Figure 3.13 LabVIEW force monitor screen

CHAPTER 4- CALIBRATION OF STRAIN-GAUGED STRUTS

4.1 Introduction

This Chapter details the procedures used to calibrate the strain-gauged struts, which measured the vertical and horizontal forces on the bend.

Ideally, the force measurements from the strain-gauged struts would equal the actual forces on the bend. However, this was not the case, due to the isolation joints and the cross-talk effects between the struts. It was necessary that the strain-gauged struts be calibrated prior to any test work, so that the readings from the struts could be quantified. The struts were calibrated before installation on the bend (free-hanging tests) and whilst installed on the bend (isolation joint and cross-talk tests).

The isolation joint and cross-talk calibration tests quantified these effects in terms of calibration coefficients. These calibration coefficients were then applied to the strain-gauged strut data. Therefore, during testing, the forces indicated on the DAS screen were not calibrated, these readings were the forces measured by the struts and did not take into account the isolation or cross-talk effects.

The calibration coefficients were applied to the DAS screen vertical and horizontal force data, by copying the data into a MS Excel master spreadsheet, where columns FV ' and FH ' represented the actual vertical and horizontal forces on the bend.

4.2 Free-Hanging Strain-Gauged Strut Calibration

This calibration was performed to obtain the calibration factors of the vertical and horizontal struts, before they were installed on the bend. These calibration factors were entered into the LabVIEW calibration screen (Refer to Chapter 3, Section 3.5.1 and Figure 3.9), of the data acquisition system, prior to any test work and recording of measurements taking place.

4.2.1 Free-Hanging Strain-Gauged Strut Tests

In the free-hanging state, the strain-gauged struts were hung from a hook, which was attached to a metal beam. Dead weights were then hung from each of the free-hanging struts, so as to put the struts into tension. The struts were connected to a signal conditioning box, from which a corresponding output voltage reading, V_{out}, was taken. The dead weights were hung in 2.2kg increments, for the range 0-8.8kg (0-86.33N).

4.2.2 Determination of Free-Hanging Calibration Factors

From the tests carried out in Section 4.2.1, a graph of output voltage, V_{out}, versus the force applied to each strut, F_{free}, was plotted (Figure 4.1). The linear relationships shown in Figure 4.1, were then used to determine the free-hanging calibration factors:

For the strut measuring vertical forces:

$$V_{out} = -0.0164 F_{free} \tag{4.a}$$

Therefore, the calibration factor of the vertical strut, C_V:

$$C_V = \frac{F_{free}}{V_{out}} \quad \text{in N/V} \tag{4.b}$$

$$C_V = \frac{1}{-0.0164} = -60.98 \quad N/V \tag{4.c}$$

Similarly, the calibration factor of the horizontal strut, C_H:

$$C_H = \frac{1}{-0.0173} = -57.80 \quad N/V \tag{4.d}$$

4.2.3 Polarity of Free-Hanging Calibration Factors

In Figure 4.1, when the struts were in tension the output voltage was negative. For all the test work carried out, the convention chosen was that the free-hanging calibration factor should be such, to give a positive force reading when the strut was in compression and a negative force reading when the strut was in tension.

Therefore, based on the free-hanging strain-gauged strut tests and the chosen convention:

In tension,

$$F_{free}\ (-ve) = C V_{out}\ (-ve) \tag{4.e}$$

In compression,

$$F_{free}\ (+ve) = C V_{out}\ (+ve) \tag{4.f}$$

For Equations (4.e) and (4.f) to be true, the free-hanging calibration factors had to be positive. Therefore, the calibration factors entered into the 'span' column of the LabVIEW calibration screen (Figure 3.9) were, $C_V = 60.98$ and $C_H = 57.80$.

4.3 Isolation Joint and Cross-Talk Effects

To isolate the bend from the surrounding pipework, two rubber isolation joints were installed on either side of the bend. It was necessary to investigate if the stiffness of these rubber joints restricted the movement of the bend and hence, what effect this had on the horizontal and vertical strain-gauged strut readings.

The test work involved measuring the horizontal and vertical forces on the bend, using two strain-gauged struts, refer to Figure 3.5. With this set-up, there was the possibility of cross-talk between the two struts. The cross-talk effect was a combination of the cross-talk between, a) the horizontal strut to the vertical strut- a force on the bend in the horizontal direction causing a force in the vertical direction and b) the vertical strut to the horizontal strut- a force on the bend in the vertical direction causing a force in the horizontal direction.

The isolation joint and cross-talk effects were investigated by carrying out the tests described in Section 4.3.1 below. The experiments quantified these effects in terms of calibration coefficients, Section 4.4. Therefore, by applying these calibration coefficients to the strain-gauged strut readings, the actual slug force on the bend was determined. The actual force, was the force observed by the strain-gauge struts, assuming there were no cross-talk and isolation joint effects.

4.3.1 Isolation Joint and Cross-Talk Tests

The isolation joint and cross-talk tests were carried out at a system pressure of 2 bara, as the single phase and two phase tests were conducted at this pressure. Refer to Appendix B- operating procedures for the riser test facility, for details of how the system pressure was set.

The tests were carried out using a spring–balance to apply known forces to the bend, in the vertical direction, V, and horizontal direction, H, putting the struts in compression (C) and tension (T), as shown in Figure 4.2. Forces were applied for approximately 5 seconds, before returning the applied (spring-balance) force to 0 N. Each test was repeated twice.

NB The range of the applied forces were restricted by the position of the bend (in particular its closeness to the laboratory walls, which affected the tests in the horizontal direction) and the location of the bend, which had to be accessed using a ladder.

The strain-gauged strut signals were recorded using the DAS (having entered the free-hanging calibration factors, as described in Section 4.2.3).

4.3.2 Data Analysis Procedures

4.3.2.1 Isolation Joint Tests

Figures 4.3 and 4.4 show the results from Tests 1 and 2, applied (spring-balance) force in the vertical direction, with the vertical strut in compression and tension, respectively. Figures 4.5 and 4.6 show the results from Tests 3 and 4, applied (spring-balance) force in the horizontal direction, with the horizontal strut in compression and tension, respectively.

NB The screen force, Fs, was the force measured by the strut, shown on the DAS screen.

To analyse the effect of the isolation joints, on the vertical strain-gauged strut readings; the applied (spring-balance) vertical forces were compared to the screen vertical forces. Similarly, for the effect of the isolation joints on the horizontal strain-gauged strut readings, the applied (spring-balance) horizontal forces were compared to the screen horizontal forces. Test 1 is used as an example to show how the data was analysed. In Figure 4.7, four peaks; $FVpeak_{(10)}$, $FVpeak_{(15)}$, $FVpeak_{(20)}$ and $FVpeak_{(25)}$ can be seen. These peaks were due to applied (spring-balance) vertical forces, FV, of 10, 15, 20 and 25N, respectively.

At FVoff, there was no force applied to the bend (FV = 0N) but, Figure 4.7 shows that FVoff was not equal to 0N and that the value of FVoff varied after each applied (spring-balance) force. This was because the strain gauges were not re-zeroed before each test and that FVoff was shown to vary, as the bend did not always return to it's original position when a force was applied (due to the isolation joints and the fact that the bend was not fully isolated, see Section 4.5). For example, at $FVoff_{(25)}$ there was an offset value of ~6N. This 'zero' offset value was subtracted from the peak value, $FVpeak_{(25)}$, so that the screen force seen by the strut, $FVs_{(25)}$, can be determined:

$$FVs_{(25)} = FVpeak_{(25)} - FVoff_{(25)} \qquad (4.g)$$

therefore,

$$FVs_{(x)} = FVpeak_{(x)} - FVoff_{(x)} \qquad (4.h)$$

$$FHs_{(x)} = FHpeak_{(x)} - FHoff_{(x)} \qquad (4.i)$$

Where x represents the applied (spring-balance) force, F.

By using the start and end times of the peak region and the zero region, average values of Fpeak and Foff, were calculated. Using Equations (4.h) and (4.i), values of screen vertical force, FVs, and screen horizontal force, FHs, were determined for Tests 1 to 4. Isolation joint calibration coefficients were then determined by plotting graphs of applied (spring-balance) vertical force versus screen vertical force (Figure 4.8) and of

applied (spring-balance) horizontal force versus screen horizontal force (Figure 4.9). This is described in Section 4.4.

4.3.2.2 Cross-Talk Tests

To analyse the cross-talk effect of the horizontal strut to the vertical strut, the applied (spring-balance) horizontal forces were compared to the corresponding screen vertical forces. Similarly, for the effect of the vertical strut to the horizontal strut, the applied (spring-balance) vertical forces were compared to the corresponding screen horizontal forces. Figure 4.10 shows an example of the corresponding horizontal force, when a vertical force is applied, putting the vertical strut into compression. The same data analysis procedure, as described in Section 4.3.2.1 above, was used to analyse the cross-talk tests and determine values of FVs and FHs.

Cross-talk calibration coefficients were then determined by plotting graphs of applied (spring-balance) horizontal force versus corresponding screen vertical force (Figure 4.11) and of applied (spring-balance) vertical force versus corresponding screen horizontal force (Figure 4.12). This is described in Section 4.4.

4.3.3 Polarity of Force Traces

In Section 4.2.3, the polarity of the free-hanging calibration factor was chosen, so that there was a positive screen force when a strut was in compression and a negative screen force when the strut was in tension. Figures 4.3 to 4.6 show that when the vertical or horizontal strut went into compression, the force went in a positive direction, and when the vertical or horizontal strut went into tension, the force went in a negative direction. Figure 4.13 shows that when 'zero' offset values are accounted for, compression still gives a positive force and tension still gives a negative force.

4.4 Calculation of Isolation Joint and Cross-Talk Calibration Coefficients

From Figure 4.8, the graph of applied (spring-balance) vertical force, FV, versus screen vertical force, FVs:

$$FVs=0.5475FV \tag{4.j}$$

Therefore the isolation joint calibration coefficient in the vertical direction, E_V, is 0.5475.

Similarly from Figure 4.9, the graph of applied (spring-balance) horizontal force, FH, versus screen horizontal force, FHs:

$$FHs=0.9282FH \tag{4.k}$$

Therefore the isolation joint calibration coefficient in the horizontal direction, E_H, is 0.9282.

From Figure 4.11, the graph of applied (spring-balance) horizontal force, FH, versus corresponding screen vertical force, FVs:

$$FVs = 0.0462FH \tag{4.l}$$

Therefore the cross-talk calibration coefficient (horizontal gauge to vertical gauge), C_{HV}, is 0.0462.

From Figure 4.12, the graph of applied (spring-balance) vertical force, FV, versus corresponding screen horizontal force, FHs:

$$FHs = 0.1355FV \tag{4.m}$$

Therefore the cross-talk calibration coefficient (vertical gauge to horizontal gauge), C_{VH}, is 0.1355.

Applying isolation joint and cross-talk effects to the actual forces on the bend, letting ' denote actual force:

$$FVs = E_V FV' + C_{HV} FH' \tag{4.n}$$

similarly,

$$FHs = E_H FH' + C_{VH} FV' \tag{4.o}$$

Please refer to Appendix D- derivation of screen force to actual force, for the detailed derivation of Equations (4.n) and (4.o).

FV ' and FH ' can be deduced by substitution in Equations (4.n) and (4.o):

Hence, the actual vertical force, FV ', is given by:

$$FV' = \frac{\left(FHs - \frac{FVsE_H}{C_{HV}}\right)}{C_{VH} - \frac{E_V E_H}{C_{HV}}} \tag{4.p}$$

The actual horizontal force, FH ', is given by:

$$FH' = \frac{\left(FHs - \frac{FVsC_{VH}}{E_V}\right)}{E_H - \frac{C_{HV}C_{VH}}{E_V}} \tag{4.q}$$

Substituting in the calibration coefficients to Equations (4.p) and (4.q):

$$FV' = \frac{\left(FHs - \frac{FVs * 0.9282}{0.0462}\right)}{0.1355 - \frac{0.5475 * 0.9282}{0.0462}}$$

$$FV' = (FHs - (FVs * 20.09)) / -10.86 \qquad (4.r)$$

$$FH' = \frac{\left(FHs - \frac{FVs * 0.1355}{0.5475}\right)}{0.9282 - \frac{0.0462 * 0.1355}{0.5475}}$$

$$FH' = (FHs - (FVs * 0.25)) / 0.92 \qquad (4.s)$$

NB Equations (4.r) and (4.s) are used in the two columns, FV ' and FH ', in a MS Excel master spreadsheet to calculate the actual vertical and horizontal forces on the bend, from the screen vertical and horizontal forces, FVs and FHs.

4.5 Discussion

4.5.1 Isolation Joint Tests

From Figure 4.8, the graph of applied vertical force versus the screen vertical force, the force reading from the vertical strain-gauged strut was 55% of the vertical force being applied to the bend. Figure 4.9, the graph of applied horizontal force versus the screen horizontal force, the horizontal strut read 93% of the horizontal force being applied to the bend. Assuming that the behaviour of the isolation joints were identical before being installed on the bend, then the set-up of the bend, when the isolation joints were installed, must have accounted for the difference in force readings.

The aim of the isolation joints was to isolate the bend from the surrounding pipework. The results of the isolation joint tests showed that the characteristics of the isolation joints were not the same when installed on the bend (the readings from the vertical strain-gauged strut were lower, compared to the horizontal strut). In the case of the vertical strut in particular, as the applied force was not equal to the force seen by the strut, this showed that the bend was not fully isolated from the surrounding pipework. The bend was less isolated in the vertical direction than the horizontal direction, due to the weight of the riser, induced during installation, as the riser was not completely supported. This suggested that the weight of the riser stretched the rubber isolation joint, therefore making it stiffer and more resistant to any movement.

As the bend was not fully isolated, the effect of the hydrostatic force due to the riser filling with liquid, was registered by the strain-gauged struts, during the single phase and two phase tests (described in Chapter 5).

4.5.2 Cross-Talk Tests

Figures 4.11 and 4.12 show the cross-talk between the horizontal strut to the vertical strut and the vertical strut to the horizontal strut, respectively. When applying a horizontal force, the vertical strut saw 5% of the applied force and when applying a vertical force, the horizontal strut saw 14% of the applied force. Hence, there was less cross-talk between the horizontal strut to the vertical strut. This was expected, as the bend was less isolated in the vertical direction, as shown by the isolation joint tests. Therefore a larger force needed to be applied in the horizontal direction, to counteract the static force.

4.6 Summary

This Chapter detailed the procedures used to calibrate the strain-gauged struts, which measured the vertical and horizontal forces on the bend. Due to the isolation joints and the cross-talk effects between the struts, it was necessary that the strain-gauged struts were calibrated, so that the readings from the struts could be quantified, in terms of calibration coefficients. These calibration coefficients were applied to the screen strain-gauged strut readings, to determine the actual vertical and horizontal forces on the bend.

Even though metal scaffolds supported the pipework surrounding the bend, the isolation joint tests showed that the bend was not fully isolated. The bend was less isolated in the vertical direction, compared to the horizontal direction, due to the riser not being fully supported. Therefore, the struts were not only measuring the dynamic force (due to slug flow around the bend), but also the hydrostatic force (due to the weight of liquid in the riser).

The following Chapter describes the lazy 'S' riser single phase and two phase tests.

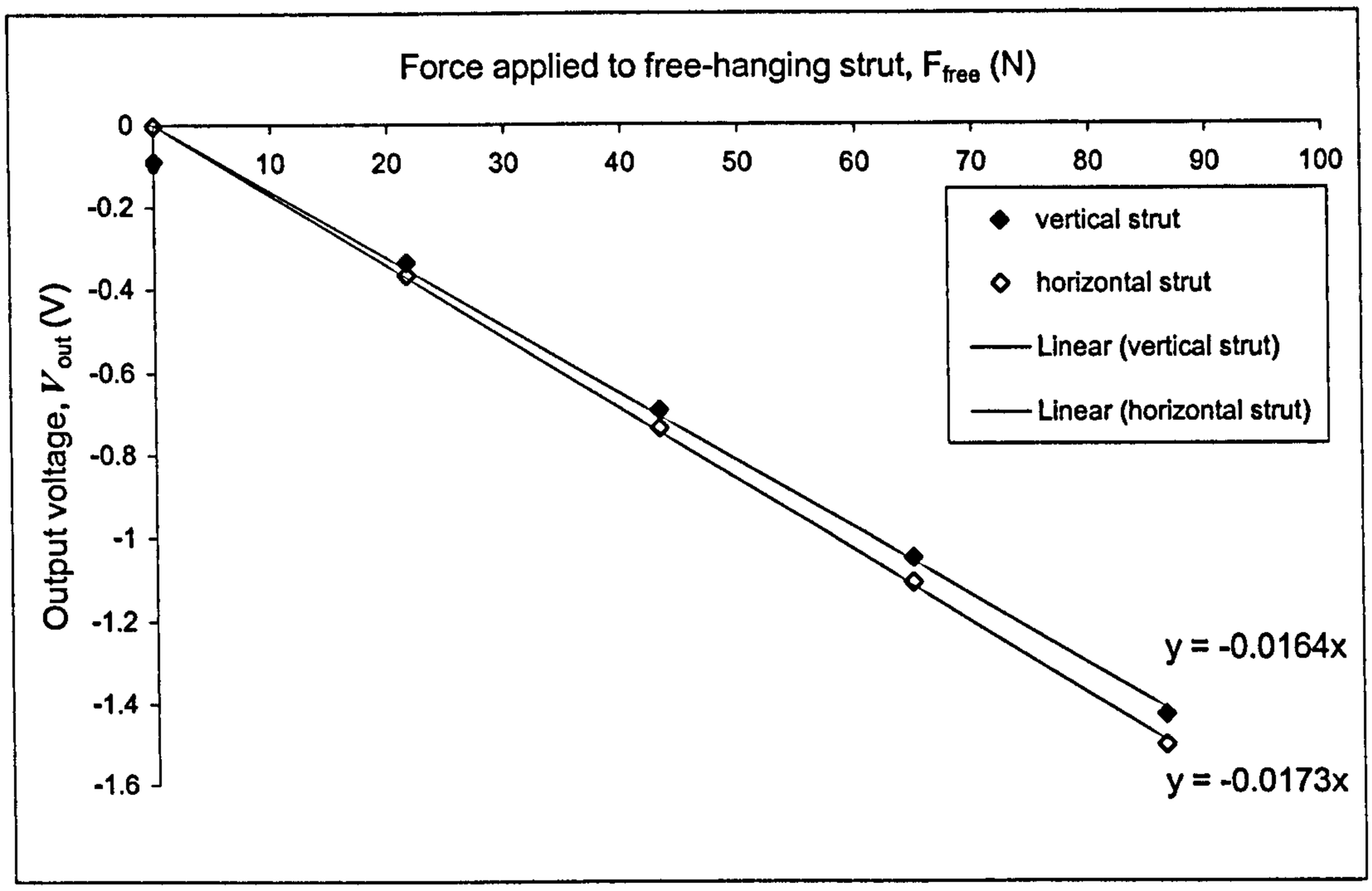

Figure 4.1 Free-hanging strain-gauged strut calibration

Test Number	Applied Force Condition (N)	Applied Force Range (N)
1	V, (C)	0-40
2	V, (T)	0-25
3	H, (C)	0-25
4	H, (T)	0-20

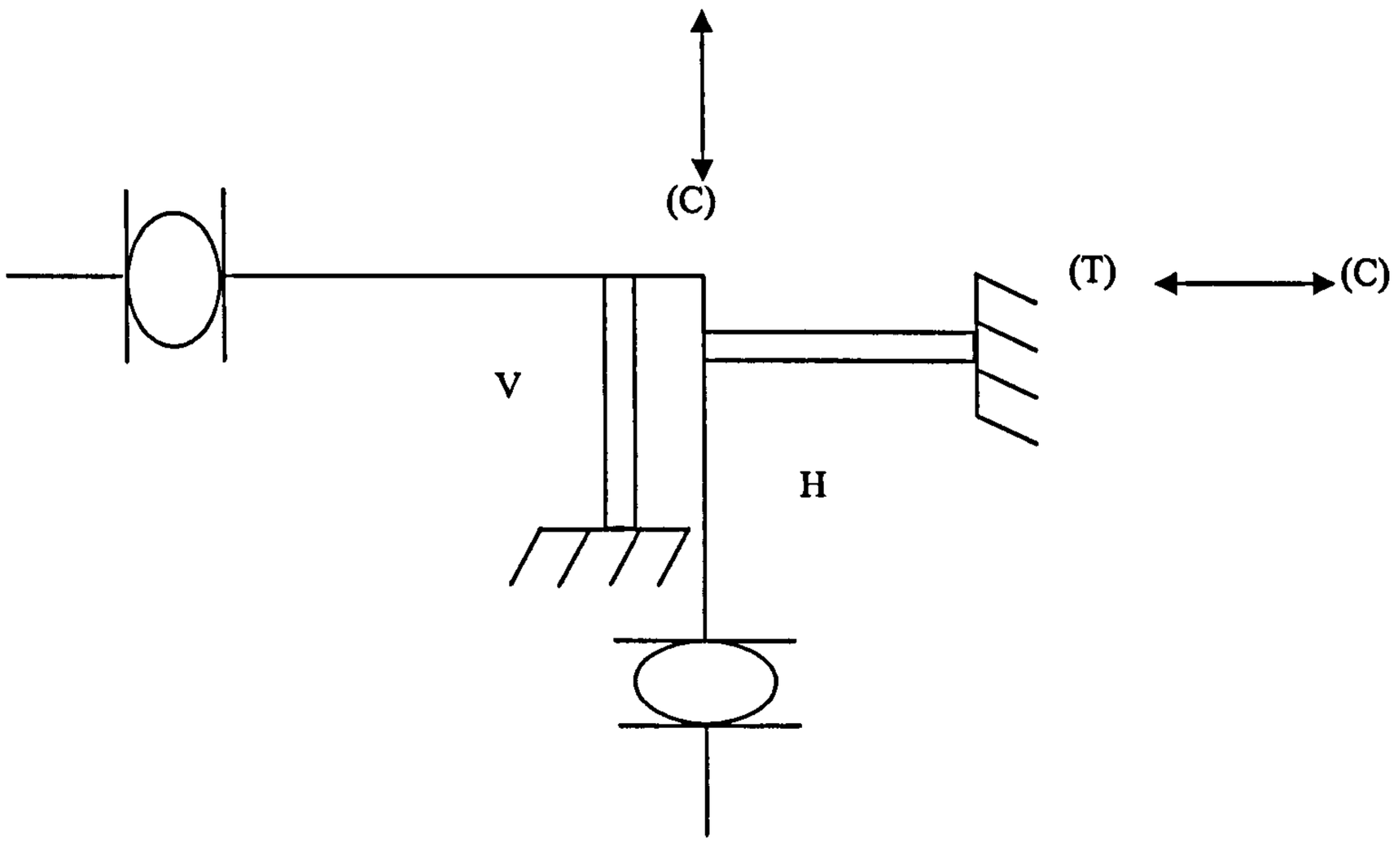

Figure 4.2 Isolation Joint and Cross-Talk Tests

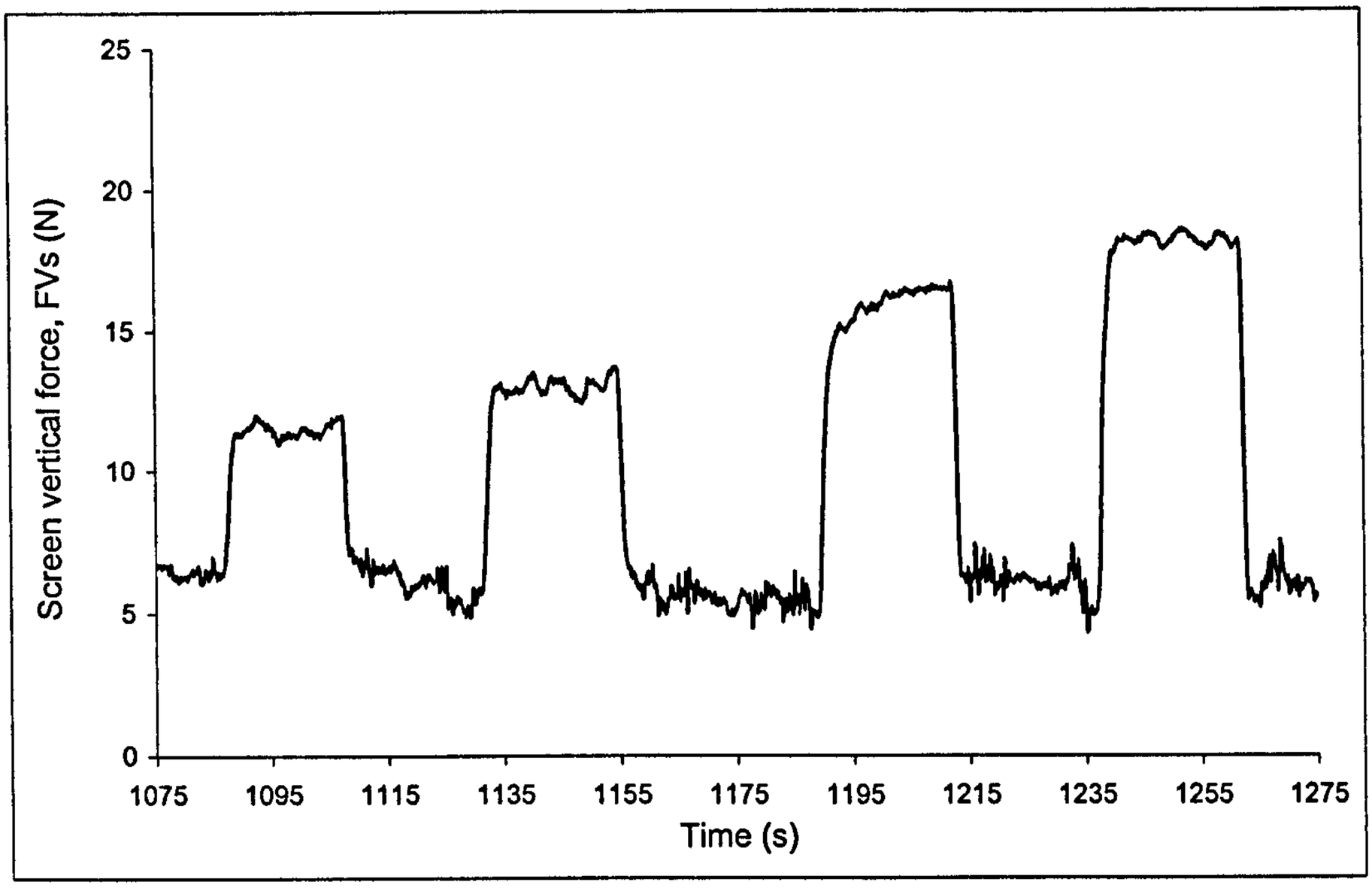

Figure 4.3 Isolation joint test 1: applied (spring-balance) force in vertical direction, vertical strut in compression

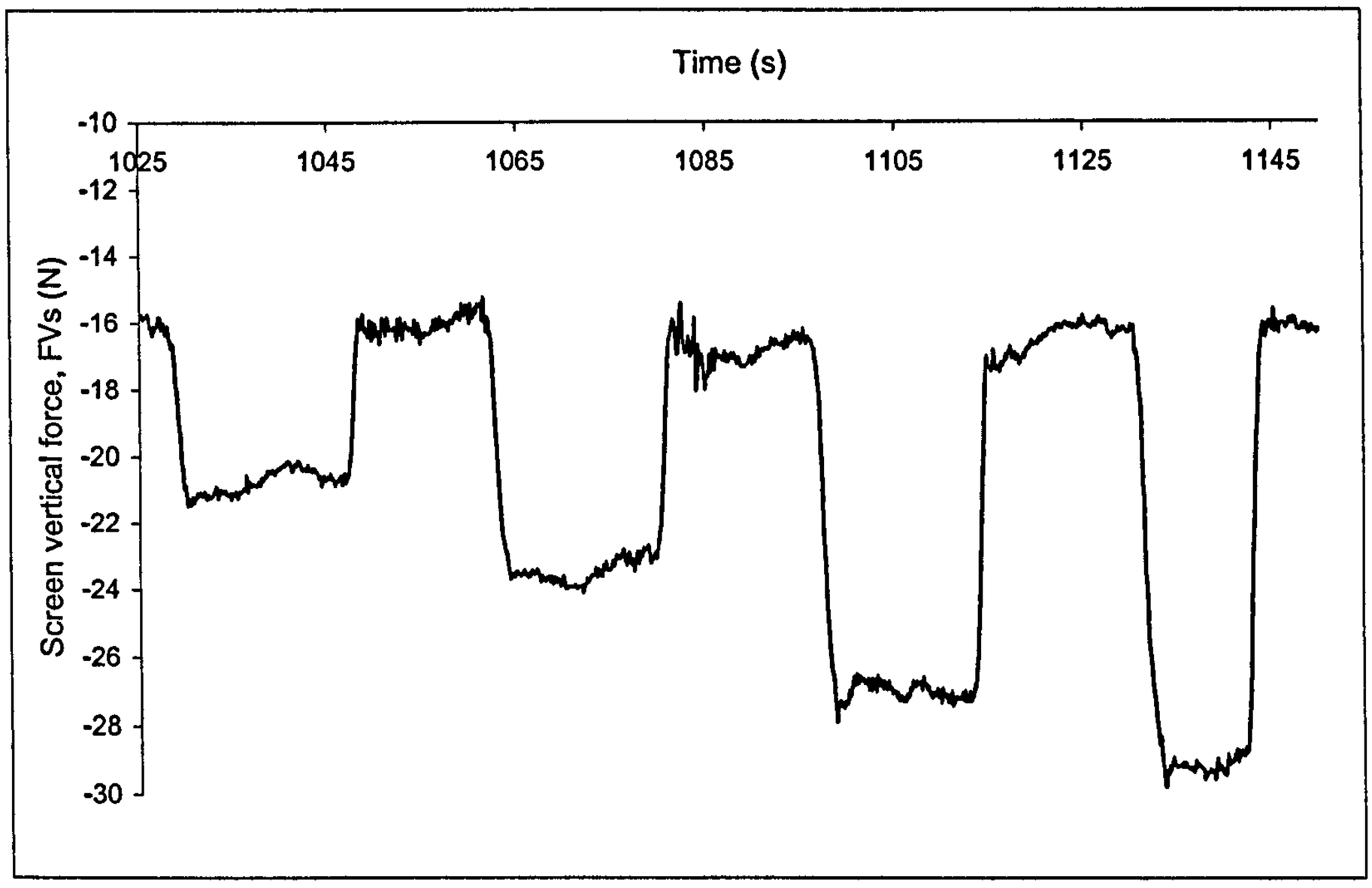

Figure 4.4 Isolation joint test 2: applied (spring-balance) force in vertical direction, vertical strut in tension

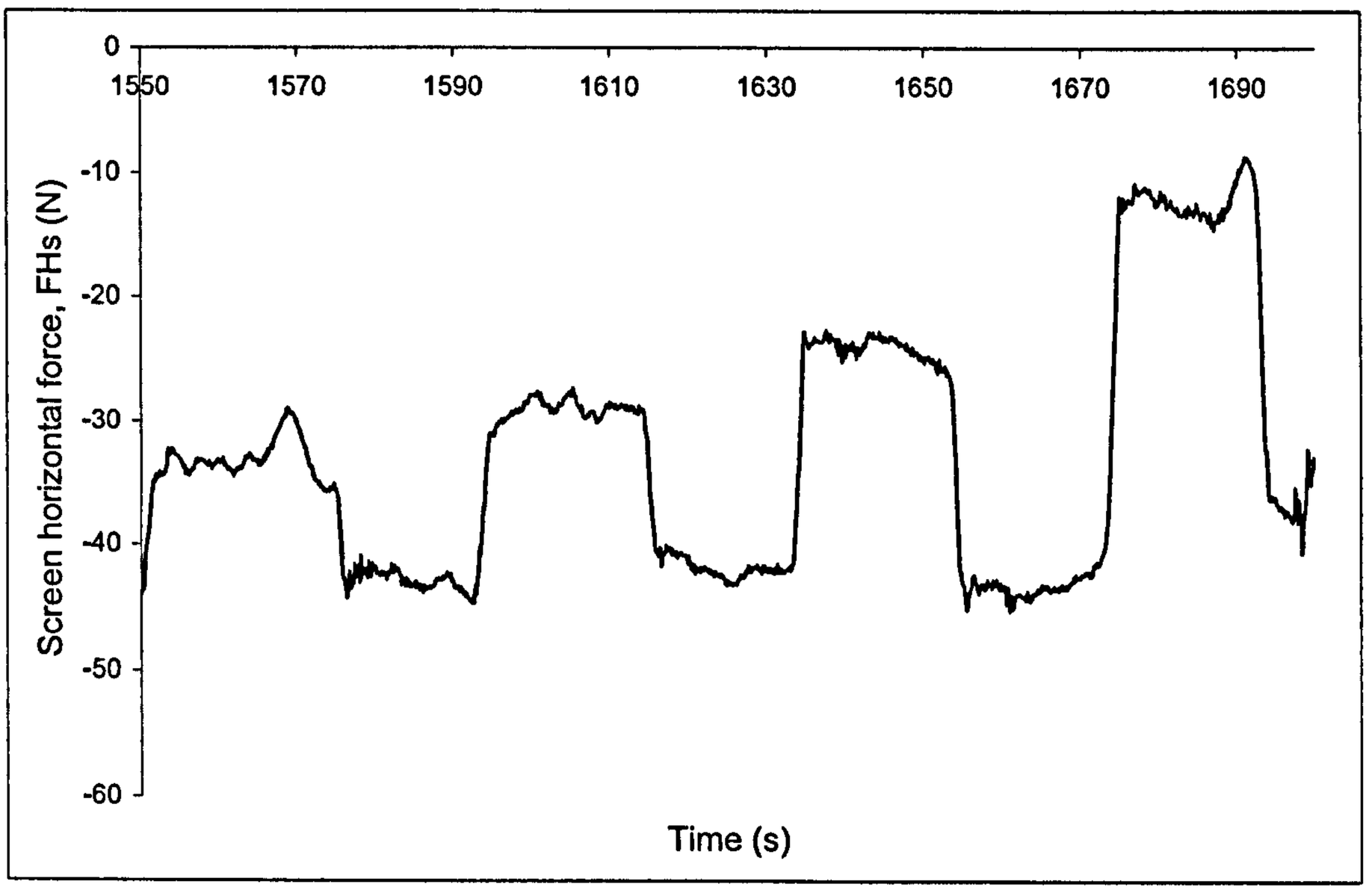

Figure 4.5 Isolation joint test 3: applied (spring-balance) force in horizontal direction, horizontal strut in compression

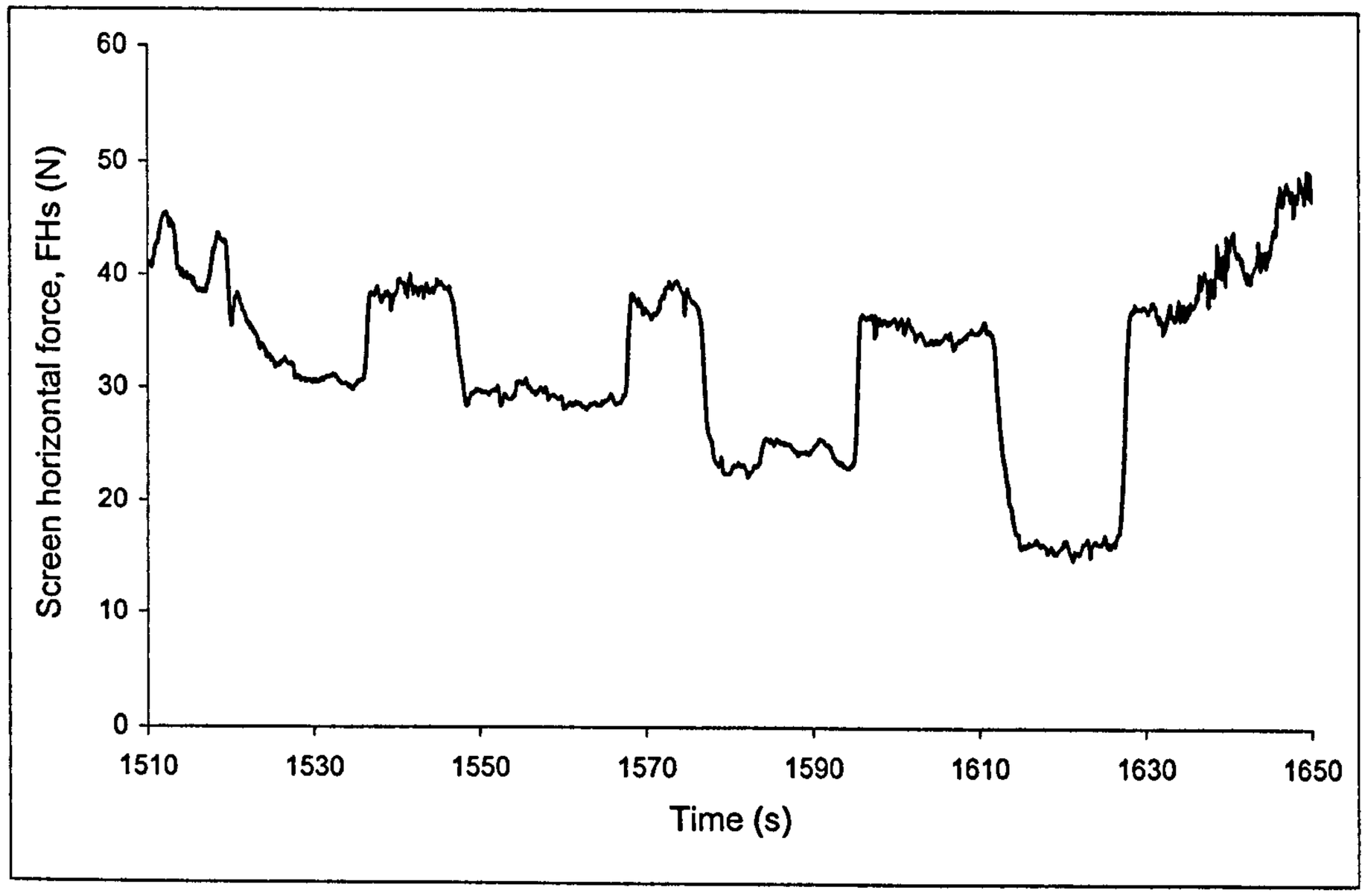

Figure 4.6 Isolation joint test 4: applied (spring-balance) force in horizontal direction, horizontal strut in tension

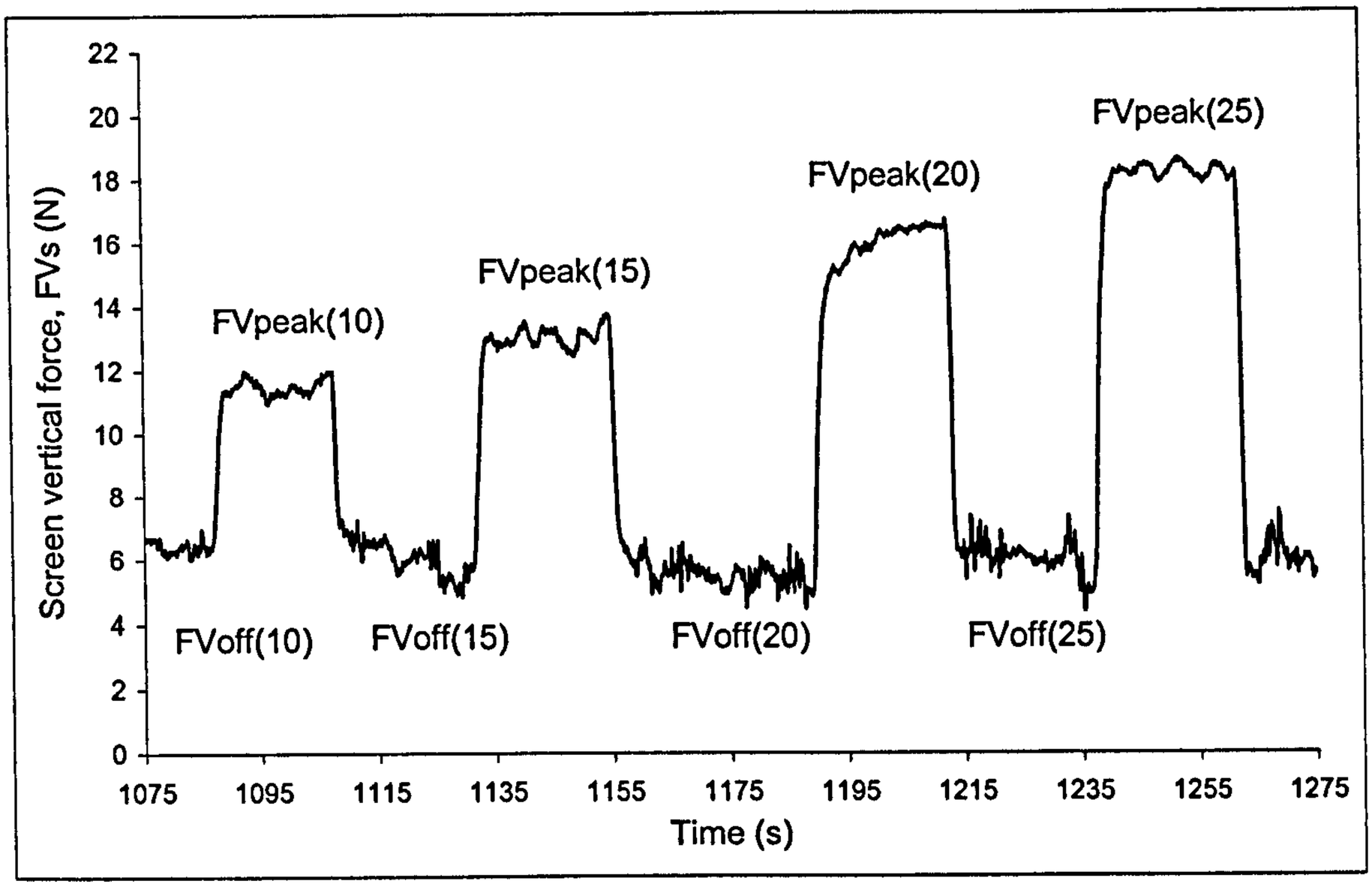

Figure 4.7 Example of isolation joint test data analysis procedure

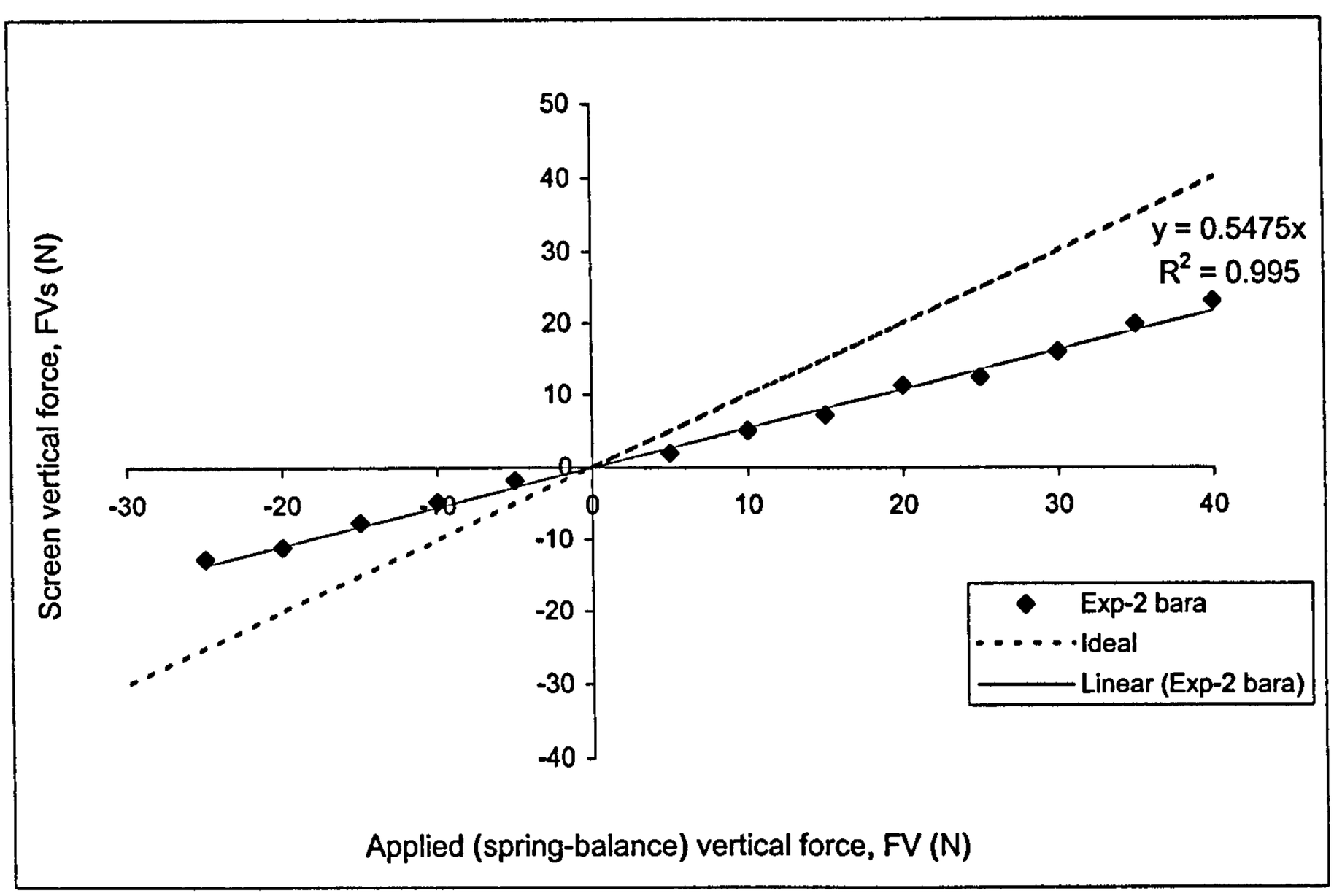

Figure 4.8 Determination of isolation joint calibration coefficient (vertical strut)

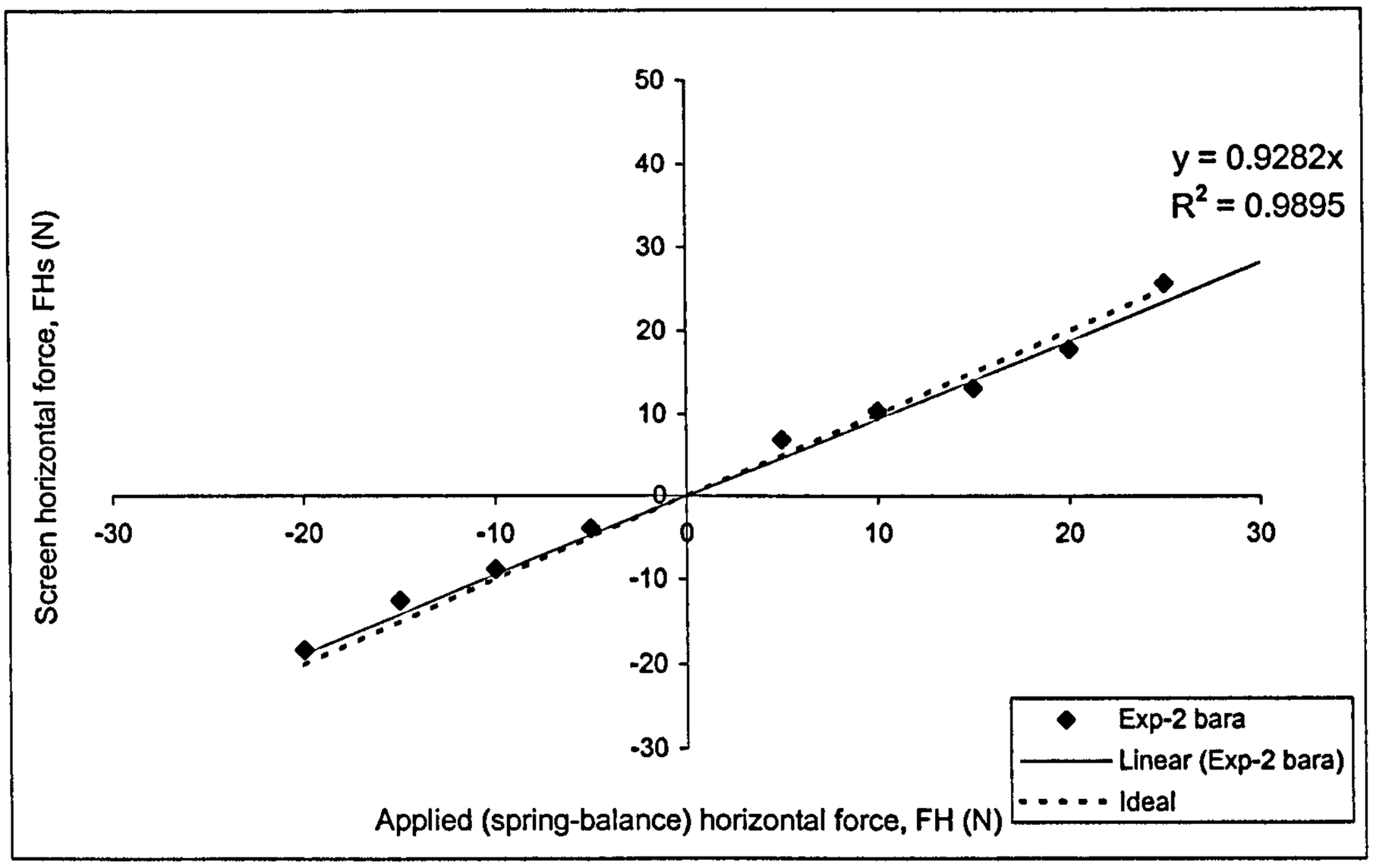

Figure 4.9 Determination of isolation joint calibration coefficient (horizontal strut)

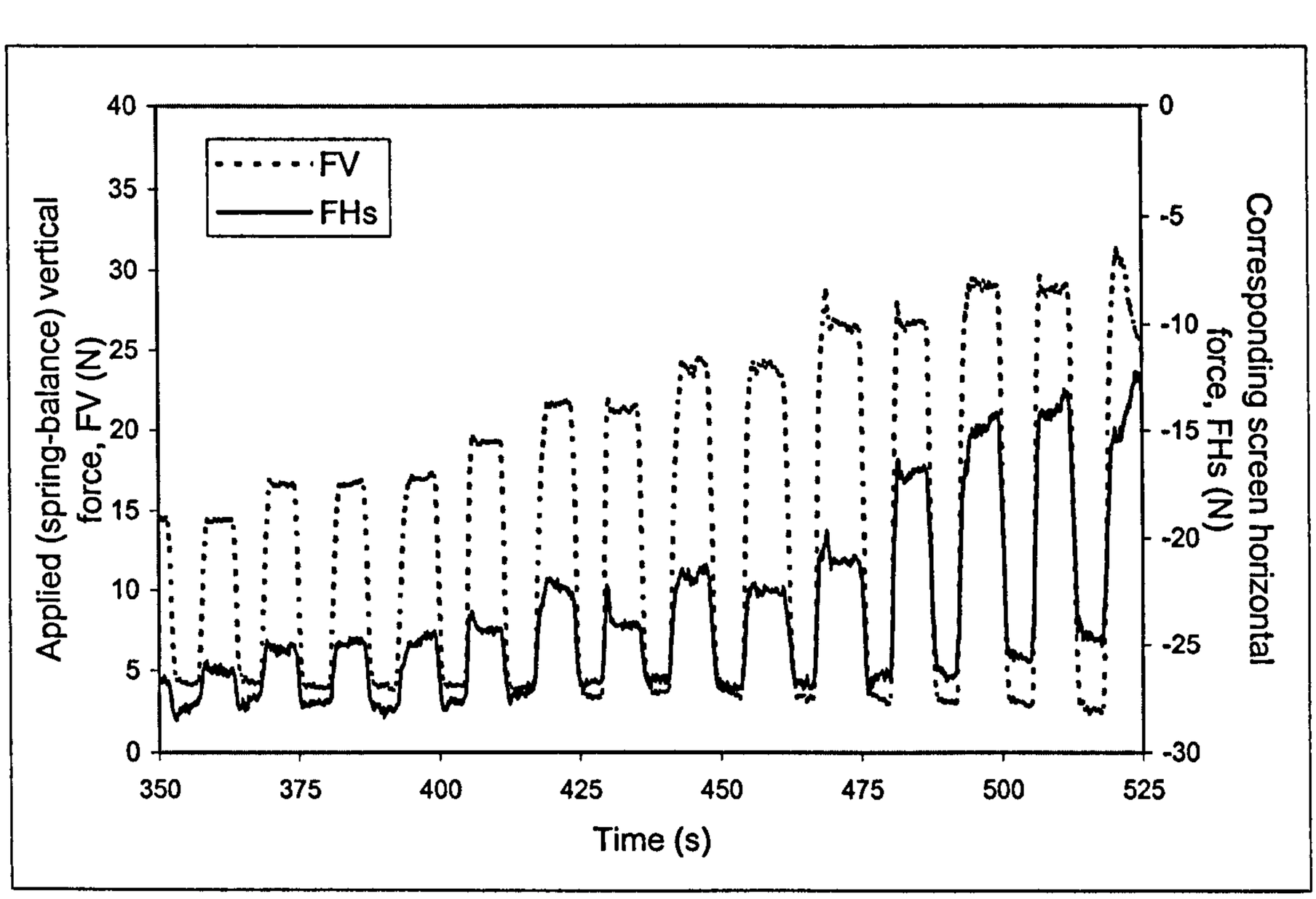

Figure 4.10 Example of cross-talk (vertical strut to horizontal strut)

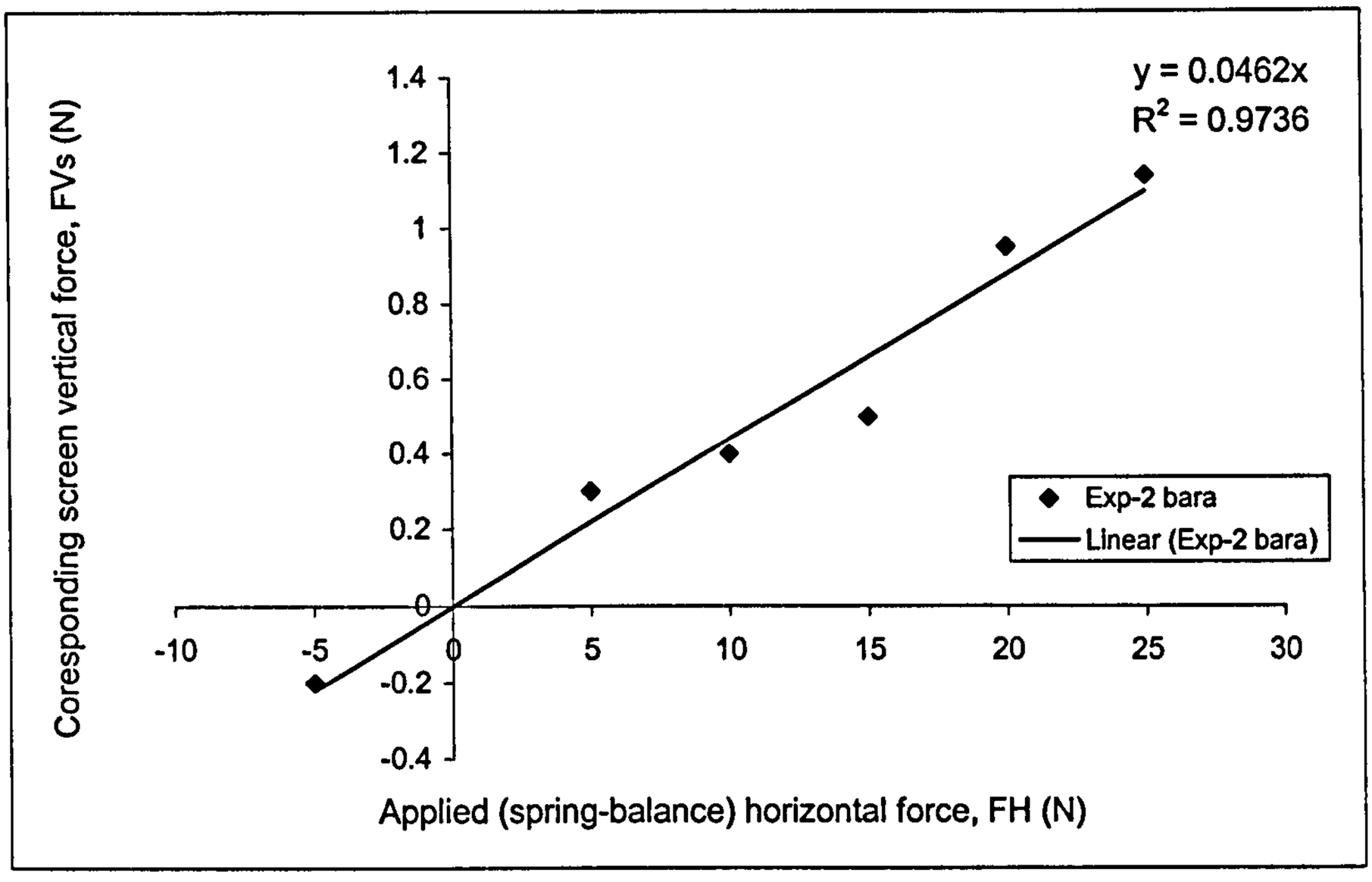

Figure 4.11 Determination of cross-talk calibration coefficient (horizontal strut to vertical strut)

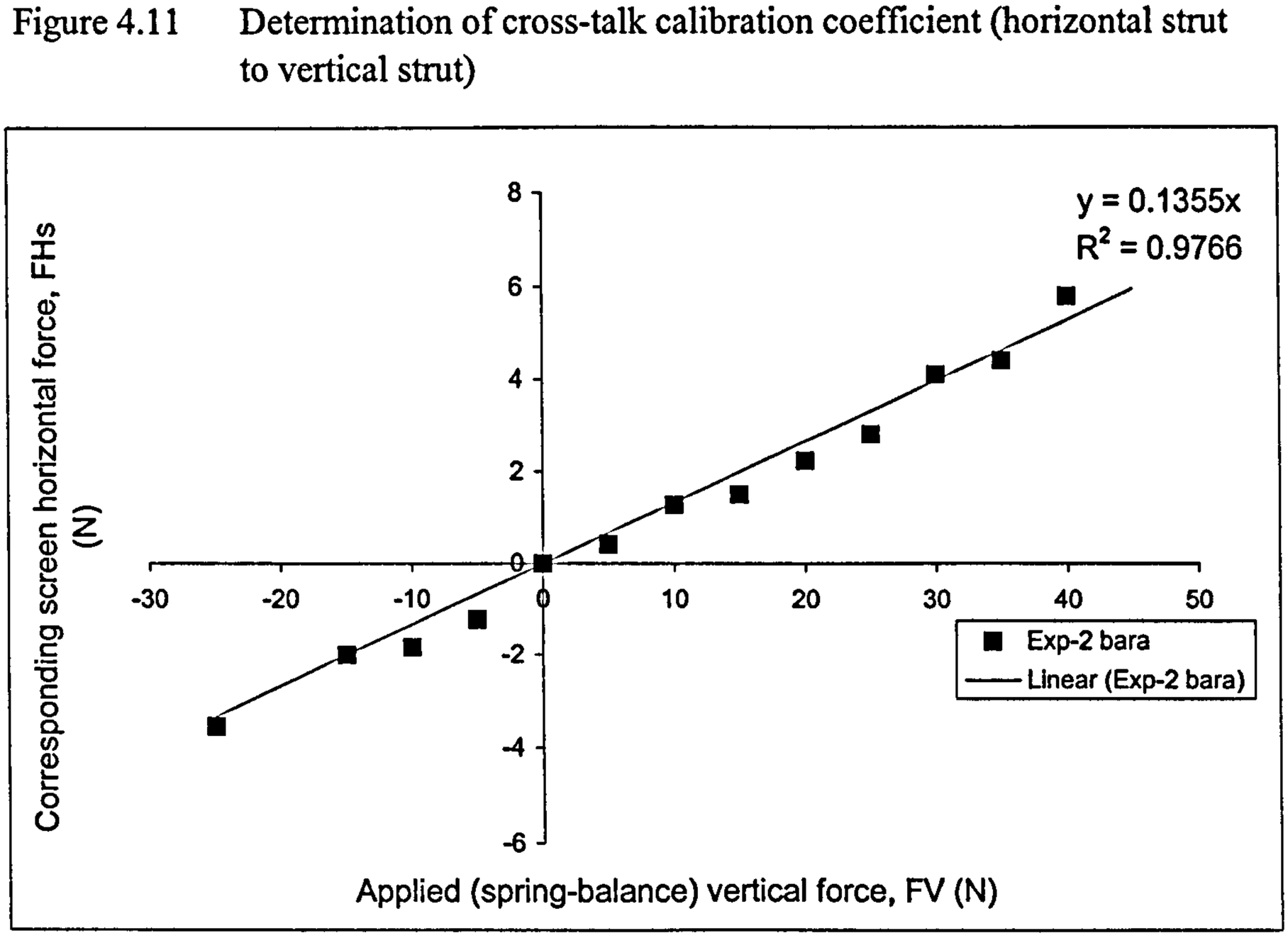

Figure 4.12 Determination of cross-talk calibration coefficient (vertical strut to horizontal strut)

Force Traces in Compression

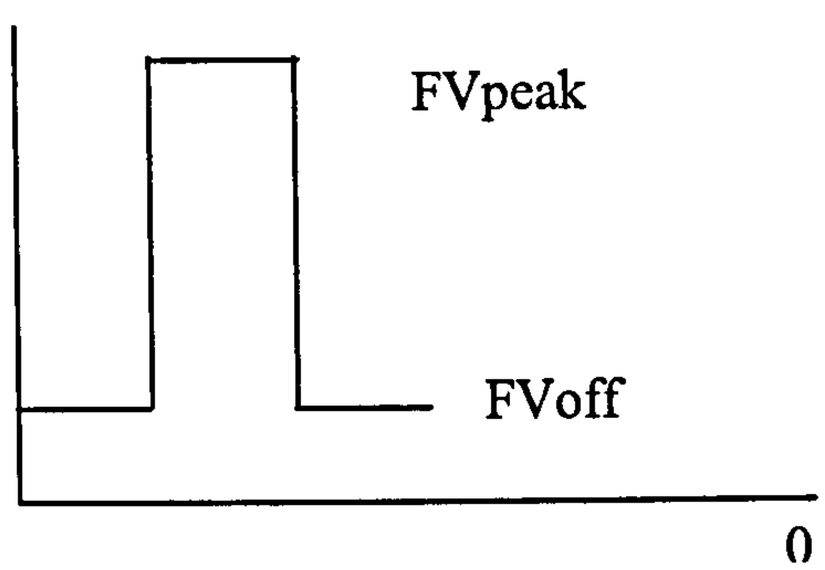

FVpeak – FVoff ⇒ +ve

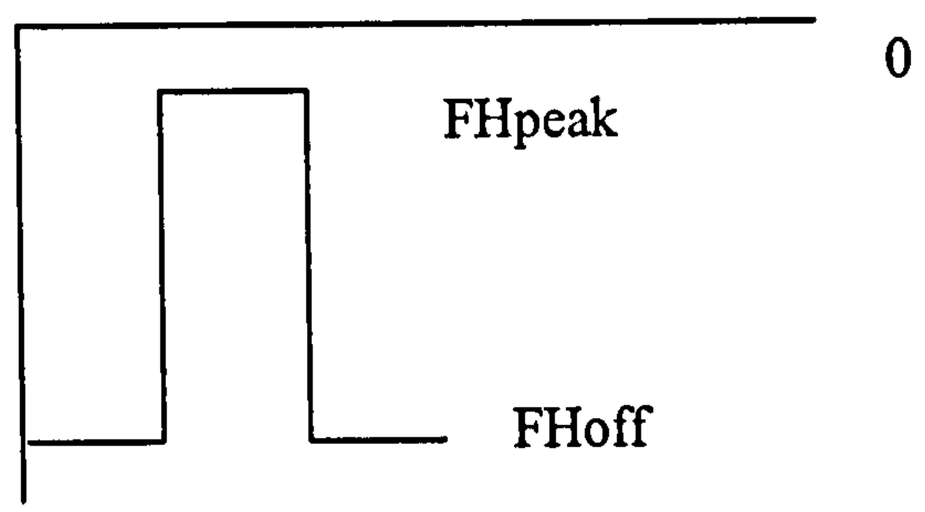

FHpeak – FHoff ⇒ +ve

Force Traces in Tension

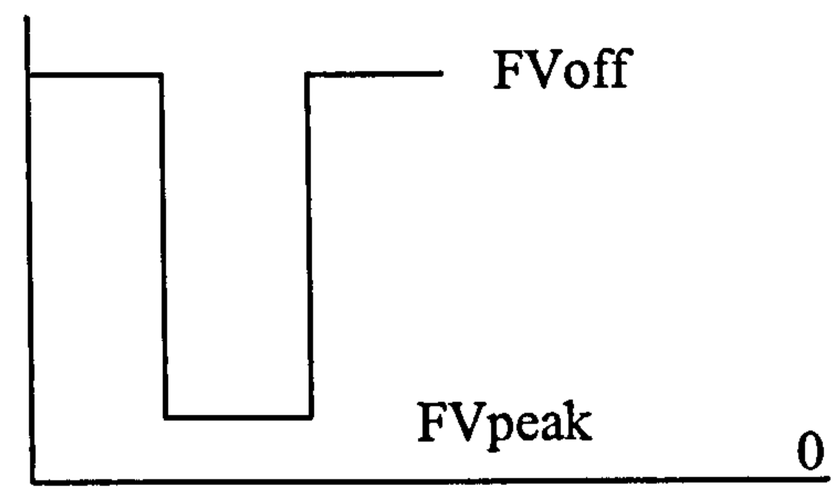

FVpeak – FVoff ⇒ -ve

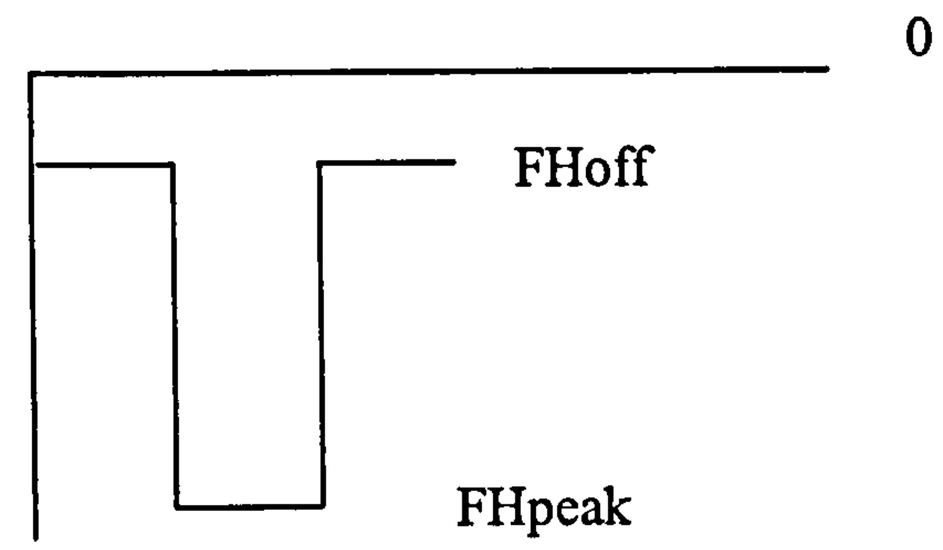

FHpeak – FHoff ⇒ -ve

Figure 4.13 Polarity of force traces

CHAPTER 5- LAZY 'S' RISER SINGLE PHASE AND TWO PHASE TESTS

5.1 Introduction

This Chapter describes the lazy 'S' riser single phase and two phase tests.

The objective of the single phase tests was to help to understand the two phase data, in particular, the pressure and force versus time traces, during the slug build-up and slug production stages of the severe slugging cycle (described in Chapter 2, Section 2.2.2).

To investigate the forces on the bend due to liquid only, two sets of tests were carried out:

(i) The pipeline-riser was filled at different liquid flowrates to measure the forces on the bend due to the slug front. These tests simulated the slug build-up stage.

(ii) To simulate the slug production stage, a steady liquid flowrate was passed through the pipeline-riser. The liquid flowrate was increased and decreased to determine the loading on the bend, due to momentum change.

The objectives of the two phase tests were; (i) to investigate severe slugging characteristics which included, slug lengths and cycle, build-up, production, bubble penetration and gas blowdown times; (ii) to determine the liquid inventory in the riser downward limb during severe slugging, and, (iii) to model the forces on a bend during the slug build-up, production and bubble penetration and gas blowdown stages of the severe slugging cycle.

The two phase tests covered a range of flow regimes, but concentrated on collecting data within the severe slugging region.

The single phase and two phase tests were carried out at a system pressure of 2 bara.

5.2 Test Programme

Sections 5.2.1 and 5.2.2 describe test procedures and include brief descriptions of how system pressure and flowrates were set. These operating procedures are described in more detail in Appendix B- operating procedures for the riser test facility.

5.2.1 Single Phase Tests

5.2.1.1 Test Matrix

BHR Group Limited[14] carried out previous experimental studies using the riser test facility described in Chapter 3, but with a 10m high catenary riser, in place of the lazy 'S' shaped riser. At 2 bara, severe slugging occurred at superficial liquid velocities less than 0.5m/s and during the bubble penetration and gas blowdown stages of the severe

slugging cycle, slug velocities of between 1.7 to 2.5m/s were observed. Therefore, these velocities were reproduced in the single phase tests.

5.2.1.2 Build-Up Stage Simulation Test Procedure

The pressure was set initially by adjusting a pressure control valve on the three-phase separator. Gas was then supplied to the flow loop, by a compressor, and the pressure in the system increased, until it reached the set pressure of 2 bara (this was checked using the reading of the pressure transducer, P9, on the 'pipeline-riser' screen of the DAS, refer to Figure 3.12). The compressor was not shutdown, as high gas flowrates were used to blow the flow loop dry between each build-up simulation test. To prevent the flow of gas into the flow loop, valves VI21, VI19 and VI20, shown in Figure 3.1, were closed.

Water was delivered into the flow loop using a positive displacement pump, P3. The liquid velocity was set (the flowrates and velocities were shown on the 'meters' screen of the DAS, Figure 3.11), prior to the data being recorded. When the flow loop had filled (the 'pipeline-riser' screen, Figure 3.12, showed that all the conductance probes were on) and the velocity had stabilized, the pump was switched off. Valves VI21, VI19 and VI20 were then opened to dry the flow loop. The conductance probe readings were checked, to ensure that no liquid was left in the flow loop i.e. conductance probes were off.

When the flow loop was dry, the recording of the data was started by using the 'data file control' screen, Figure 3.10. The water pump was switched on and the liquid filled the flow loop at the previously set velocity. The progression of the liquid was tracked by observing the conductance probe readings. The recording was stopped 1 minute after the riser had completely filled with liquid. The next test velocity was then set-up. This procedure was repeated for a range of velocities, 0.2 to 2.0m/s.

5.2.1.3 Production Stage Simulation Test Procedure

The pressure was set, as in Section 5.2.1.2, by adjusting the pressure control valve on the three-phase separator. The compressor was then shutdown.

The production stage simulations were recorded as one continuous test. Therefore, for these tests the water flowrate was measured using the large electromagnetic flowmeter, FL2, as it had a greater range of flowrates available (0-6.25m/s) compared to the smaller flowmeter, FL1, (0-0.84m/s).

The water pump was switched on and starting with a low velocity, a velocity of 0.5m/s was set. When the flow loop, including the horizontal section into the separator, were filled the flow was left to stabilize. Recording of the data was then started. The flow was left at this velocity, 0.5m/s, for 2 minutes. The velocity was then increased in approximately 0.5m/s steps, up to 3.0m/s; again each velocity was left for 2 minutes. The velocity was then decreased, until the water in the tank reached its minimum, $2m^3$.

5.2.2 Two Phase Tests

5.2.2.1 Test Matrix

The test matrix for the two phase tests, was based on previous experimental studies[34] using the riser test facility described in Chapter 3. The provisional test matrix covered a range of flow regimes (severe slugging, transitional severe slugging, oscillation, slug flow) but concentrated on collecting data within the severe slugging regions.

5.2.2.2 Test Procedure

Using the 'calibration screen' of the DAS, Figure 3.9, the appropriate gas and liquid flowmeters were selected (FG1/FG2, FL1/FL2), whose operating range suited the test conditions. When the set system pressure of 2 bara had been reached, the gas control valve, VI21, refer to Figure 3.1, was adjusted to give the required flowrate. Water was then delivered into the flow loop and the required liquid flowrate was set. The flowrates and velocities were checked using the 'meters' screen of the DAS, Figure 3.11. The flow conditions were allowed to reach a steady state (i.e. for severe slugging to adopt repeatable cycles). The data was then recorded using the 'data file control' screen of the DAS, Figure 3.10. For severe slugging and transitional severe slugging, the data was recorded for 25 minutes and for oscillation and slug flow, the recording time was 15 minutes.

The test programme consisted of 28 test points, with superficial gas velocities ranging from 0.07 to 1.12m/s and superficial liquid velocities from 0.02 to 0.95m/s. All tests were performed at a system pressure of 2 bara.

5.3 Description of Observed Flow Regimes

The flow pattern map showing all the test points is shown in Figure 5.1. Two types of severe slugging phenomenon were identified, severe slugging 1 and severe slugging 1b (the observed severe slugging boundary is represented by a bold line). In addition to severe slugging 1 and 1b, a severe slugging transitional region, SS2 was also observed. Outside the severe slugging region oscillation flow and slug flow were also found.

5.3.1 Severe Slugging

Two types of severe slugging were observed, severe slugging 1 and severe slugging 1b. These severe slugging flow regimes were categorised based on the analysis of the following:

- The pressure difference over the riser
- Liquid production from the riser, based on a liquid mass balance on the separator
- Slug length
- Liquid hold-up at the base of the riser, measured using a gamma densitometer.

5.3.1.1 Severe Slugging 1 (SS1)

Based on the observations by Tin[17, 22] and Schmidt[13], severe slugging 1 was described by:

- The pressure difference over the riser, during the slug production stage, was equal to or greater than the hydrostatic head of the riser.
- The slug length was greater than one riser height.
- There were distinct times of no liquid production and pure liquid production within each cycle.
- The riser base was blocked by liquid during the build-up and production stages.

Figure 5.2 shows a typical pressure over the riser versus time trace, for the severe slugging 1 (SS1) cycle.

5.3.1.2 Severe Slugging 1b (SS1b)

Severe slugging 1b was distinguished from severe slugging 1 by:

- The slug length was just greater than one riser height.
- No slug production stage or short production time.
- No liquid backed-up the pipeline during the slug build-up stage.

Figure 5.3 shows a typical pressure over the riser versus time trace, for the severe slugging 1b (SS1b) cycle.

5.3.2 Transitional Severe Slugging

5.3.2.1 Severe Slugging 2

Severe slugging 2 was described by:

- The slug length was less than one riser height.
- No slug production stage.
- No liquid backed-up the pipeline during the slug build-up stage.
- Exhibited characteristics of intermediate cycles (pressure increments in the slug build-up stage of the cycle) on the lower limb.
- Occurred at a higher range of flowrates compared to SS1.

Figures 5.4 and 5.5 show typical pressure over the riser versus time traces, for the severe slugging 2 cycle (SS2) and severe slugging 2 cycle with intermediate cycles on the lower limb (SS2i), respectively.

5.3.3 Oscillation Flow and Normal Slug Flow

The oscillation and normal slug flow regimes were based on the analysis of:

- Pressure difference over the riser
- Liquid density at the base of the riser.

Oscillation flow was distinguished from normal slug flow, as pressure difference over the riser was higher and slug frequency was lower, with oscillation flow.

Figure 5.6 shows a typical pressure difference over riser versus time trace, during the oscillation flow regime.

For oscillation flow, slug frequencies of 0.02Hz were observed, with the pressure over the riser varying by 0.6 bar.

Figure 5.7 shows a typical pressure difference over riser and density versus time trace, for normal slug flow.

The riser base density trace showed the sequence of high density liquid slugs followed by a bubble/film region. The frequency of these slugs was approximately 0.14Hz. The pressure trace showed a variation in pressure of each slug of 0.35 to 0.4 bar, showing that there was a regular progression of slugs through the riser.

5.4 Data Analysis Procedures

5.4.1 Analysis of Force Data- Single Phase Tests

5.4.1.1 Slug Build-Up and Production Simulations

Figure 5.8 summarises the pressure over the riser versus time and resultant force versus time traces, observed in the build-up and production simulations.

The pressure versus time trace was divided into two regions; (i) a build-up region, where the pressure over the riser increased as the riser filled with liquid and (ii) a slug production region. In this region the liquid had reached the top of the riser and was passing around the bend and along the horizontal section of pipeline, into the separator. The pressure over the riser was at a maximum.

As liquid started to accumulate at the base of the riser, an offset force was observed. As explained in Chapter 4, Section 4.3.2.1, this offset force was equivalent to a force of 0N.

A peak in the force, FR'pk, was due to the liquid impacting upon the bend. This peak force was a combination of the hydrostatic force, $FR'bu_{hy}$, (due to weight of liquid in the riser), the dynamic force, $FR'bu_{dy}$, as the liquid front hit the bend and the 'zero' offset, FR'off.

As the liquid passed around the bend and into the separator, the force on the bend decreased and began to stabilize. The forces on the bend at this stage were due to the hydrostatic force, FR'p_{hy}, (due to the weight of liquid in the riser and the horizontal section), dynamic force, FR'p_{dy}, as the slug passed around the bend and the 'zero' offset, FR'off.

The following equations were used to determine the resultant forces on the bend, during the build-up and production stages.

Resultant force during build-up stage:

$$FR'bu_{dy,\,hy} = FR'bu_{hy} + FR'bu_{dy} = FR'pk - FR'off \qquad (5.a)$$

Resultant force during production stage:

$$FR'p_{dy,\,hy} = FR'p_{hy} + FR'p_{dy} = FR'p - FR'off \qquad (5.b)$$

The hydrostatic force was extrapolated from the graph of resultant dynamic and hydrostatic force versus liquid velocity, v_L (liquid velocity at the outlet of the riser, based on the liquid mass balance, Chapter 3, Section 3.3.6.2), by assuming that at v_L = 0m/s, the force on the bend was due to hydrostatic force only.

5.4.2 Analysis of Force Data- Two Phase Tests

5.4.2.1 Slug Build-Up Stage

From the single phase build-up simulation tests, referring to Equation (5.a), the force on the bend was described by:

$$FR'bu_{dy,\,hy} = FR'bu_{hy} + FR'bu_{dy} = FR'pk - FR'off \qquad (5.c)$$

The single phase build-up simulations showed that at low liquid velocities, the force on the bend was dominated by the FR'$_{hy}$ term. The single phase tests were performed at liquid velocities ranging from 0.23-2.06m/s, whereas for the severe slugging tests, mixture velocities of 0.14-0.59m/s were observed. Due to these low velocities, the single phase data analysis procedure was not suitable for the severe slugging tests, as the dynamic force was too small to measure, hence Equation (5.c) becomes:

$$FR'pk - FR'off = FR'_{hy} \qquad (5.d)$$

Therefore, an alternative method was used to determine the dynamic force on the bend, during the build-up stage of the severe slugging cycle.

Taking the time at which the liquid front reached probes L9 and L10 (located nearest to the bend), as t_9 and t_{10}, respectively, then the time taken for the liquid front to travel the 0.5m between L9 and L10 is given by:

$$\Delta t_{9-10} = t_{10} - t_9 \qquad (5.e)$$

The distance between L10 and the bend is 0.9m, so the time at which the liquid front would hit the bend:

$$t_{bend} = \Delta t_{9-10} \frac{0.9}{0.5} + t_{10} \qquad (5.f)$$

To calculate the resultant dynamic force, FR'_{dy}, referring to Figure 5.9, using the time references above, the resultant force trace can be extrapolated (as shown by the dashed line) to get the resultant force on the bend, FR'_{bend} at time t_{bend}.

From Equation (5.d), the resultant hydrostatic force is described by:

$$FR'_{hy} = FR'pk - FR'off \qquad (5.g)$$

Using the results from the extrapolation:

$$FR'_{hy} + FR'_{dy} = FR'_{bend} - FR'off \qquad (5.h)$$

Substituting Equation (5.g) into (5.h) and rearranging, the resultant dynamic force on the bend during the build-up stage is:

$$FR'_{dy} = FRbu'_{dy} = FR'_{bend} - FR'pk \qquad (5.i)$$

5.4.2.2 Bubble Penetration and Gas Blowdown Stage

Figures 5.10 and 5.11 show a typical resultant force versus time trace, observed during the severe slugging flow regime. Large fluctuations in the force were seen during the bubble penetration and gas blowdown stage.

Referring to Figure 5.11, the maximum resultant peak-to-peak force on the bend was given by:

$$FR'pk\text{-}pk = FR'_{max} - FR'_{min} \qquad (5.j)$$

Therefore, the amplitude of this force was:

$$FR'_{amp} = \frac{FR'pk - pk}{2} = FR'bg_{dy} \qquad (5.k)$$

The mixture velocity, v_{mix}, from the top of the riser into the separator, was calculated based on a liquid and gas mass balance on the separator, refer to Chapter 3, Sections 3.3.6.2 and 3.3.7.2 respectively:

$$v_{mix} = v_G + v_L \qquad (5.l)$$

where,

v_G gas production from the riser
v_L liquid production from the riser

Therefore, by plotting a graph of v_{mix} versus time, the mixture velocity at the corresponding maximum resultant peak-to-peak force was deduced.

5.5 The Effect of Trapped Gas in Riser Downward Limb

Referring to Figure 3.3, transducers P4 and P5, P6 and P9, and P5 and P6 could be used to measure the pressure difference, and hence the liquid inventory, in the lower limb, upper limb and downward limb, respectively, where:

Pressure difference over upper limb,

$$P6 - P9 = \rho g h_u \qquad (5.m)$$

Pressure difference over lower limb,

$$P4 - P5 = \rho g h_l \qquad (5.n)$$

If the lower and upper limbs of the riser were full of liquid, but there was trapped gas in the riser downward limb, then the amount of trapped gas would affect the pressure difference over the riser, as shown in Cases 1 to 3 below:

Case 1

The downward limb is not filled with liquid due to trapped gas. Therefore, $h_{d'} = 0m$ and P6 = P5. The pressure difference over the riser becomes:

$$P4 - P9 = (P6 - P9) + (P4 - P5) - (P6 - P5) \qquad (5.o)$$

$$P4 - P9 = \rho g(h_u + h_l) \qquad (5.p)$$

$$P4 - P9 = \rho g(7.348 + 4.685) \qquad (5.q)$$

Case 2

The downward limb is completely filled with liquid i.e. no gas is trapped. Therefore, $h_{d'} = h_d$. Therefore, the pressure difference over the riser in this case:

$$P4 - P9 = \rho g(h_u + h_l - h_d) \qquad (5.r)$$

$$P4 - P9 = \rho g(7.348 + 4.685 - 2.331) \qquad (5.s)$$

Case 3

Unknown volume of liquid in downward limb, where $0 > h_{d'} < h_d$. Therefore, pressure difference over the riser:

$$P4 - P9 = \rho g(h_u + h_l - h_{d'}) \qquad (5.t)$$

$$P4 - P9 = \rho g(7.348 + 4.685 - h_{d'}) \qquad (5.u)$$

5.5.1 Determination of Liquid Inventory in Riser Downward Limb

To investigate if gas was trapped in the downward limb during the slug production stage of the severe slugging 1 cycle, the pressure difference over the riser and the downward limb were measured. From the pressure difference and by considering frictional losses, the actual liquid inventory in the downward limb was calculated.

Referring to Case 3 above, for an unknown volume of liquid in the downward limb, the pressure difference over the riser, considering frictional losses, is:

$$P4 - P9 = \rho g h_u + \Delta P_{fu} + \rho g h_l + \Delta P_{fl} - \rho g h_{d'} + \Delta P_{fd} \qquad (5.v)$$

From measurements of pressure difference over the downward limb and over the riser, Equation (5.v) becomes:

$$\rho g h_{rmeas} - \Delta P_{ful} + \rho g h_{d'meas} - \Delta P_{fd} = \rho g(h_u + h_l) \qquad (5.w)$$

where,

$$h_{rmeas} = \frac{(P4 - P9)_{meas}}{\rho g} \qquad (5.x)$$

$$h_{d'meas} = \frac{(P6 - P5)_{meas}}{\rho g} \qquad (5.y)$$

Frictional losses for the liquid were given by,

$$\Delta P_f = f\rho\, v_L^{\,2} \frac{L}{2D} \qquad (5.z)$$

where,

f	friction factor
D	riser diameter
v_L	average outlet liquid velocity (based on a liquid mass balance, see Chapter 3)
L	length ($L = L_d = 3.3$m, for ΔP_{fd} and $L = L_u + L_l = 14.6$m, for ΔP_{ful})

NB ΔP_f for gas were approximately zero.

The actual liquid inventory can be described by:

$$h_{actual} = h_{meas} - h_f \qquad (5.aa)$$

Therefore, Equation (5.w) can be written as:

$$h_{ractual} + h_{d'actual} = h_u + h_l \qquad (5.ab)$$

5.6 Discussion of Results

5.6.1 Severe Slugging Flow Characteristics

The flow pattern maps in Figures 5.12 to 5.16 show the trends of cycle time, slug build-up time, slug production time, bubble penetration and gas blowdown time and slug length with superficial gas and liquid velocities. The values shown on the flow pattern maps, were average values for each severe slugging test.

5.6.1.1 Cycle Time

Figure 5.12 shows that longer cycle times were observed at lower gas and liquid velocities.

At a constant gas velocity of $v_{SG} \sim 0.35$m/s, the cycle time decreased by 3 times (265.1s to 86.2s), as the liquid velocity increased by 0.28m/s (0.02m/s to 0.3m/s). At a constant liquid velocity of $v_{SL} \sim 0.1$m/s, for an increase in gas velocity from 0.07m/s to 0.35m/s, the cycle time decreased by 4 times (544.8s to 133.3s).

At low liquid velocities, it took longer for the liquid to block the base of the riser, resulting in slower slug build-up times. At low gas velocities, the time taken for the gas pressure to build-up in the pipeline and to overcome the hydrostatic head of liquid in the riser was slower.

The longest cycle time observed was 544.8s (~ 9 minutes), this occurred in the severe slugging region, and the shortest cycle time, 30.5s, was observed within the transitional severe slugging region.

5.6.1.2 Slug Build-Up Time

Figure 5.13 shows that, (i) the time for the slug to build-up in the riser, occurred more quickly as liquid and gas velocity increased and (ii) slug build-up was more sensitive to changes in liquid velocity than gas velocity.

At a constant gas velocity of $v_{SG} \sim 0.35$m/s, the build-up time decreased by 5 times (233.1s to 44.5s), as the liquid velocity increased by 0.28m/s (0.02m/s to 0.3m/s). At a

constant liquid velocity of $v_{SL} \sim 0.1$m/s, for a 0.28m/s increase in gas velocity (0.07m/s to 0.35m/s), the build-up time decreased, but by only 1.5 times (136.7s to 97.7s).

As liquid velocity increased, the time for the slug to build-up in the riser occurred more quickly because, at lower liquid velocities, it took longer for the liquid to accumulate at the base of the riser and hence, for the riser base to become blocked. At higher gas velocities, the build-up time reduced because the slug did not back as far up the pipeline, due to the faster gas pressure build-up in the pipeline.

The longest slug build-up time observed was 233.1s (~ 4 minutes) and the shortest was 21.3s, both occurred in the transitional severe slugging region.

5.6.1.3 Slug Production Time

Figure 5.14 shows that, (i) as the gas velocity increased, the slug production time became shorter until the transitional severe slugging region was entered, where there was no slug production stage, (ii) slug production was more sensitive to changes in gas velocity than liquid velocity and (iii) there was a large variation in production times within the severe slugging region.

At a constant liquid velocity of $v_{SL} \sim 0.1$m/s, the production time decreased by 25 times (376.6s to 15.3s), as the gas velocity increased by 5 times from 0.07m/s to 0.35m/s. At a constant gas velocity of $v_{SG} \sim 0.28$m/s, by increasing the liquid velocity by 5 times (0.06m/s to 0.3m/s), the production time changed by only 3 times (8s to 26.7s). The ratio between the longest and shortest production times observed was 47.

At higher gas velocities, the increase in gas pressure in the pipeline overcame the hydrostatic head of liquid in the riser more quickly, therefore, the slug moved faster along the pipeline and into the riser, resulting in a shorter production time. Another reason for this effect, was that at higher gas velocities the slug lengths were shorter (see below) therefore it took less time for the liquid to be pushed out from the top of the riser.

5.6.1.4 Bubble Penetration and Gas Blowdown Time

Figure 5.15 shows that, (i) bubble penetration and gas blowdown tended to occur more quickly as gas and liquid velocity increased.

Within the severe slugging region, the bubble penetration and gas blowdown time decreased from 28.6s to 14.6s, with an increase in gas and liquid velocity.

In the severe slugging region, at lower gas velocities, slug lengths were longer. Therefore bubble penetration and gas blowdown tended to occur more slowly as it took longer for the bubbles to penetrate the liquid in the riser and for blowdown to take place.

5.6.1.5 Slug Length

The flow pattern map in Figure 5.16 shows that as the gas velocity increased, the slug lengths became shorter.

At a liquid velocity, v_{SL} ~ 0.18m/s, the slug length decreased from 29.3m, at v_{SG} = 0.18m/s, to 8.3m at v_{SG} = 1m/s.

As described in Section 5.6.1.2, at higher gas velocities, the slug did not recede as far up the pipeline, due to the gas having more energy and gas pressure build-up in the pipeline being faster.

For a 9.9m high lazy 'S' riser, slug lengths varied from 5.7m, seen in the transitional severe slugging region, to 70.2m (7 times the riser height), in the severe slugging region.

5.6.1.6 Comparisons to Previous Work

The literature review in Chapter 2 highlighted some of the experimental and theoretical studies of the hydraulics of severe slug flow, in pipeline-riser systems. Many of these investigations looked at vertical risers that were coupled to inclined pipelines therefore, research into severe slugging in flexible shaped riser systems has been limited.

As described in Chapter 2, Tin[17, 22] carried out extensive experimental work to investigate severe slugging using a 33m high, catenary shaped and lazy 'S' shaped riser. More recently, BHR Group Limited[14, 15] and Cranfield University[36] have performed experimental work using the test facility described in Chapter 3, with the BHR Group test work replacing the lazy 'S' riser with a 10m high catenary riser. Cranfield University[36] conducted experiments over a range of pressures to investigate the effect of pressure on the stability of severe slugging.

Although Tin, BHR Group and Cranfield University carried out extensive experimental work, many of the investigations into the characteristics of severe slugging are confidential. Hence, comparisons of the results from the two phase tests outlined in this research could only be compared to the limited published results.

5.6.1.6.1 Flow Pattern Maps

Comparing the flow pattern map in Figure 5.1, to the 4 bara and 7 bara flow pattern maps generated by Cranfield University[36], Figures 5.17 and 5.18, it can be seen that an increase in the pressure caused the severe slugging region to contract. The effect of pressure on the severe slugging boundary, was that it reduced the maximum superficial gas and liquid velocities at which severe slugging was experienced and consequently, shifted the severe slugging region to lower superficial gas and liquid velocities.

The flow pattern maps show that pressure had a greater effect on the superficial gas velocity boundary, i.e. the severe slugging region moved towards the left hand section

of the flow pattern map. This shift to the left of the severe slugging boundary was also observed in the vertical riser experiments carried out by Fuchs[38]. There are two reasons for the change in the severe slugging boundary:

(i) The effect of gas compressibility on the flow regime. As the pressure increased, the gas in the pipeline became less compressible. Due to the reduction in compressibility, back up of liquid in the pipeline was more difficult and as a consequence, slug lengths became shorter. As the definition of a severe slugging flow regime, was dependent on the slug length being greater than the height of the riser, then the reduction in slug length at higher pressures, accounted for the contraction of the severe slugging.

(ii) The effect of pressure on the ability of the pipeline gas to lift the liquid from the riser. Cranfield University[36] stated that the reduction in the potential lift energy was attributable to the reduction in the gas expansion during blowdown. An increase in the pressure reduced the expansion ratio of the gas by approximately 1.5, 1.3 and 1.1, for 2, 4 and 7 bara respectively.

Figure 5.19 compares the 9.9m lazy 'S' riser severe slugging boundary to the free hanging catenary flow pattern map generated by BHR Group Limited[15]. As the BHR Group tests were at a higher pressure (3 bara compared to 2 bara), then referring to the effects of pressure described above, the severe slugging region for the BHR Group tests would be expected to be smaller. However, Figure 5.19 shows that the catenary riser severe slugging boundary extended to a superficial gas and liquid velocity of 1m/s and 2.3m/s, respectively. Therefore, even accounting for pressure effects, the catenary severe slugging region was still larger. This suggested that the lazy 'S' riser configuration limited the occurrence of severe slugging.

This trend of a smaller severe slugging region with a lazy 'S' riser, agreed with the observations of Tin[17, 22], refer to Figures 2.3 and 2.4. Tin described that the lazy 'S' riser configuration had a considerable effect on the severe slugging boundary and cycle characteristics, due to trapped gas in the riser downward limb. Tin observed during some of the severe slugging cycles, that the trapped gas shortened the cycle time and reduced slug lengths. Referring to Figure 2.14, the slug lengths observed by Tin[22] for the catenary and lazy 'S' riser are presented. Even though gas and liquid velocities are not shown, comparisons between the different riser configurations can be made based on the maximum, minimum and average slug lengths, as shown in Table 5.1 below.

		Catenary Riser	Lazy 'S' Riser
Slug Length (m)	Minimum	55	50
	Maximum	230	185
	Average	118	91

Table 5.1 Slug Length Comparisons

The flow pattern map in Figure 2.4 was based on experiments carried out at atmospheric pressure, with a 33m high lazy 'S' riser. Comparing Figure 2.4 to Figure 5.1 it is seen that the flow regimes and layout of the maps were similar. Both maps have a severe slugging and a transitional severe slugging region; although in Figure 5.1, the transition region was only observed to the right of the severe slugging boundary, at higher gas velocities. Tin[17] also observed severe slugging 1, with intermediate cycles on the lower limb, which was not seen in the 2 bara lazy 'S' experiments. Transitional severe slugging, with intermediate cycles on the lower limb, was experienced in both sets of experiments, as was oscillation and stable flow. The severe slugging region in Figure 2.4 was larger and shifted more to the right (to a superficial gas velocity of 3.6m/s), compared to the severe slugging region in Figure 5.1, as the experiments were carried out at a lower pressure.

5.6.1.6.2 Severe Slugging Characteristics

Some similar trends were seen between the different riser configurations. The 9.9m lazy 'S' riser and the 10m catenary riser[15] both saw a decrease in cycle time and slug length with an increase in gas superficial velocity. Pot's[19] vertical riser, saw a decrease in cycle time with an increase in liquid superficial velocity, which also agreed to the lazy 'S' riser results.

Severe slugging is characterised by periods of no liquid production followed by large volumes of liquid i.e. long liquid slugs. This research has shown that slug length was affected by the superficial gas velocity, system pressure and riser configuration. For the 9.9m lazy 'S' riser, slug lengths of up to seven times the riser height were observed. In a 1000m riser, this could mean slug lengths of 7km are possible.

For the period of no liquid production during the slug build-up stage, the 9.9m lazy 'S' riser experienced a maximum build-up time of 204.8s. At similar gas and liquid flowrates, a 1000m riser would expect to see longer build-up times, based on the 9.9m lazy 'S' results this could mean a no flow period of up to 6 hours.

5.6.2 Liquid Inventory in Riser Downward Limb

Figure 5.20 shows the results from the investigations of the liquid inventory in the riser downward limb, during severe slugging. For each of the severe slugging conditions, the pressure difference over the riser, $(P4\text{-}P9)_{meas}$, exceeded the hydrostatic head due to the riser being full of liquid i.e. $(P4\text{-}P9)_{meas} > 0.95$ bar. This effect was explained using the measurements of pressure difference over the riser downward limb. If the downward limb were filled with liquid, then the liquid inventory (taking frictional losses into account), $h_{d'actual}$, would correspond to 2.331m, the height of the downward limb. Figure 5.20 shows that $h_{d'actual} < 2.331$m, in fact the maximum height of liquid observed was 0.659m (which corresponded to the downward limb being 28% full of liquid), hence gas was trapped in the downward limb, during each of the severe slugging conditions. The results of these investigations showed that due to trapped gas, the pressure difference over the riser exceeded the hydrostatic head, this agreed with Case 3 in Section 5.5:

For an unknown volume of liquid in the downward limb, where $0 > h_{d'} < h_d$, the pressure difference over the riser:

$$P4 - P9 = \rho g(h_u + h_l - h_{d'}) = \rho g(7.348 + 4.685 - h_{d'}) \qquad (5.ac)$$

The pressure difference over the riser when frictional losses were considered was:

$$P4 - P9 = \rho g h_u + \Delta P_{fu} + \rho g h_l + \Delta P_{fl} - \rho g h_{d'} + \Delta P_{fd} \qquad (5.ad)$$

By measuring the pressure differences over the riser and downward limb, Equation (5.ad) could be written as:

$$\rho g h_{rmeas} = \rho g(h_u + h_l) - \rho g h_{d'meas} + \Delta P_{fd} + \Delta P_{fu} + \Delta P_{fl} \qquad (5.ae)$$

hence,

$$h_{rmeas} - h_{ful} + h_{d'meas} - h_{fd} = h_u + h_l = 12.033 \text{ m} \qquad (5.af)$$

Figure 5.20 shows that by substituting the measured liquid inventories into Equation (5.af), the Equation is proved as $h_{d'actual} + h_{ractual} = 12.033$m.

Due to the low velocities during the slug production stage of the severe slugging cycle, frictional losses were small, the maximum frictional loss calculated was 0.15m over a total riser length of 17.9m (0.8%).

Figure 5.21 shows a graph of liquid inventory in the downward limb, $h_{d'actual}$, versus liquid velocity, for the severe slugging tests. As the liquid velocity increased, the liquid inventory in the downward limb decreased from 0.66m to 0.35m, i.e. more gas became trapped. As the liquid velocity increased, the lower limb of the riser filled more quickly, therefore when the liquid reached the top of the lower limb, the base of the upper limb would then become blocked more quickly, resulting in more gas being trapped in the downward limb. With an increase in the liquid velocity, the decrease in the liquid inventory in the downward limb would result in a decrease in the hydrostatic force, as there was less liquid in the riser.

It should be noted that for the severe slugging tests, the gas velocities during the slug production stage were very small (< 0.07m/s). The gas velocity was found to have a negligible affect on the volume of trapped gas in the downward limb, as shown in Figure 5.22, graph of liquid inventory in the downward limb versus mixture velocity.

As mentioned in Section 5.6.1.7, Tin[17, 22] observed during some severe slugging cycles, that trapped gas shortened the cycle time and reduced slug lengths. To see if the same trend applied to the 2 bara two phase tests, a graph of slug length and cycle time versus liquid inventory in the downward limb was plotted, as shown in Figure 5.23. As the liquid inventory decreased i.e. as more gas became trapped, the cycle times did become shorter and in some cases, slug length reduced.

The riser used in these tests was approximately 10m high, with lower limb, downward limb and upper limb heights of, 4.685m, 2.331m and 7.348m, respectively. As the riser dimensions were based on a real-life riser; for an actual riser height of 1000m, the downward limb would be nearly 250m high. The variation in trapped gas with velocity would make the maximum pressure difference over the riser and hydrostatic force, difficult to predict. If the downward limb is filled with gas, then the maximum pressure difference over the riser would be 118 bar, compared to 98 bar when no gas is trapped. Large differences in hydrostatic force could lead to mechanical stresses and fatigue.

5.6.3 Forces on a Bend during the Build-Up and Production Stages of the Severe Slugging Cycle

5.6.3.1 Single Phase Simulations

5.6.3.1.1 Description of Pressure-Time Traces

The pressure-time traces from the build-up stage simulations could be used to describe the build-up stage of a severe slugging cycle. The pressure-time traces shown in Figures 5.24 and 5.25 were from a simulation test at a system pressure of 2 bara, where the riser was filled with a liquid velocity of 0.234m/s.

Figure 5.24 shows the pressure over the riser, P4-P9, versus time, refer to Figure 3.3 for the location of the instrumentation. The pressure-time trace could be divided into three regions; (i) a region approximately equal to 0.03 bar; (ii) a build-up region and (iii) a region where the pressure over the riser was at a maximum.

The trace can be explained by looking at the progression of the liquid in the pipeline-riser (using the conductance probe readings) and the pressure over the lower limb, P4-P5, upper limb, P6-P9, and riser downward limb, P6-P5.

Figure 5.24 shows that region (i) covered the time period 50.0 to 179.4s. The pressure over the riser was equal to approximately 0.03 bar. This suggested that before any liquid entered the flow loop, there was already liquid in the riser. If this were not the case, then the pressure difference between the base and the top of the riser would be equal to zero.

From pressure transducer readings, this liquid was found to have accumulated at the base of the riser. This liquid was from the previous build-up stage simulation test, where remaining liquid had not been blown out by the gas. The liquid was from the film left on the riser walls, which fell back down the riser and accumulated at the base. This was similar to the process seen during severe slugging, as explained in Chapter 2, Section 2.2.2.

Region (ii) covered the time period, 179.4 to 246.6s. In this region, the pressure over the riser increased. This was due to the riser filling with liquid, and was confirmed by the fact that the conductance probes along the riser turned on in sequence. L4 turned on at 183.2s, L6 at 214.4s, L8 at 235.4s, L9 at 238.0s and L10, the probe nearest the top of the riser, at 240.6s.

A kink in the pressure over the riser was observed around 210s. The pressure increased steadily from 179.4 to 207.4s, then the pressure decreased, until at 209.7s, at which point, the pressure increased steadily again. This can be explained by looking at the individual limbs of the riser. Figure 5.25 shows the pressure over the lower limb and upper limb during this time period. From 179.4 to 207.4s, the increase in pressure over the riser was due to the lower limb filling with liquid. From 207.4s, the pressure over the lower limb increased at a slower rate, reaching a maximum at 209.5s (as the liquid reached the top of the lower limb), the pressure then decreased (as the liquid drained into the base of the upper limb), then the pressure stabilized, as there was a steady flow of liquid over the top of the lower limb into the base of the upper limb. The increase in pressure over the riser from 209.7 to 246.6s, was due to the upper limb filling with liquid.

Liquid was detected by the conductance probe nearest the base of the riser, L4, at 183.2s. Along the pipeline, L3 detected liquid at 186.6s and L2 at 207.8s. Therefore, liquid accumulated at the base of the riser, the riser began to fill with liquid and then the liquid began to back-up the pipeline. Even though liquid was continuously flowing along the pipeline, probes L2 and L3 did not detect this liquid initially because the probes were inserted a quarter of the way through the top of the pipe, so the liquid was only detected when the pipeline was nearly full.

In region (iii), 246.6 to 300s, the pressure over the riser reached a maximum value of 1.1 bar. In this region, the liquid had reached the top of the riser and was passing around the bend and along the horizontal section of pipeline, into the separator. Probes L11 and L12 indicated the presence of liquid at 246.6 and 251.7s respectively. Using $\Delta P = \rho gh$, a pressure difference of 1.1 bar, corresponded to a liquid height of 11.20m, but the actual height of the riser was 9.9m. During region (iii), the maximum pressure difference over the riser downward limb, P6-P5, was 0.094 bar. This corresponded to a liquid height of 0.96m. The height of the downward limb was 2.331m; therefore the riser was not completely filled with liquid, due to trapped gas in the downward limb. The effect of this trapped gas on the pressure difference over the riser is discussed in Section 5.5.

5.6.3.1.2 Description of Force-Time Traces

The force-time traces from the build-up stage simulations were used to describe the build-up stage of a severe slugging cycle. As in Section 5.6.3.1.1, these traces were from a simulation test at a system pressure of 2 bara, where the riser was filled with a liquid velocity of 0.234m/s.

From the pressure-time trace in Figure 5.24, for the time period 50.0 to 179.4s, liquid flowed along the pipeline and started to accumulate at the base of the riser. Figures 5.26 and 5.27 showed that in this region, the vertical and horizontal forces on the bend were approximately –3.7N and –6.6N, respectively. As explained in Chapter 4, Section 4.3.2.1, these vertical and horizontal forces were offset values, equivalent to a force of 0N. Therefore, as the liquid entered the pipeline and accumulated at the base of the riser, the dynamic forces on the bend were equivalent to zero, as expected.

During this time period, a cycling effect was noticed in the force traces, with this effect being more apparent in the vertical trace. The period and amplitude of the cycles were approximately, 5s and 3N, respectively.

Figure 5.28, shows a trace of vertical 'zero' offset, FV 'off versus time, taken from a test where there was no gas or liquid entering the flow loop and the water pump and compressor were turned off. Fluctuations in the force were shown, which were probably due to temperature effects and/or electrical noise, but cycles similar to those seen in Figure 5.26 were not shown here. This suggested that the cycling of the force was due to the vibration of the pipework, due to the water pump and/or compressor.

In Figure 5.24, the pressure over the riser increased during the time period 179.4 to 246.6s, due to the riser filling with liquid. During this period, it was expected that the strain- gauged struts would register no force, until the liquid front impacted upon the bend. Figures 5.26 and 5.27 show no force on the bend until 209.7s, when vertical and horizontal forces were observed. As described earlier, at 209.5s the liquid reached the top of the lower limb, with the upper limb filling with liquid from 209.7s. At the top of the lower limb there was a support attaching the limb to the laboratory wall. This support isolated the bend from the hydrostatic force, due to the lower limb filling with liquid. Therefore, up until 209.5s the vertical and horizontal strain-gauged struts did not register the effect of this increasing force. As the upper limb filled at 209.7s, the hydrostatic force came into effect, as the bend was not fully isolated.

The vertical and horizontal forces on the bend reached a peak at 242.7s. At this point the riser was full of liquid, as conductance probes L8, L9 and L10 were on, but liquid had not passed around the bend, as probes L11 and L12 were off. These peaks were due to the liquid front impacting upon the bend. For the single phase tests, these peak forces were a combination of the hydrostatic force (due to weight of liquid in the downward limb and upper limb), the dynamic force, as the liquid front hit the bend and the 'zero' offset. Due to the very low velocities during the build-up and production stages of the two phase severe slugging tests, the dynamic force was very small and dominated by the hydrostatic force. Therefore it was assumed that the peak force was equivalent to the hydrostatic force (due to liquid in the downward limb and upper limb) and the 'zero' offset.

Referring to Chapter 4, Section 4.3.3, there was a positive screen force when a strut was in compression and a negative screen force when a strut was in tension. When the vertical or horizontal strut went into compression, the force went in a positive direction, and when the vertical or horizontal strut went into tension, the force went in a negative direction. Therefore, as the riser filled with liquid the vertical strut went into tension (-3.7 to -45.1N) and the horizontal strut went into compression (-6.6 to 11.0N).

As the liquid passed around the bend, along the horizontal section and into the separator, the vertical and horizontal forces on the bend decreased (as the weight of liquid in the horizontal section, reduced the effect of the hydrostatic force due to the liquid in the riser). The forces then began to stabilise, as there was a steady liquid production into the separator. For the single phase tests, the forces on the bend at this

stage were due to the hydrostatic force (due to the weight of liquid in the riser and the horizontal section), dynamic force, as the slug passed around the bend and the 'zero' offset. Again, due to the low velocities during the build-up and production stages of the two phase severe slugging tests, this steady force was assumed to be equivalent to the hydrostatic force and the 'zero' offset.

As the riser filled with liquid, the vertical strut went into tension. It was expected that the weight of the liquid in the riser would pull the bend downwards, therefore putting the vertical strut into compression. On the horizontal section, after the isolation joint, the pipe was supported by an I-beam that was positioned underneath the pipe, refer to Figure 3.5. At the end of the horizontal section, the pipe was flanged to the separator. This combination of supports prevented the bend from being pulled downwards, so the vertical strut went into tension. The tension decreased when the liquid flowed along the horizontal section, moving the pipe in a downward direction, towards its initial position.

5.6.3.1.3 Results and Comparisons to Theory

Figures 5.29 and 5.30 present the results from the build-up stage and production stage simulations. Figure 5.29 shows the graph of resultant dynamic force during the build-up stage, $FR'bu_{dy,}$ versus liquid velocity and Figure 5.30 shows the graph of resultant dynamic force during the production stage, $FR'p_{dy,}$ versus liquid velocity. Each graph is compared to the theoretical resultant force, from Appendix A:

$$FR = \sqrt{2}\rho_L A v_L^2 \qquad (5.ag)$$

The build-up simulation tests and the production stage simulation tests showed that the resultant dynamic force on the bend was proportional to the square of the liquid velocity, but the experimental resultant dynamic force was lower than expected.

A possible reason for these lower values, was that the data analysis procedure described in Section 5.4.1, assumed that the hydrostatic force was independent of the liquid velocity, i.e. the liquid inventory in the riser remained constant, as liquid velocity was varied. This assumption was proved to be incorrect, by the investigation of trapped gas in the riser downward limb. The results of this investigation showed that with an increase in the liquid velocity, the liquid inventory in the lower limb decreased and hence, the hydrostatic force would decrease, as there was less liquid in the riser. As the hydrostatic force was assumed to be equal to the force at 0m/s, when the riser was full of liquid, for liquid velocities greater than 0m/s, this hydrostatic force would overestimate the actual hydrostatic force, as it did not account for trapped gas effects. Therefore this overestimate in the hydrostatic force resulted in the dynamic force being underestimated.

5.6.3.2 Two Phase Tests

Figure 5.31, shows a typical vertical, horizontal and resultant force trace during the slug build-up and slug production stage of the severe slugging 1 cycle (please refer to Appendix E for the force-time traces for each severe slugging test condition). Comparing the vertical and horizontal force traces to Figures 5.26 and 5.27 showed the similarities between the severe slugging build-up and production stages and the single phase build-up and production simulations.

Referring to Figure 5.31, between 220s to 240s the pressure over the riser increased as the lower limb of the riser filled with liquid. During this stage the resultant force on the bend was approximately 51N. This was an offset force, equivalent to a dynamic force of 0N. At 240s the upper limb began to fill with liquid and the resultant force increased. This increasing force was a hydrostatic force due to the bend not being fully isolated.

The resultant force reached a peak at 282s as the liquid front impacted upon the bend. Due to the very low velocities during the build-up stage, the dynamic force was very small and dominated by the hydrostatic force. Therefore it can be assumed that the peak force was equivalent to the hydrostatic force (due to liquid in the downward limb and upper limb) and the 'zero' offset.

As the liquid passed around the bend, along the horizontal section and into the separator, the resultant force on the bend decreased (as the weight of liquid in the horizontal section, reduced the effect of the hydrostatic force due to the liquid in the riser). The forces then began to stabilise, as there was a steady liquid production into the separator. Again, due to the low velocities during the production stage, this steady force can be assumed to be equivalent to the hydrostatic force and the 'zero' offset.

5.6.3.2.1 Slug Build-Up Stage

For the severe slugging data, the resultant dynamic force on the bend during the slug build-up stage, $FR'bu_{dy}$, was determined, using the data analysis procedure described in Section 5.4.2.1.

Figure 5.32 shows the graph of $FR'bu_{dy}$ versus mixture velocity, v_{mix}. Each data point on the graph represents a slug at a particular severe slugging test condition. The mixture velocity was based on the liquid and gas mass balances on the separator at the top of the riser. The mixture velocity, see Equation (5.l), was the average mixture velocity over the slug production stage. The graph does not include the data where $v_{mix} < 0.14$m/s. At these velocities, the dynamic forces were too small (less than 0.06N) to be measured using the data analysis procedure.

Figure 5.32 shows that the resultant dynamic force on the bend, due to the slug front impacting upon the bend during the build-up stage was equal to $2.834v_{mix}^2$. Referring to Appendix A, the resultant force on the bend was given by:

$$FR = \sqrt{2}\rho A v^2 \qquad (5.ah)$$

Applying Equation (5.ah) to the measured resultant force during the build-up stage:

$$FR'bu_{dy} = \sqrt{2}\,\rho_{mix} A v_{mix}^{\ 2} = 2.834 v_{mix}^{\ 2} \qquad (5.ai)$$

As the density of the slug at the bend was not measured, the slug density was assumed to be equal to the density of water, therefore the density term in Equation (5.ai), $\rho_{mix} = \rho_L = 1000 kg/m^3$. Therefore, based on this assumption, the predicted resultant force on the bend would be:

$$FR'bu_{dy} = \sqrt{2}\,\rho_L A v_{mix}^{\ 2} = 2.867 v_{mix}^{\ 2} \qquad (5.aj)$$

Comparing Equations (5.ai) and (5.aj), it was seen that the measured resultant force matched very closely to the predicted resultant force on the bend, during the slug build-up stage. The error between measured and predicted resultant force was 1.2%.

Therefore, during the slug build-up stage of the severe slugging cycle, the resultant dynamic force on the bend:

$$FR'bu_{dy} = \sqrt{2}\rho A v_{mix}^{\ 2} \qquad (5.ak)$$

Where the density term is equal to the liquid density, if the mixture density is unknown.

Figure 5.33, shows a graph of resultant force during the slug build-up stage versus slug build-up time. As slug build-up in the riser occurred more slowly, the resultant force on the bend decreased. This trend was expected, because as shown in Equation (5.ak), the resultant force during build-up was dependent on velocity. Therefore, as slug build-up occurred more slowly, the slug would be travelling at a lower velocity and hence, would impart a lower force on the bend.

The flow pattern map in Figure 5.34 shows the trend of $FR'bu_{dy}$ and cycle time, with superficial liquid and gas velocities. The values shown on the flow pattern map, are average values for each severe slugging test. The map shows that, (i) the force was more sensitive to changes in the superficial liquid velocity, than the superficial gas velocity and (ii) with an increase in the superficial gas and liquid velocities, the cycle time decreased and the resultant force on the bend increased.

At a constant gas velocity, $v_{SG} \sim 0.18m/s$, the force increased by 6 times (from 0.129N to 0.791N) for a liquid velocity increase of 0.2m/s. At a constant liquid velocity, $v_{SL} \sim 0.2m/s$, for a 0.2m/s increase in gas velocity, the force increased, but by only 1.5 times (from 0.267N to 0.423N).

At a superficial gas and liquid velocity of 0.07m/s and 0.1m/s respectively, the cycle time was 544.8s and the resultant force was 0.076N. For a test condition at a higher superficial gas and liquid velocity (v_{SG} and $v_{SL} = 0.31m/s$), the cycle time and resultant force was 86.2s and 0.971N respectively. Therefore, at higher superficial gas and liquid

velocities, within the severe slugging region, there were more cycles imparting higher forces on the bend, leading to a greater risk of structure and fatigue damage.

5.6.3.2.2 Slug Production Stage

Assuming that that the flow into the bend was equal to the flow out of the bend and considering that Equation (5.ak) was based on the average mixture velocity over the slug production stage, therefore the dynamic resultant force was the same for each stage. Hence, Equation (5.ak) can be used to describe the dynamic resultant force on the bend during the slug production stage:

$$FR'bu_{dy} = FR'p_{dy} = \sqrt{2}\rho A v_{mix}^{\ 2} \qquad (5.al)$$

5.6.3.2.3 Theoretical Force-Time Traces

As it was difficult to determine the dynamic force on the bend from the force-time traces, another method was considered to enable the dynamic force behaviour to be examined. From Equation (5.ak) and (5.al), the resultant dynamic force was described by:

$$FR'_{dy} = \sqrt{2}\rho A v_{mix}^{\ 2} \qquad (5.am)$$

For each two-phase severe slugging test, the mixture velocity at the outlet of the riser was measured, therefore, by substituting the mixture velocity into Equation (5.am) a theoretical resultant dynamic force trace could be plotted, as shown in Figure 5.35.

During the slug build-up stage there was no dynamic force on the bend. As the slug passed around the bend, the bend registered an increasing force that then stabilised to approximately 0.23N during the slug production stage.

5.6.4 Forces on a Bend during the Bubble Penetration and Gas Blowdown Stages of the Severe Slugging Cycle

Referring to Figures 5.10 and 5.11, the bubble penetration and gas blowdown stage was characterised by the rapid depressurisation over the riser. During this stage, large fluctuations in the force were observed.

To understand the forces on the bend and what was happening in the riser during the bubble penetration and gas blowdown stage, reference is made to the description of liquid production during a severe slugging 1 cycle by Montgomery and Yeung[36]. Figure 5.36 shows the liquid velocity at the outlet to the riser (based on the mass balance on the separator at the top of the riser) and Figure 5.37 shows a close-up of the liquid velocity with the resultant force on the bend. From Point A (at 633s) to Point B (at 640s) on Figure 5.37, the bubble front penetrated the base of the riser and this resulted in the acceleration of the liquid as the lower limb was blown down. During this stage, the resultant force on the bend increased by approximately 3N. This dynamic

resultant force was due to the accelerated liquid in the upper limb passing around the bend.

As the gas penetrated the base of the upper limb, a secondary acceleration of the liquid occurred (Point B) up to a maximum liquid velocity of 1.70m/s, three times higher than the velocity during the slug production stage. The peak velocity corresponded to the arrival of the liquid from the upper limb at the separator.

From Point B to about 643s, the resultant force on the bend decreased. During this period, even though the liquid velocity was increasing and hence the dynamic force was getting larger, the more dominant hydrostatic force decreased, due to liquid emptying from the upper limb and therefore, the resultant force decreased.

At 643s fluctuations in the force were observed. Figure 5.37 shows a series of large peaks that acted on the bend for approximately 4s, with the peak force on the bend occurring near the maximum velocity. The fluctuations in force did not correspond to any large fluctuations in the velocity therefore, this suggested that the bend was vibrating. This theory was supported, as the fluctuations quickly decreased in amplitude.

At 649s, a second peak in the liquid velocity corresponded to the liquid from the lower limb exiting the riser into the separator. An effect of this second peak on the resultant force was difficult to determine, but as the riser emptied, the hydrostatic force and dynamic force on the bend would decrease, until the resultant force reached a minimum. This minimum resultant force would comprise of an offset force and a hydrostatic force, due to any liquid that had not been blown out and had therefore accumulated in the riser.

Figure 5.38, shows the conductance probe trace from probe L11, which was on the horizontal section, nearest the bend. During slug production and the start of the bubble penetration stage at 633s, the conductance probe reading was 1 i.e. the liquid slug body was passing around the bend. After the gas front penetrated the upper limb, at approximately 643.5s gas bubbles penetrated the body of the slug as the probe began to detect gas and liquid. This gas entrainment coincided with the start of the large fluctuations in force. At 649s, the liquid from the lower limb exited from the riser. Figure 5.38 suggested that the liquid from the lower limb was less dense than that from the upper limb. This could have been amplified, as the gas trapped in the downward limb moved through the upper limb of the riser, when the liquid from the upper limb was delivered into the separator[36]. From 649s, the amount of gas increased, until at 651.8s, only gas was detected.

From Figures 5.36 to 5.38 a region of peak forces was observed as liquid from the upper limb exited from the riser. The forces occurred as the tail of the slug passed around the bend. Due to bubble penetration, the slug from the upper limb was not 100% liquid. The high velocity slug tail, resulted in a sudden increase in the dynamic force on the bend and as the slug tail travelled around the bend, it caused the bend to vibrate and fluctuations in the force were observed. The liquid from the lower limb exited the riser

at a lower velocity and was less dense compared to the liquid from the upper limb and therefore exerted a smaller force on the bend.

For the severe slugging data, the resultant dynamic force on the bend during the bubble penetration and gas blowdown stage, $FR'bg_{dy}$, was determined, using the data analysis procedure described in Section 5.4.2.2.

Figure 5.39 shows the graph of $FR'bg_{dy}$ versus mixture velocity, v_{mix} (where v_{mix} was based on the liquid and gas mass balances on the separator at the top of the riser, described in Chapter 3). The mixture velocity for each severe slugging cycle, corresponded to the maximum peak-to-peak resultant force.

Figure 5.39 shows that the resultant dynamic force on the bend during the bubble penetration and gas blowdown stage was equal to $2.744v_{mix}^2$. From the build-up stage analysis, described in Section 5.6.3.2.1, the resultant dynamic force on the bend could be described by:

$$FR'bu_{dy} = \sqrt{2}\,\rho_L A v_{mix}^{\ 2} = 2.867 v_{mix}^{\ 2} \qquad (5.an)$$

Comparing the results from the bubble penetration and gas blowdown analysis to the build-up results, showed that the density term during the bubble penetration and gas blowdown stage could not be assumed to be 100% liquid. This agreed to Figure 5.38. From the results shown in Figure 5.39, the slug density during the bubble penetration and gas blowdown stage is $957kg/m^3$. Therefore, during the bubble penetration and gas blowdown stage of the severe slugging cycle, the expected resultant dynamic force on the bend would be:

$$FR'bg_{dy} = \sqrt{2}\,\rho_{mix} A v_{mix}^{\ 2} \qquad (5.ao)$$

Where the mixture density term can be assumed to be $957kg/m^3$, if the actual mixture density is unknown.

It was noted that one severe slugging test condition did not follow the trend shown in Figure 5.39. At $v_{SG} = 0.32m/s$ and $v_{SL} = 0.19m/s$, the measured resultant dynamic force on the bend was up to 2.7 times larger than expected, as shown in Figure 5.40. Referring to Equation (5.ao), a possible explanation for these larger forces could have been that the mixture velocity had been underestimated, but the slug velocities for this test were within the reliable range of the flowmeters.

Looking at the worst case (where the measured resultant dynamic force was 2.7 times greater than theory), Figure 5.41 shows the resultant force and liquid velocity versus time. As the liquid from the upper limb exited from the riser, the liquid reached a maximum velocity at 220.5s (1.8m/s), decreased, then the velocity peaked again at 223s (1.7m/s). The conductance probe L11 began to detect gas at 219.5s. Comparing Figure 5.37 to Figure 5.41, as the liquid from the upper limb passed around the bend, only one distinct peak in the liquid velocity was observed.

This difference suggested that for the worse case scenario, these two peaks in the velocity in quick succession caused two sets of large dynamic forces to be imparted on the bend, causing the bend to vibrate and resulting in large fluctuations in the force.

Therefore, for this particular test condition, during the bubble penetration and gas blowdown stage of the severe slugging cycle, the resultant dynamic force on the bend, is described by:

$$FR'bg_{dy} = B\sqrt{2}\,\rho_{mix} A v_{mix}^{\ 2} \qquad (5.ap)$$

Where B varies between 1.7-2.9, as shown in Table 5.2.

$FR'bu_{dy}$ (N)	B
20.08	2.9
12.34	1.6
16.59	1.7
17.06	2.2
13.25	1.7

Table 5.2 Variable B (v_{SG} =0.32m/s, v_{SL} =0.19m/s)

As the back of a slug passes around a bend, BP[39] calculated the force on the bend using the following equation:

$$FR_{dy} = 2\sqrt{2}(\rho_s - \rho_G) A v_{mix}^{\ 2} \qquad (5.aq)$$

Where a dynamic factor of 2 was applied due to 'spring-back' of the bend. Considering this, the variable B in Equation (5.ap) and Table 5.2 can be described as a spring-back factor.

5.7 Forces on a Bend during Normal Slug Flow

Even though the objective of the research was to investigate the forces on a bend due to severe slug flow, this section briefly examines the forces due to normal slug flow and the potential risk of fatigue damage due to this highly fluctuating flow regime.

Normal slug flow comprises of a bubbly mass of liquid interspersed by a long bubble/film region. Referring to Figure 5.7, a typical example of the pressure difference over the riser during normal slug flow, the frequency of the pressure difference fluctuations shows that there was a regular progression of slugs through the riser. The faster the slugs moved through the riser, the greater the frequency of these fluctuations. The magnitude of the pressure difference fluctuation depends on the liquid inventory in the riser i.e. the size of the slugs.

The normal slug flow and severe slugging pressure traces (refer to Appendix E), show that during normal slug flow the maximum pressure difference over the riser was less than that experienced during severe slugging. Due to the structure of the slugs in normal slug flow, the liquid inventory in the riser was less due to the lower density of the slugs. The frequency of the fluctuations during normal slug flow was also much higher than those seen during severe slugging. The slug cycle time in Figure 5.7 is approximately 7s, compared to the shortest severe slugging cycle time of 86.2s.

If during normal slug flow the liquid inventory in the riser was less and the frequency of the slugs was higher, this suggests that the hydrostatic forces were lower and the dynamic forces were higher, compared to severe slugging.

Figure 5.42 shows the resultant force on the bend and liquid production traces during normal slug flow.

The composition of the slugs can be seen from the liquid production traces. Peaks in the liquid production are due to the arrival of the liquid slug body at the separator. Where the gas bubble arrives, the peaks are interspersed by regions where the liquid production is equal to zero.

As discussed earlier, the resultant force consisted of an offset force, hydrostatic force and dynamic force. The resultant force trace represents the slugs as they impacted and then passed around the bend. Figure 5.42 suggests that the peaks in the force were due to the liquid slug body, with the maximum force corresponding to the maximum liquid velocity. When the gas bubble impacted and moved around the bend, the resultant force was approximately 80N. This resultant force can be assumed to be equal to the offset force and the hydrostatic force, as the dynamic force is negligible because the gas velocities are very small (< 0.01m/s). Therefore, by making this assumption the maximum dynamic force on the bend during normal slug flow is approximately 22N. Due to higher velocities, the normal slug flow dynamic forces are greater than those observed during the severe slugging build-up and production stages and more than some of the forces seen during bubble penetration and gas blowdown.

Due to the higher velocity of the slugs coupled with large dynamic forces, normal slug flow is potentially more problematic in terms of fatigue damage, than severe slugging.

5.8 Summary

This Chapter described the lazy 'S' riser single phase and two phase tests. The single phase tests simulated the build-up stage and production stage of the severe slugging cycle. The two phase tests investigated the characteristics of severe slug flow, determined the liquid inventory in the riser downward limb and modelled the forces on a bend during the slug build-up, production and bubble penetration and gas blowdown stages of the severe slugging cycle.

Chapter 2 gave an overview of the major investigations into the forces due to normal slug flow. The overview showed that previous studies have been performed to determine the forces on pipe bends, but unlike the experimental work presented here using a pipeline-riser system, the studies concentrated on the forces on a bend in a horizontal pipeline. From the previous investigations the slug force models were based on the fact that the force on a bend resulted from the momentum transfer, in changing the slug direction around the bend. This was as expected, but had not been proved experimentally.

The single phase tests supported the two phase tests by proving that the resultant dynamic force on a bend, at the top of the riser, was proportional to the square of the liquid velocity. From the single phase tests, the following model was developed to describe the resultant dynamic force on the bend:

$$FR'_{dy} = \sqrt{2}\rho_L A v_L^{\,2} \qquad (5.ar)$$

Severe slugging is characterised by periods of no liquid production followed by large volumes of liquid i.e. long liquid slugs. From the comparisons of this work to previous investigations, it was shown that slug length was affected by the superficial gas velocity, system pressure and riser configuration. For the 9.9m lazy 'S' riser, slug lengths of up to seven times the riser height were observed

The occurrence of severe slugging was found to be reduced at higher system pressures and using a lazy 'S' shaped riser instead of a free hanging catenary configuration.

For each severe slugging test, the pressure difference over the riser, exceeded the hydrostatic head due to the riser being full of liquid, due to trapped gas in the riser downward limb. As liquid velocity increased, the liquid inventory in the downward limb decreased, as more gas was trapped. The trapped gas led to a reduction in cycle times and slug lengths.

The slug build-up and slug production stages of the severe slugging cycle were characterised by low velocities therefore, the resultant dynamic forces on the bend were small. The dynamic forces on the bend were dominated by the hydrostatic forces due to liquid in the downward limb and upper limb (build-up stage) and downward limb, upper limb and horizontal section into the separator (production stage). At each stage the density of the slug could be assumed to be equal to the liquid density.

During the bubble penetration and gas blowdown stage, high velocities and large fluctuations in the force were observed. Peak velocities (up to 15 times the velocity during the production stage) and forces corresponded to the arrival of the slug from the upper limb, at the separator. Fluctuations in the force occurred as the tail of the slug passed around the bend, causing the bend to vibrate. At one severe slugging test condition (which was characterised by two peaks in the liquid velocity), the forces on the bend were up to 2.9 times higher than expected.

From the two phase tests, the following models were developed to describe the forces on a bend during the slug build-up, production and bubble penetration and gas blowdown stages, of a severe slugging cycle.

During the slug build-up stage the resultant dynamic force on a bend, could be described by:

$$FR'bu_{dy} = \sqrt{2}\rho_{mix} A v_{mix}^{2} \qquad (5.as)$$

During the slug production stage the resultant dynamic force on a bend, could be described by:

$$FR'p_{dy} = \sqrt{2}\rho_{mix} A v_{mix}^{2} \qquad (5.at)$$

In Equations (5.as) and (5.at) if the mixture density is unknown, ρ_{mix} can be assumed to be equal to the liquid density.

For the bubble penetration and gas blowdown stage the resultant dynamic force on the bend, could be described by:

$$FR'bg_{dy} = \sqrt{2}\rho_{mix} A v_{mix}^{2} \qquad (5.au)$$

Where the mixture density term can be assumed to be 957kg/m^3, if the actual mixture density is unknown.

In certain cases, during the bubble penetration and gas blowdown stage, the resultant dynamic force on the bend is described by:

$$FR'bg_{dy} = B\sqrt{2}\,\rho_{mix} A v_{mix}^{2} \qquad (5.av)$$

Where B is a dynamic 'spring-back' factor which varies between 1.7-2.9.

This Chapter included a brief examination of the forces on a bend due to normal slug flow. By comparing normal and severe slug flow pressure traces, it was found that normal slugs were less dense and the frequency of the normal slugs was much higher.

The dynamic forces due to normal slug flow were found to be greater than the forces observed during the severe slugging build-up and production stages and in some cases, greater than the forces seen during bubble penetration and gas blowdown. Hence, normal slug flow is potentially more problematic in terms of fatigue damage, than severe slugging.

The following Chapter summarises the research undertaken and details the conclusions from each research topic. The Chapter also highlights the further work required.

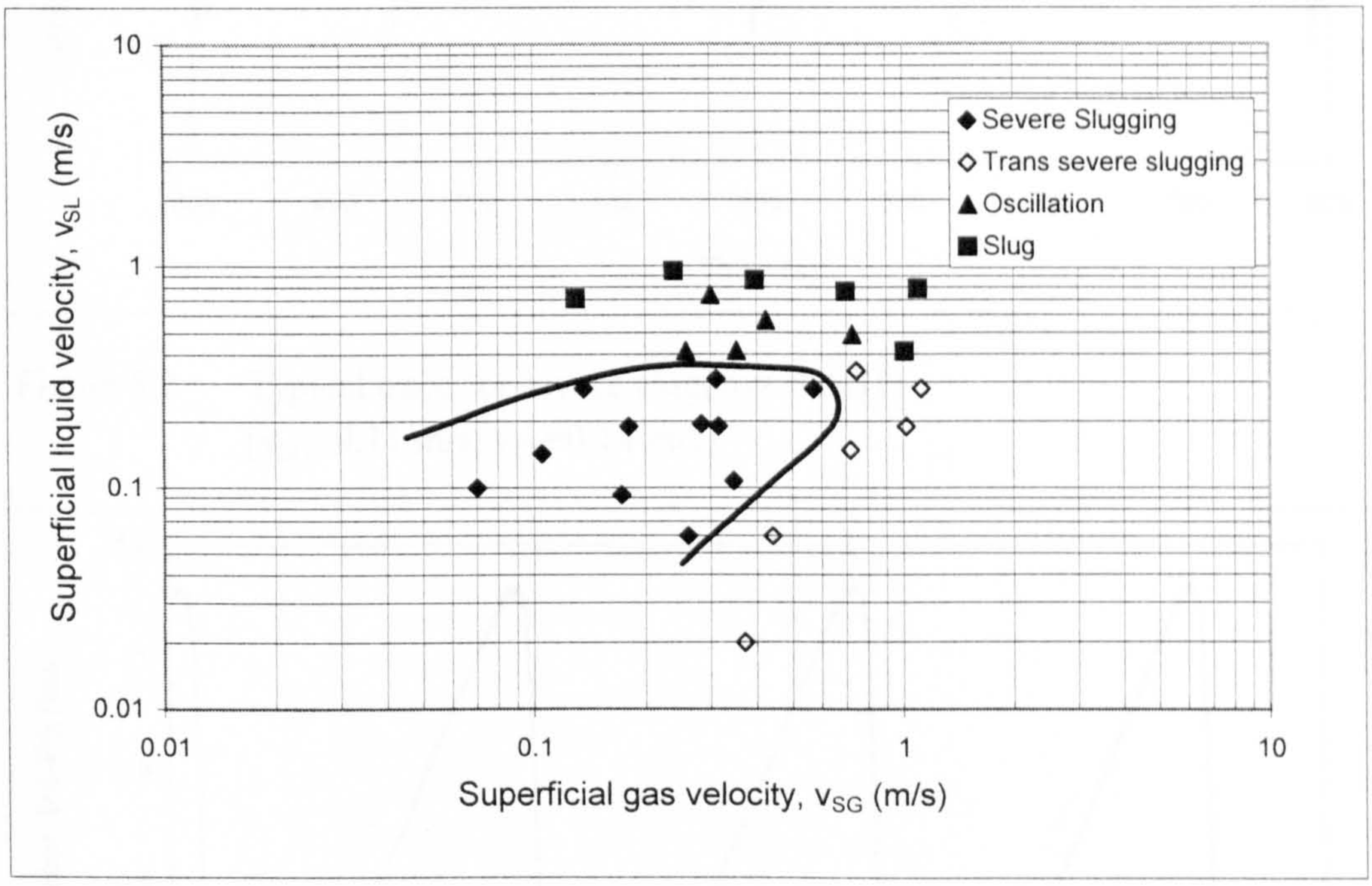

Figure 5.1 Flow pattern map showing test points and observed flow regimes

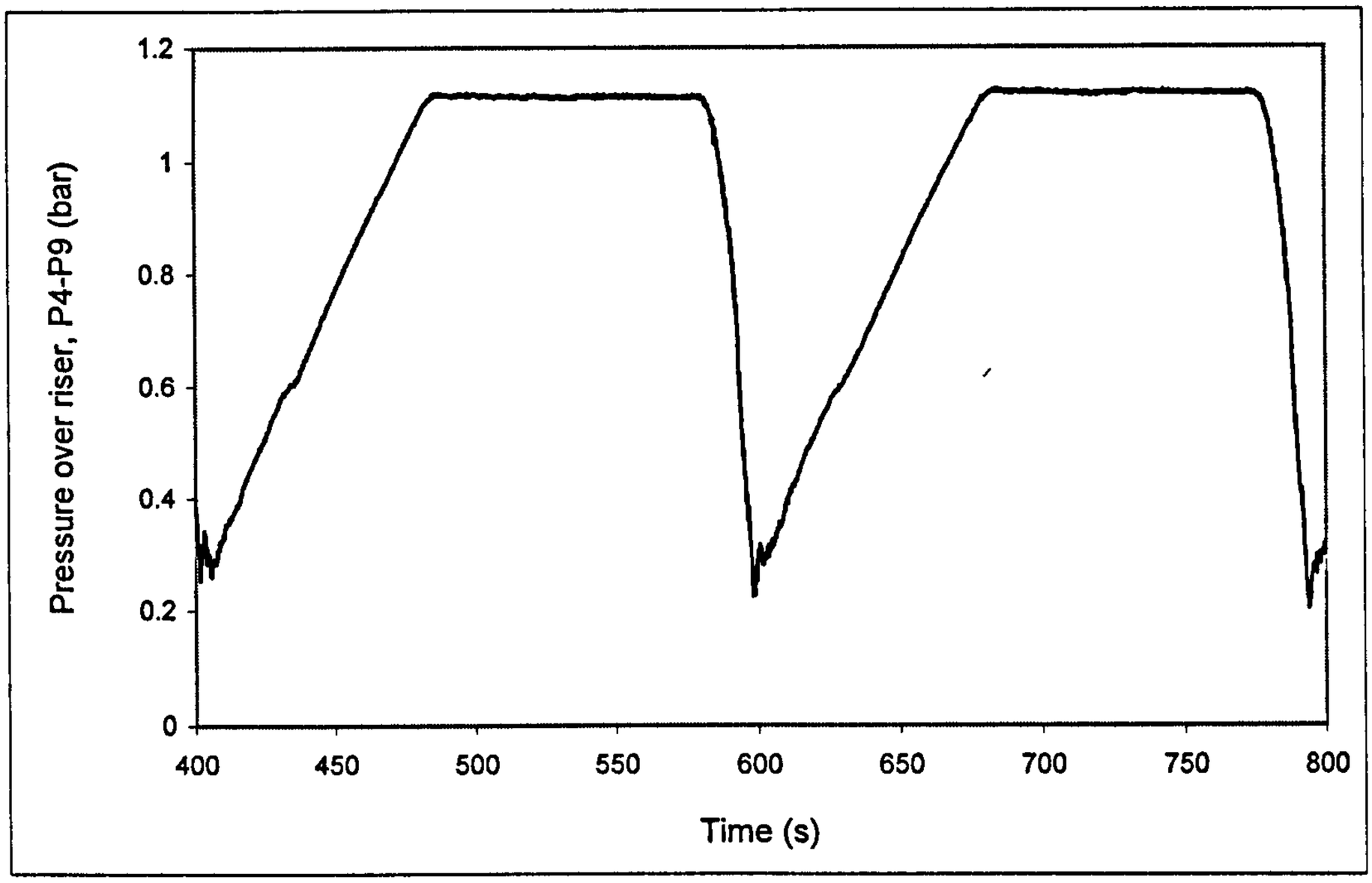

Figure 5.2 Typical trace for severe slugging 1 (SS1)
[v_{SG}=0.11 m/s, v_{SL}=0.14 m/s]

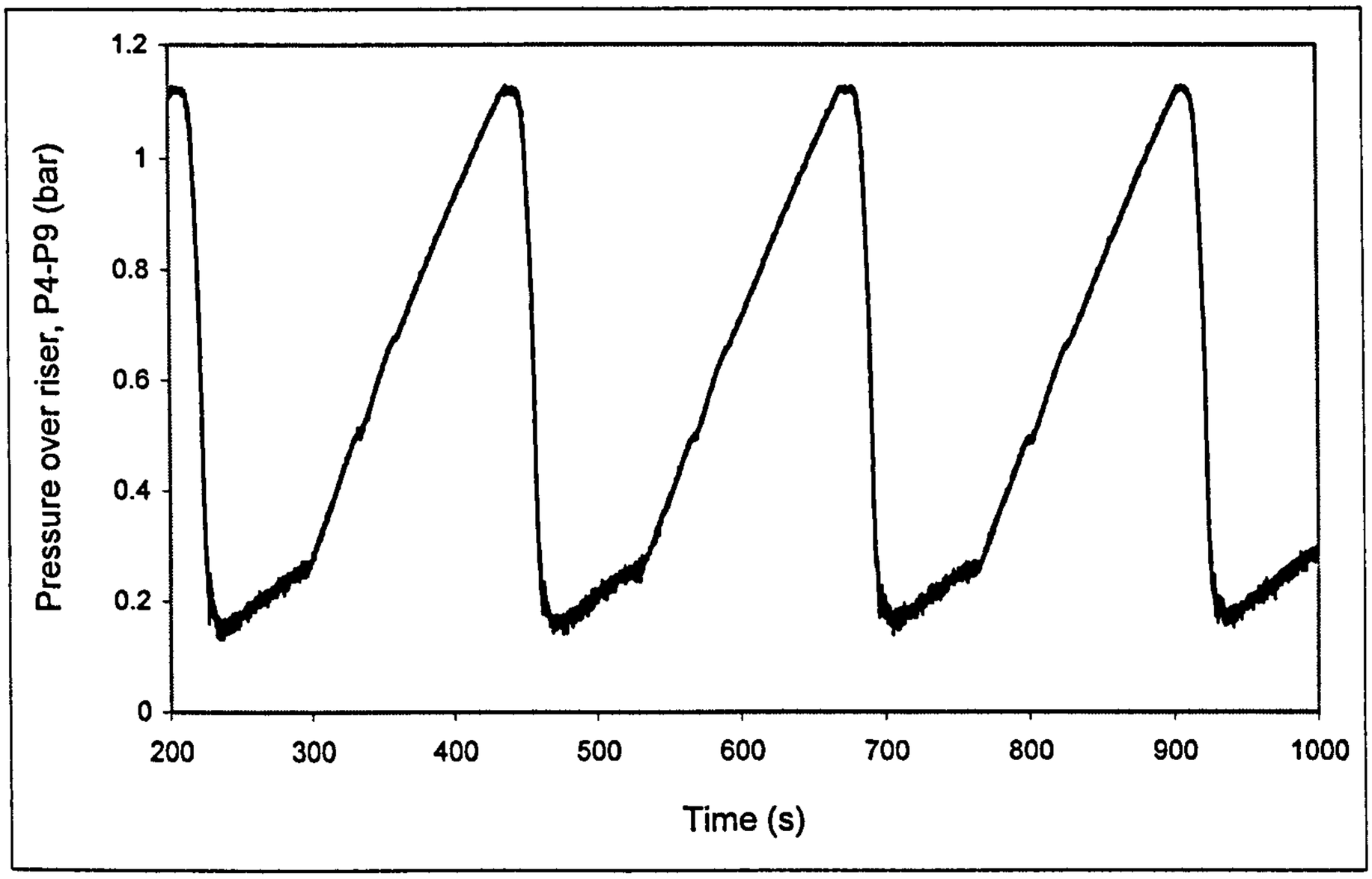

Figure 5.3 Typical trace for severe slugging 1b (SS1b)
[v_{SG}=0.26 m/s, v_{SL}=0.06 m/s]

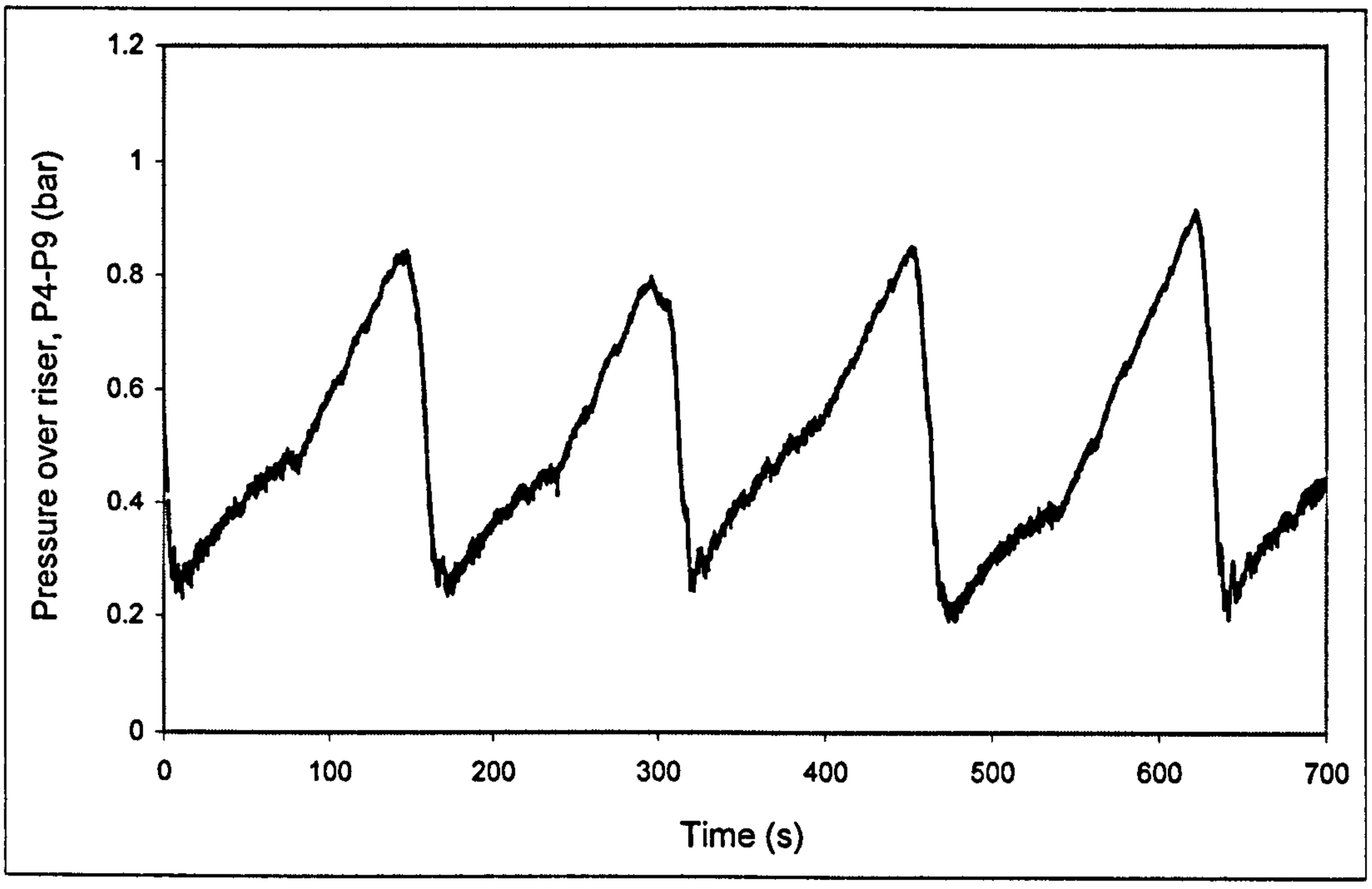

Figure 5.4 Typical trace for severe slugging 2 (SS2)
[v_{SG}=0.74 m/s, v_{SL}=0.34 m/s]

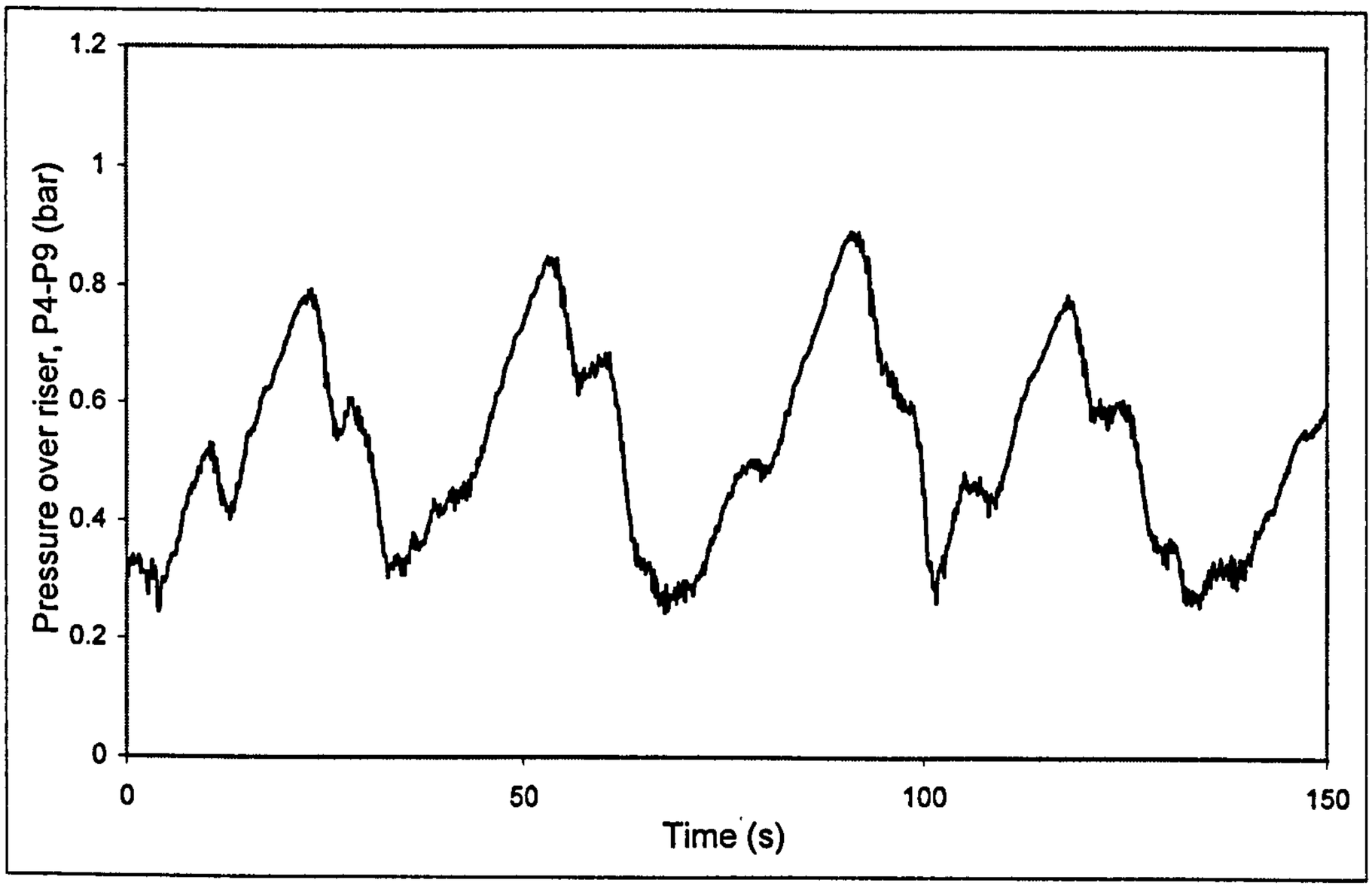

Figure 5.5 Typical trace for severe slugging with intermediate cycles on the lower limb (SS2i)
[v_{SG}=1.12 m/s, v_{SL}=0.28 m/s]

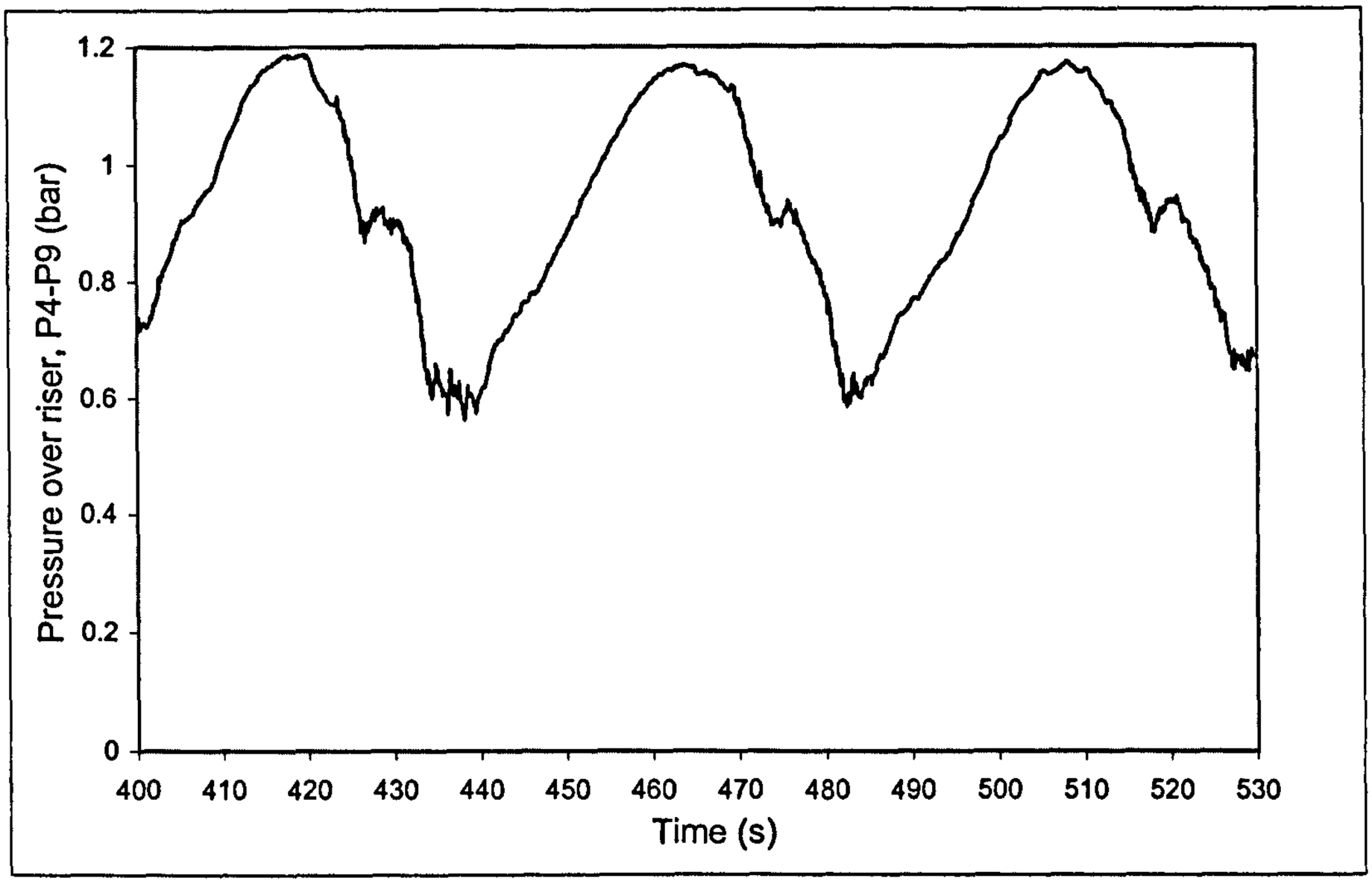

Figure 5.6 Typical trace for oscillation flow

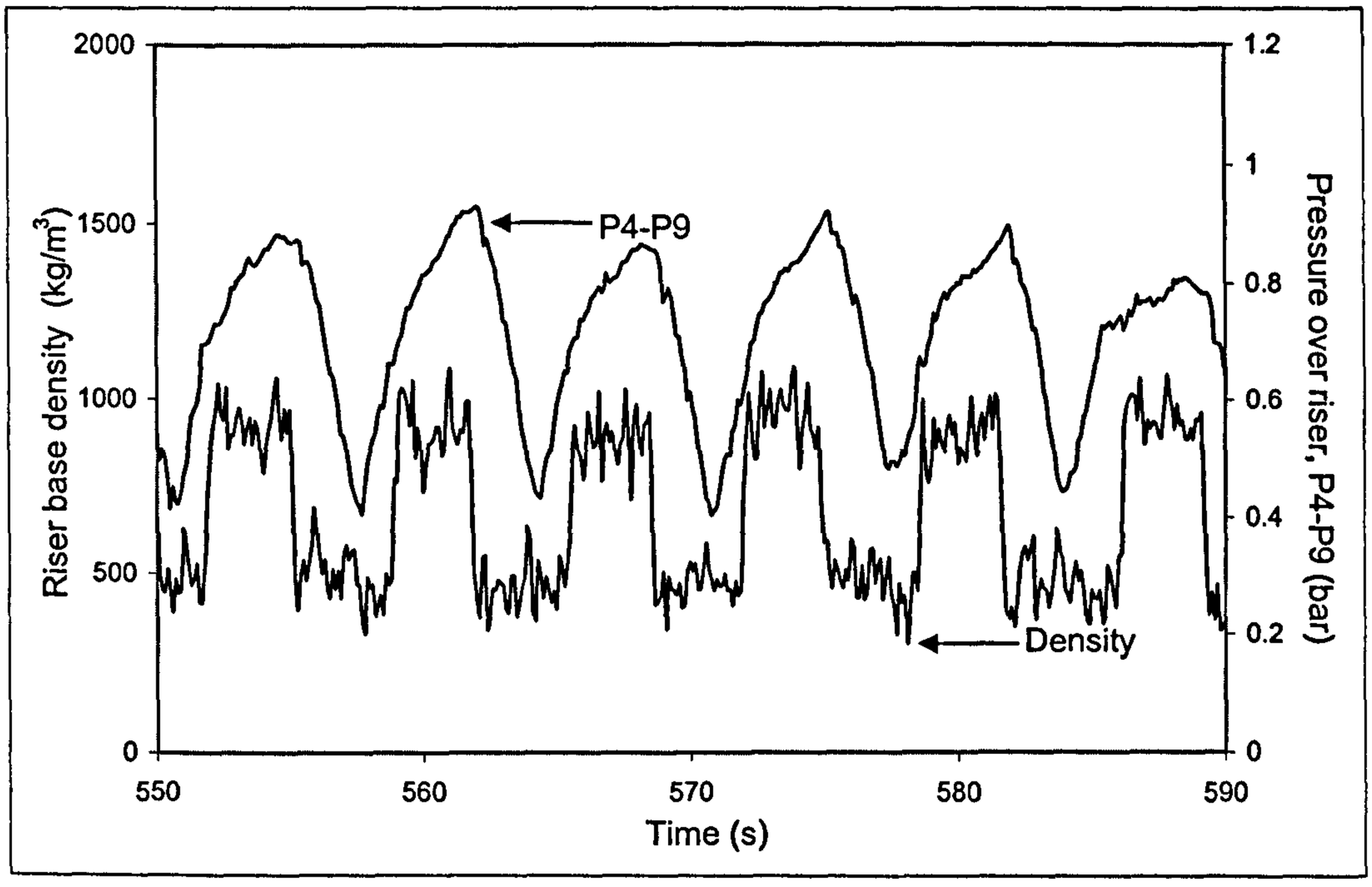

Figure 5.7 Typical trace for slug flow

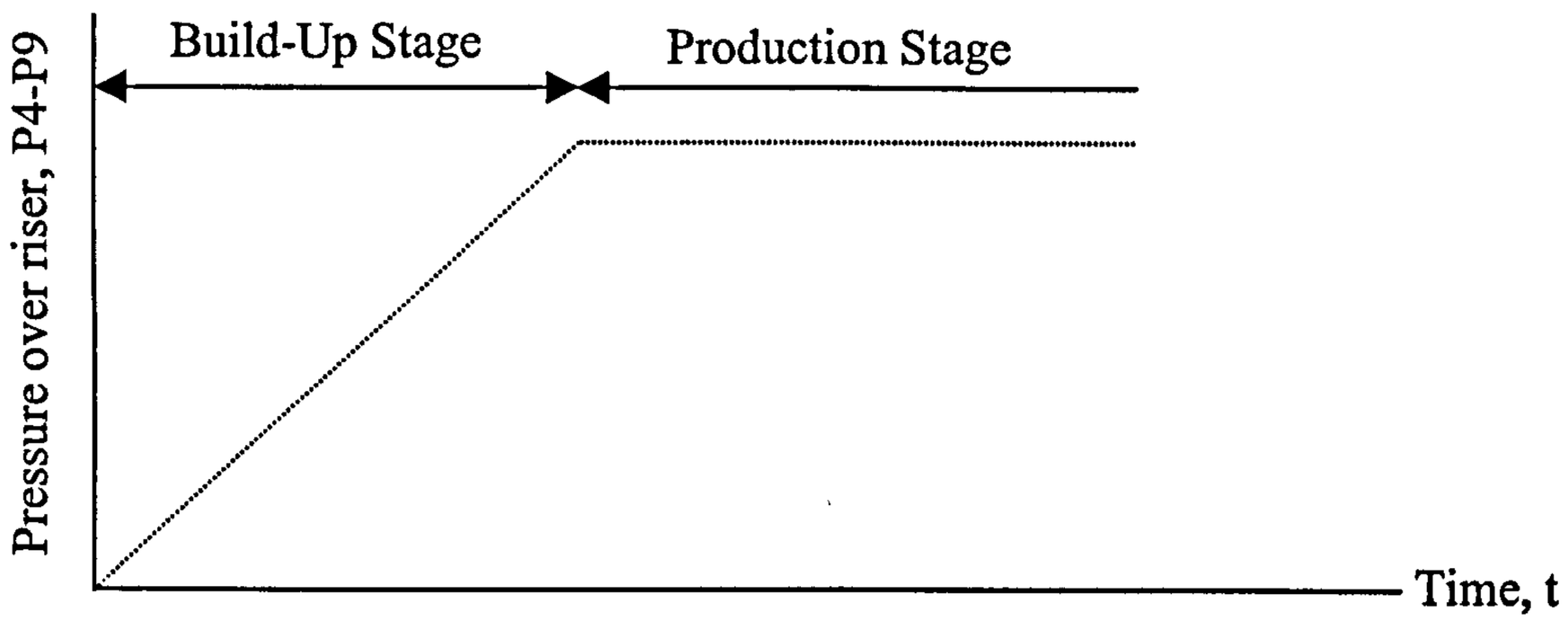

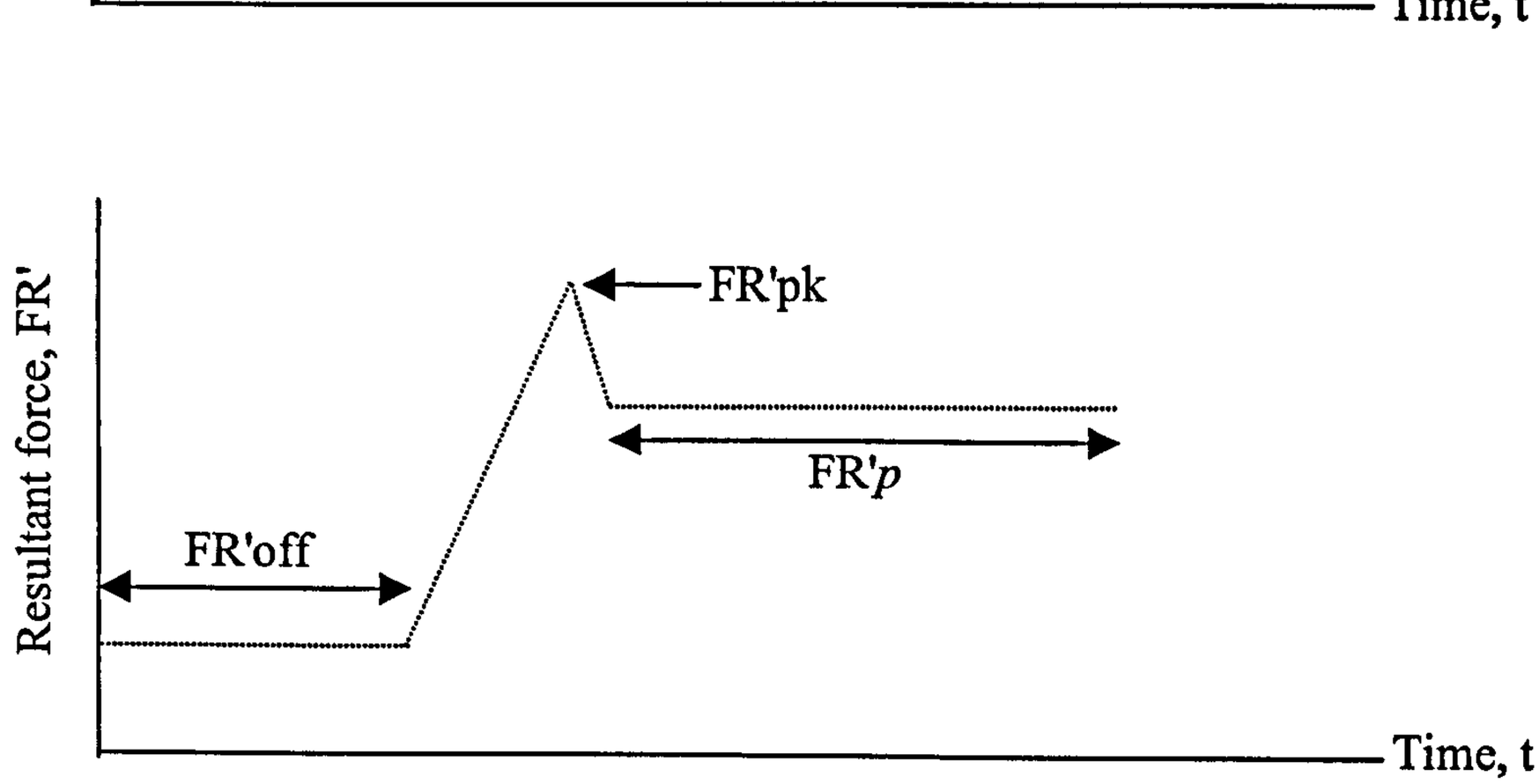

Figure 5.8 Pressure over the riser and resultant force versus time traces

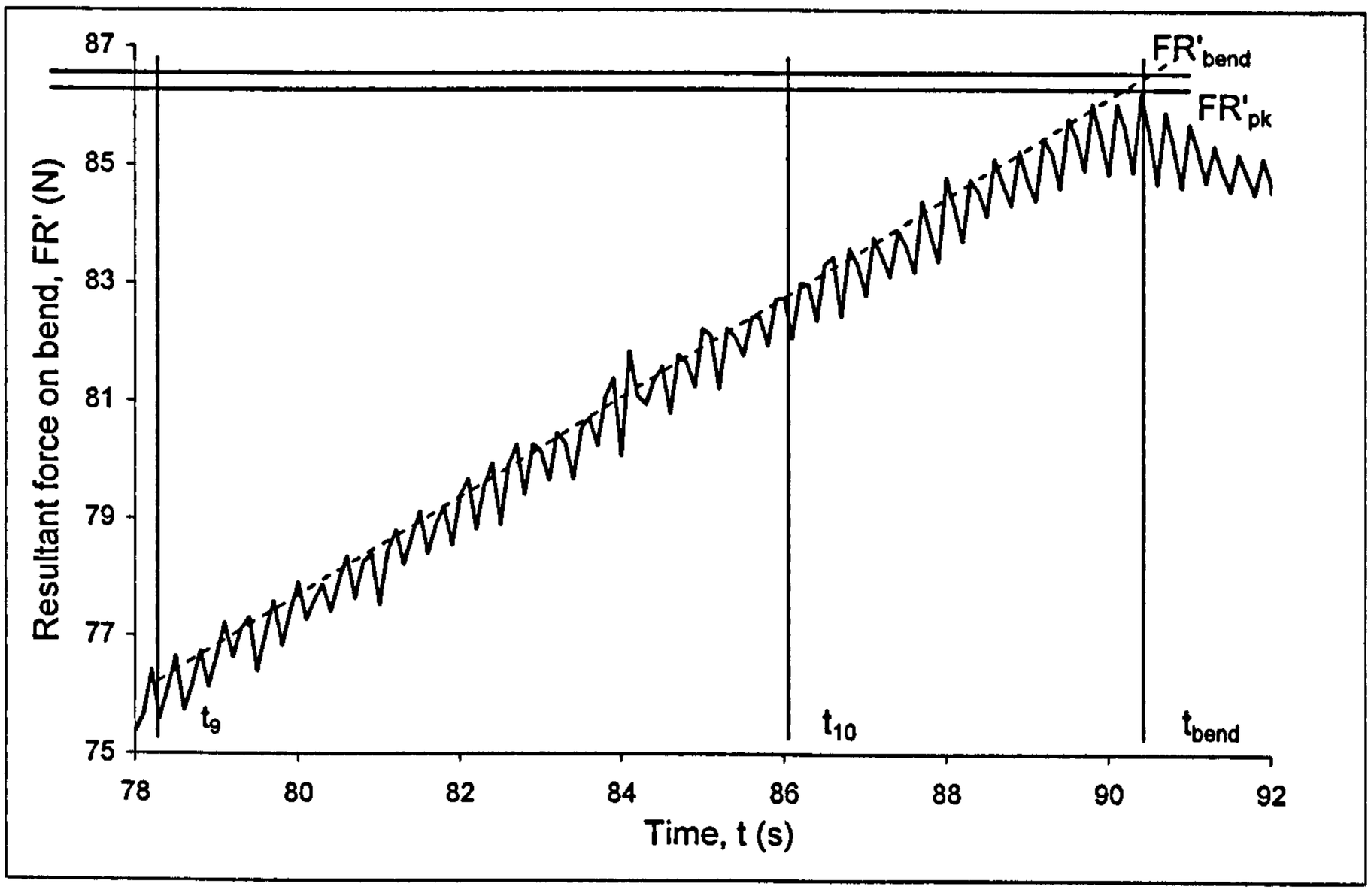

Figure 5.9 Extrapolation technique used to determine the dynamic and vertical force on the bend during slug build-up

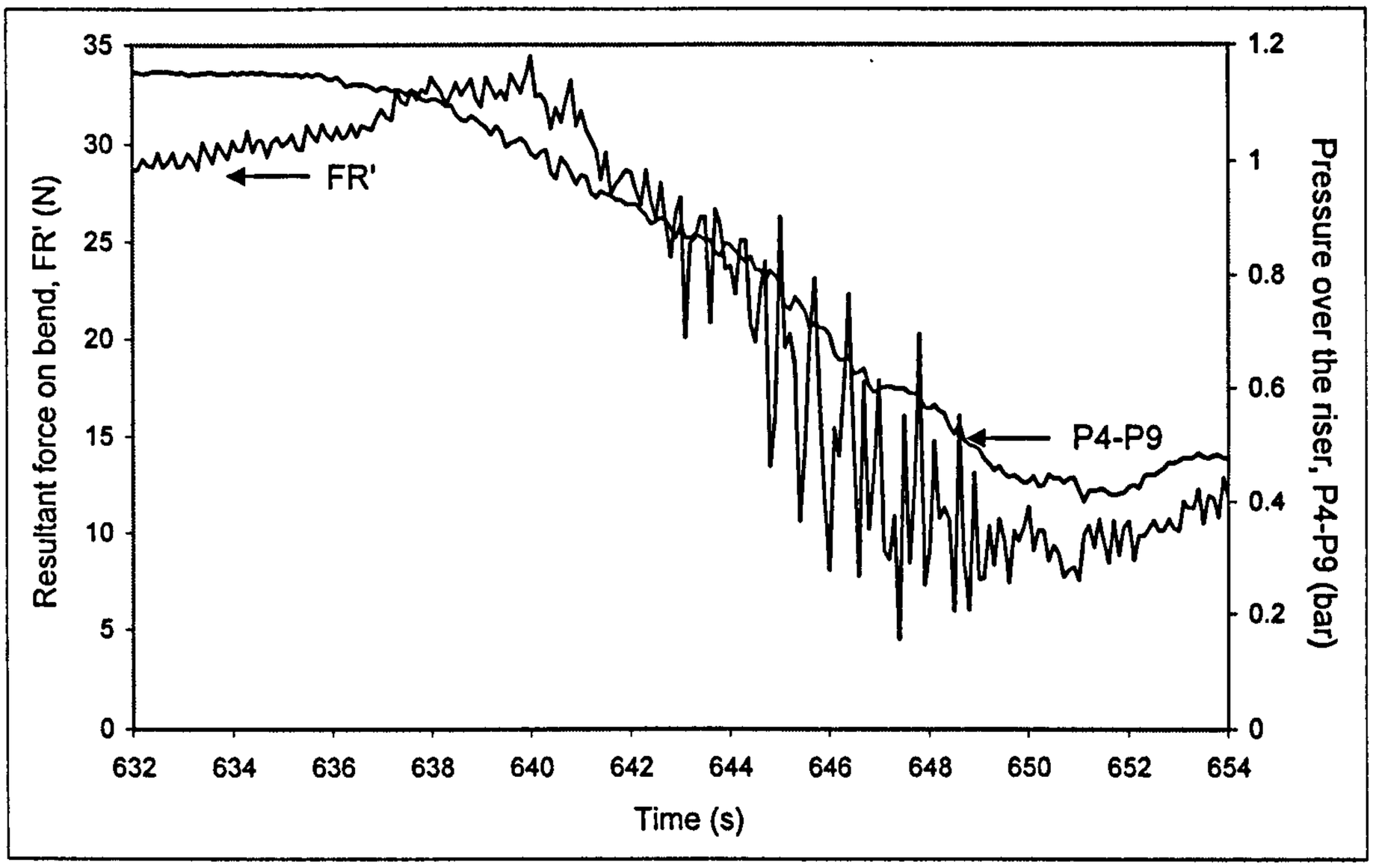

Figure 5.10 Typical resultant force during the bubble penetration and gas blowdown stage, of a severe slugging cycle
[v_{SG} = 0.14 m/s, v_{SL} = 0.28 m/s]

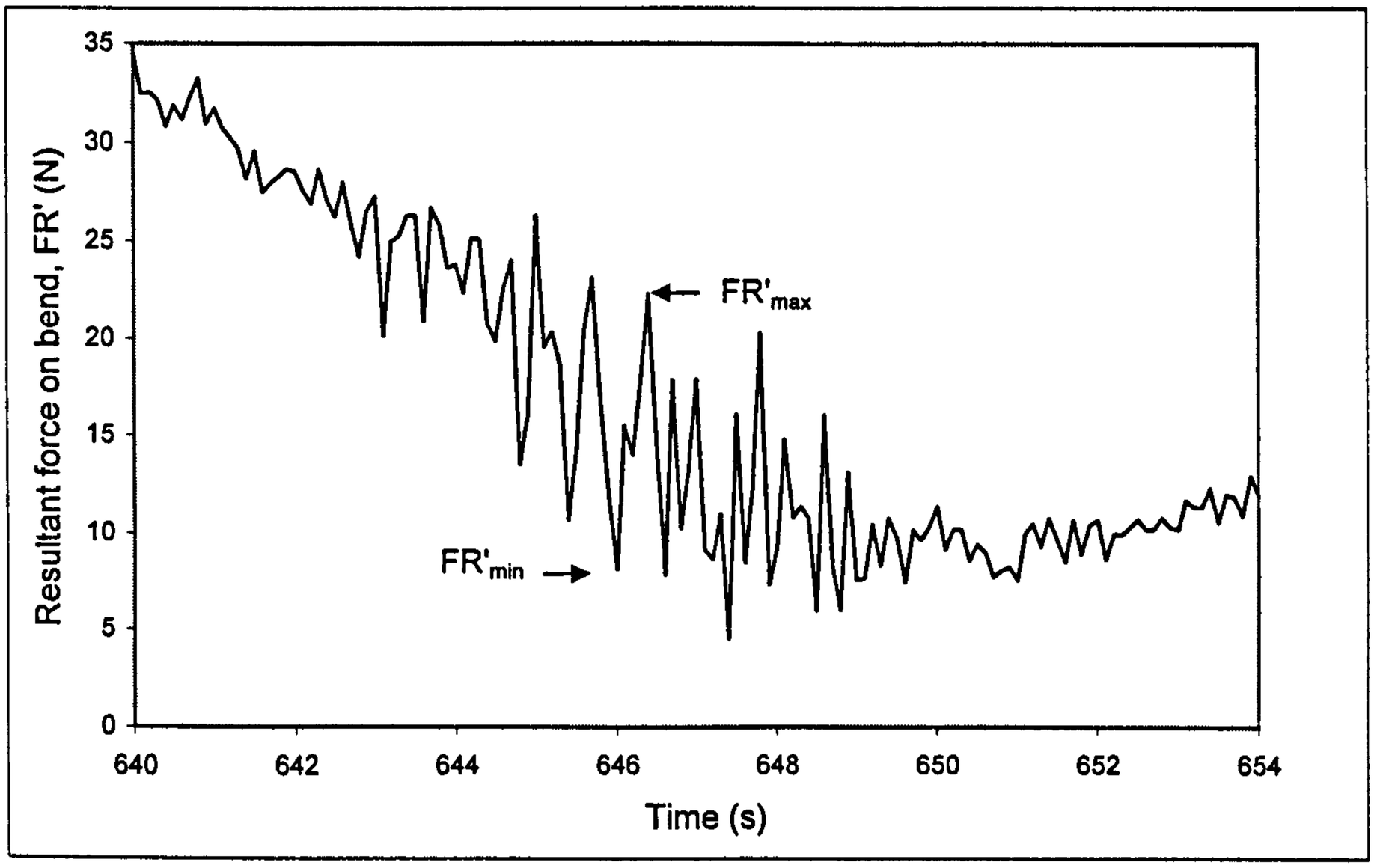

Figure 5.11 Close-up of the resultant force during the bubble penetration and gas blowdown stage, of a severe slugging cycle
[v_{SG} = 0.14 m/s, v_{SL} = 0.28 m/s]

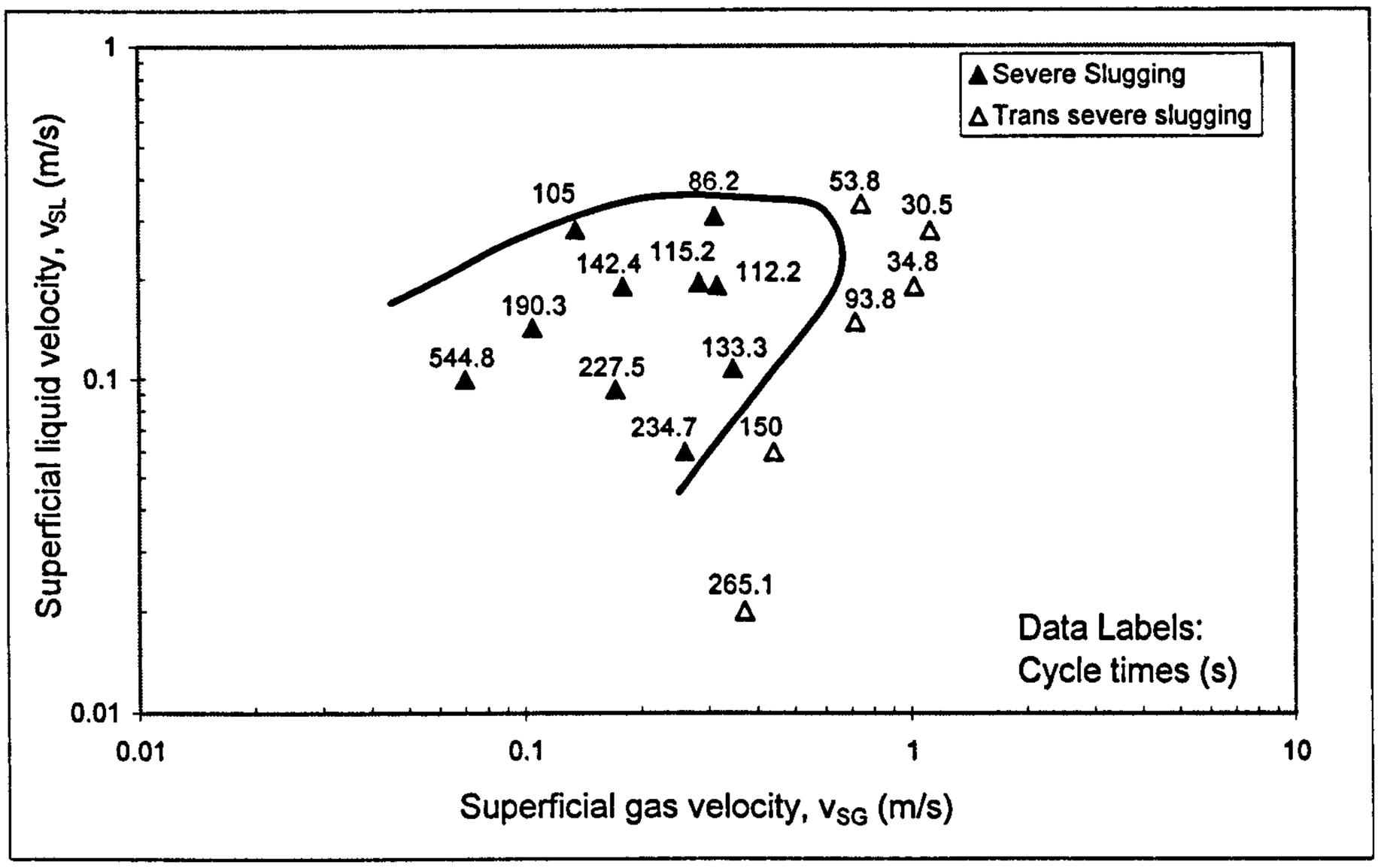

Figure 5.12 Flow pattern map showing cycle times

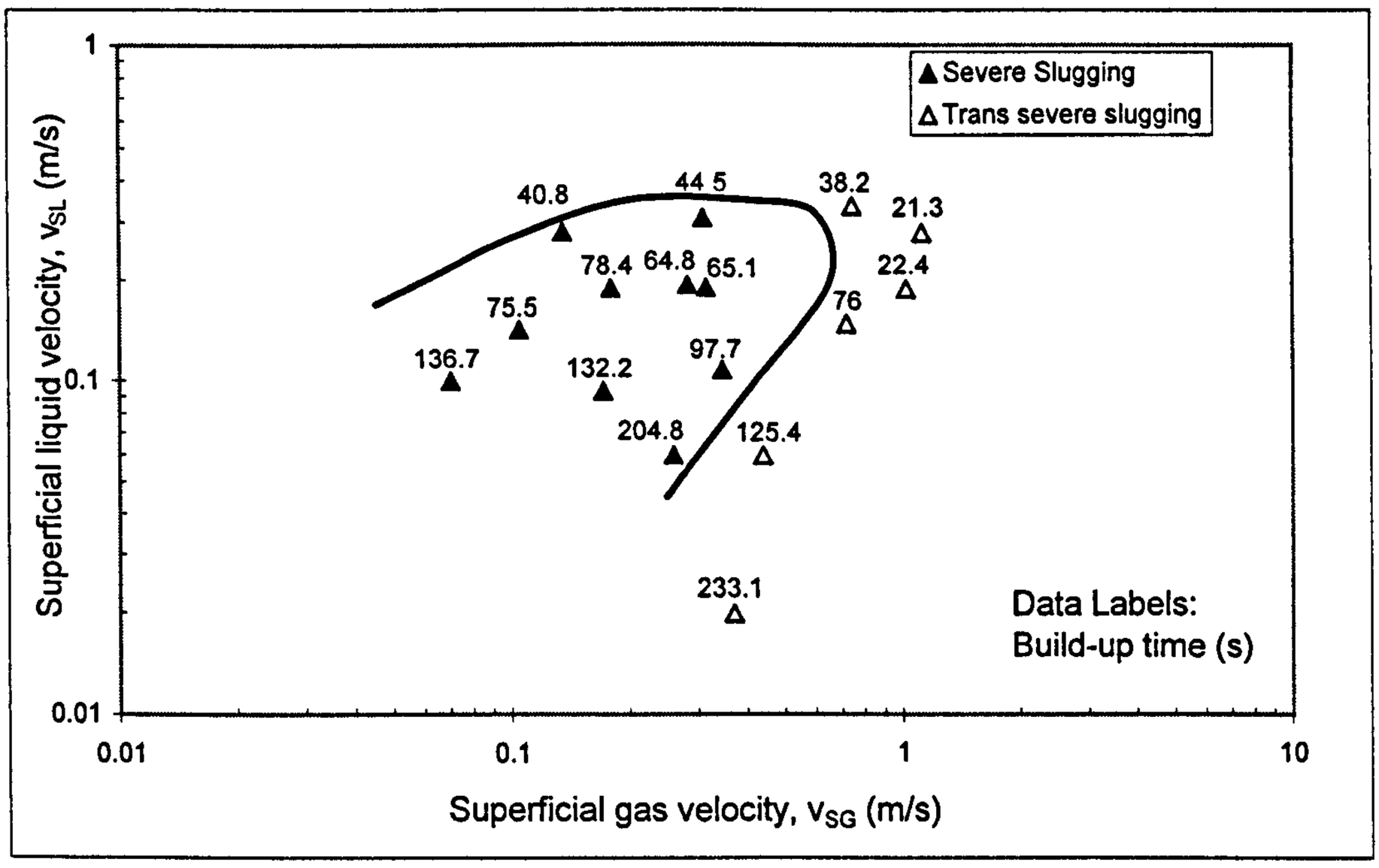

Figure 5.13 Flow pattern map showing slug build-up times

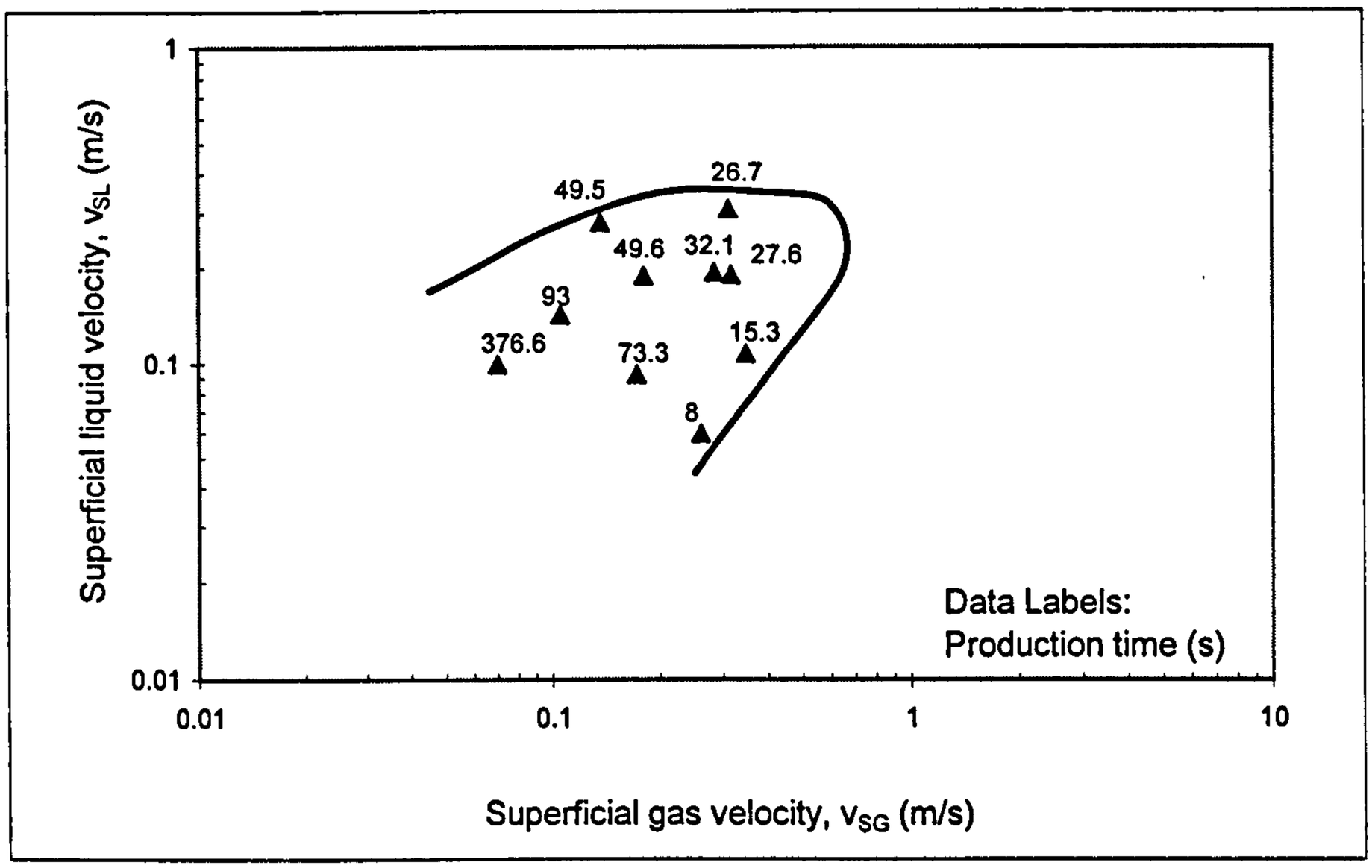

Figure 5.14 Flow pattern map showing slug production times

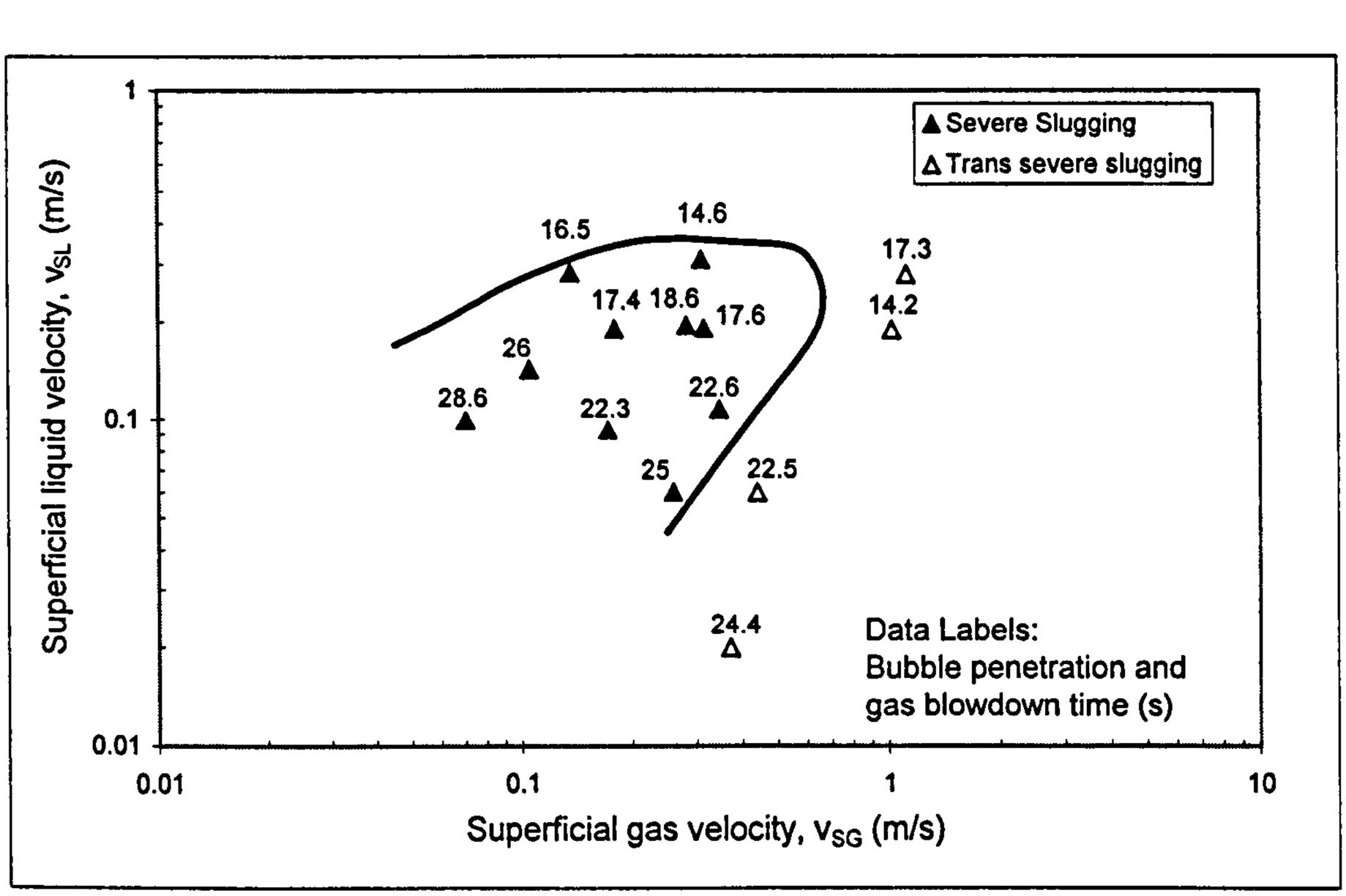

Figure 5.15 Flow pattern map showing bubble penetration and gas blowdown times

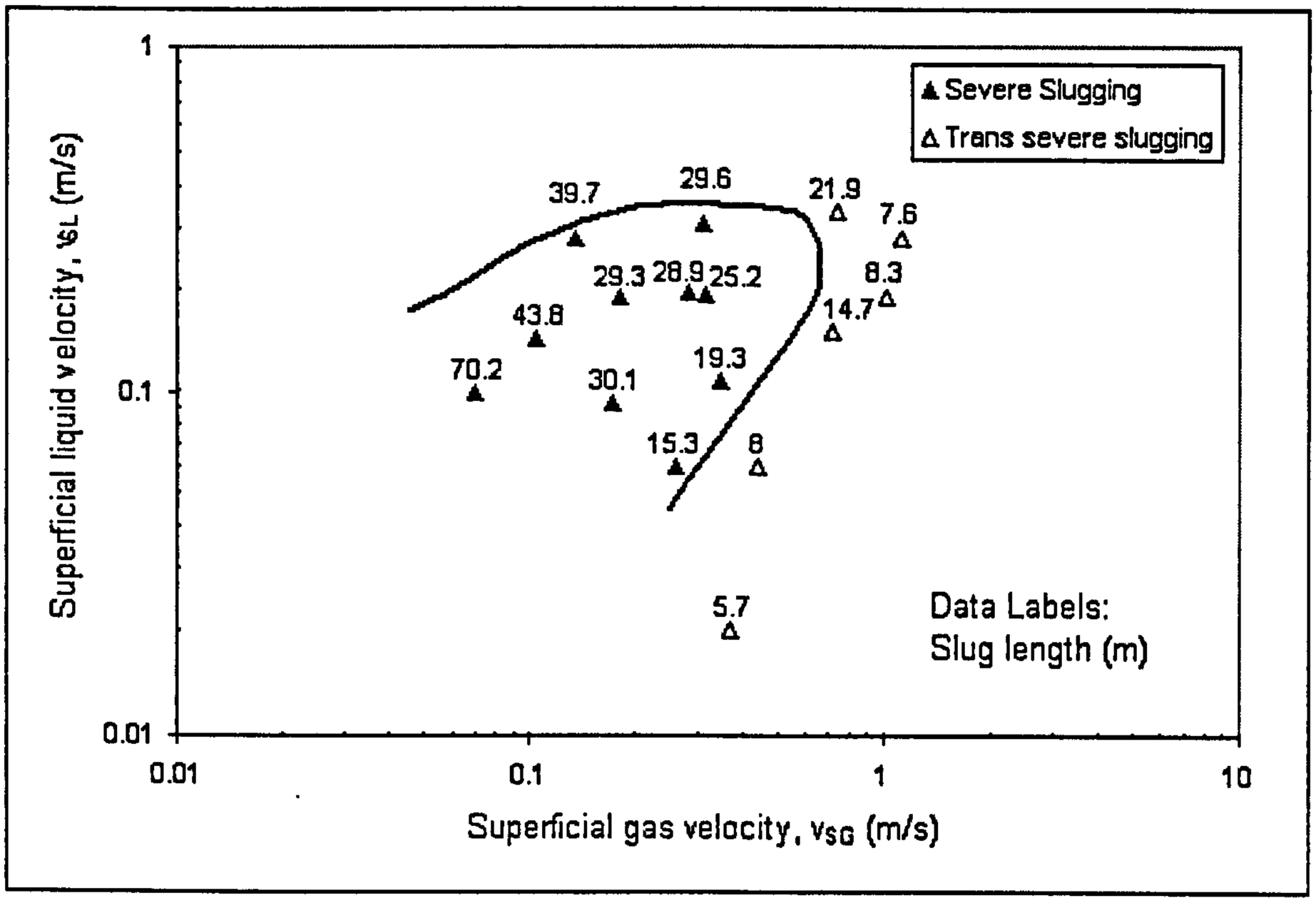

Figure 5.16 Flow pattern maps showing slug lengths

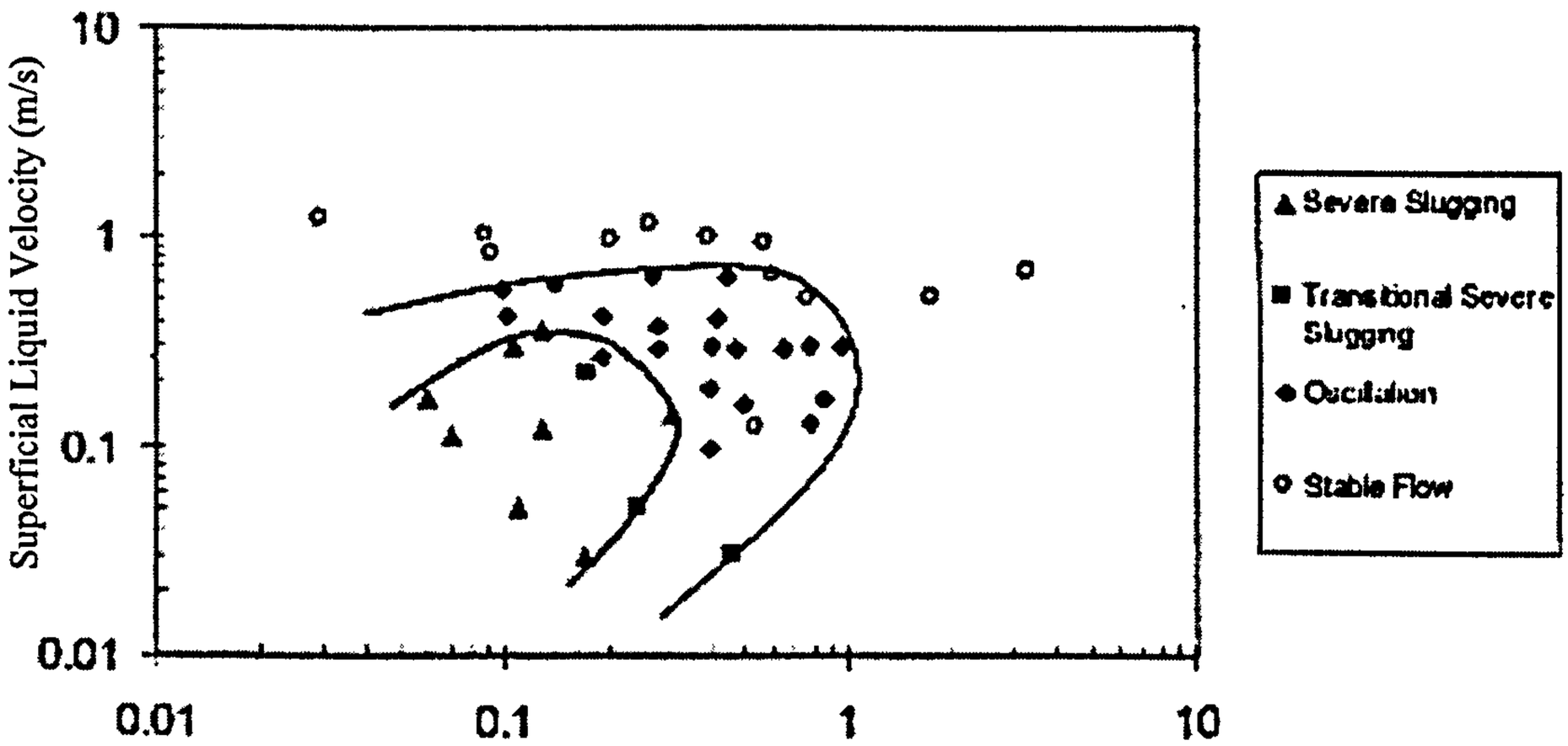

Figure 5.17 Cranfield University lazy 'S' riser flow pattern map, 4 bara[36]

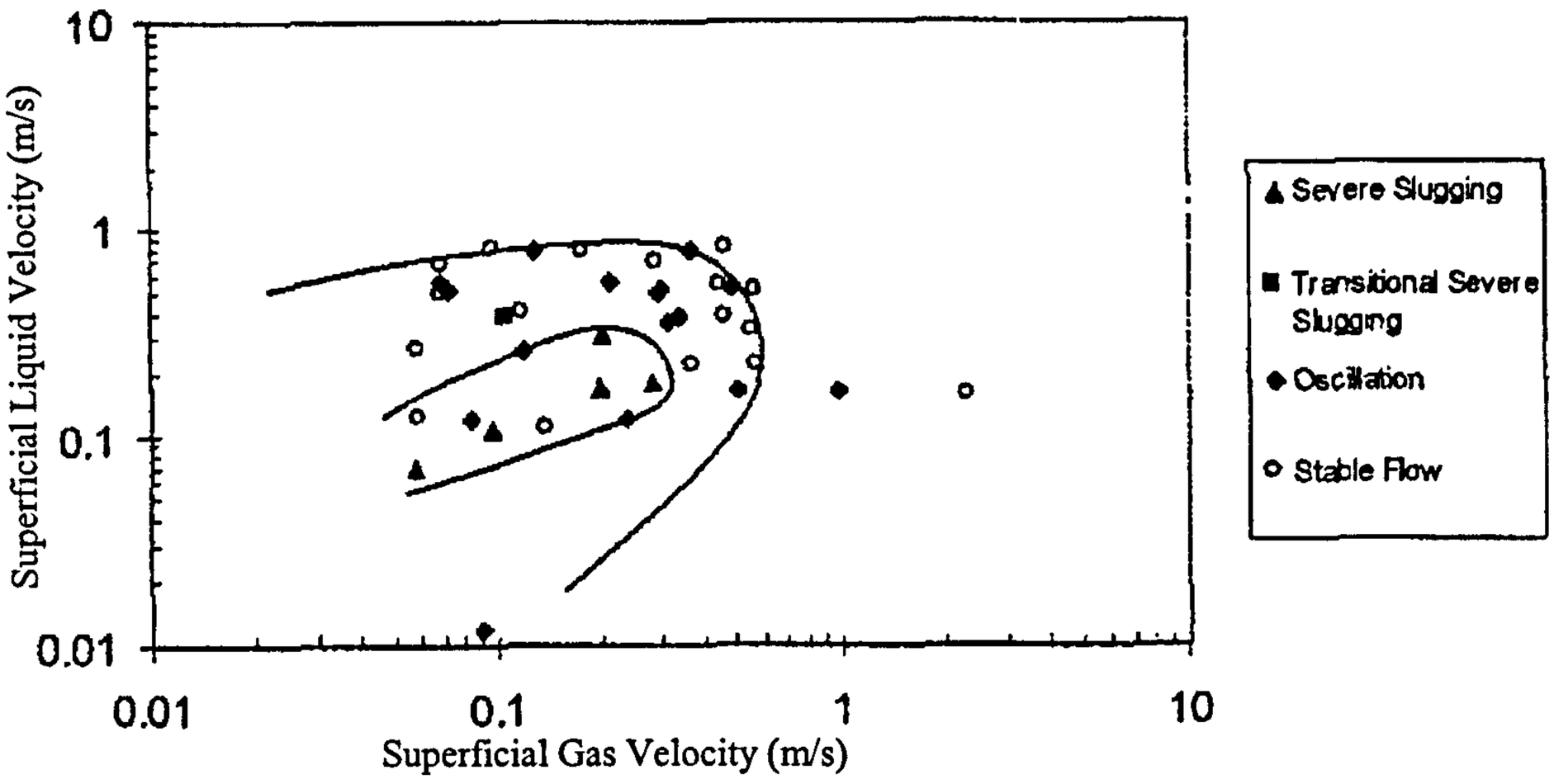

Figure 5.18 Cranfield University lazy 'S' riser flow pattern map, 7 bara[36]

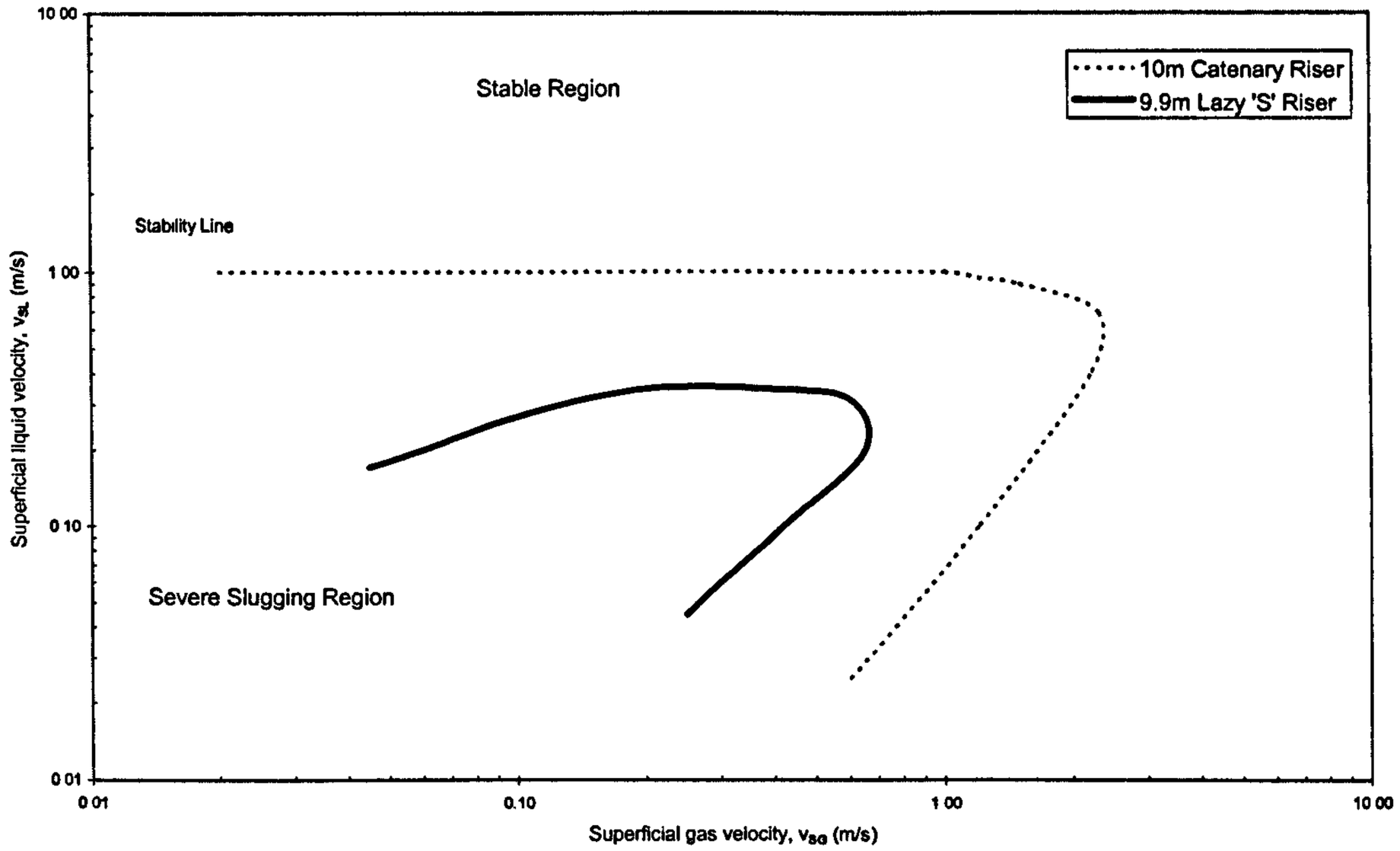

Figure 5.19 Comparison between free-hanging catenary riser[15] and lazy 'S' riser severe slugging boundaries

v_{SG} (m/s) v_{SL} (m/s)	cycle no.	v_L (m/s)	$(P6-P5)_{meas}$ (bar)	$h_{d'meas}$ (m)	ΔP_{fd} (bar)	h_{fd} (m)	$h_{d'actual}$ (m)	$(P4-P9)_{meas}$ (bar)	h_{rmeas} (m)	ΔP_{ful} (bar)	h_{ful} (m)	$h_{ractual}$ (m)	$h_{d'actual}$ + $h_{ractual}$ (m)
0.105	1	0 291	0.062	0.632	0.0008	0.0084	0.624	1.121	11.427	0 0037	0 0372	11.390	12.013
0.143	2	0.292	0 063	0 642	0.0008	0 0085	0.634	1.117	11.386	0.0037	0.0375	11 349	11.983
	3	0.284	0 061	0.622	0.0008	0.0080	0.614	1.116	11.376	0.0035	0.0354	11.341	11.955
	4	0.272	0 055	0.561	0 0007	0.0074	0.553	1.122	11.437	0 0032	0 0326	11.405	11.958
	5	0.269	0 063	0.642	0.0007	0 0072	0 635	1.115	11.366	0.0031	0.0319	11.334	11.969
	6	0 278	0.061	0 622	0 0008	0 0077	0.614	1.118	11.397	0.0033	0.0339	11.363	11.977
	7	0.277	0.063	0.642	0 0007	0.0076	0.635	1.116	11.376	0.0033	0.0337	11.342	11.977
0.172	1	0.198	0 064	0 652	0 0004	0 0039	0.648	1.120	11.417	0 0017	0 0173	11 400	12 048
0.093	2	0.197	0 061	0.622	0.0004	0 0038	0.618	1.119	11.407	0.0017	0 0170	11.390	12.008
	3	0 200	0.064	0 652	0 0004	0 0040	0 648	1.121	11.427	0 0017	0 0175	11.410	12 058
	4	0.183	0 065	0 663	0 0003	0 0033	0.659	1.118	11.397	0 0014	0.0146	11.382	12.041
	5	0.188	0.063	0.642	0.0003	0.0035	0 639	1.121	11.427	0.0015	0.0155	11.412	12 050
0.136	1	0.492	0 045	0 455	0 0024	0 0240	0.431	1.152	11.743	0 0104	0.1063	11 637	12 067
0.282	2	0 472	0 043	0 434	0 0022	0 0221	0 412	1.152	11.743	0 0096	0.0980	11 645	12 057
	3	0 479	0 042	0 424	0.0022	0 0227	0.401	1.151	11.733	0 0099	0.1006	11 632	12 034
	4	0 480	0 046	0 465	0 0022	0 0228	0.442	1.151	11.733	0 0099	0.1011	11 632	12 074
	5	0 489	0 045	0.455	0 0023	0 0238	0 431	1.151	11.733	0 0103	0.1053	11 628	12.059
	6	0.492	0.047	0.475	0.0024	0 0241	0.451	1.150	11.723	0.0105	0.1065	11.616	12.067
	7	0.476	0 046	0.465	0.0022	0.0225	0.442	1.148	11.702	0.0098	0 0994	11.603	12 045
0.283	1	0.382	0.046	0.469	0 0014	0.0145	0.454	1.142	11.641	0.0063	0.0641	11.577	12.032
0.195	2	0.377	0.044	0.449	0 0014	0.0141	0.434	1.137	11.590	0.0061	0.0624	11.528	11.962
	3	0.373	0 045	0.459	0 0014	0.0139	0.445	1.141	11.631	0.0060	0.0613	11.570	12.015
	4	0.364	0 045	0.459	0 0013	0.0132	0.446	1.139	11.611	0.0057	0.0583	11.552	11.998
	5	0.380	0 046	0.469	0.0014	0 0143	0.455	1.141	11.631	0.0062	0.0634	11.568	12.022
	6	0.373	0 046	0.469	0.0014	0.0139	0.455	1.140	11.621	0.0060	0.0613	11.560	12.015
	7	0.362	0 047	0.479	0 0014	0.0145	0.465	1.142	11.641	0.0063	0.0641	11.577	12.042
0.346	1	0.104	0 054	0.550	0.0001	0 0011	0.549	1.123	11.448	0 0005	0.0047	11 443	11.992
0.108	2	0 092	0 058	0.591	0 0001	0 0008	0 590	1.122	11.437	0.0004	0 0037	11.434	12 024
	3	0 065	0 055	0 561	0 0000	0 0004	0.560	1.123	11.448	0 0002	0 0018	11.446	12.006
	4	0.090	0.055	0.561	0.0001	0.0008	0.560	1.123	11.448	0.0004	0.0036	11.444	12.004
0.315	1	0 327	0 043	0.438	0.0010	0 0106	0.428	1.138	11.600	0.0046	0.0469	11.554	11.981
0.191	2	0.379	0 042	0.428	0.0014	0.0143	0.414	1.138	11.600	0.0062	0.0632	11.537	11.951
	3	0.350	0 046	0 469	0.0012	0.0122	0.457	1.140	11.621	0.0053	0.0539	11.567	12.024
	4	0.279	0.045	0.459	0.0008	0 0077	0 451	1.137	11.590	0.0034	0.0343	11.556	12.007
	5	0.362	0.045	0 459	0.0013	0.0130	0 446	1.140	11.621	0.0057	0.0576	11.563	12.009
	6	0.368	0 047	0.479	0 0013	0.0134	0.466	1.138	11.600	0.0058	0.0594	11.541	12.007
	7	0.361	0 046	0.469	0.0013	0.0129	0.456	1.135	11.570	0.0056	0.0572	11.513	11.969
0.26	1	0 036	0 055	0 561	0 0000	0.0001	0 561	1.119	11.407	0 0001	0.0006	11.406	11.967
0 06	2	0.044	0 054	0.550	0 0000	0 0002	0.550	1.118	11.397	0 0001	0.0008	11.396	11 946
	3	0.041	0 055	0.561	0 0000	0 0002	0 560	1.119	11.407	0 0001	0.0007	11 406	11.966
0 07 0.1	1	0.144	0 065	0 660	0.0002	0 0021	0.657	1.122	11.437	0.0009	0.0091	11.428	12.086
0 31	1	0.538	0.037	0.378	0.0028	0.0287	0.349	1.159	11.814	0.0125	0.1271	11.687	12.037
0.31	2	0.516	0.041	0.418	0.0026	0.0264	0.392	1.162	11.845	0 0115	0.1168	11.728	12.120
	3	0 487	0 038	0 383	0 0023	0 0236	0 360	1 156	11 784	0 0102	0 1043	11 680	12 039

Figure 5.20 Results of the liquid inventory in riser downward section investigations

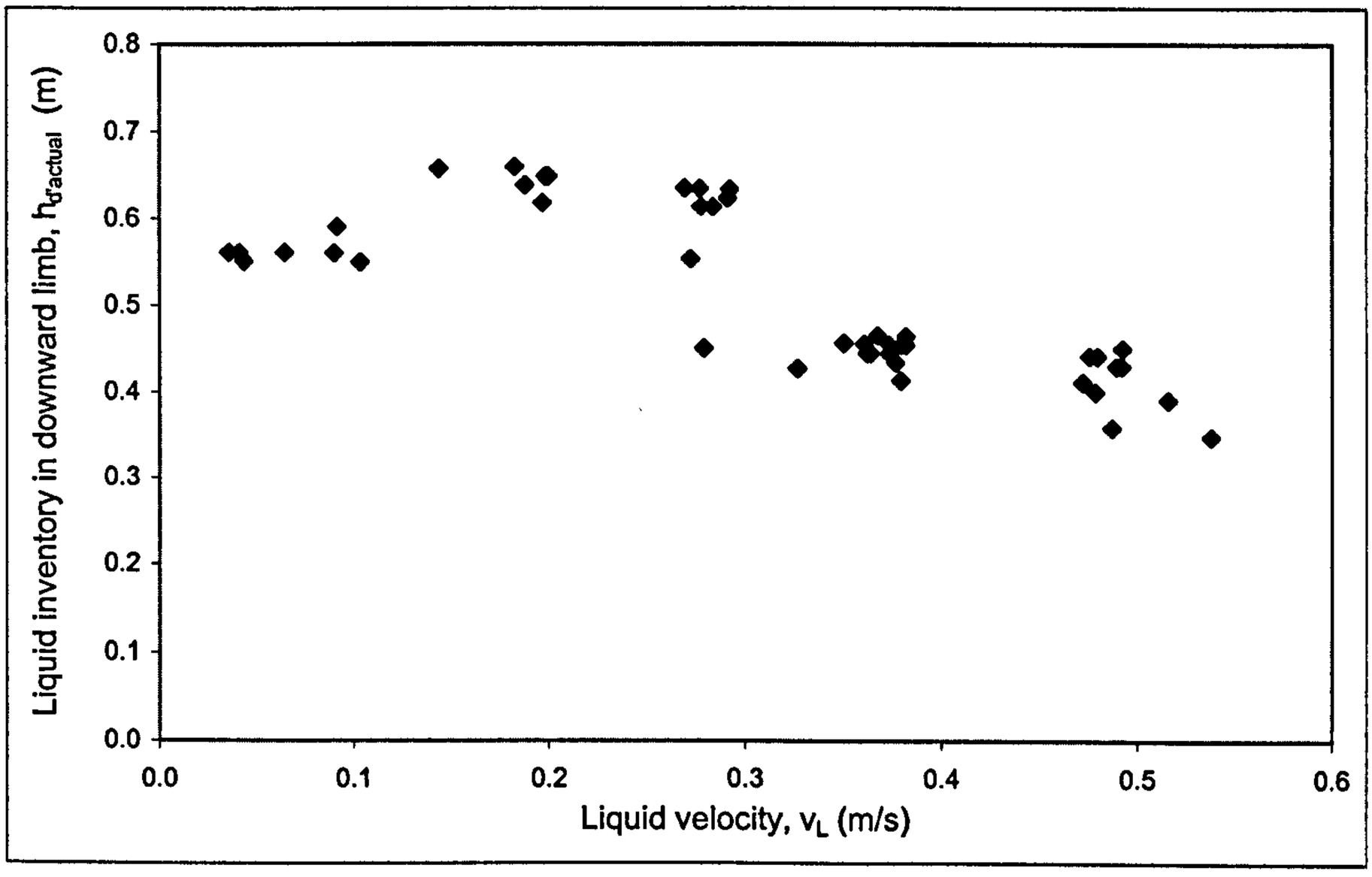

Figure 5.21 Liquid inventory in riser downward section during severe slugging versus liquid velocity

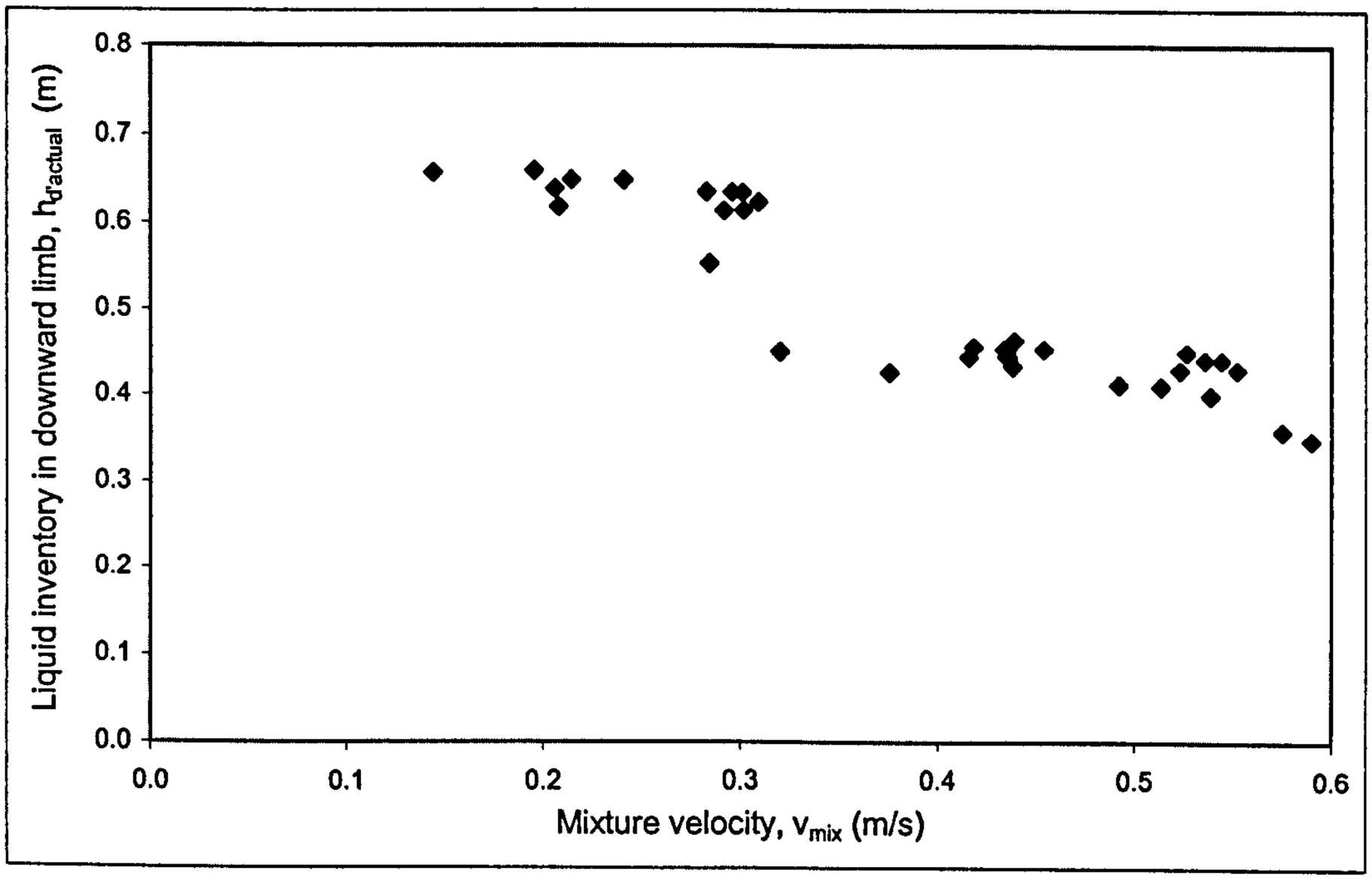

Figure 5.22 Liquid inventory in riser downward section during severe slugging versus mixture velocity

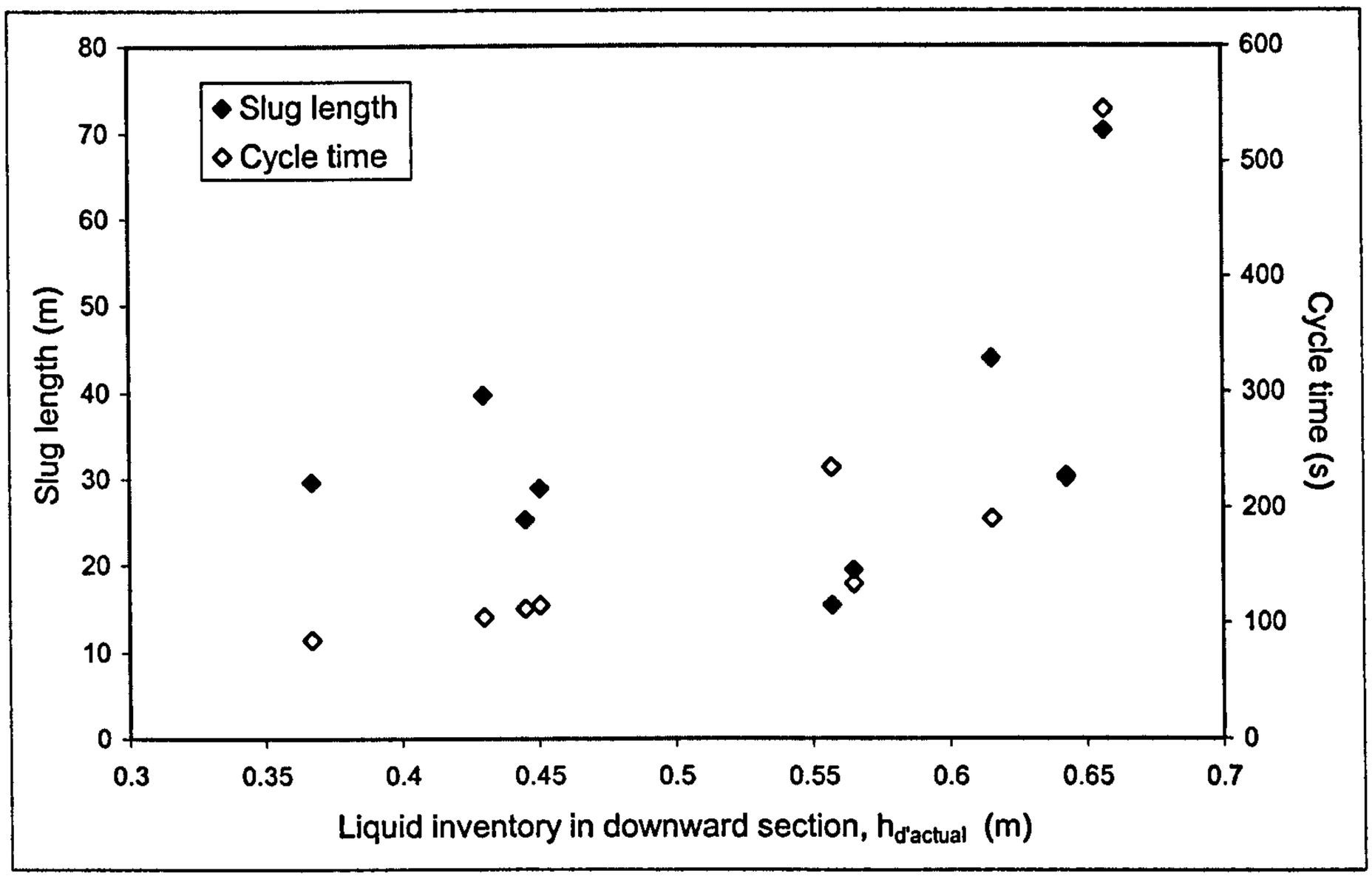

Figure 5.23 Effect of trapped gas on slug length and cycle time

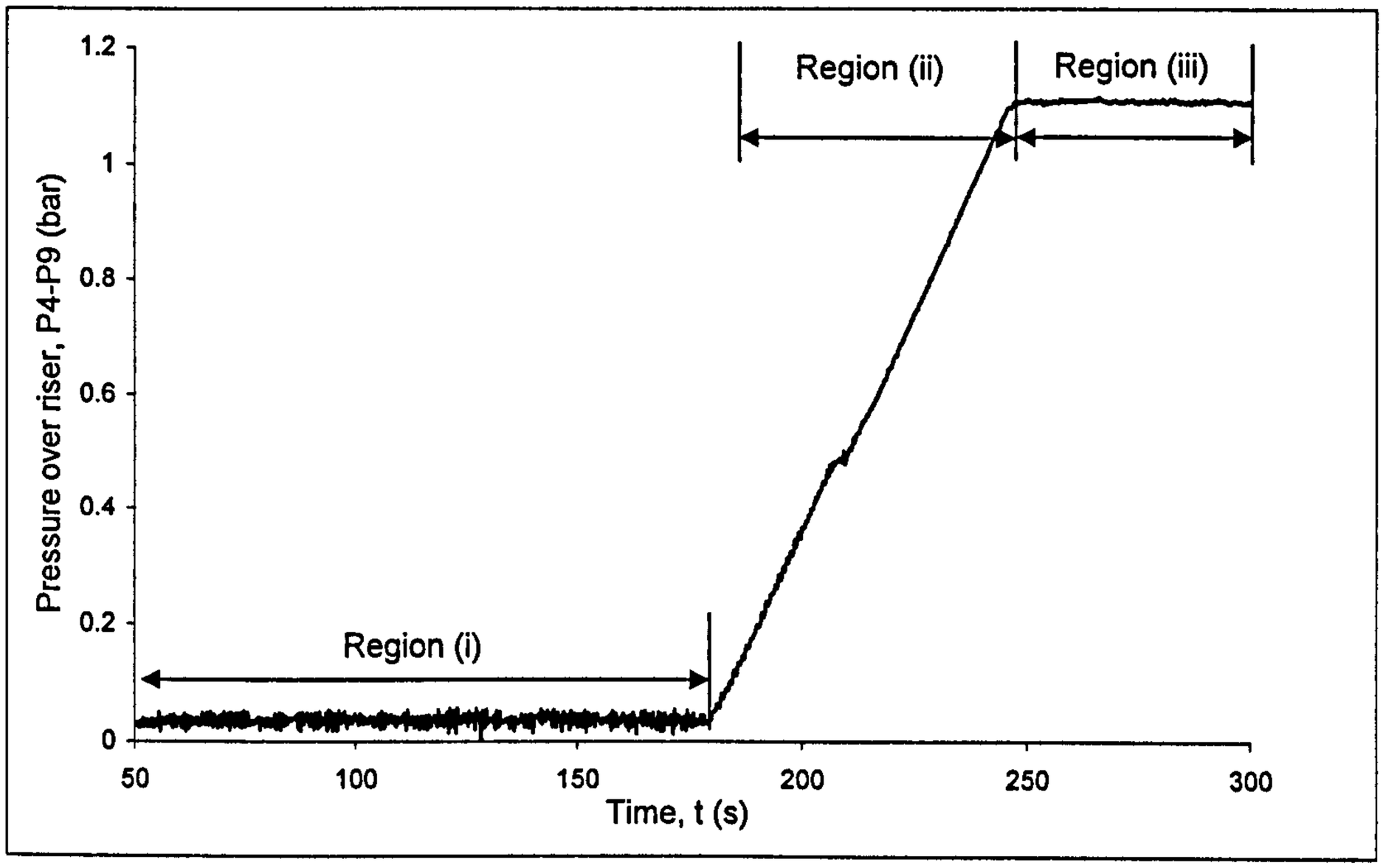

Figure 5.24 Build-up stage simulation test: pressure over riser, P4-P9 [v_L = 0.234 m/s]

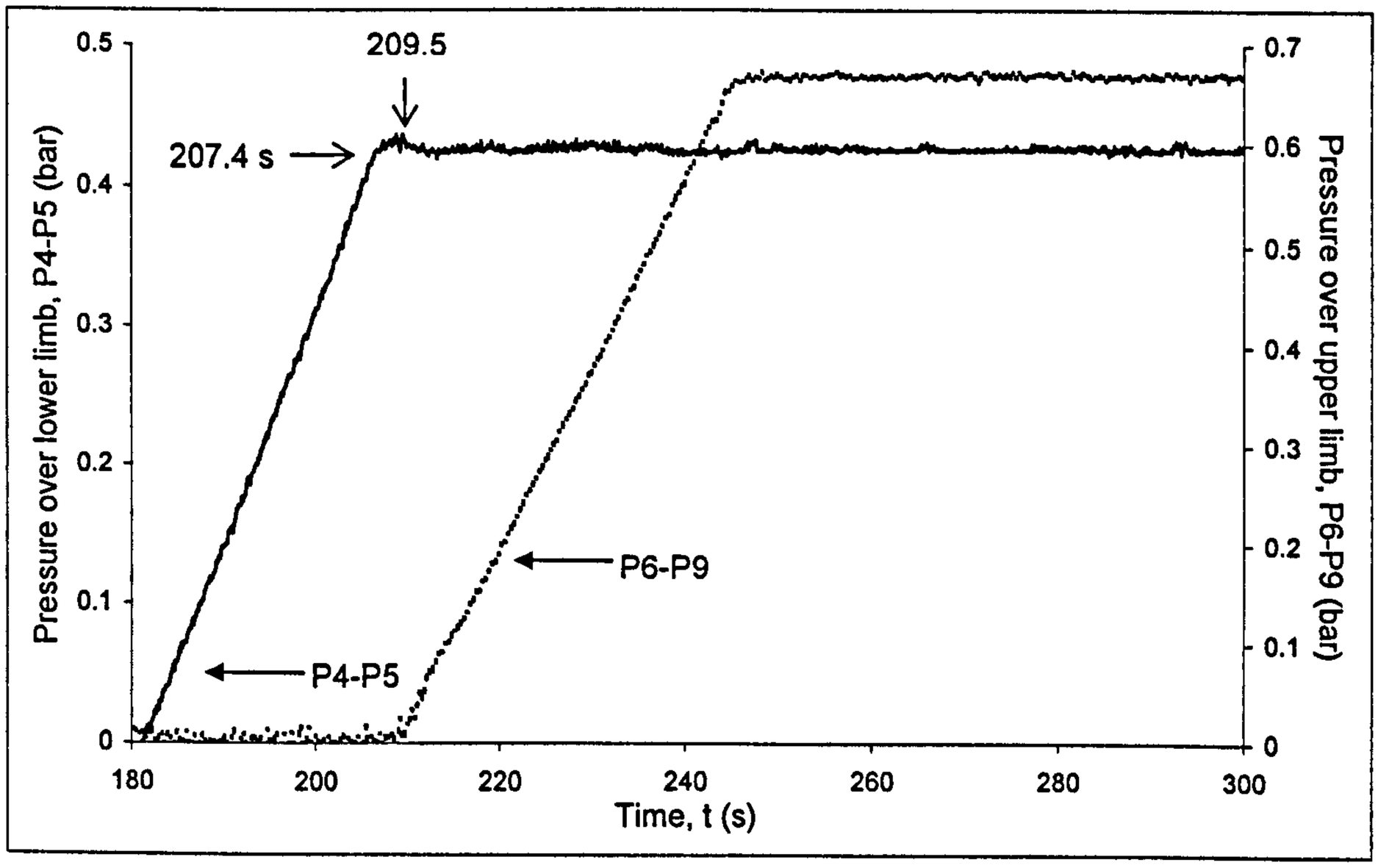

Figure 5.25 Build-up stage simulation test: pressure over lower limb, P4-P5, and upper limb, P6-P9, as riser filled with liquid [v_L = 0.234 m/s]

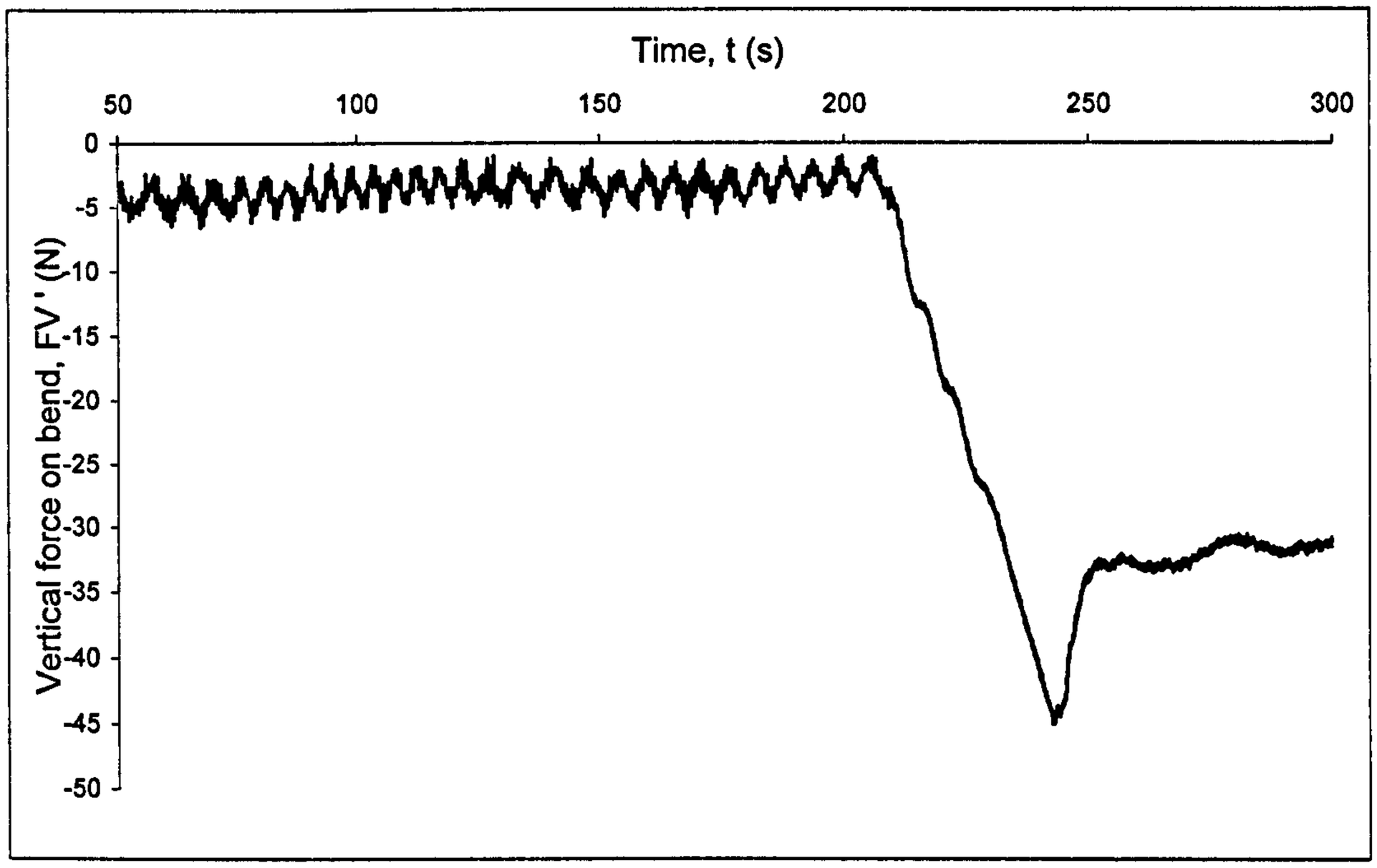

Figure 5.26 Build-up stage simulation test: vertical force on a bend
[v_L = 0.234 m/s]

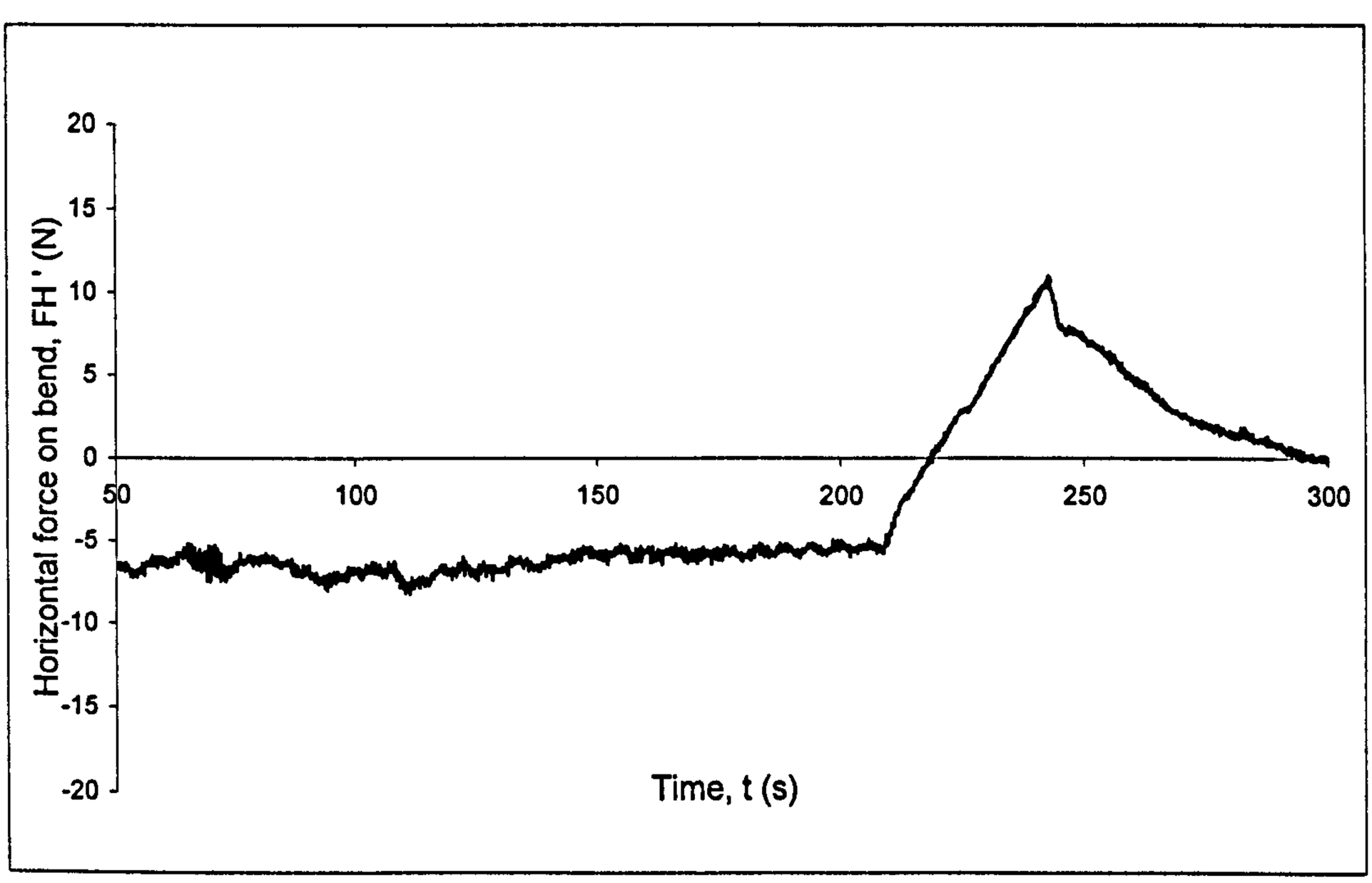

Figure 5.27 Build-up stage simulation test: horizontal force on a bend
[v_L = 0.234 m/s]

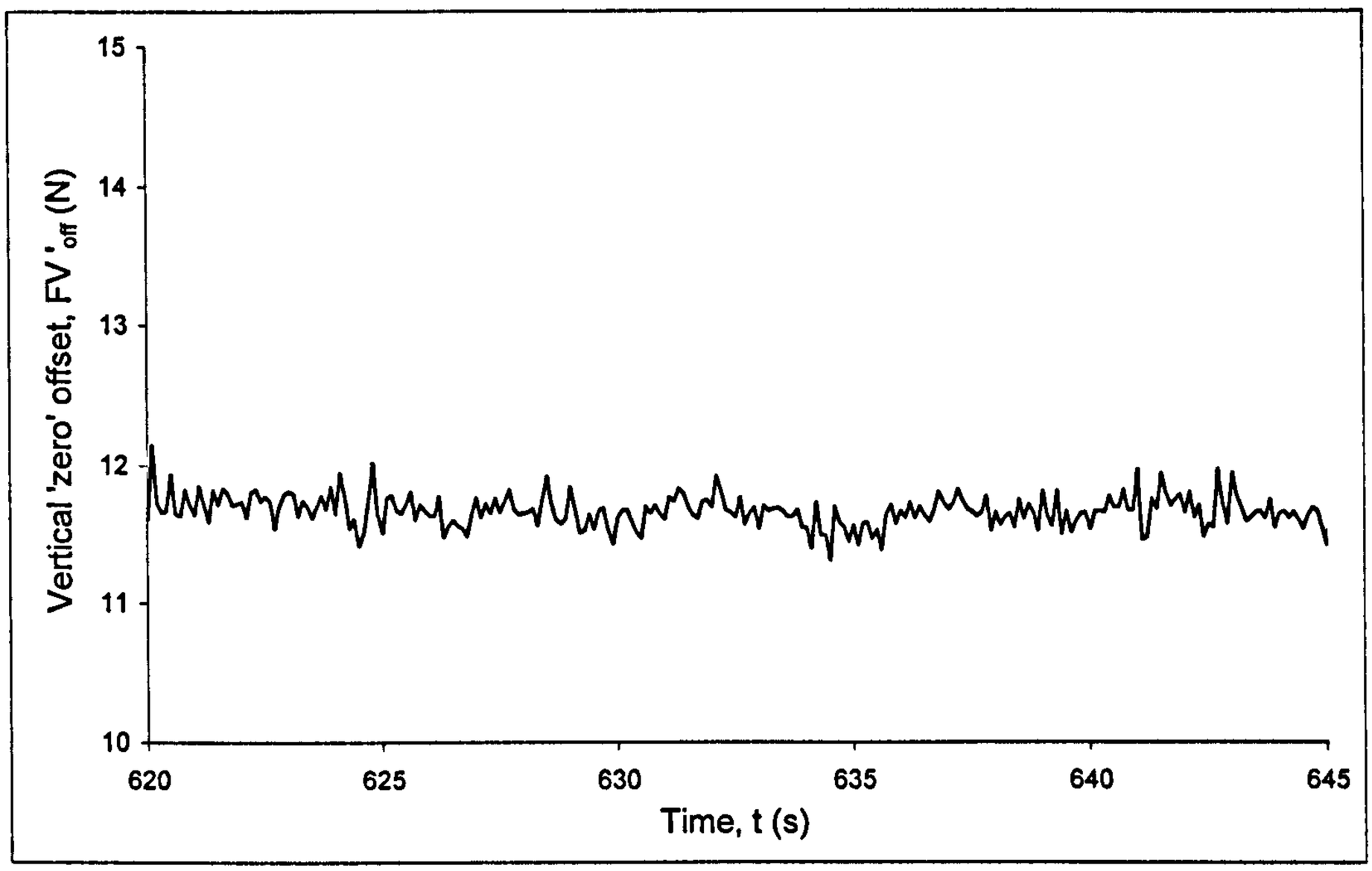

Figure 5.28 Vertical 'zero' offset under the condition of no gas or liquid in the flow loop

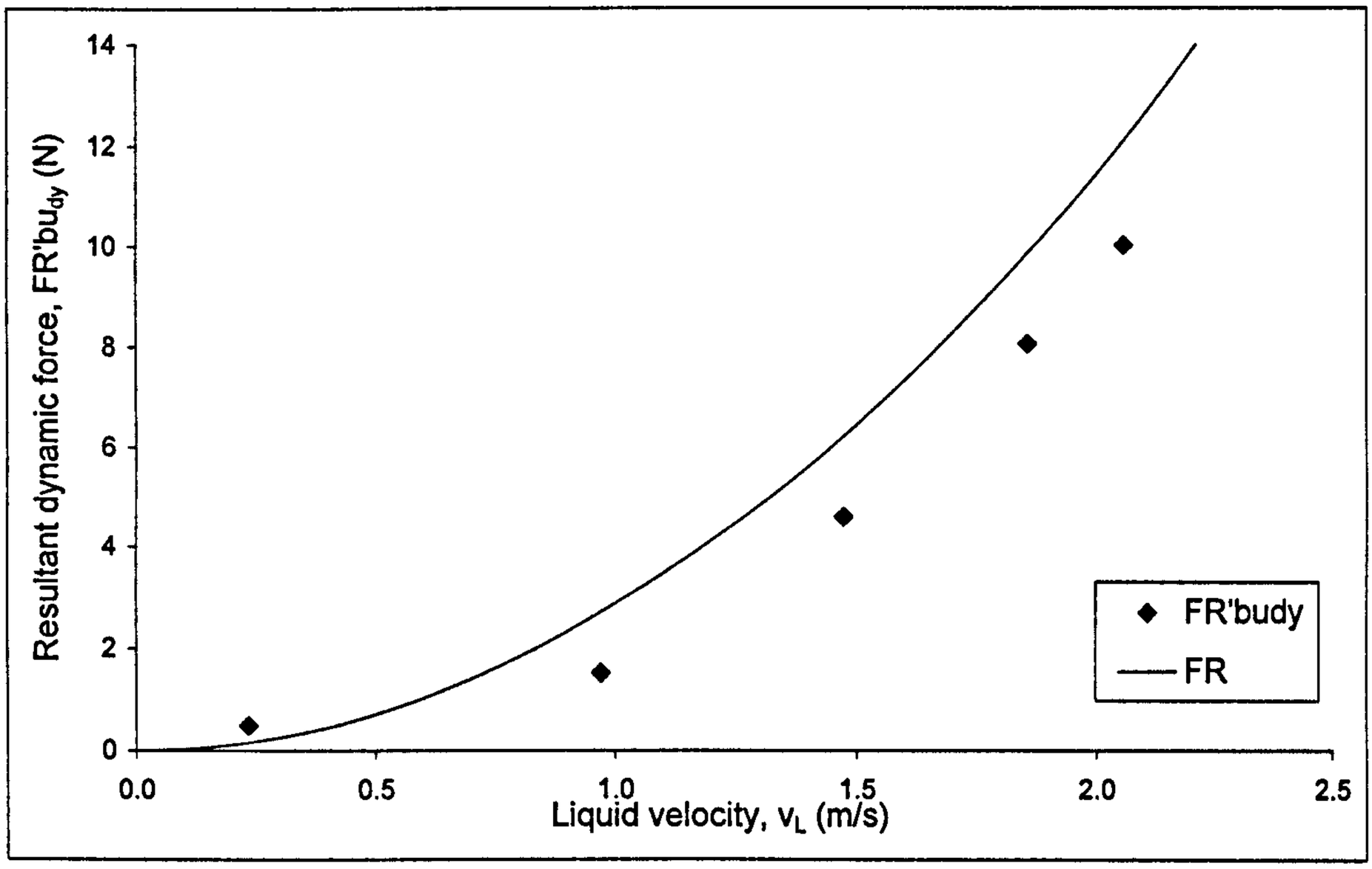

Figure 5.29 Build-up stage simulation test: resultant dynamic force on a bend compared to theory, $FR = 2^{0.5} rho_L A v_L^2$

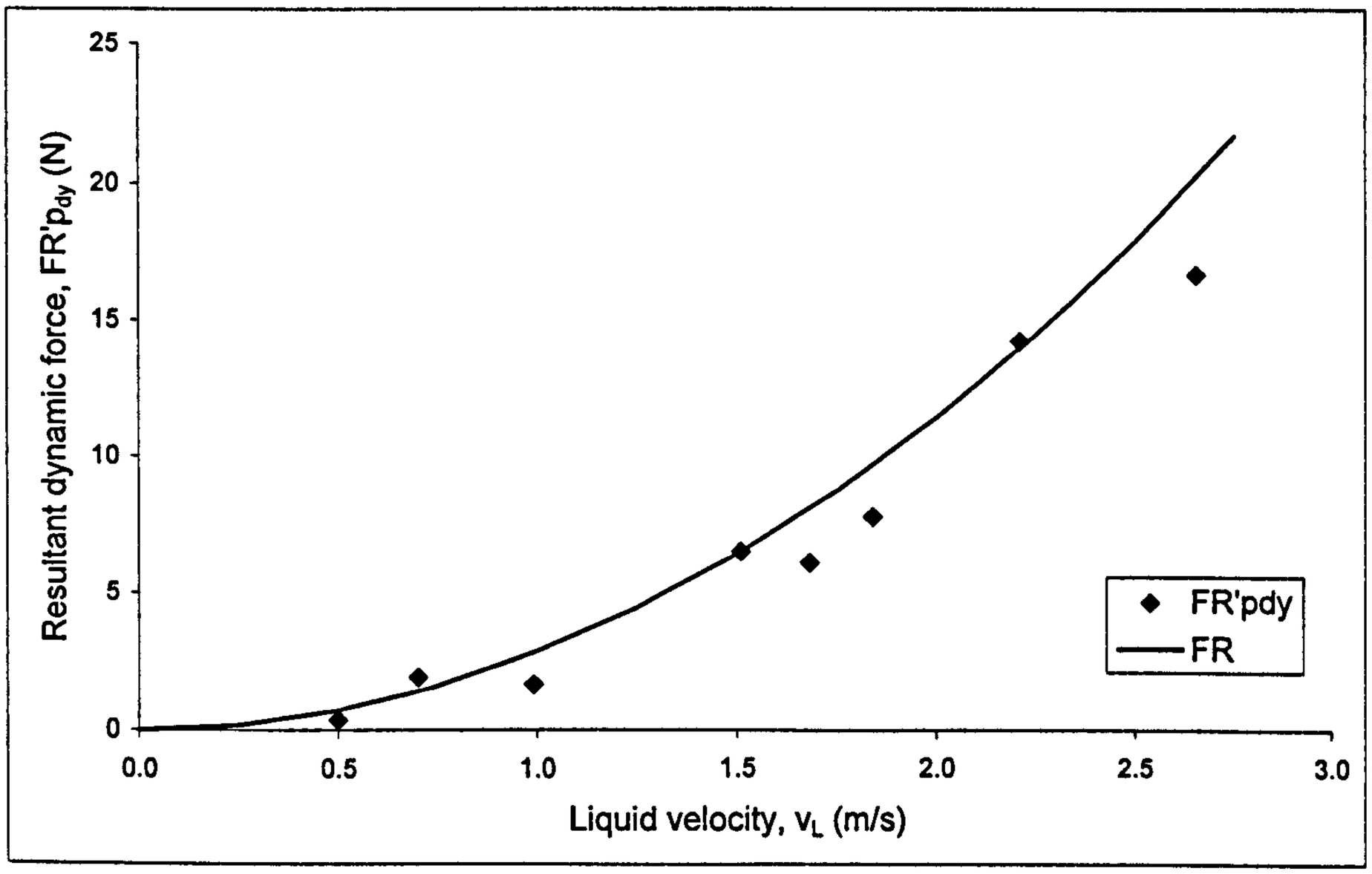

Figure 5.30 Production stage simulation test: resultant dynamic force on a bend compared to theory, $FR = 2^{0.5} rho_L A v_L^2$

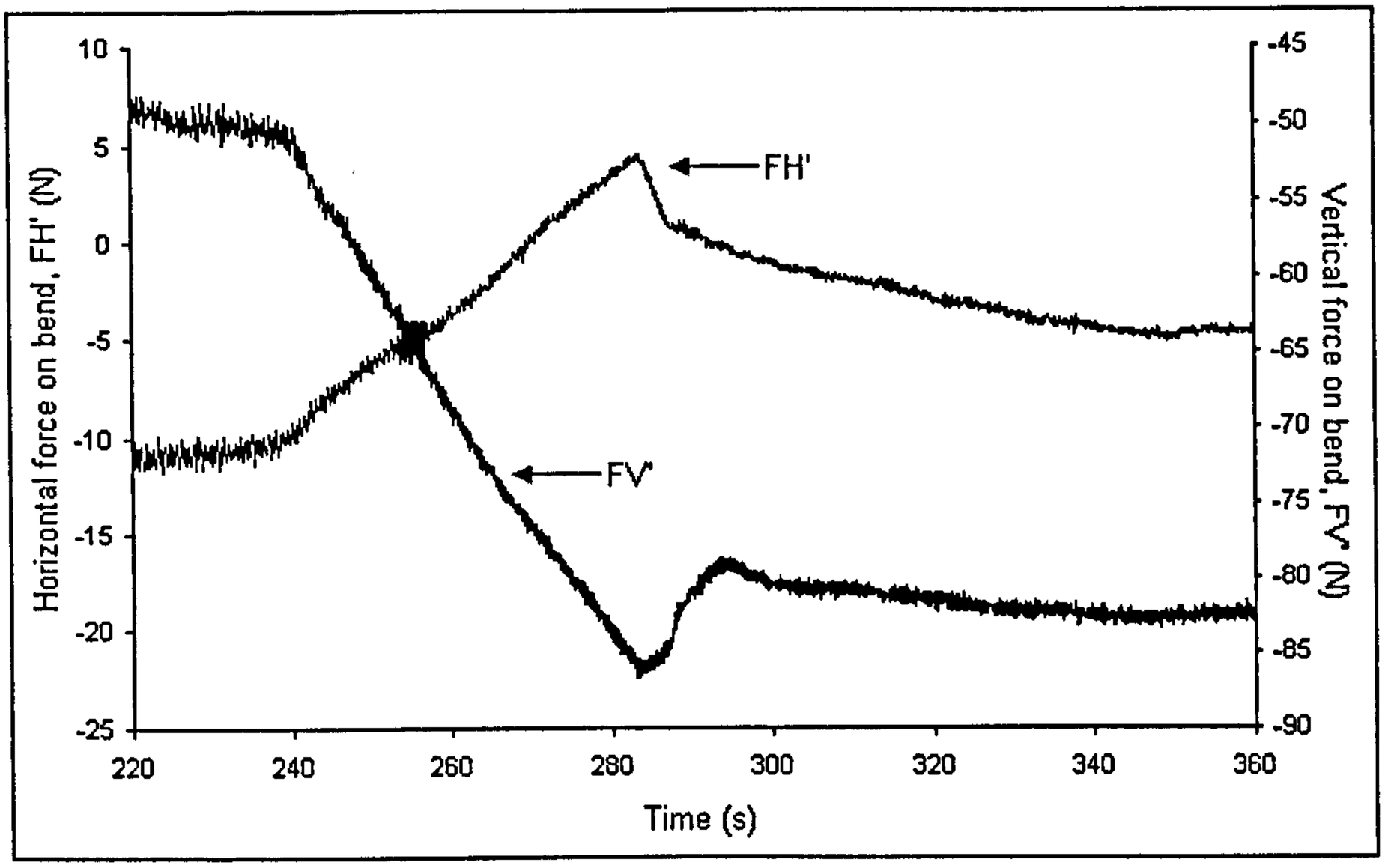

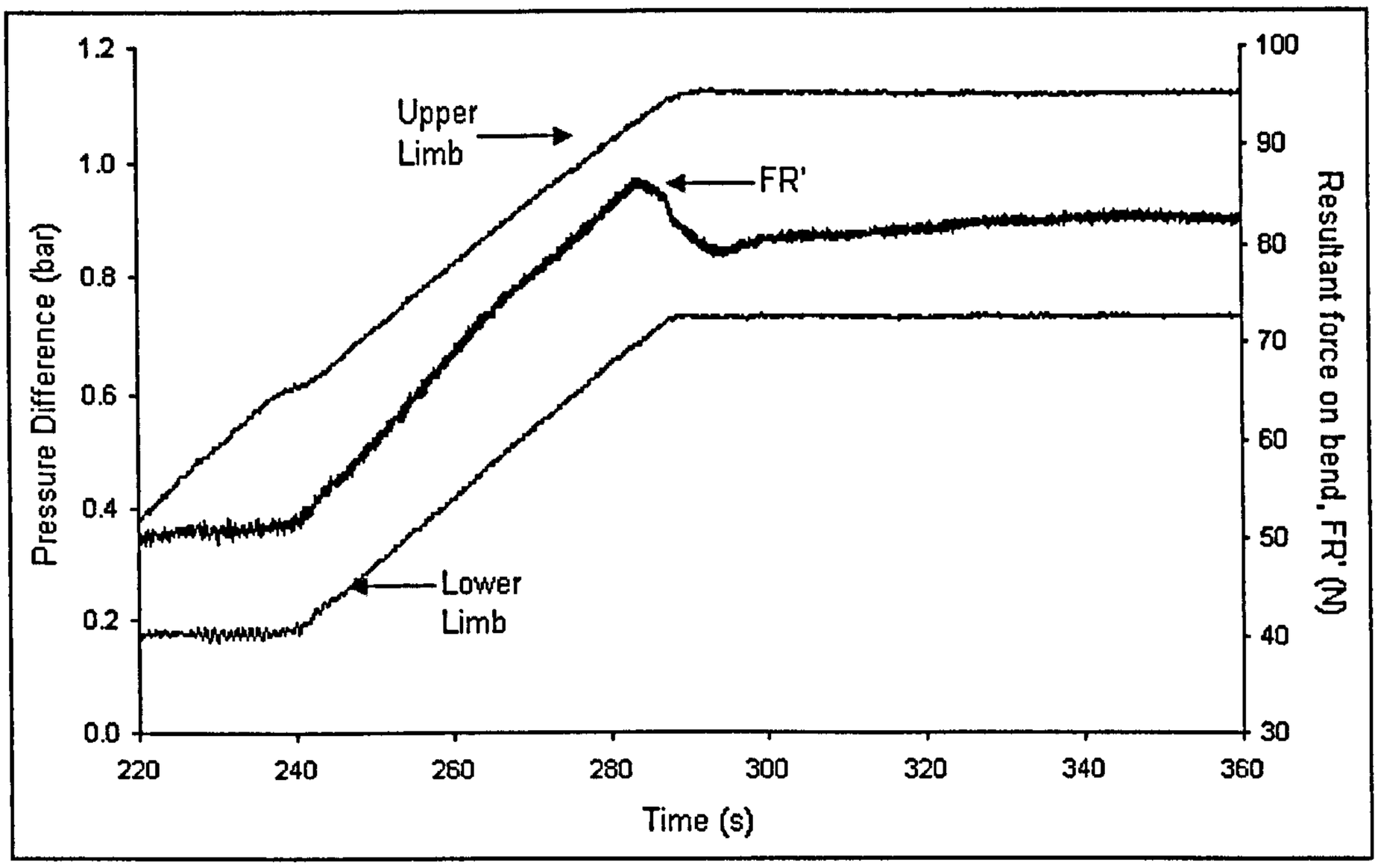

Figure 5.31 Typical traces during the slug build-up and slug production stage of the severe slugging 1 cycle

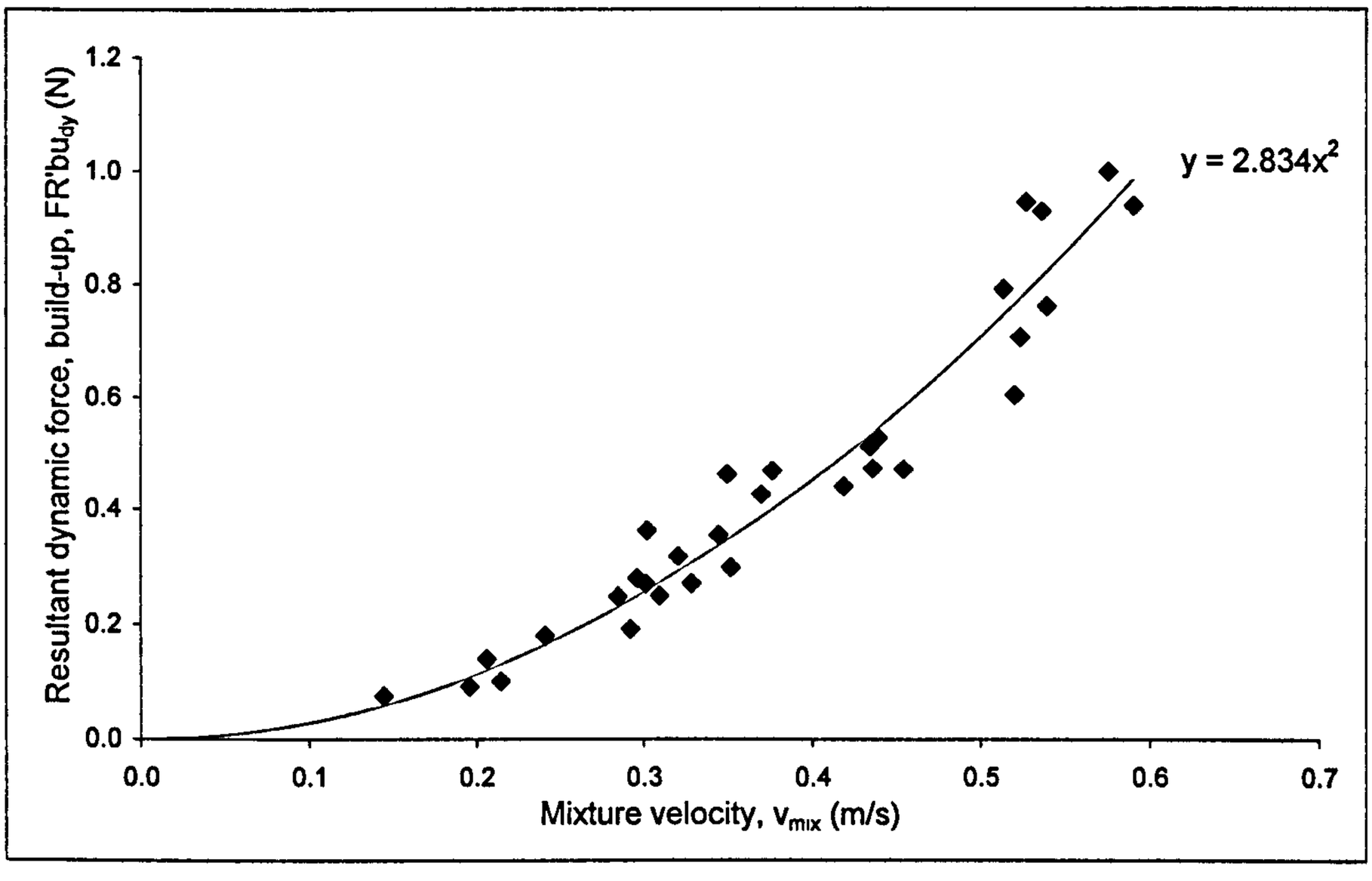

Figure 5.32 Resultant dynamic force on a bend during slug build-up

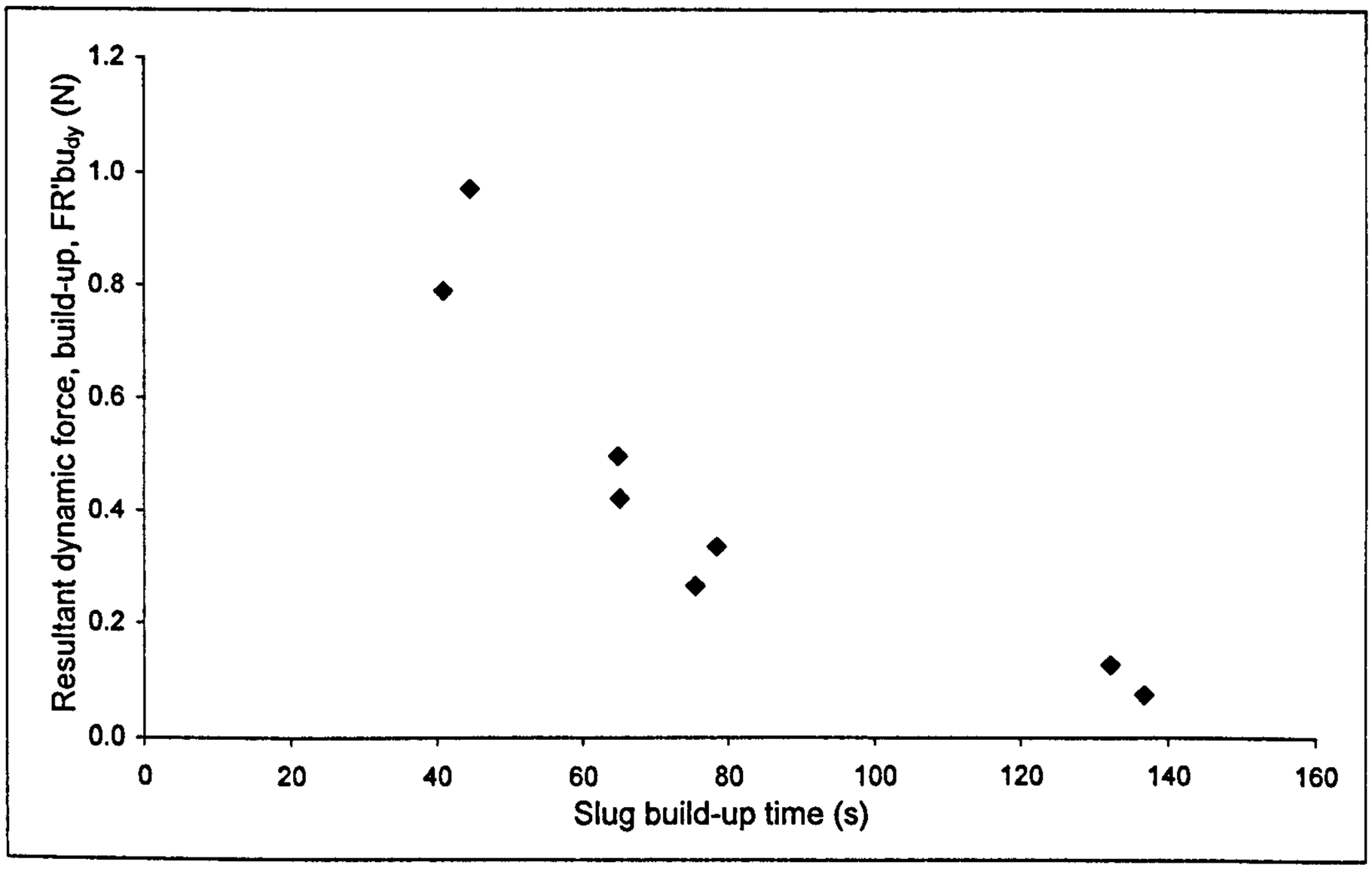

Figure 5.33 Comparison of resultant dynamic force on a bend with slug build-up time

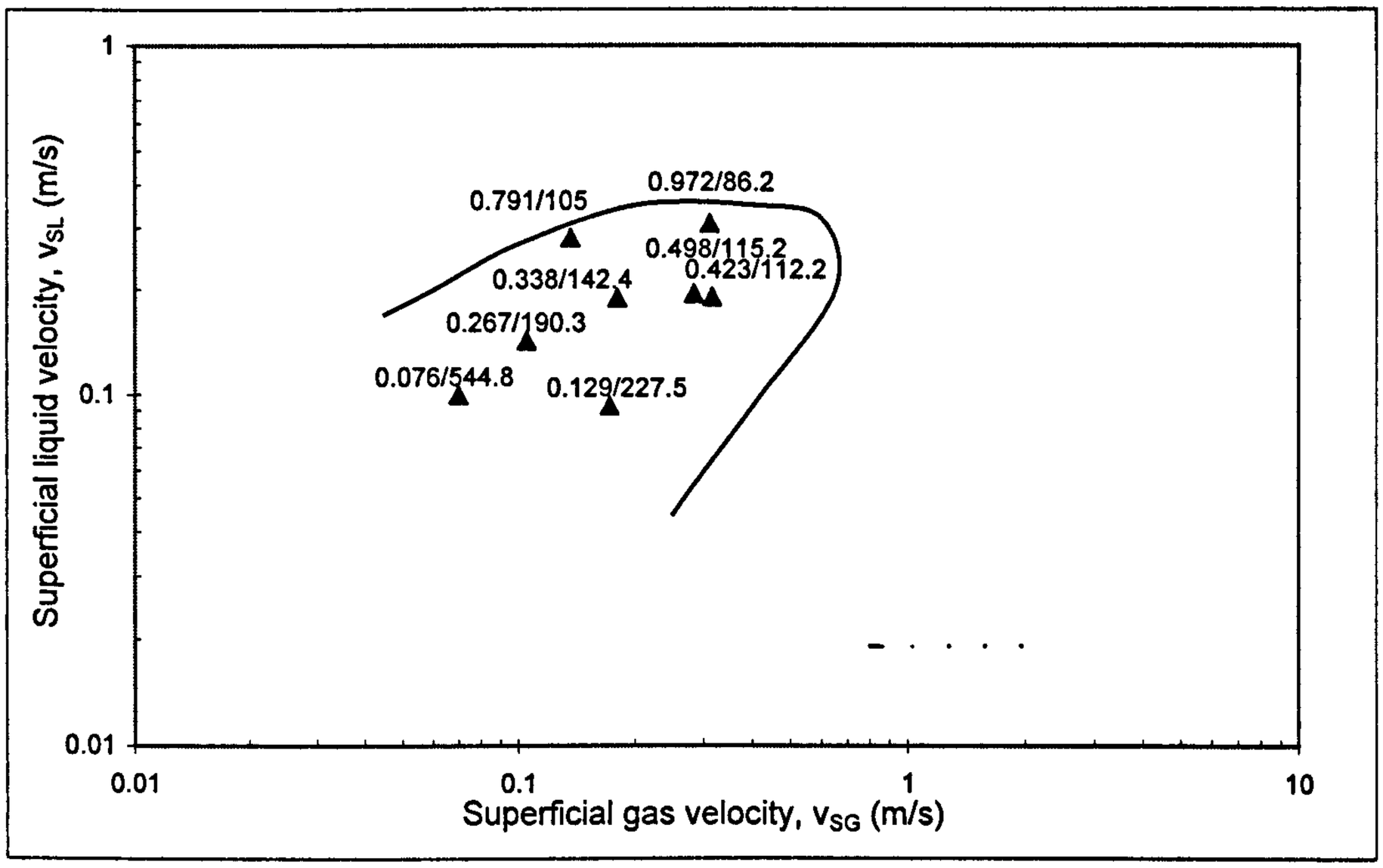

Figure 5.34 Flow pattern map showing resultant dynamic force on a bend during slug build-up and cycle times

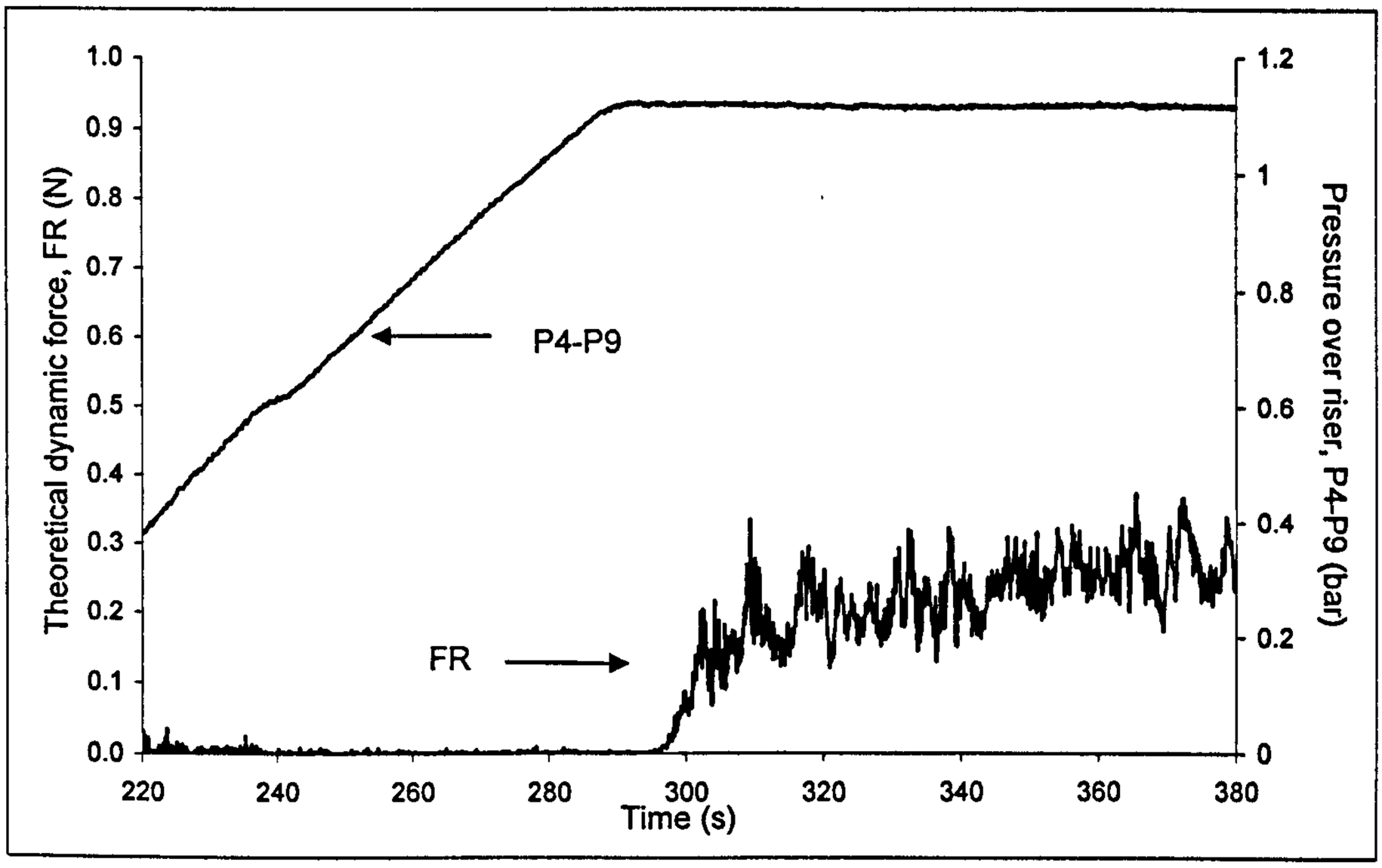

Figure 5.35 Theoretical resultant dynamic force on a bend during slug build-up and production

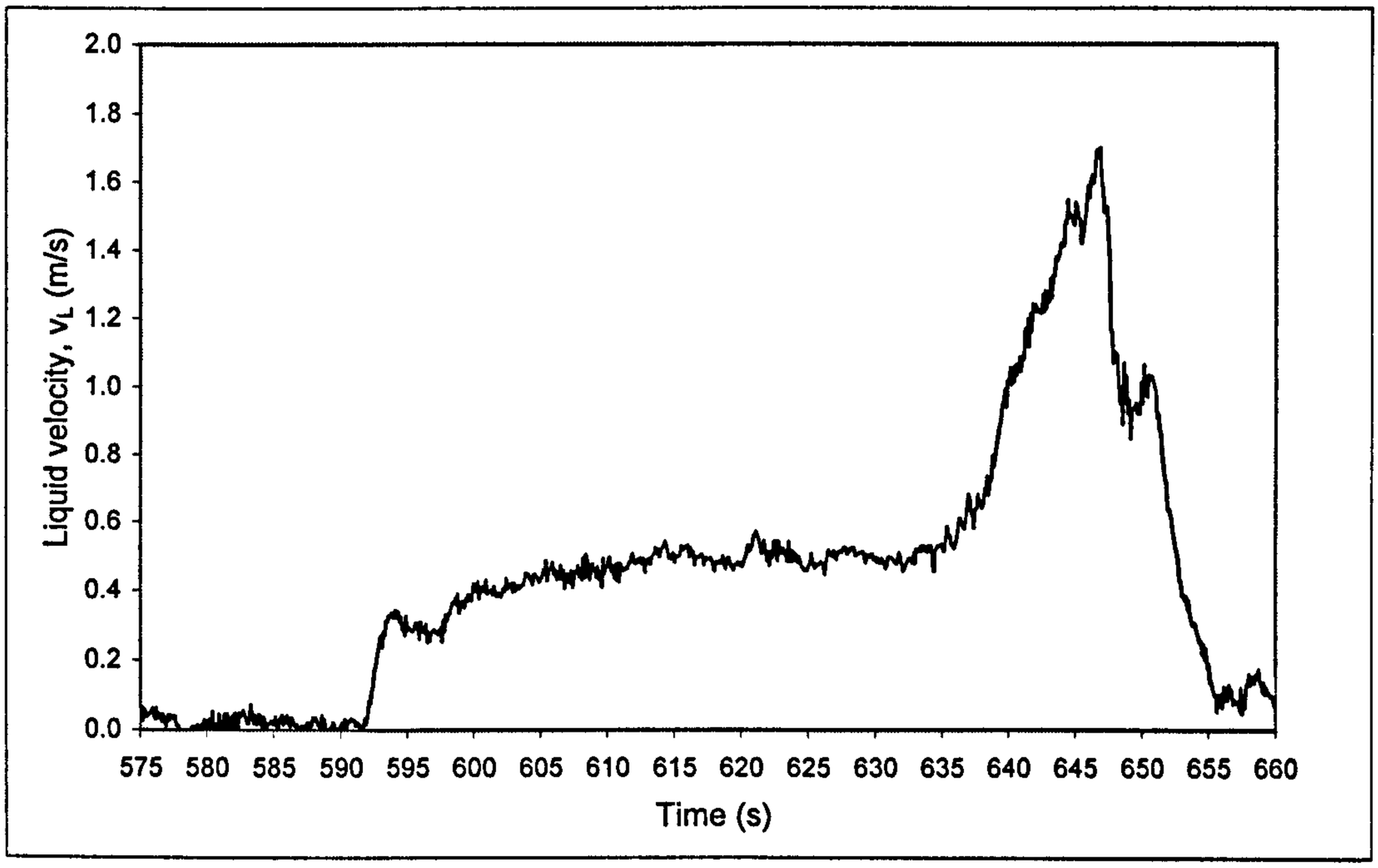

Figure 5.36 Liquid velocity at riser outlet [v_{SG} = 0.14m/s, v_{SL} = 0.28m/s]

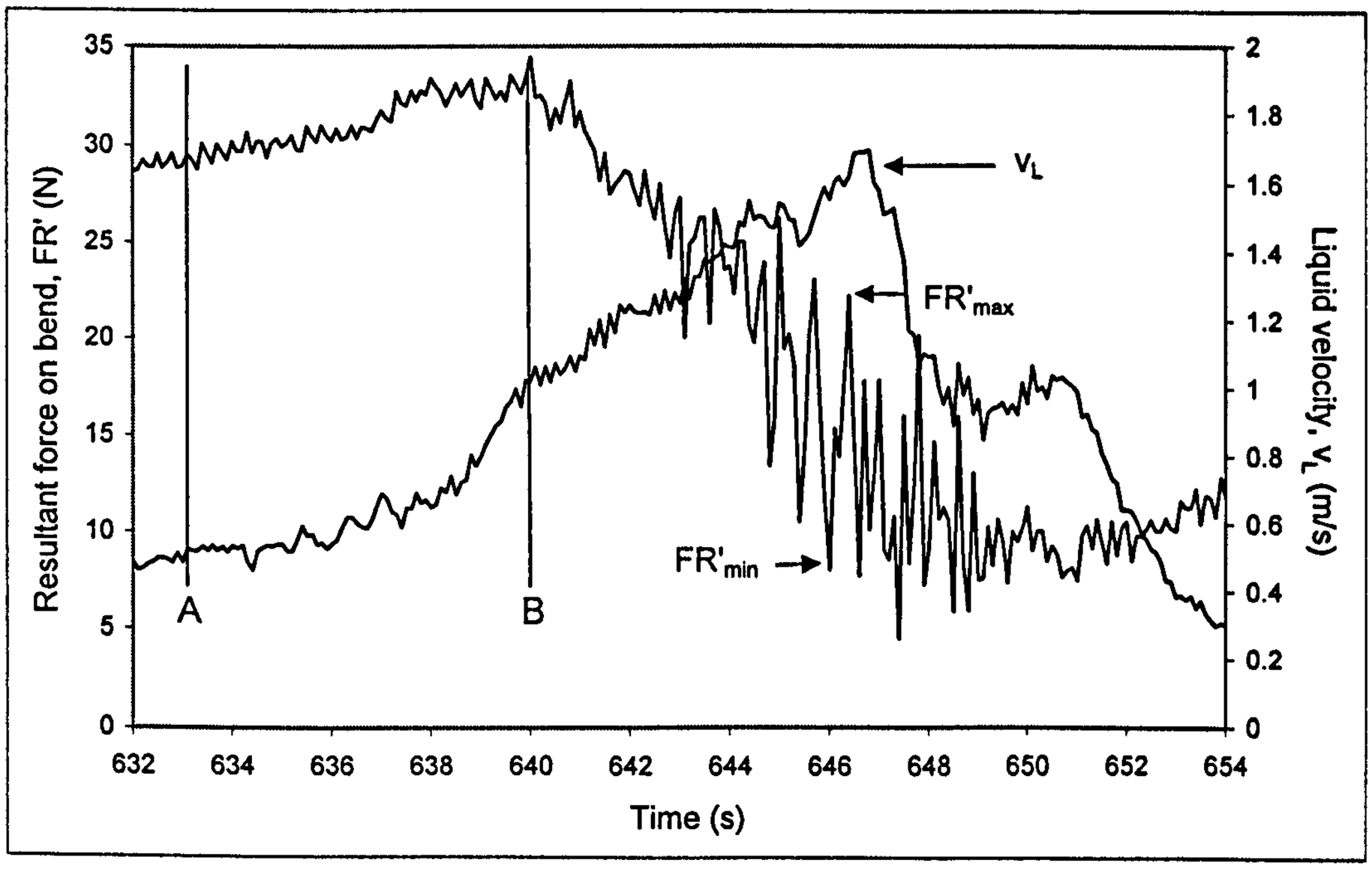

Figure 5.37 Resultant force and liquid velocity during bubble penetration and gas blowdown [v_{SG} = 0.14m/s, v_{SL} = 0.28m/s]

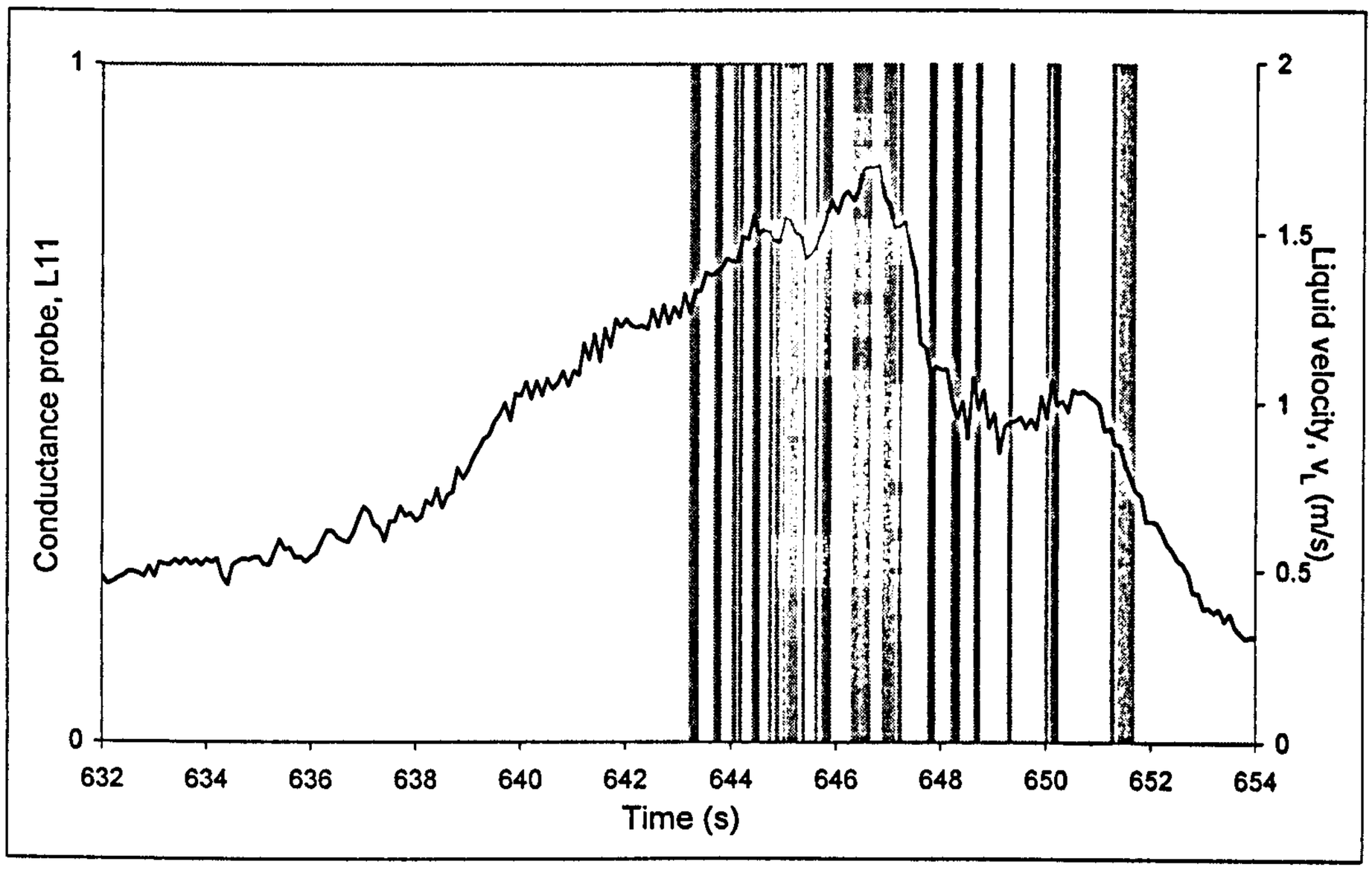

Figure 5.38 Conductance probe and liquid velocity trace during bubble penetration and gas blowdown [v_{SG} = 0.14 m/s, v_{SL} = 0.28 m/s]

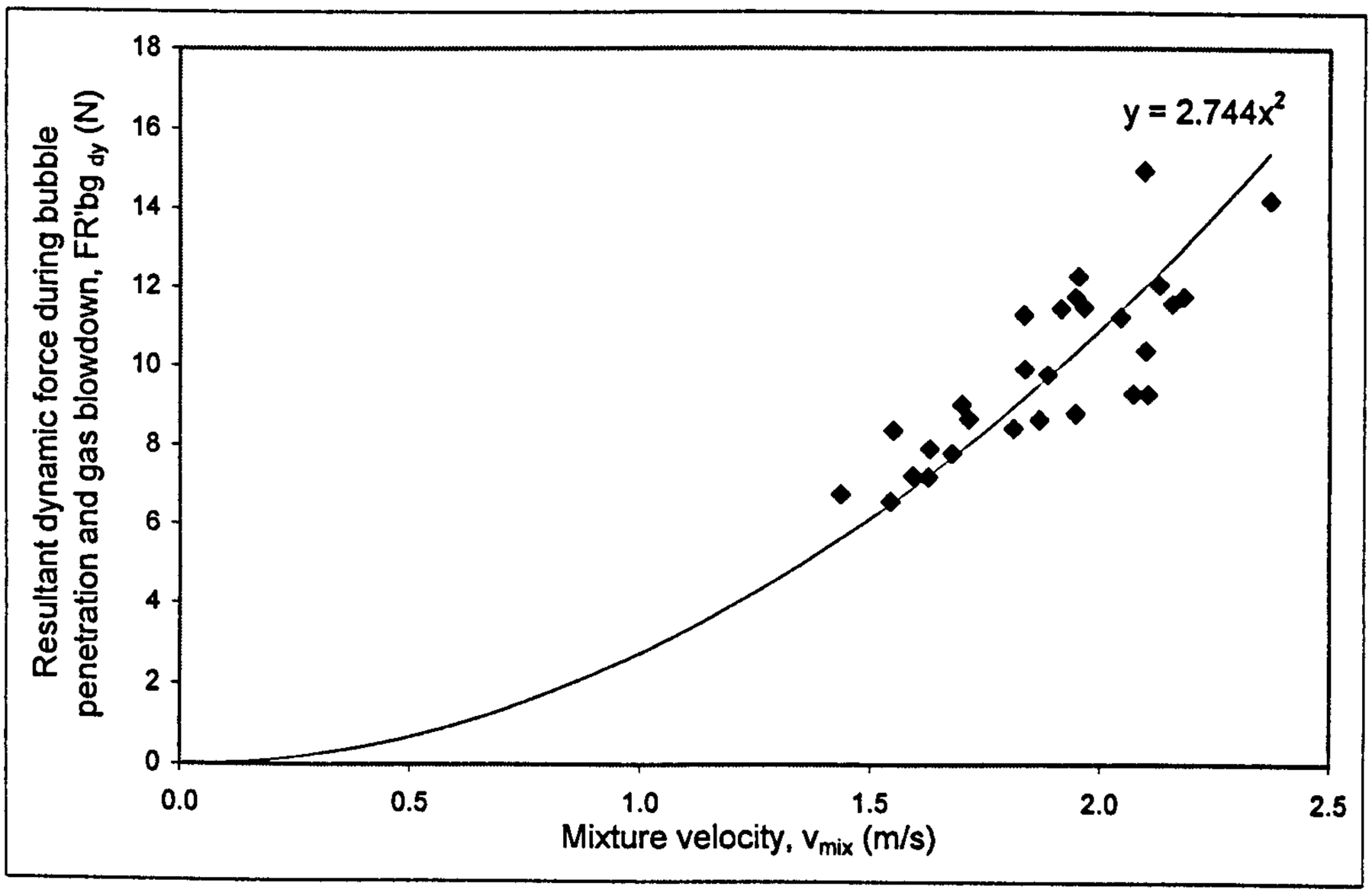

Figure 5.39 Resultant dynamic force on a bend during bubble penetration and gas blowdown

Cycle Number	Measured Resultant Dynamic Force (N)	Theoretical Resultant Dynamic Force (N)
1	20.08	7.02
2	12.34	7.65
3	16.59	9.49
4	17.06	7.65
5	13.25	7.84

Figure 5.40 Measured and predicted resultant dynamic force during bubble penetration and gas blowdown

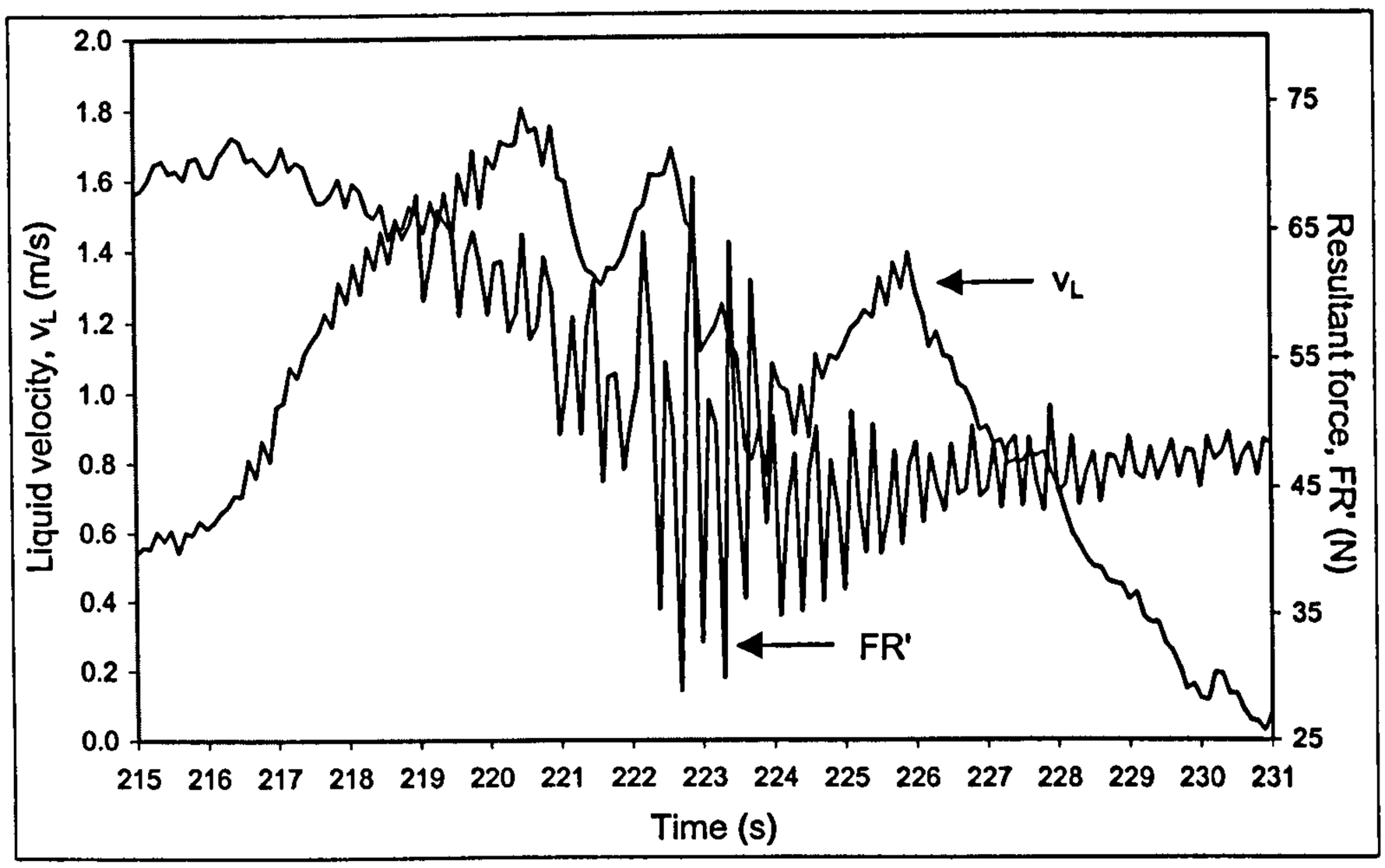

Figure 5.41 Resultant force and liquid velocity during bubble penetration and gas blowdown, worse case

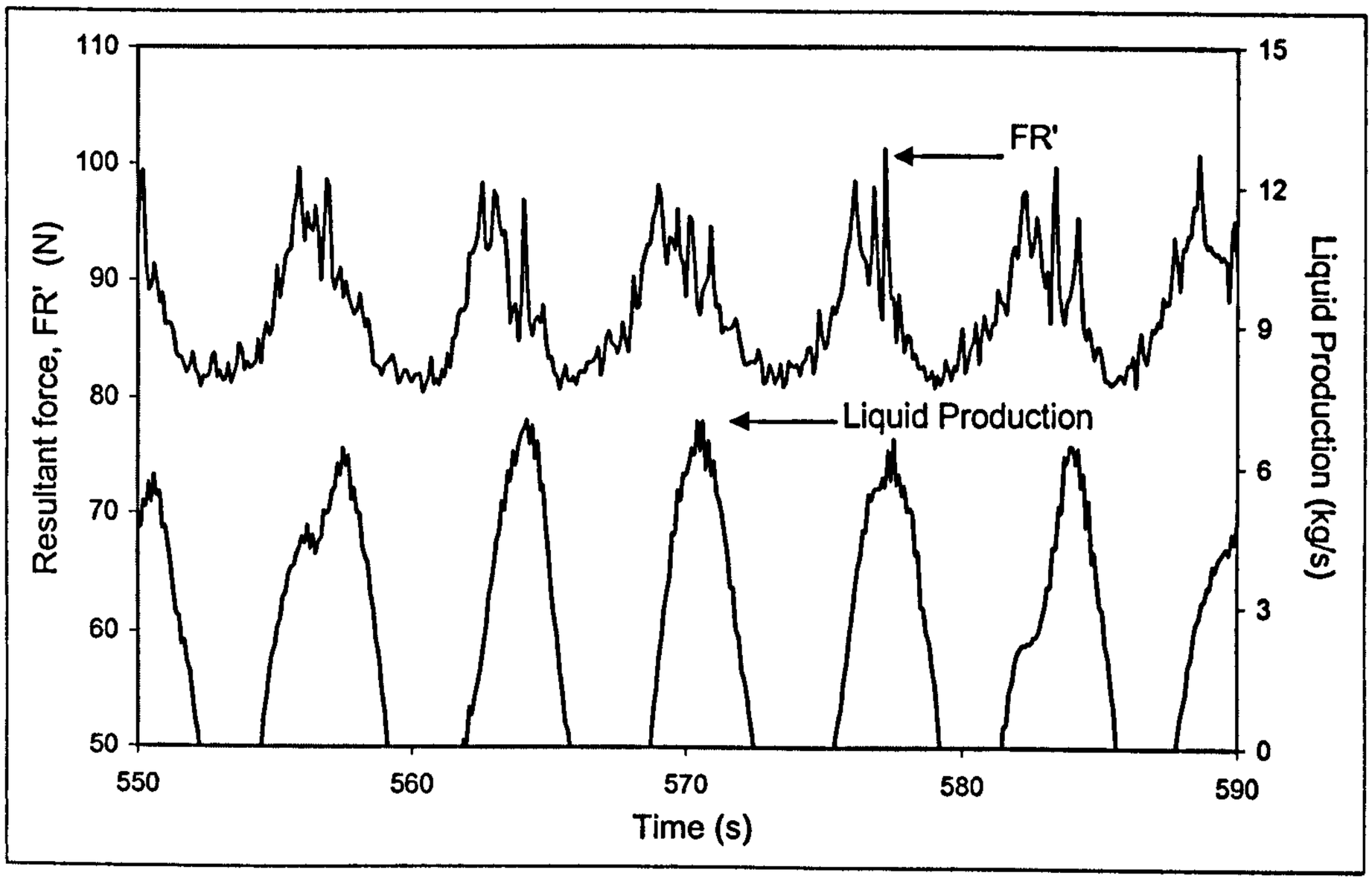

Figure 5.42 Resultant force and liquid production during normal slug flow

CHAPTER 6- CONCLUSIONS AND FURTHER WORK

This chapter presents the findings from the research. The chapter is divided into three main sections, the first two summarising the research undertaken and the conclusions for each main research topic. The third section aims to complete this research by presenting some proposals for further work.

The research presented in this thesis focused on the collection of new experimental data to determine the characteristics of severe slugging and to model the forces on a bend during the slug build-up, production and bubble penetration and gas blowdown stages of the severe slugging cycle.

The literature review in Chapter 2 highlighted the limited investigations into severe slugging in flexible shaped risers. Previous work had not provided detailed information on severe slugging characteristics or the effect of trapped gas in the riser downward limb. Investigations to determine the forces on pipe bends concentrated on the forces due to normal slug flow in horizontal pipelines. The literature review showed that no previous research into the normal and severe slug flow forces in a pipeline-riser system had been performed.

6.1 Research Summary

The following research was carried out:

(i) A set of experimental data was collected in an 'S' shaped riser, covering a range of flow regimes: severe slugging, transitional severe slugging, oscillation and normal slug flow.

(ii) Based on the experimental data, the characteristics of severe slug flow were determined. These characteristics, which included, slug lengths and cycle, build-up and production times, were compared to previous investigations into severe slugging in flexible shaped risers.

(iii) The liquid inventory in the riser downward limb during severe slugging was calculated.

(iv) For the first time experiments were undertaken to measure the forces on a bend due to slug flow, in a pipeline-riser system.

(v) Calibration tests were developed and carried out, so that the force readings from the instrumentation could be quantified.

(vi) Single phase tests in an 'S' shaped riser were completed to simulate the forces on a bend during the slug build-up and production stages of the severe slugging cycle.

(vii) Two phase tests, using air and water in an 'S' shaped riser, were carried out to measure the forces on a bend during the slug build-up, production and bubble penetration and gas blowdown stages of the severe slugging cycle.

(viii) Using the experimental data, models were developed to predict the forces on a bend during each stage of the severe slugging cycle.

6.2 Conclusions

6.2.1 Severe Slugging Characteristics

(i) Within the severe slugging region, cycle, build-up, production, bubble penetration and gas blowdown times and slug lengths decreased with an increase in superficial gas and liquid velocities. Slug build-up times were more sensitive to changes in liquid velocity than gas velocity, whereas slug production times and slug lengths were more sensitive to changes in gas velocity.

(ii) Comparing severe slugging and transitional severe slugging characteristics, it was shown that within the severe slugging region, longer cycle, build-up, production, bubble penetration and gas blowdown times and slug lengths were observed. The reason for these trends was because transitional severe slugging was characterised by higher superficial gas velocities and having no liquid backing-up the pipeline during the slug build-up stage.

(iii) From the comparisons of this work to previous investigations, the occurrence of severe slugging reduced with increasing pressure, in terms of the maximum superficial gas and liquid velocities at which severe slugging was observed on a flow pattern map. Pressure had a greater effect on the superficial gas velocity hence, the severe slugging boundary moved towards the left of the flow pattern map.

(iv) Severe slugging is characterised by periods of no liquid production followed by large volumes of liquid i.e. long liquid slugs. This research has shown that shorter slug lengths were seen at higher superficial gas velocities and system pressure and also in an 'S' shaped riser, compared to a catenary riser. During severe slugging, slug lengths of up to seven times the riser height are possible.

6.2.2 Liquid Inventory in Riser Downward Limb

(i) For each of the severe slugging conditions, the pressure difference over the riser exceeded the hydrostatic head due to the riser being full of liquid, due to trapped gas in the riser downward limb. Hence, for an unknown volume of liquid in the downward limb, where $0 > h_{d'} < h_d$, the pressure difference over the riser:

$$\Delta P_{riser} = \rho g(h_u + h_l - h_{d'}) \qquad (6.a)$$

(ii) As liquid velocity increased, the liquid inventory in the downward limb decreased, as more gas became trapped. The decrease in the liquid inventory would result in a decrease in the hydrostatic force, as there was less liquid in the riser. Large fluctuations in hydrostatic force may result in fatigue damage.

(iii) From comparisons to previous investigations, the occurrence of severe slugging was reduced using a lazy 'S' shaped riser instead of a free hanging catenary configuration. In addition, this research showed that trapped gas in the downward limb shortened the severe slugging cycle time and in some cases, reduced slug lengths.

6.2.3 Forces on a Bend during the Severe Slugging Cycle

(i) No previous research into the slug flow forces in a pipeline-riser system has been carried out. From previous investigations of the forces due to normal slug flow, the slug force models were based on the fact that the force on a bend resulted from the momentum transfer, in changing the slug direction around the bend and that force was proportional to the square of the velocity. This was as expected, but had not been proved experimentally. The experimental results from this research have proved that the force on a bend, located at the top of a riser, is proportional to the velocity squared.

(ii) From single phase tests, the following model was developed to describe the resultant dynamic force on a bend:

$$FR'_{dy} = \sqrt{2}\rho_L A v_L^{\,2} \qquad (6.b)$$

(iii) The slug build-up and slug production stages of the severe slugging cycle were characterised by low velocities therefore the resultant dynamic forces on the bend were small, compared to the bubble penetration and gas blowdown stage. The dynamic forces on the bend were dominated by the hydrostatic forces due to liquid in the downward limb and upper limb (build-up stage) and downward limb, upper limb and horizontal section into the separator (production stage). During build-up and production the density of the slug could be assumed to be equal to the liquid density.

(iv) During the bubble penetration and gas blowdown stage, high velocities and large fluctuations in the force were observed. Peak velocities (up to 15 times the velocity during the production stage) and forces corresponded to the arrival of the slug from the upper limb, at the separator. Fluctuations in the force occurred as the tail of the slug passed around the bend, causing the bend to vibrate. At one severe slugging test condition (which was characterised by two peaks in the liquid velocity in quick succession), the forces on the bend were up to 2.9 times higher than expected.

(v) At higher superficial gas and liquid velocities, within the severe slugging region, cycle time decreased and the resultant dynamic force on the bend increased. Therefore, there were more cycles imparting higher forces on the bend, leading to a greater risk of structure and fatigue damage. These dynamic forces were more sensitive to changes in superficial liquid velocity, than superficial gas velocity.

(vi) The following models were developed to describe the forces on a bend during the slug build-up, production and bubble penetration and gas blowdown stages, of a severe slugging cycle.

During the slug build-up stage, the resultant dynamic force on a bend is described by:

$$FR'bu_{dy} = \sqrt{2}\rho_{mix} A v_{mix}^{2} \qquad (6.c)$$

During the slug production stage, the resultant dynamic force on a bend is described by:

$$FR'p_{dy} = \sqrt{2}\rho_{mix} A v_{mix}^{2} \qquad (6.d)$$

In Equations (6.c) and (6.d) if the mixture density is unknown, ρ_{mix} can be assumed to be equal to the liquid density.

For the bubble penetration and gas blowdown stage, the resultant dynamic force on the bend is described by:

$$FR'bg_{dy} = \sqrt{2}\rho_{mix} A v_{mix}^{2} \qquad (6.e)$$

Where the mixture density term can be assumed to be 957kg/m^3, if the actual mixture density is unknown.

In certain cases during the bubble penetration and gas blowdown stage, the resultant dynamic force on the bend, is described by:

$$FR'bg_{dy} = B\sqrt{2}\,\rho_{mix} A v_{mix}^{2} \qquad (6.f)$$

Where B is a dynamic 'spring-back' factor which varies between 1.7-2.9.

(vii) From a preliminary analysis, normal slug flow is potentially more problematic in terms of fatigue damage than severe slug flow, due to the higher velocity of the slugs coupled with large dynamic forces.

6.3 Suggestions for Further Work

The section details suggestions for further research.

(i) The test fluids used in this research were air and water. In reality, multiphase flow comprises of oil, natural gas and water. In the current test facility, it is difficult to replicate these conditions. Therefore, it is suggested that similar experiments to those described in this work are carried out using air and oil and then repeated using a three phase system of air, oil and water. These experiments would confirm the effect of fluid properties on the severe slugging characteristics and slug flow forces on the bend.

(ii) The models developed in this research are dependent on the density of the slug at the bend. During the build-up and production stages, the slug is predominantly liquid and therefore the density of the slug can be assumed to be equal to the liquid density. This is not the case during the bubble penetration stage, where the density of the slug is described by the mixture density. To validate the bubble penetration and gas blowdown model, additional experiments should be undertaken where the slug density at the bend is measured.

(iii) Additional data is required to validate the models in respect to different riser configurations, system pressure and operating fluids, as mentioned in part (i). This is particularly applicable to the determination of the spring-back factor, which is important in terms of design aspects i.e. in restraining pipe work against structural and fatigue damage.

(iv) This research has suggested that normal slug flow could be more problematic in terms of fatigue damage, than severe slug flow. As this statement is based on a preliminary assessment, further investigations are required to determine the forces due to normal slug flow, as well as transitional severe slugging and oscillation flow, where cycle times are also higher compared to severe slug flow.

(v) Due to the cyclical nature of severe slugging and the size and energy of these slugs, the capability of conventional handling facilities may well be exceeded. It is suggested that the severe slug force data from these experiments are used in conjunction with S-N curves for known materials, so fatigue life can be determined. This suggestion can also be applied to the transitional severe slugging, oscillation and normal slug flow data.

(vi) It would be interesting to simulate the experiments described in the research using commercial codes such as OLGA and PROFES and to compare the predicted and experimental severe slugging characteristics and severe slug forces. This would highlight areas where the code had difficulty in predicting unstable flow and lead to suggestions of how the simulations may be improved.

(vii) Trapped gas in the riser downward limb has been shown to shorten severe slugging cycle times and slug lengths, suggesting that an 'S' shaped riser is advantageous in terms of severe slugging, compared to a catenary riser. Further investigations are required to develop understanding of the mechanics of the trapped gas; this may be aided by a transparent rig for flow visualisation.

REFERENCES

[1] Hart's E & P, January 2002

[2] Hill, T
"Gas-Liquid Flow Challenges in Oil and Gas Production"
Proc. 1997 ASME Fluids Engineering Division Summer Meeting, June 1997

[3] Thomas, M
"Deepwater at the Double"
Hart's E & P, pp 41-47, October 2000

[4] Hart's E & P, March 2002

[5] Hart Deepwater International, Vol 1, Issue 2, June 1999

[6] Inglis, R
"The Challenges of Developing a Large Deepwater Field"
Proc. Deep and Ultra Deep Water Offshore Technology Conference, Newcastle, March 1999

[7] Gurney, J
"Big Splash in the Deep Six"
The Shield Magazine, pp 40-43, October 1999

[8] Owen, D
"Oil Price Collapse: Fighting the Auld Enemy"
The Journal of Offshore Technology, February 1999

[9] Hart's E & P, July 2002

[10] Hart's E & P, May 2002

[11] Hassanein, T, Fairhurst, P
"Challenges in the Mechanical and Hydraulic Aspects of Riser Design for Deep Water Developments"
Proc. Deepwater Technology Conference, Norway, 1998

[12] Hatton, S, Arvid O
"Deepwater Riser Technology"
The Journal of Offshore Technology, pp 41-42, February 1999

[13] Schmidt Z, Brill J, Beggs H,
"Experimental Study of Severe Slugging in a Two Phase Flow Pipeline-Riser System"
SPE Paper 8306, 1979

[14] Wordsworth C, Das I, Loh WL, McNulty G, Lima PC, Barbuto, F
"Multiphase Flow Behaviour in a Catenary Shaped Riser- Vol 1"
BHR Group Limited Report: CR 6820, 1998

[15] McNulty, G, Wordsworth C, Das, I
"Predicting, Detecting and Controlling Slugs in Pipeline-Riser Systems"
Proc. The 9th International Conference-Multiphase '99, France, June 1999

[16] Schmidt Z,
"Experimental Study of Two-Phase Flow in a Pipeline-Riser Pipe System"
PhD Thesis, U. of Tulsa, 1977

[17] Tin V
"Severe Slugging in Flexible Risers"
Proc. The 5th International Conference on Multi-Phase Flow, 1991

[18] Bøe, A,
"Severe Slugging Characteristics Part I: Flow Regime for Severe Slugging"
Selected Topics in Two Phase Flow, Norway, 1981

[19] Pots B, Bromilow I, Konijn M,
"Severe Slug Flow in Offshore Flowline/Riser Systems"
SPE 13723, 1985

[20] Goldzberg V, McKee F,
"Model Predicts Liquid Accumulation, Severe Terrain Induced Slugging for Two Phase Lines"
Oil and Gas Journal, August 1985

[21] Fabre J, Peresson L, Corteville J, Odello R, Bourgeois T,
"Severe Slugging in Pipeline/Riser Systems"
SPE 16846, 1987

[22] Tin V, Sarshar M,
"An Investigation of Severe Slugging Characteristics in Flexible Risers"
Proc. The 6th International Conference on Multiphase Production, June 1993

[23] Dukler A, Hubbard M,
"A Model for Gas-Liquid Slug Flow in Horizontal and Near Horizontal Tubes"
Industrial and Engineering Chemistry Fundamentals, Vol 14, pp 337-347, 1975

[24] Govier G, Aziz K,
"The Flow of Complex Mixtures in Pipes"
Published by Van Nostrand Reinhold Co, pp 581-582, 1972

[25] Fenton R, Griffith P
"The Forces at a Pipe Bend due to the Clearing of Water Trapped Upstream"
Proc. ASME Piping and Pressure Vessel Conference, June 1990

[26] Neumann A, Griffith P,
"Forces on a Pipe Bend Resulting from Clearing a Pool of Liquid Upstream"
Proc. ASME Piping and Pressure Vessel Conference, June 1992

[27] Bozkus Z, Wiggert D,
"Slug Motion and Impact in a Voided Line"
Proc. Fluid Transients and Fluid Structure Interaction, 1991

[28] Sánchez S, Toledo V, Hernández G
"Slug Flow Momentum Transfer Analysis to Determine the Forces Acting on a 90° Elbow in a Horizontal Line"
Proc. The 3rd International Conference on Multiphase Flow, June 1998

[29] Boilard M,
"Experimental Study of the Slug Flow Induced Forces on Pipeline Bends"
BP Exploration Report, 1997

[30] Hargreaves C,
"Measurement of the Forces on Bends in (Oil) Pipelines Due to Multiphase Flow"
University of Cambridge, Chemical Engineering Tripos Part II Research Project, 1998

[31] Owen I, Hussein I
"The Propulsion of an Isolated Slug Through a Pipe and the Forces Produced as it Impacts Upon an Orifice Plate"
Int. Journal of Multiphase Flow, Vol 20, 1994

[32] Sakaguchi T, Ozawa M, Hamaguchi H, Nishiwaki F, Fujii E
"Analysis of the Impact Force by a Transient Liquid Slug Flowing Out of a Horizontal Pipe"
Nuclear Engineering and Design, Vol 99, 1987

[33] Santana B, Fetzner D, Edwards N, Haupt R
"Program for Improving Multiphase Slug Force Resistance at Kuparuk River Unit Processing Facilities"
SPE Paper 26104, 1993

[34] Wordsworth C, Das I, Loh W L, McNulty J G, Montgomery J
"Multiphase Flow Behaviour in a Flowline-'S' Shaped Riser System"
BHR Group Limited, Confidential Report, 1999

[35] ICI Tracero
Manufacturer Handbook- Gammatrol Density Gauge, Type PRI 121/116

[36] Montgomery J, Yeung H
"The Stability of Fluid Production From a Flexible Riser"
Proc. ETCE/OAME 2000 Joint Conference: Energy for the New Millennium, New Orleans, February 2000

[37] Foxboro
Instruction Book 3496, IDP10-1, Intelligent D/P Cell Transmitter

[38] Fuchs P
"The Pressure Limit For Terrain Slugging"
Proc. The 3rd International Conference-Multiphase Flow, Netherlands, May 1987

[39] Multiphase Flow Course, "A Presentation of Design and Operational Issues Concerning Multiphase Production Systems", BP, May 1998

PUBLICATIONS

McNulty, G, Wordsworth C, Das, I
"Predicting, Detecting and Controlling Slugs in Pipeline-Riser Systems"
Proc. The 9th International Conference-Multiphase '99, France, June 1999

Das, I, McNulty, G, Wordsworth C
"Living with Slugs on Floaters"
Proc. The Institute of Marine Engineers Deep and Ultra Deep Water Offshore Technology Conference, March 1999

Appendix A

Derivation of the Resultant Force on a Bend

The force on a bend results from the momentum transfer, in changing the fluid flow direction around the bend.

If we consider the flow into the bend is from the y-direction, then the flow out will be in the x-direction:

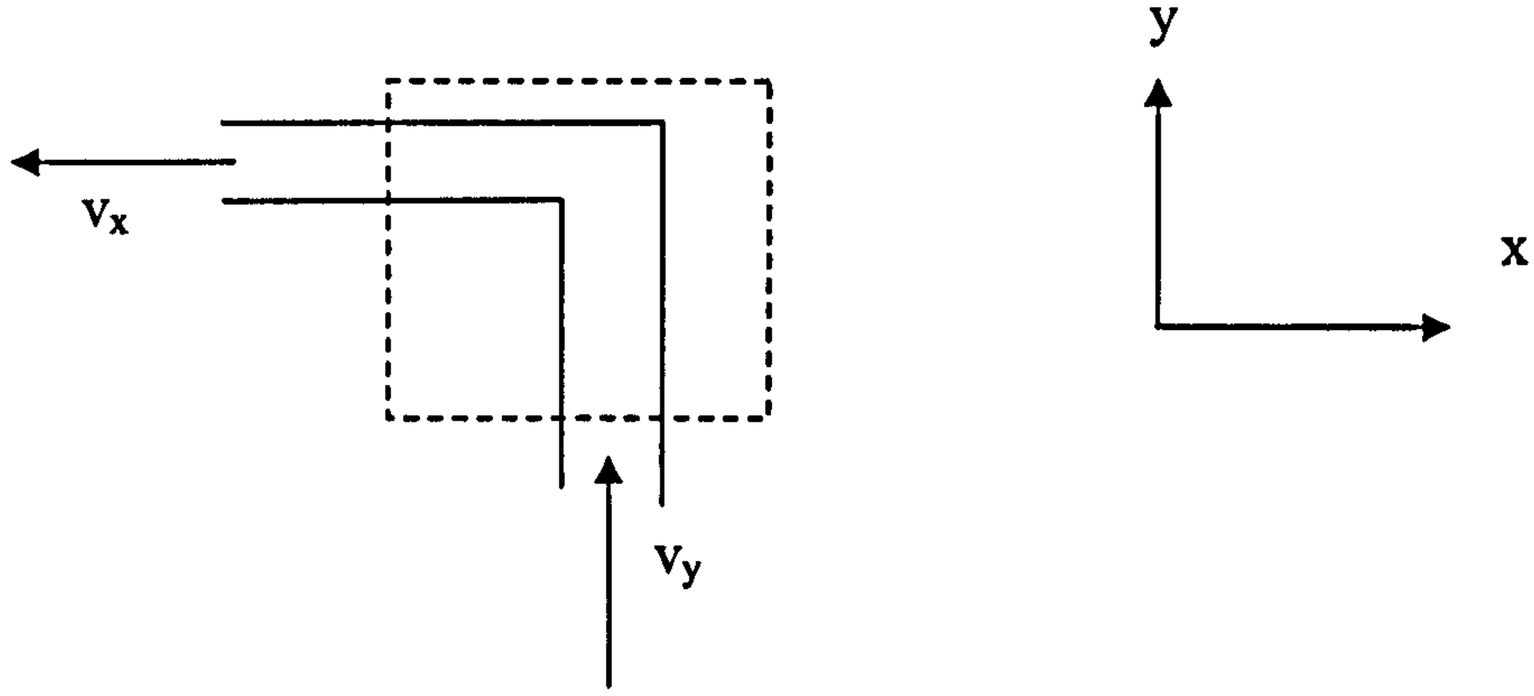

Therefore, drawing a control volume around the bend, the momentum in the y-direction is completely destroyed (giving the force in the y-direction) and the momentum in the x-direction is generated.

Momentum, *M*, is given by:

$$M = Ft = mv \qquad \text{(A.a)}$$

Rearranging Equation (A.a) to give the force in the y-direction, F_y:

$$F_y = \frac{mv}{t} = \rho A v_y^{\,2} \qquad \text{(A.b)}$$

Similarly, the force in the x-direction, F_x:

$$F_x = \frac{mv}{t} = \rho A v_x^{\,2} \qquad \text{(A.c)}$$

The resultant force on the bend, FR, is given by:

$$FR = (F_x^{\,2} + F_y^{\,2})^{0.5} \qquad \text{(A.d)}$$

The forces in the x- and y- directions (for fluid flow) are equal and opposite:

$$F_y = -F_x \qquad \text{(A.e)}$$

Therefore,

$$F_x^{\,2} = -F_y * -F_y = F_y^{\,2} \qquad \text{(A.f)}$$

Substituting Equation (A.f) into (A.d):

$$FR = (F_y^{\,2} + F_y^{\,2})^{0.5} \qquad \text{(A.g)}$$

$$FR = (2F_y^{\,2})^{0.5} = \sqrt{2}F_y \qquad \text{(A.h)}$$

Substituting Equation (A.b) into Equation (A.h):

$$FR = \sqrt{2}\rho A v^2 \qquad \text{(A.i)}$$

Appendix B

Operating Procedures for Lazy 'S' Riser Test Facility

1. Operating Procedures for Lazy 'S' Riser Test Facility

1.1 Pre Start-up Checks

1. Ensure the high pressure test facility is isolated from the existing low pressure 3-phase test facility and motion simulator by checking all the isolation valves to the high pressure test facility and the motion simulator are closed (**VI24, VI25 & V10**).
2. Ensure water outlet valve from 3-phase separator is open (**VA3**).
3. Ensure all vents and drains in the test facility are closed.
4. Ensure main vent valve (**VI6**) is closed.
5. Ensure all outlets valves (**VM10, VA1**) from the oil coalescer are fully closed and (**VM8**) the oil outlet from the water coalescer is also closed.
6. Ensure by-pass valve (**VM11**) of the water feeder pump (**P3**) is fully open. (The water pump is a positive displacement pump and should never be operated against a closed valve.).
7. Check the water level on the water tank to ensure that it contains enough water
to perform your tests (a level of at least 5 is recommended).
8. Check the oil/water levels on the 3-phase separator.
9. Ensure the gas flow valve (**VM5**) is open and gas control valve (**VI21**) is closed.
10. Ensure main drain valve (**VI26**) on the gas buffer vessel is closed.
11. Ensure that the outlet valve (**VN4**) on the buffer vessel is open.
12. Ensure the flow control valve (**VM1**) of the water feeder pump (**P3**) is open.
13. Ensure the main booster pump's (**P1**) flow control valve and inlet valve are fully open (**VI3 & VI1**).
14. Drain works compressor using the drain valve, which is located at the base of the compressor.
15. Drain the pressure regulator on the actuated valve (**VA6**) in the tower.
16. Turn on data acquisition system.

1.2 Operating Procedures

1. Switch on the works compressor, which supplies the works compressor air line.
2. Ensure that the works compressor has achieved a minimum pressure of 20 psi before any further steps are performed, it is advisable to check the pressure level on the pressure gauge of the 3-phase separator.
3. Check that the correct pressure is supplied to the pneumatic control equipment (i.e. 20 psi).
4. Ensure that the main vent valve (**VI6**) is closed before any tests are performed.
5. Ensure flowmeter FL1 and FL2 are switched on and are operational.
6. Make sure that the automatic level control valve (**VA3**) on the 3-phase separator is operational and the required liquid level is already set correctly (you can test it using the controller).
7. See that the pressure control valve of the 3-phase separator (**VA5**) is set to required test pressure or a minimum pressure of 1 bar (for the liquid in the 3-phase separator to be able to flow into the coalescers).

8. Check that the manual water and oil outlet valves on the oil coalescer are closed (**VM10, VA1** respectively). The water outlet valve on the water coalescer should be opened (**VM9**) whilst the oil outlet valve (**VM8**) on the water coalescer should be closed (the water outlet valve on the water coalescer is pneumatically controlled)
9. Make sure that the drain valve (**VI26**) on the buffer vessel is closed.
10. Check the gas valve (**VM5**) is open and the isolation valve for the relevant flowmeter is open.
11. Ensure that the outlet valve (**VN4**) on the buffer vessel is open.
12. Ensure that the gas control valve (**VI21**) is closed.
13. Check the current total operating time on the compressor to see if a service check is needed (service checks needed every 100 hours).
14. Check cooling water pump is primed before operation.
15. Check oil level in compressor BEFORE starting and record the quantity of any oil added.
16. Drain condensate from after cooler and intercooler moisture traps.
17. Start cooling water pump against closed valve, then fully open, slowly.
18. Check coolant flow return into sump.
19. Open air outlet valve.
20. Turn on cooling water temperature display.
21. Make sure the unload/loaded switch is in the UNLOAD position.
22. Turn on main isolator.
23. Turn the switch on the cream box from off to manual.
24. Once the motor has changed over from star to delta (listen for the clunk) the compressor can be switched to the loaded position.
25. Follow checks **4 to 12** on the daily check list (section 8) just after start up and then every four hours.
26. Open the gas valve (**VM5**) to give a gas flowrate into the riser.
27. Open gas flow control valve (**VI21**) to give required gas flowrate.
28. Ensure that the pressure in the system has achieved the required set value before any further procedures are performed. This can be performed by checking the pressure the 3-phase separator; a minimum pressure of 0.6 bar should be obtained before any further work is performed.
29. Check the pressure control on the three phase separator, i.e. the pneumatic pressure control valve is operating.
30. Check the pressure in the system on the data acquisition system to ensure that no problems have occurred in the riser.
31. Switch on the water feeder pump (**P3**).
32. Using the bypass control valve (**VM11**) and the speed of the main feeder pump, slowly adjust the water flowrate until the required flowrate conditions are met. If low flowrates are required it is possible to obtain the required flowrate by having the pump speed set on it's lowest setting and just using the bypass valve to control the flowrate.
33. With water flowing through the riser test loop, check that the level control (LC on 3 phase separator), i.e. the level control valves, on both separators are operating correctly.

34. Turn on the liquid flowmeters **FL3** and **FL4** at the top of the tower, these flowmeters have to be turned on only when there is water flowing through the system.
35. With water flowing through the test loop, check the oil/water interface level in the water colaescer.
36. Check the level of the water in the water tank, to make sure that there is sufficient water in the tank, the water level should not be allowed to fall below 2 on the scale.

1.3 Operating Procedure Whilst Equipment is in Use

1. Check the level controllers (**LC**) on the 3-phase separator, if the levels rise then adjust using the controller, the levels should ideally be checked every **15 minutes.**
2. Check the level in the main water tank, the level should not be allowed to fall below the No. 2 mark on the water level indicator, it should also not be allowed to rise higher then the No. 8 mark. Again this should ideally be checked every **15 minutes.**
3. Follow checks 4 to 12 on the compressor daily checklist every **4 hours.**

1.4 Shut Down Procedure

1. Ensure flowmeters **FL3** & **FL4** are turned off, **FL3** & **FL4** should not be operated if there is no water flowing through them.
2. Open bypass valve (**VM11**) on the main feeder pump, If high flowrates are being used then the speed of the pump should be reduced prior to the bypass valve being opened.
3. Switch off the water feeder pump (**P3**).
4. Move compressor from loaded to unloaded position.
5. Close air outlet valve.
6. Turn switch on cream box from manual to off
7. Turn off main isolator box.
8. Drain the manual condensate valves.
9. Turn off the cooling water temperature display.
10. Shut down the cooling water pump and close its discharge valve.
11. Close the gas control valve (**VI21**).
12. Slowly vent the 3-phase separator using the main vent valve (**VI6**), to relieve the pressure.
13. Check that both pneumatic outlet valves on the 3-phase separator are closed (due to no more flow in water and oil).
14. Shut down works compressor.

1.5 Emergency Shutdown Procedure

This procedure should only be used in the case of an emergency.

1. Hit emergency stop button located near the buffer vessel.
2. Check to see if the main compressor is off.
3. Check to see if the water feeder pump **(P3)** is off.
4. Vent the 3-phase separator using the main vent valve **(VI6)**.

1.6 Computer Start-up Procedure

1. Turn on power supply at plug socket.
2. Turn on computer, the computer will automatically load LabVIEW and the data acquisition system.
3. Press run on the main screen, this is indicated by a small arrow, which flashes to indicate that the program is running.
4. Press the red button labelled View/Edit, the program now enters the calibration tables.
5. Change any information needed whilst in the calibration section.
6. Press the green run button twice, this then sets the calibration which you have chosen.
7. Enter menu and select which screen you want.

1.7 Computer Shut Down Procedure

1. Go to menu and select main panel.
2. Press the red button labelled run/stop, this now stops the DAS programme running.
3. Exit LabVIEW programme.
4. Exit Windows.
5. Shut off computer.
6. Turn off power.

2. Checklist For Riser Operation

No.	OPERATION
1	Close main vent valve VI6.
2	Ensure valve VA3 on the 3-phase separator is open.
3	Ensure the isolator valves VI24, VI25 and V10 are closed to isolate the riser rig.
4	Ensure the water tank contains sufficient water to complete the test work.
5	Close the main drain valve on the buffer vessel (VI26).
6	Switch on works compressor and wait until 20 psi has been achieved.
7	Close gas flow control valve VI21.
8	Complete items 1 to 3 on compressor daily checklist.
9	Start the cooling water pump against closed valve.

10	Check coolant flow return to the sump.
11	Make sure the load/unload switch is in the UNLOAD position.
12	Turn on compressor and when motor has switched from star to delta switch to loaded.
13	Complete compressor daily checklist, items 4 to 12.
14	Vary gas flow control valve VI21 to get required flowrate.
15	Check the pressure level on the data acquisition system to ensure there are no problems.
16	Open main feeder pump bypass valve VM11.
17	Switch on water feeder pump P3.
18	Using bypass valve VM11 and pump speed adjust flowrate to obtain the required conditions.
19	With water flowing through the test loop switch on the liquid flowmeters FL3 & FL4, at the top of the tower.
20	Whilst the system is running check the water level on the water tank and the oil/water interface levels on the 3-phase separator at regular intervals (» every 15 minutes)

3. Checklist For Riser Shutdown

No.	OPERATION
1	Switch off liquid flowmeters FL3 & FL4
2	Open bypass valve VM11 on main feeder pump
3	Switch off main feeder pump
4	Switch compressor from load to unload.
5	Turn off compressor
6	Turn off cooling water temperature display.
7	Shutdown the cooling water pump and close its discharge valve.
8	Close gas control valve VI21
9	Slowly vent the air pressure in the 3-phase separator using vent VI6
10	Shut down works compressor

4. Daily Instrumentation Calibration Checklist

	OPERATION	
1	Before start-up check the zero readings of the strain gauges on the data acquisition system	V: H:
2	Check conductance probe values on the DAS and record any that are on.	
3	Start compressor and obtain 2 bar on the 3-phase separator, then check the pressure transducer readings on the DAS.	
4	Turn on the water pump and allow the pipe to fill with water. Check and record densitometer reading on DAS.	
5	Whilst there is water passing through the pipeline check the conductance probes and record any that are not working.	

5. Daily Compressor Checklist

	Time	:	:	:	:
No.	**OPERATION**	Start -Up	+4 hrs	+8 hrs	+12 hrs
1	Check cooling water pump is primed before operation.				
2	Check oil level before starting. Record oil quantity added.				
3	Drain condensate from aftercooler and intercooler moisture traps before starting. Also from main air receiver.				
4	Check oil pressure 2-3 bar (min 1.2 bar)				
5	Check intercooler pressure (3.4 bar @ 16 bar working pressure)				
6	Check air intake filter service indicator.				
7	Check lubricator oil delivery rate LP 8 drops/min : HP 4 drops/min (right : left)				
8	Drain condensate from control air filter housing.				
9	Check air outlet temperature (175 °C Max)				
10	Check operation of aftercooler and intercooler float valves. Watch drain outlet for condensate flow.				
11	Check loading and unloading pressures.				
12	Check cooling water inlet/outlet temperature	/	/	/	/
	INITIAL				

Shut down time	
Total hours run from previous sheet	
Total hours run	

Appendix C

Strain-Gauged Strut Design Calculations

The struts that the strain gauges were bonded to, had to be of suitable dimensions, so that the force range of the strain-gauged struts, could measure the forces on the bend.

From Chapter 2, Section 2.5, the resultant force on a bend, F, due to momentum change, was described by:

$$FR = \sqrt{2}\rho_L A v_s^{\,2} \qquad \text{(C.a)}$$

where,

ρ_L liquid density
A cross sectional area of the pipe
v_s velocity of the slug

From the work carried out by BHR Group Limited[14] the maximum slug velocity observed, during severe slugging, was 5.6m/s. Using Equation (C.a) and assuming the slug was 100% liquid, the force due to a slug travelling at 5.6m/s in a 2". pipeline-riser was:

$$F=\sqrt{2} * 1000 * 0.002027 * 5.6^2 = 89.9\,\text{N} \qquad \text{(C.b)}$$

This value was used to determine the upper force range of the strain-gauged struts, which was assumed to be two times the expected maximum force.

To determine the dimensions of the struts, where:

F = 200N
Young's Modulus, **E** = $190x10^9$ (mild steel)
Let the strain, $\epsilon = 100x10^{-6}$

The stress, σ, in the struts was determined using:

$$\sigma = \mathbf{E}\varepsilon \qquad \text{(C.c)}$$

hence,

$$\sigma = 190x10^9 * 100x10^{-6} = 19\,\text{MPa} \qquad \text{(C.d)}$$

The area of the strut, A, was calculated using:

$$\sigma = \frac{F}{A} \qquad \text{(C.e)}$$

therefore,

$$A = \frac{F}{\sigma} = \frac{200}{19x10^6} = 1.05x10^{-5}\,\text{m}^2 \qquad \text{(C.f)}$$

If the strut is rectangular in shape, with a width, w, and thickness, *t*:

$$A = wt \tag{C.g}$$

For a width of 10 mm:

$$t = \frac{A}{w} = \frac{1.05x10^{-5}}{0.01} = 1.05x10^{-3}\ m \tag{C.h}$$

Therefore, the struts were designed to be 10mm wide and 1mm thick, with a length of 25mm. At each end of the struts, sections were added for gauges to be bonded and to enable the struts to be attached to the pipe clamps and supports.

Appendix D

Derivation of Screen Force to Actual Force

Applying isolation and cross-talk effects to the actual forces on the bend, where the applied (spring-balance) forces are analogous to the actual forces, letting ' denote actual force, then Equations (4.j) to (4.m) become:

$$FVs = E_V FV' \quad \text{(D.a)}$$

$$FHs = E_H FH' \quad \text{(D.b)}$$

$$FVs = C_{HV} FH' \quad \text{(D.c)}$$

$$FHs = C_{VH} FV' \quad \text{(D.d)}$$

If there were no isolation or cross-talk effects then the screen readings would be,

$$FVs = FV' \quad \text{(D.e)}$$

$$FHs = FH' \quad \text{(D.f)}$$

If there were no cross-talk effects,

$$FVs = E_V FV' \quad \text{(D.g)}$$

$$FHs = E_H FH' \quad \text{(D.h)}$$

If there were no isolation effects,

$$FVs = FV' + C_{HV} FH' \quad \text{(D.i)}$$

$$FHs = FH' + C_{VH} FV' \quad \text{(D.j)}$$

Use Equations (D.g) and (D.j) to apply isolation joint and cross-talk effects to the actual forces on the bend to give Equations (4.n) and (4.o).

Appendix E

Severe Slugging Force Traces

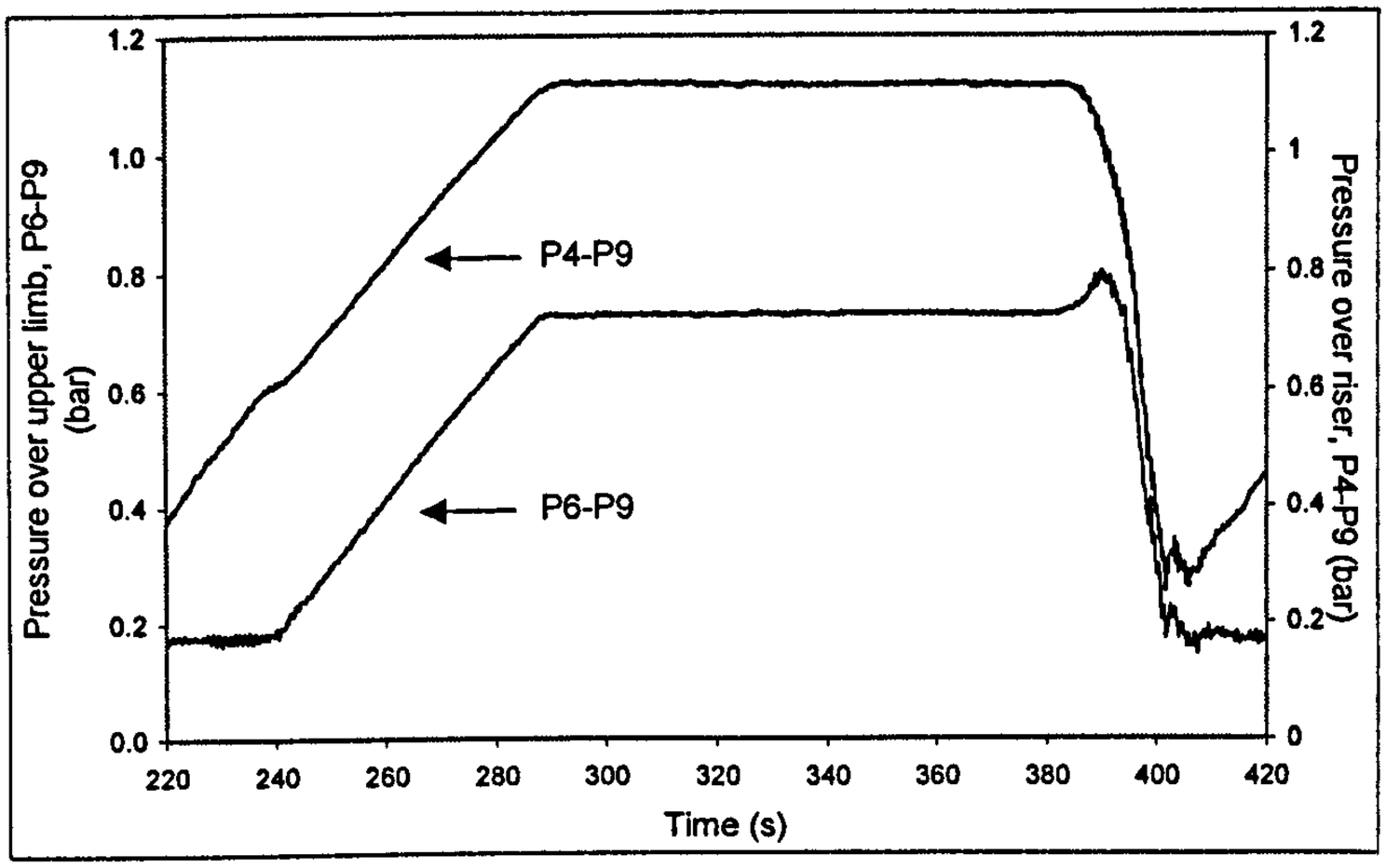

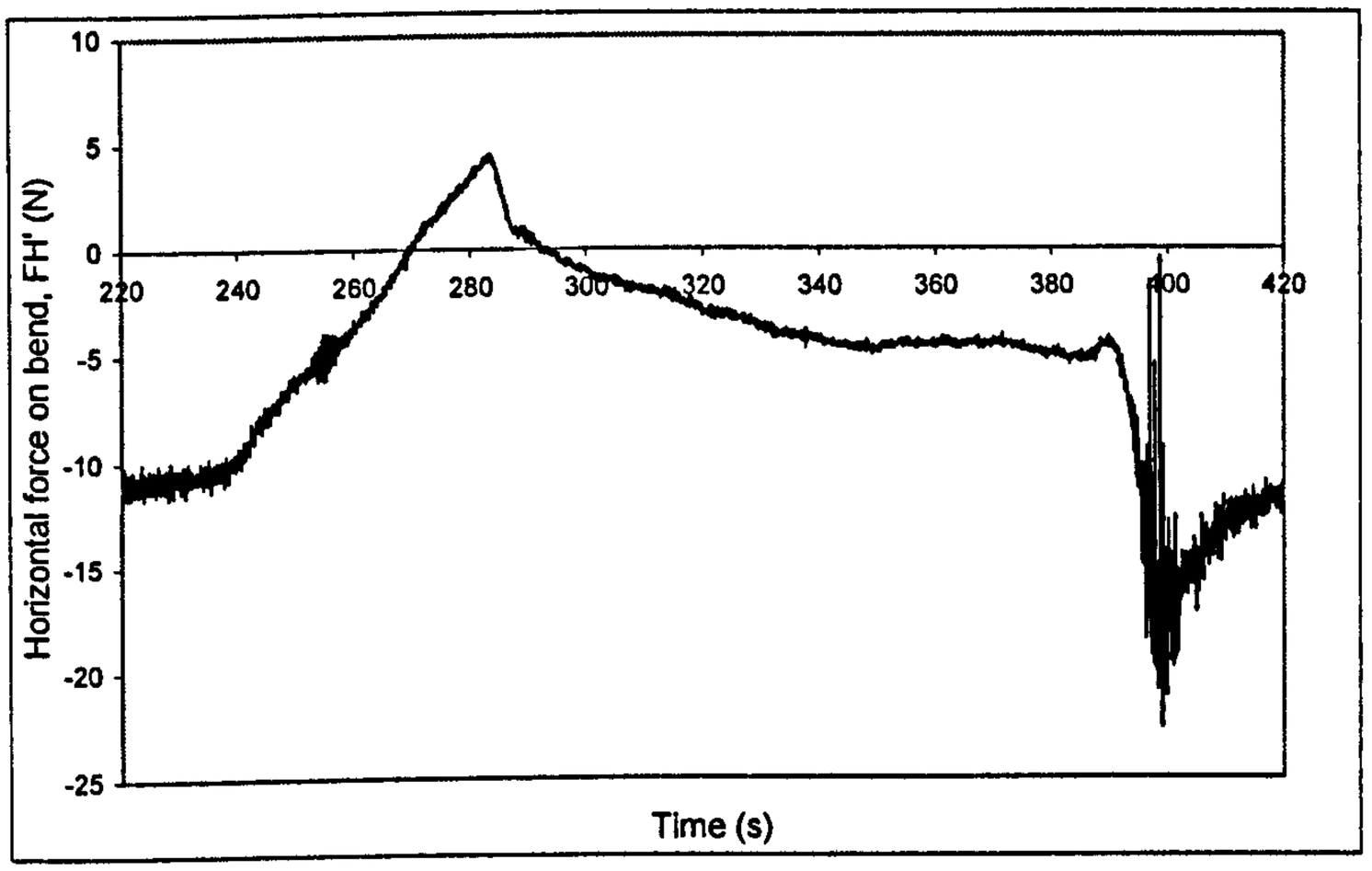

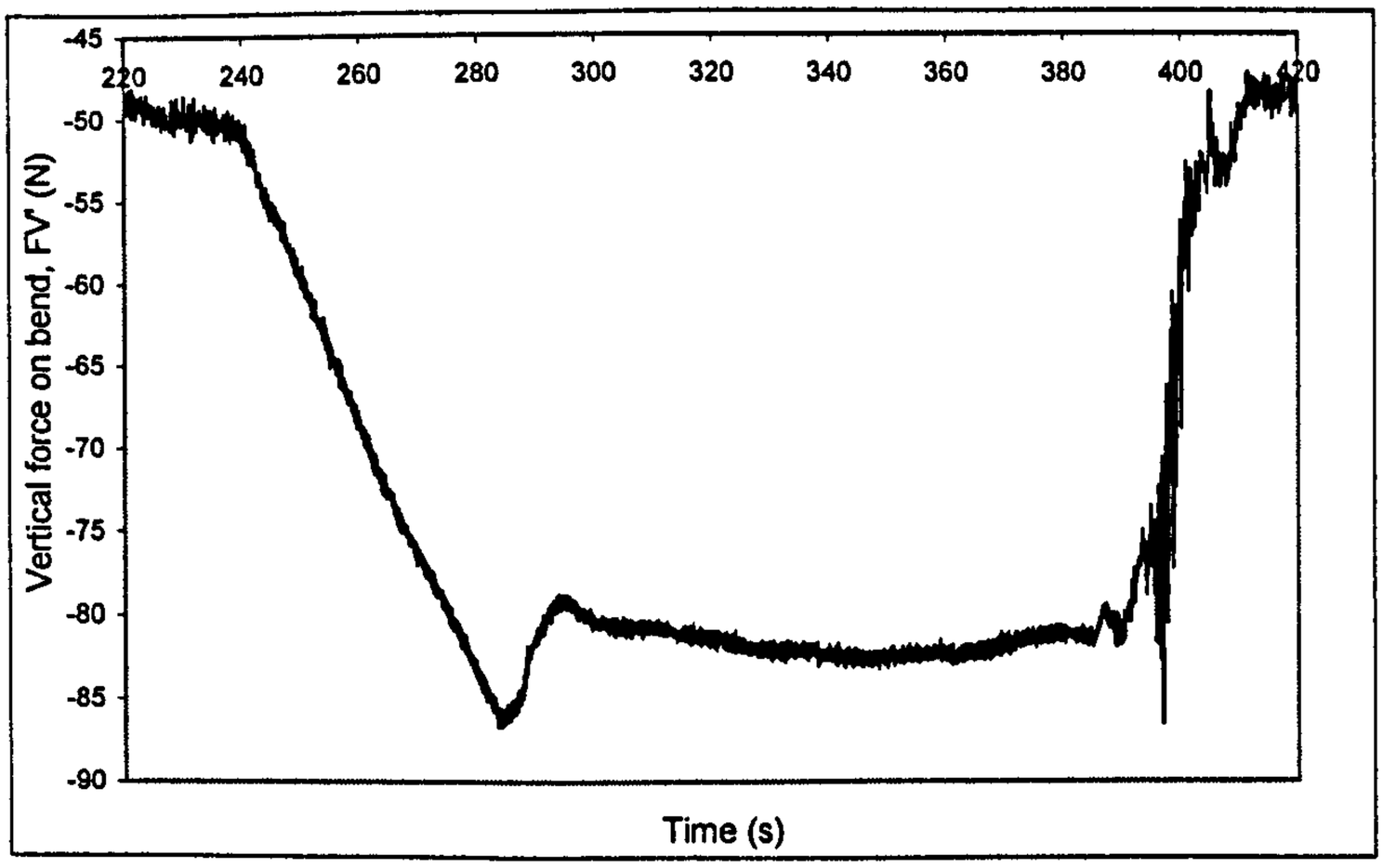

Figure E1.1 Severe slugging 1 traces [v_{SG}=0.11m/s, v_{SL}=0.14m/s]

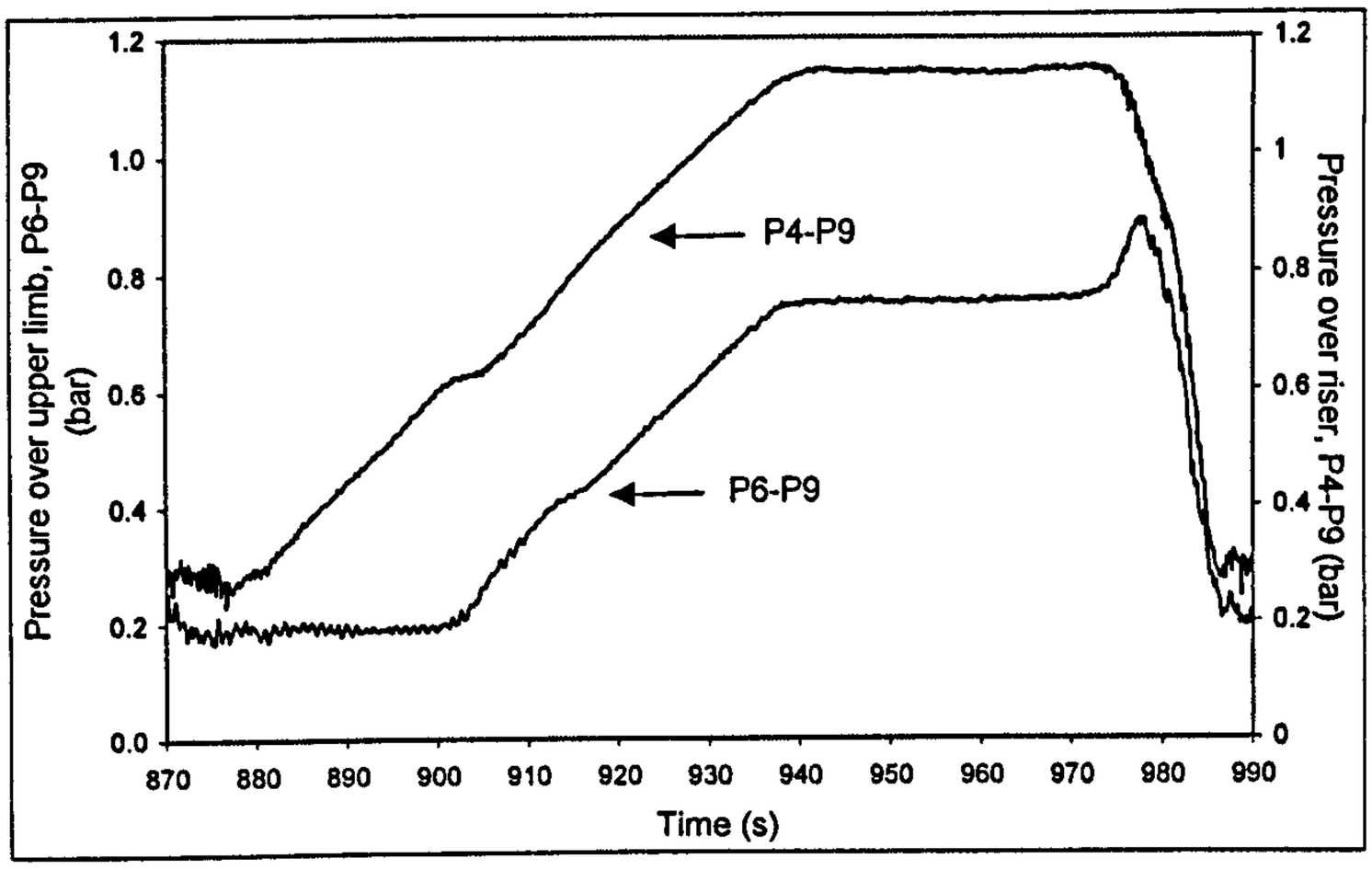

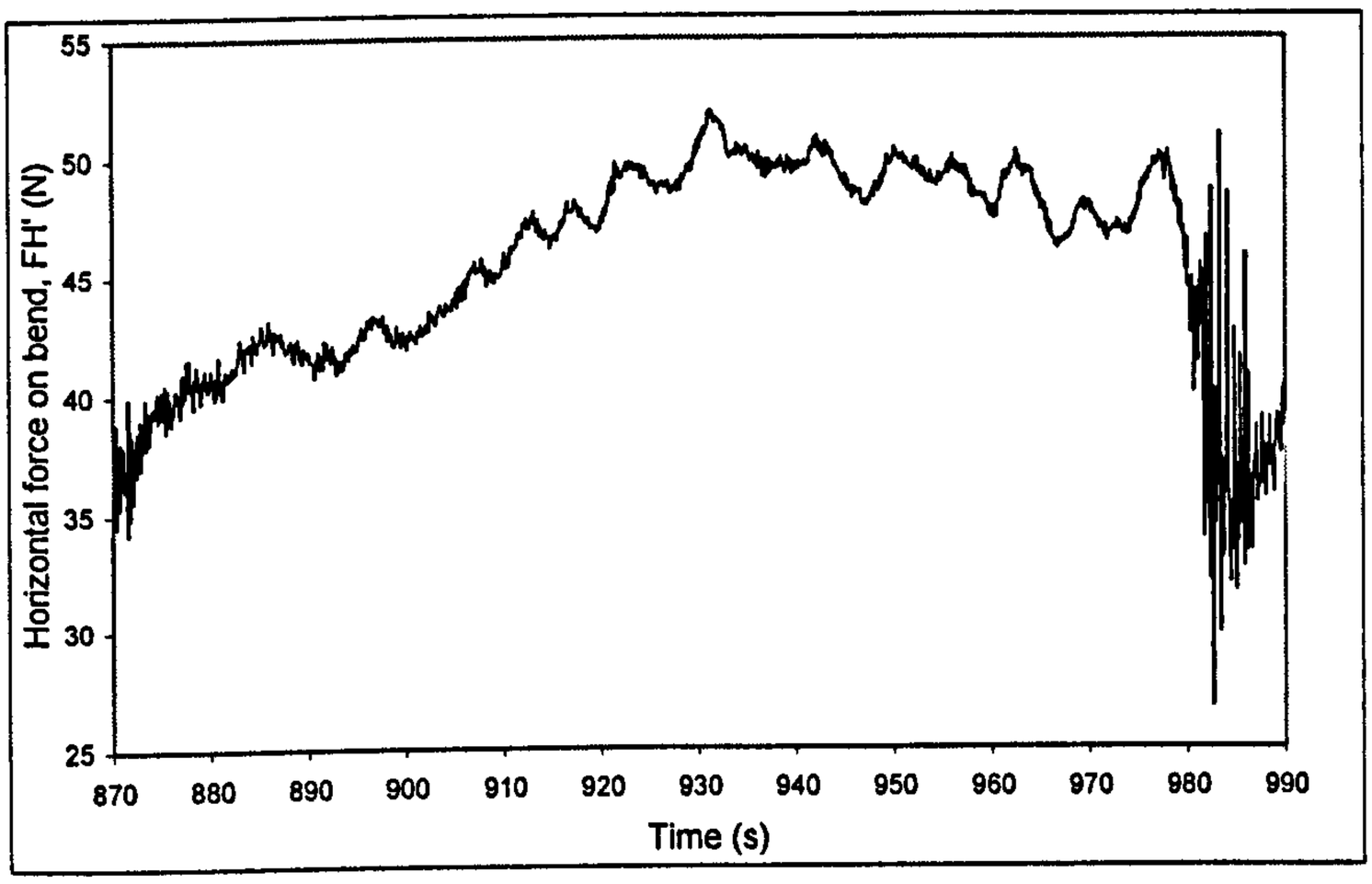

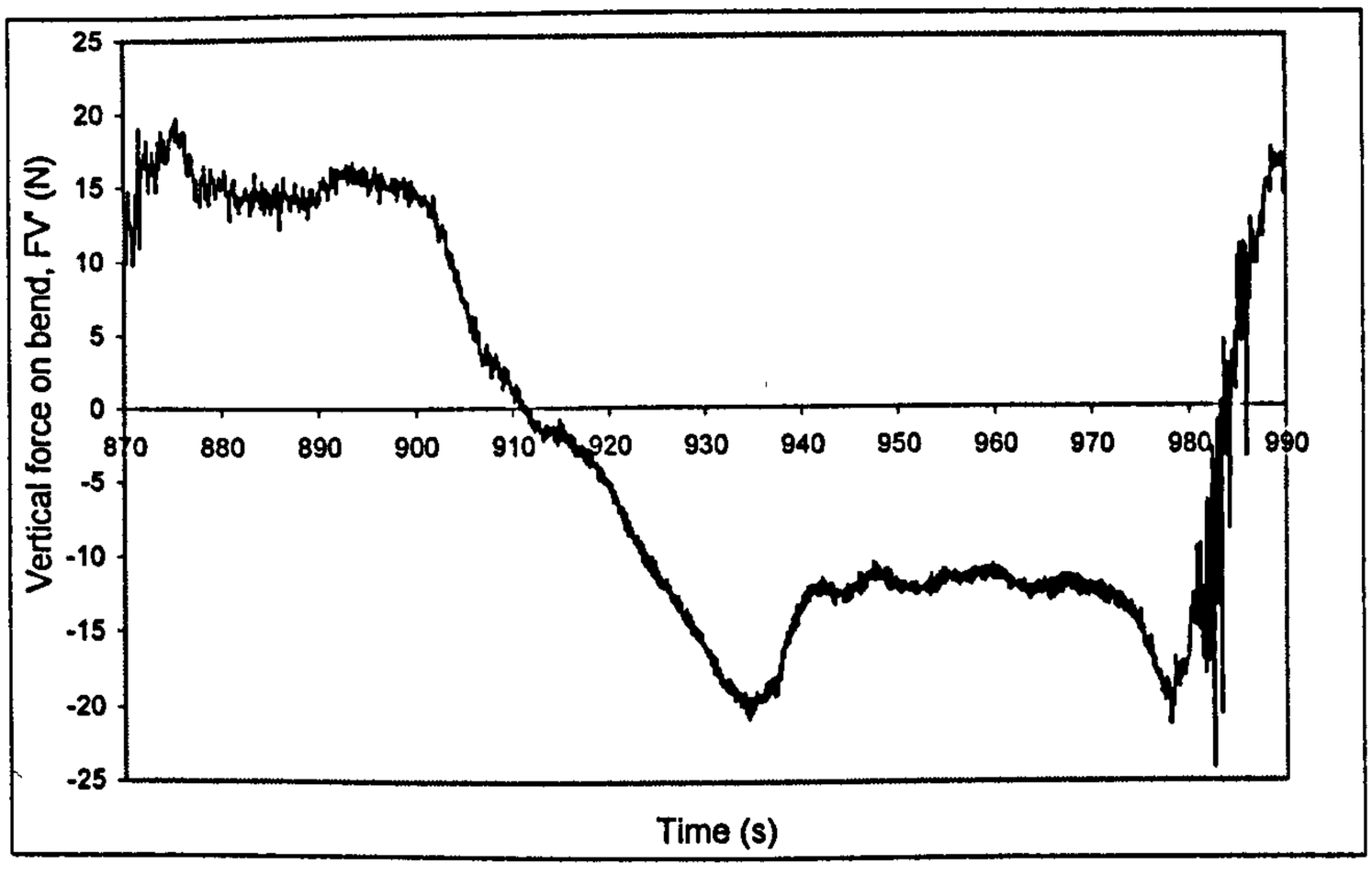

Figure E1.2 Severe slugging 1 traces [v_{SG}=0.28m/s, v_{SL}=0.20m/s]

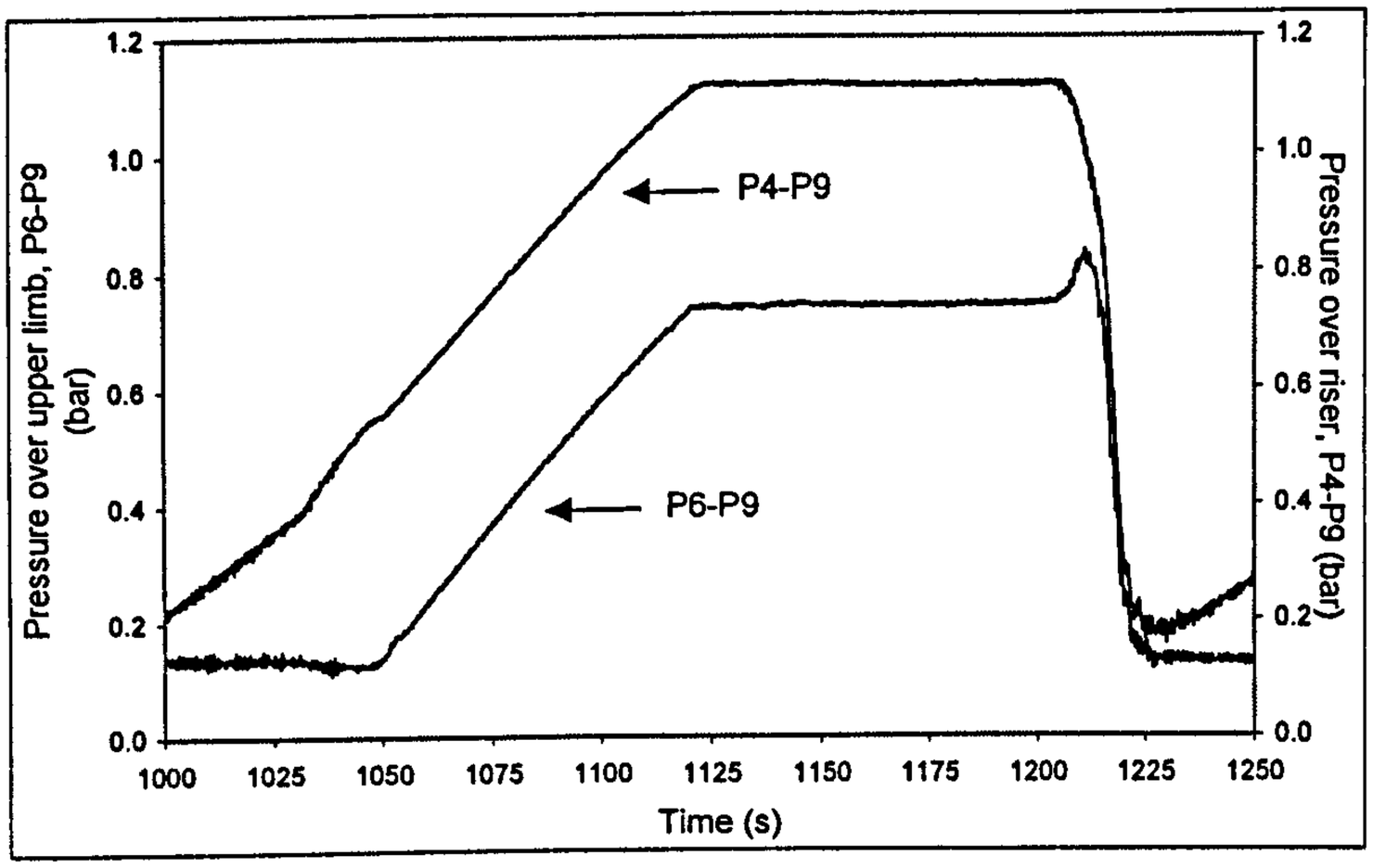

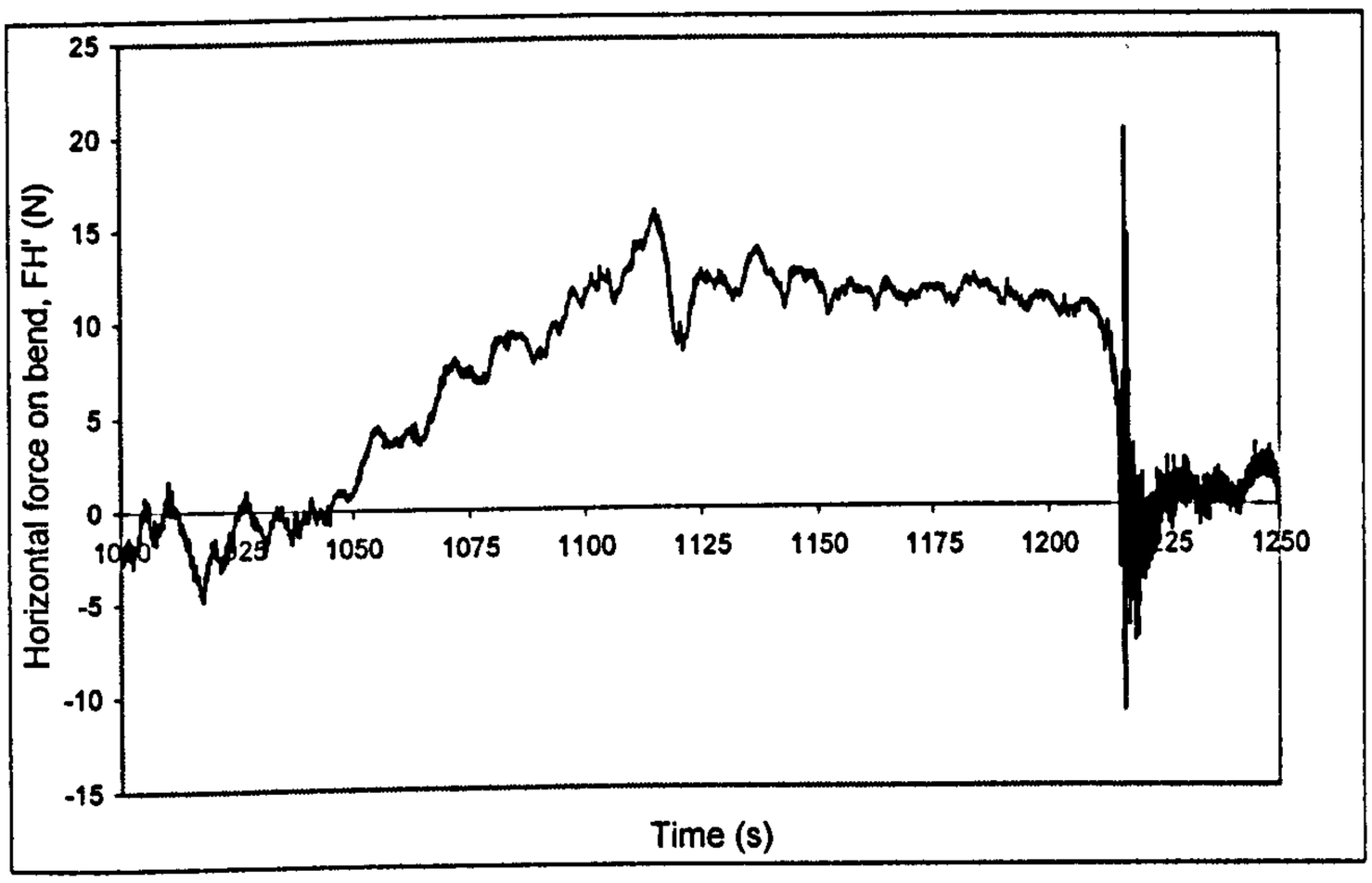

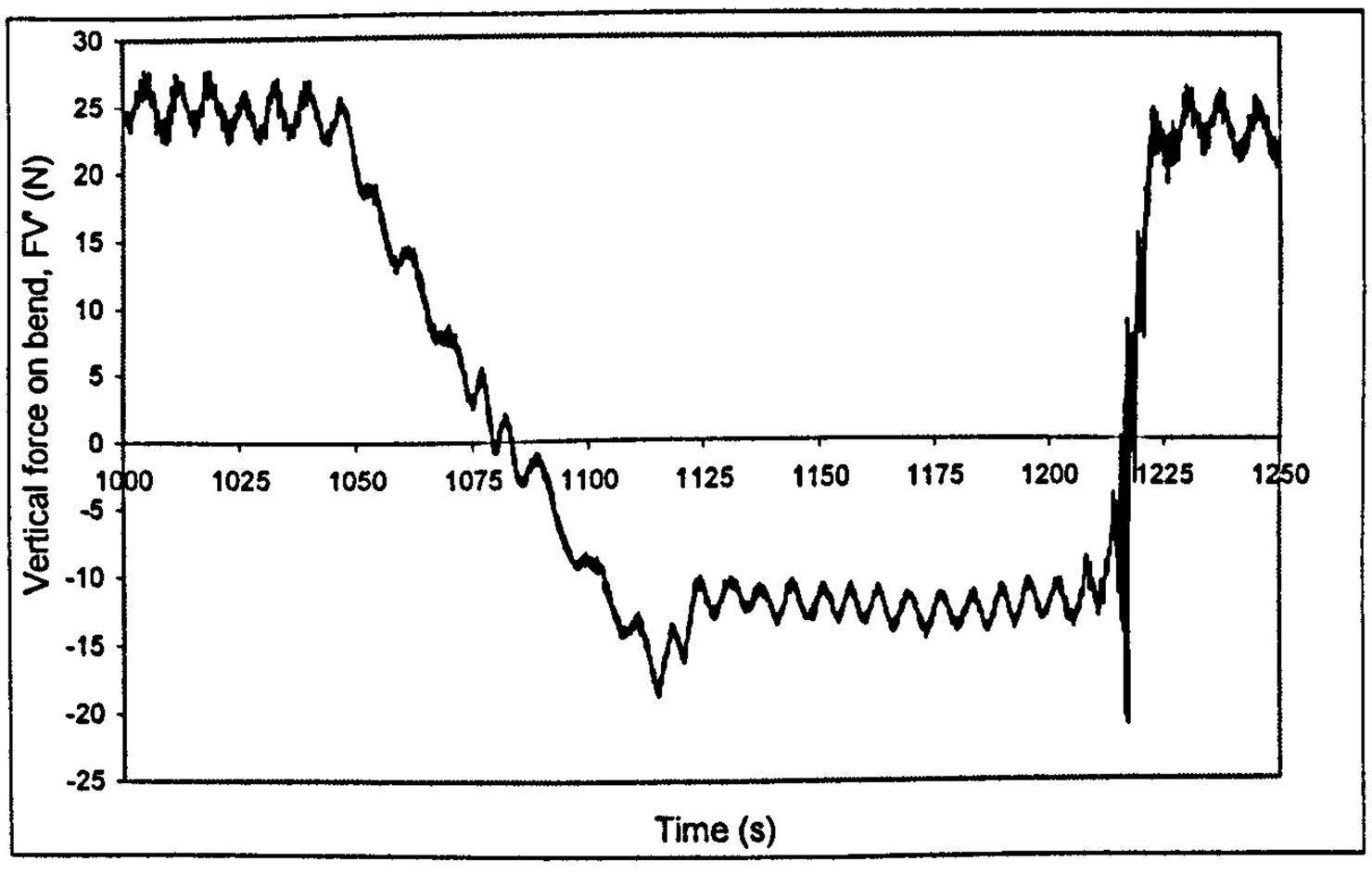

Figure E1.3 Severe slugging 1 traces [v_{SG}=0.17m/s, v_{SL}=0.09m/s]

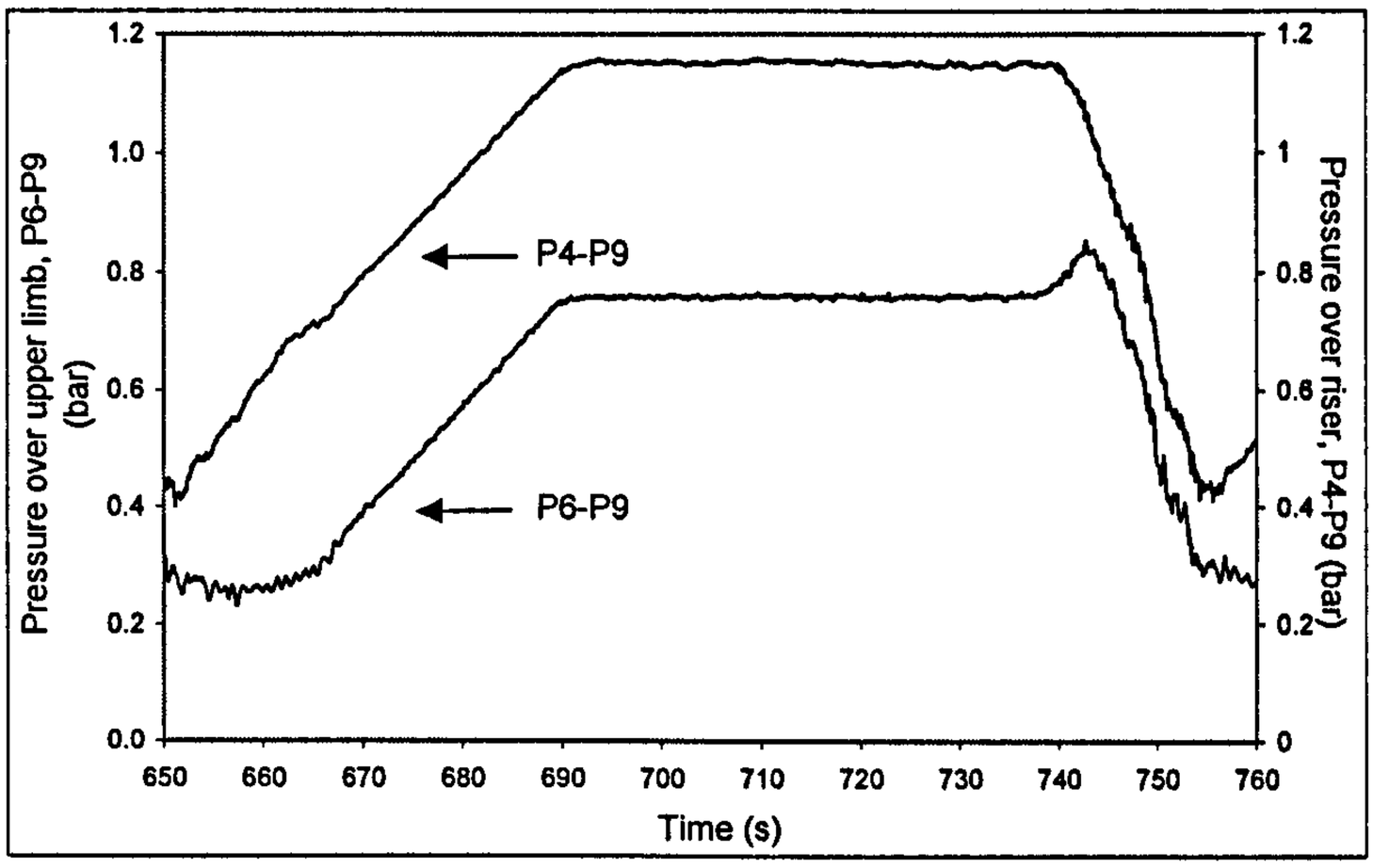

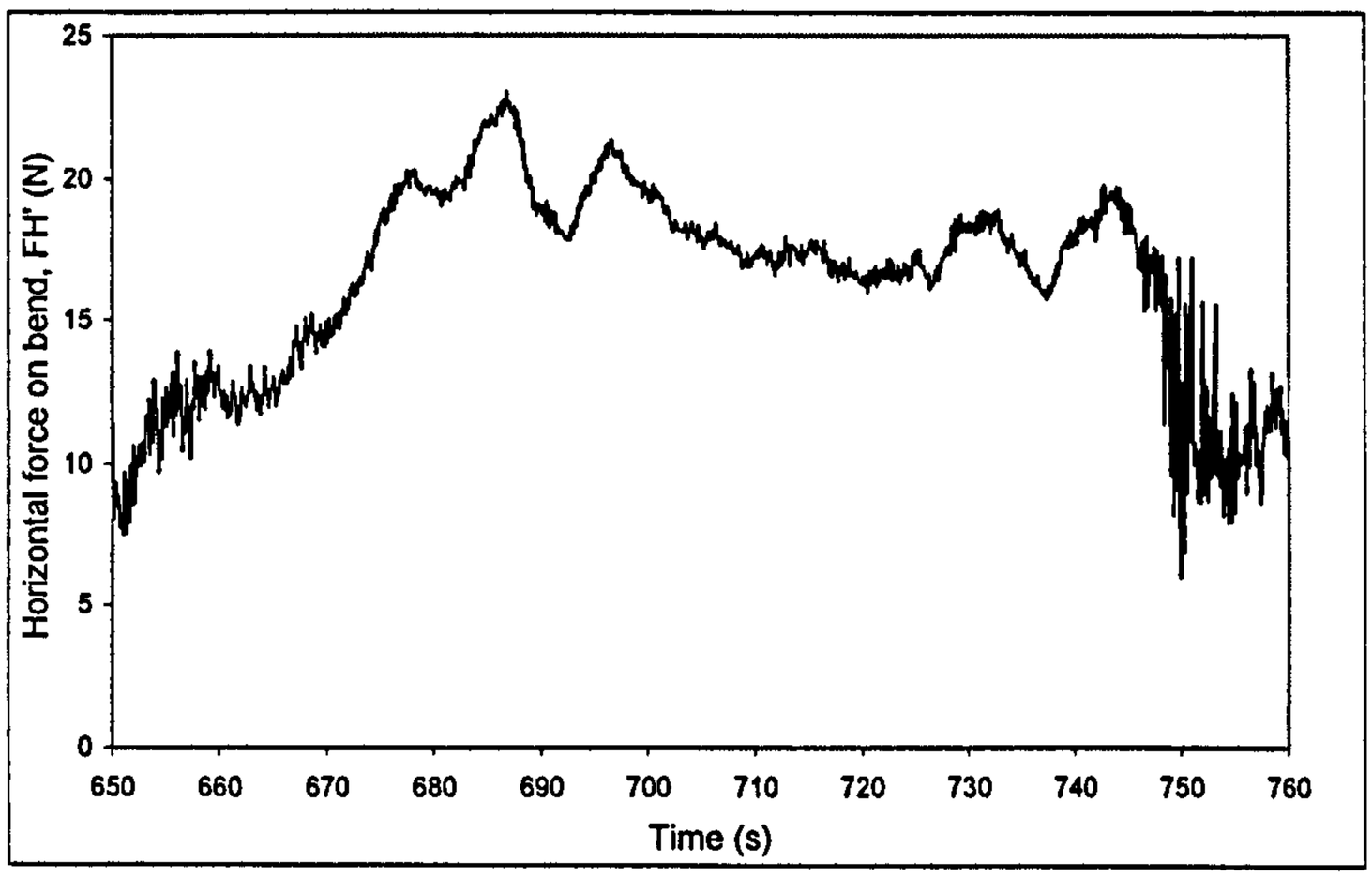

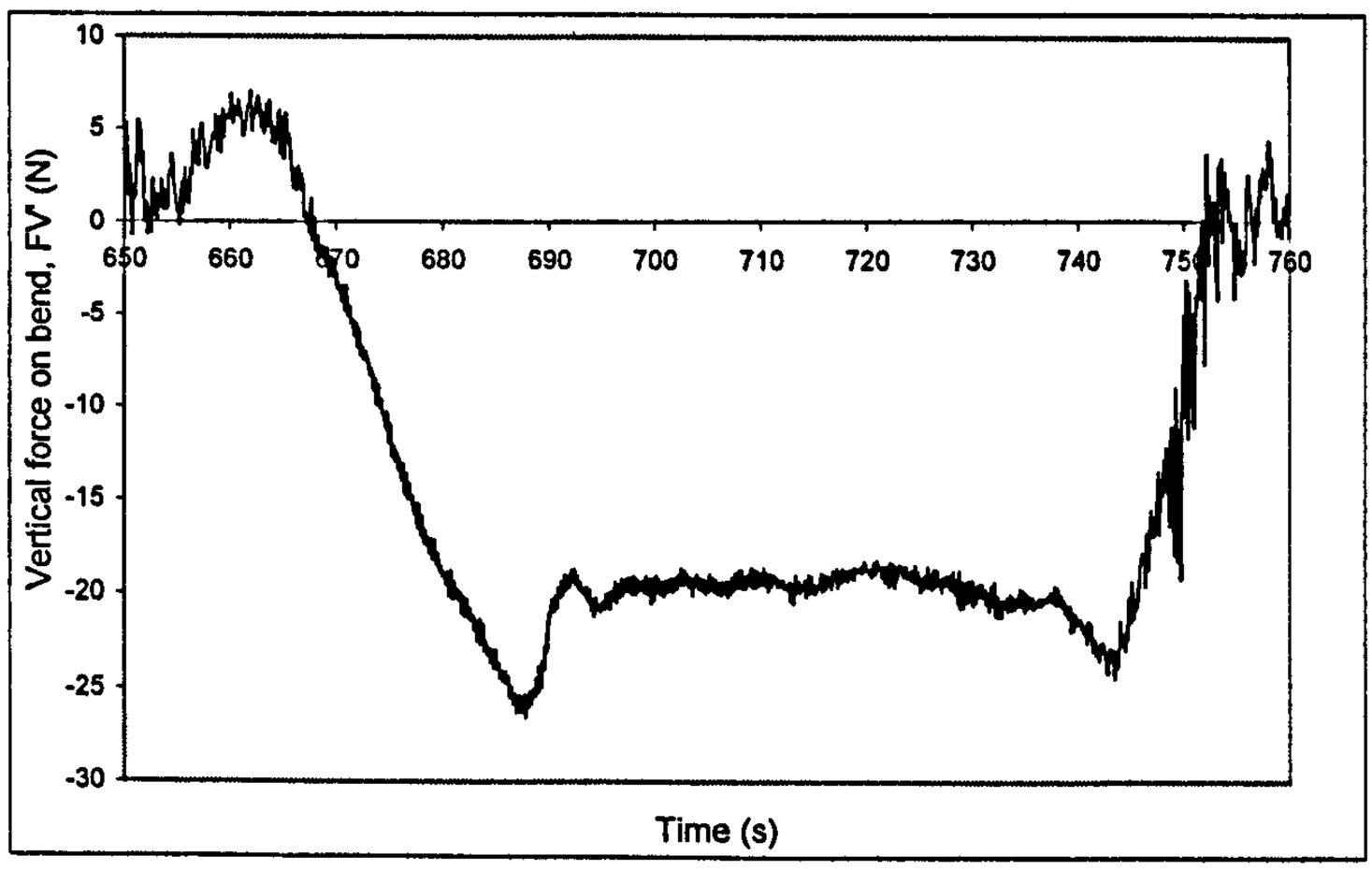

Figure E1.4 Severe slugging 1 traces [v_{SG}=0.14m/s, v_{SL}=0.28m/s]

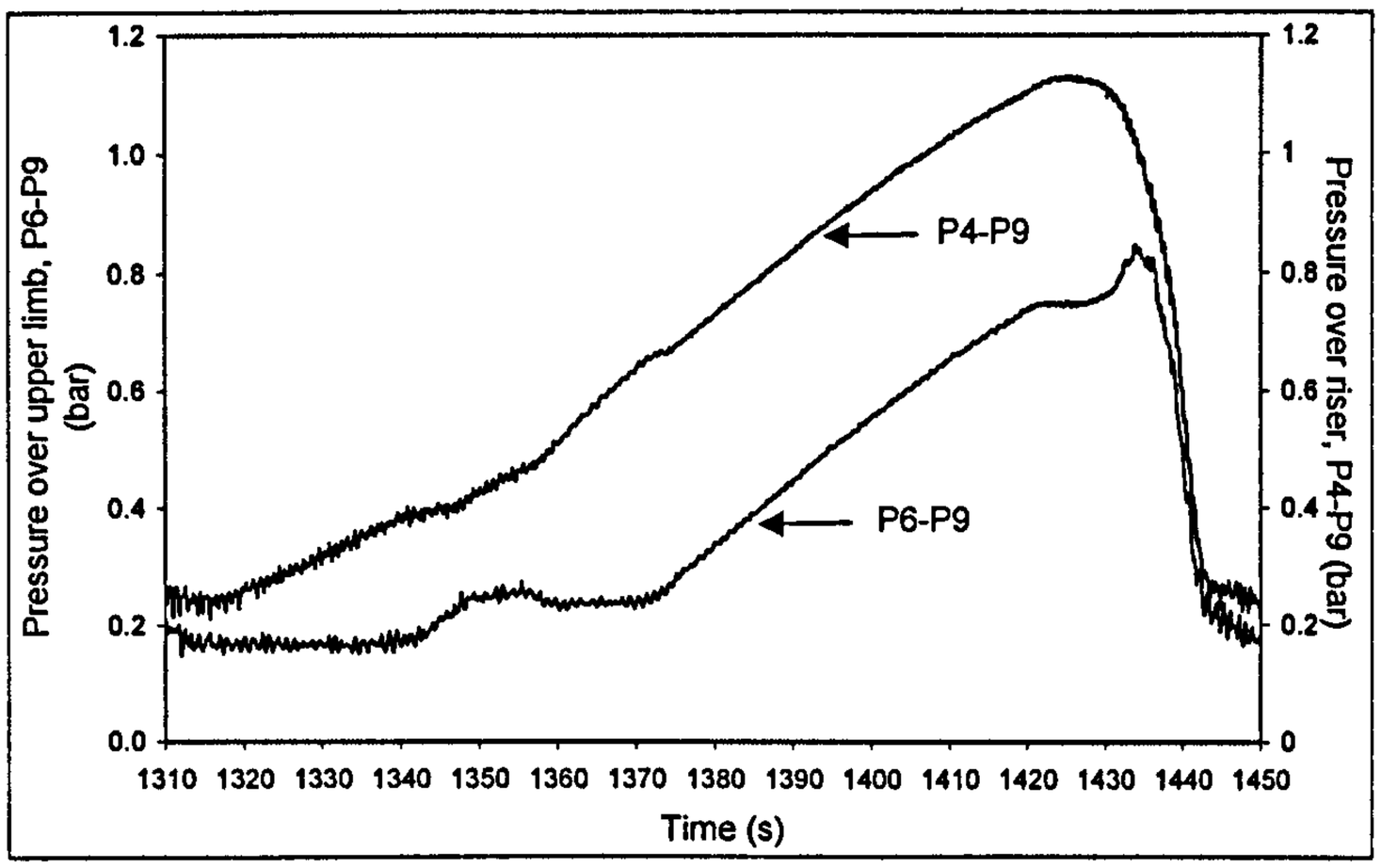

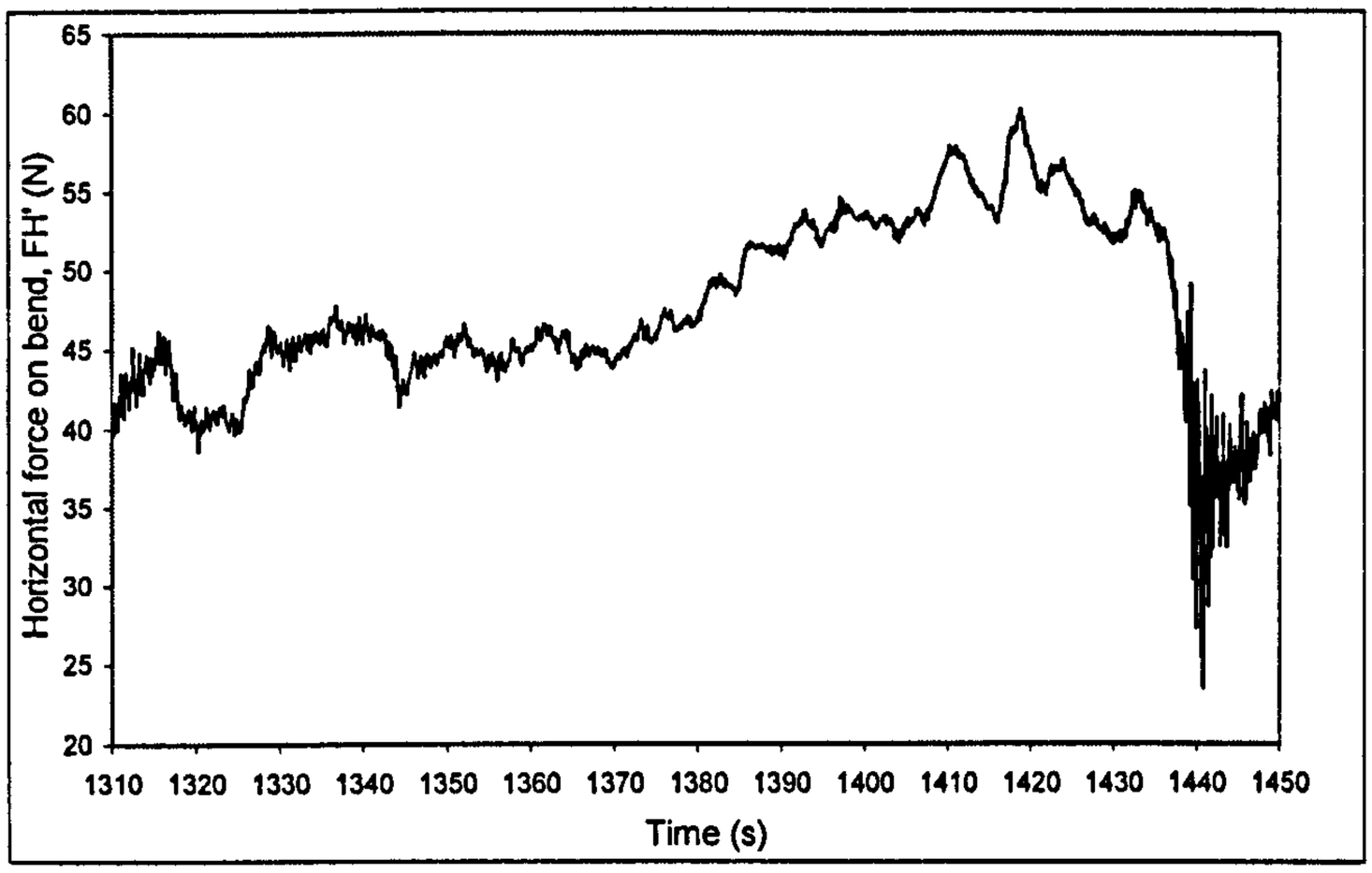

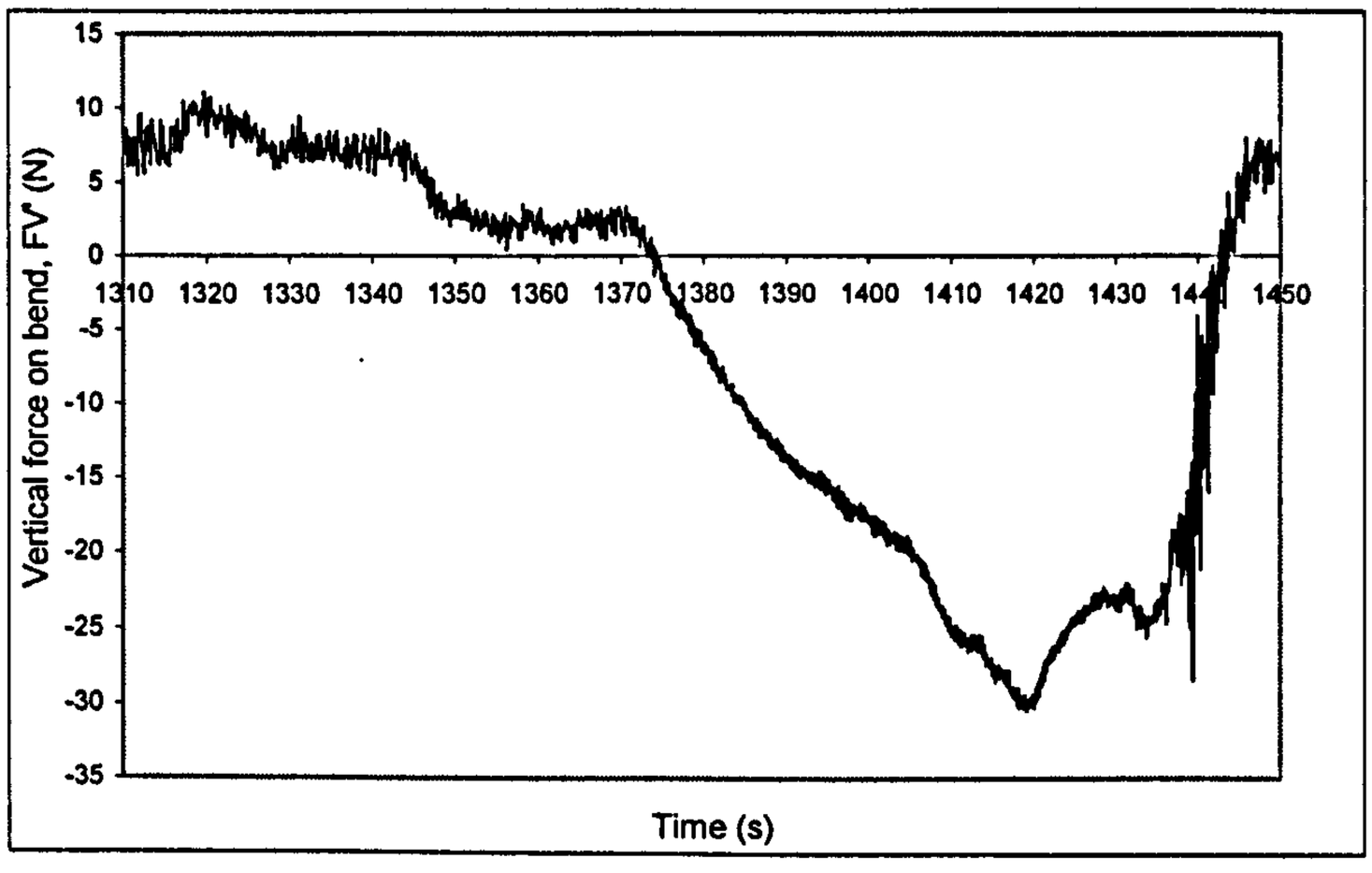

Figure E1.5 Severe slugging 1b traces [v_{SG}=0.35m/s, v_{SL}=0.11m/s]

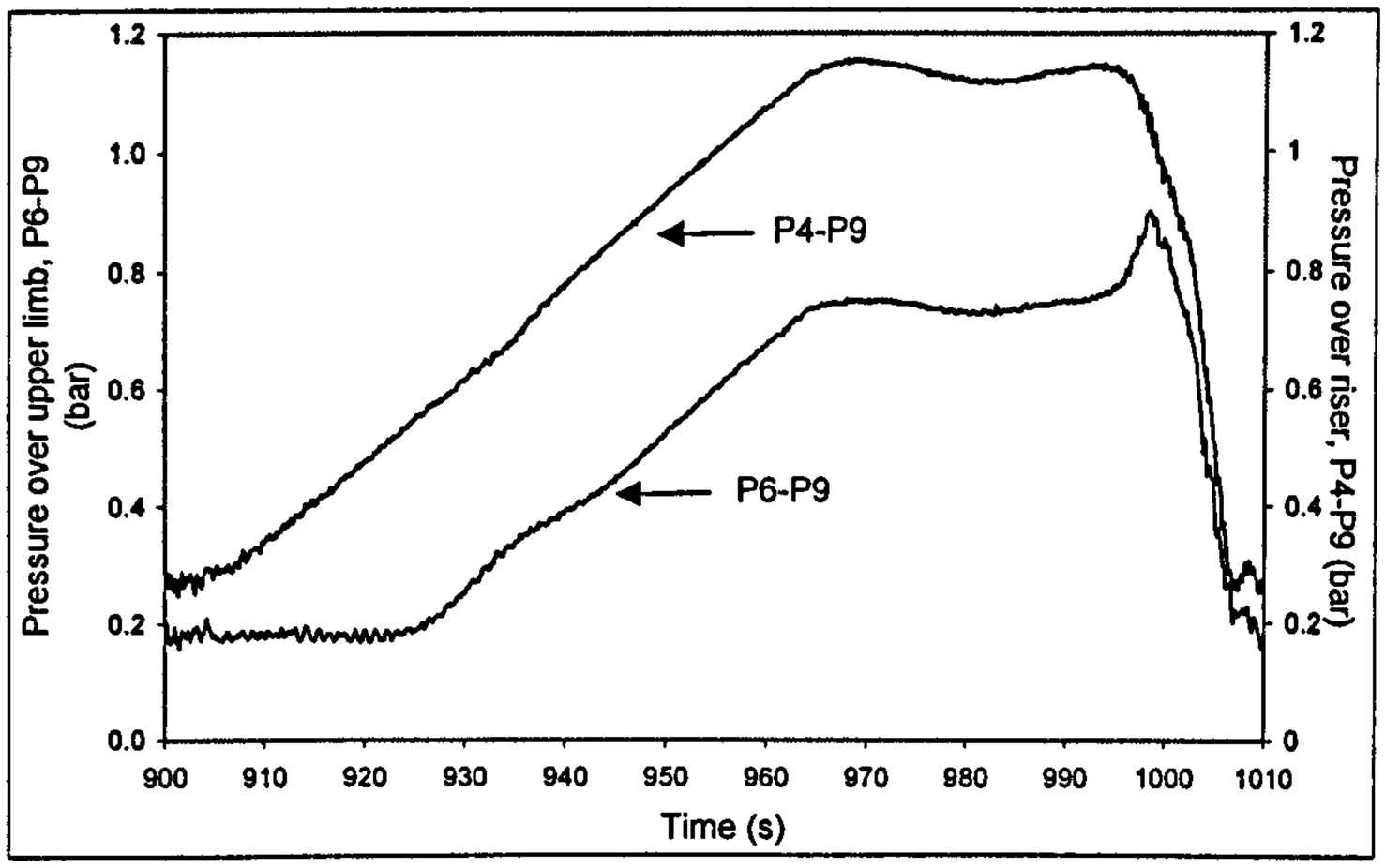

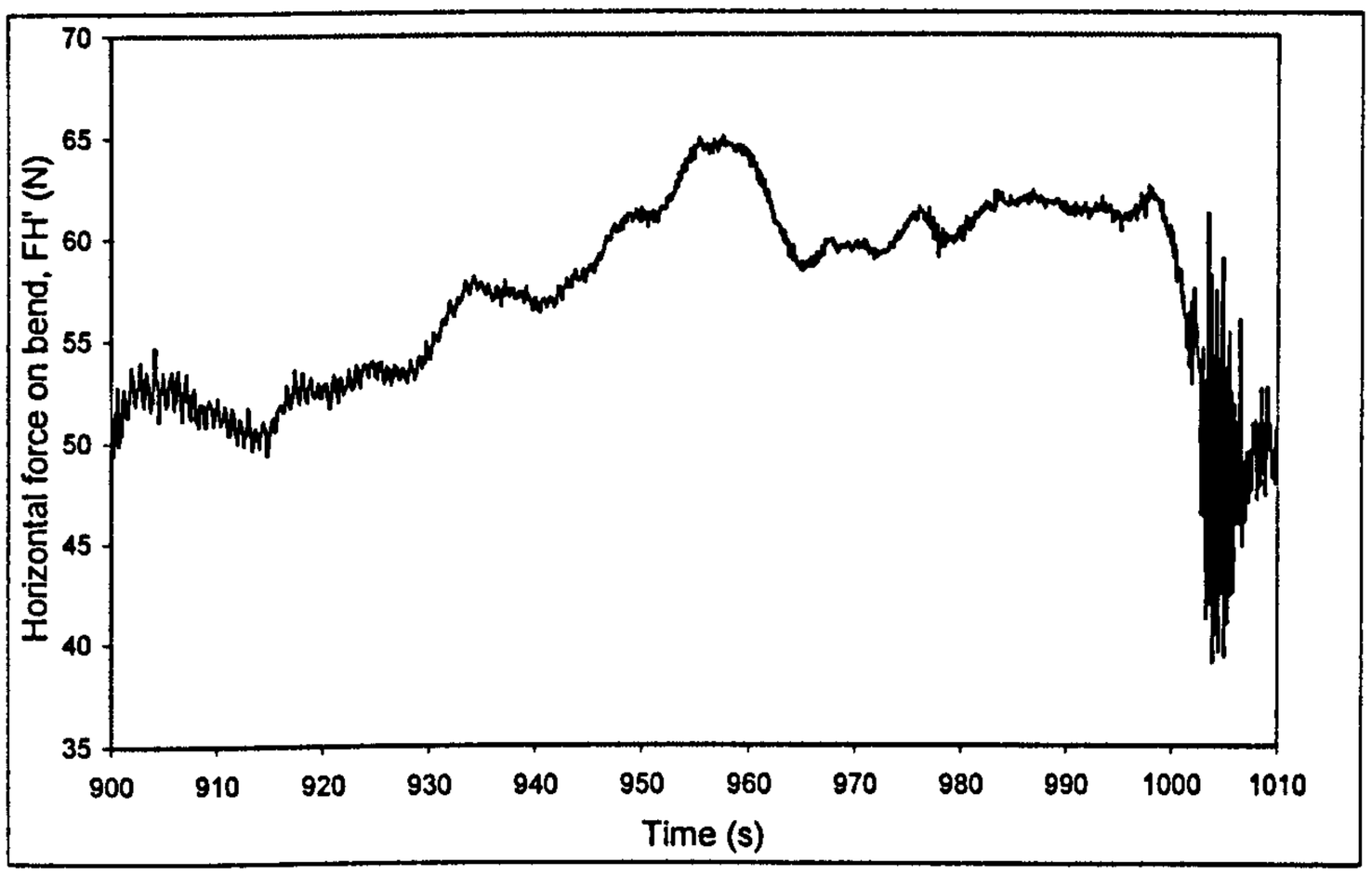

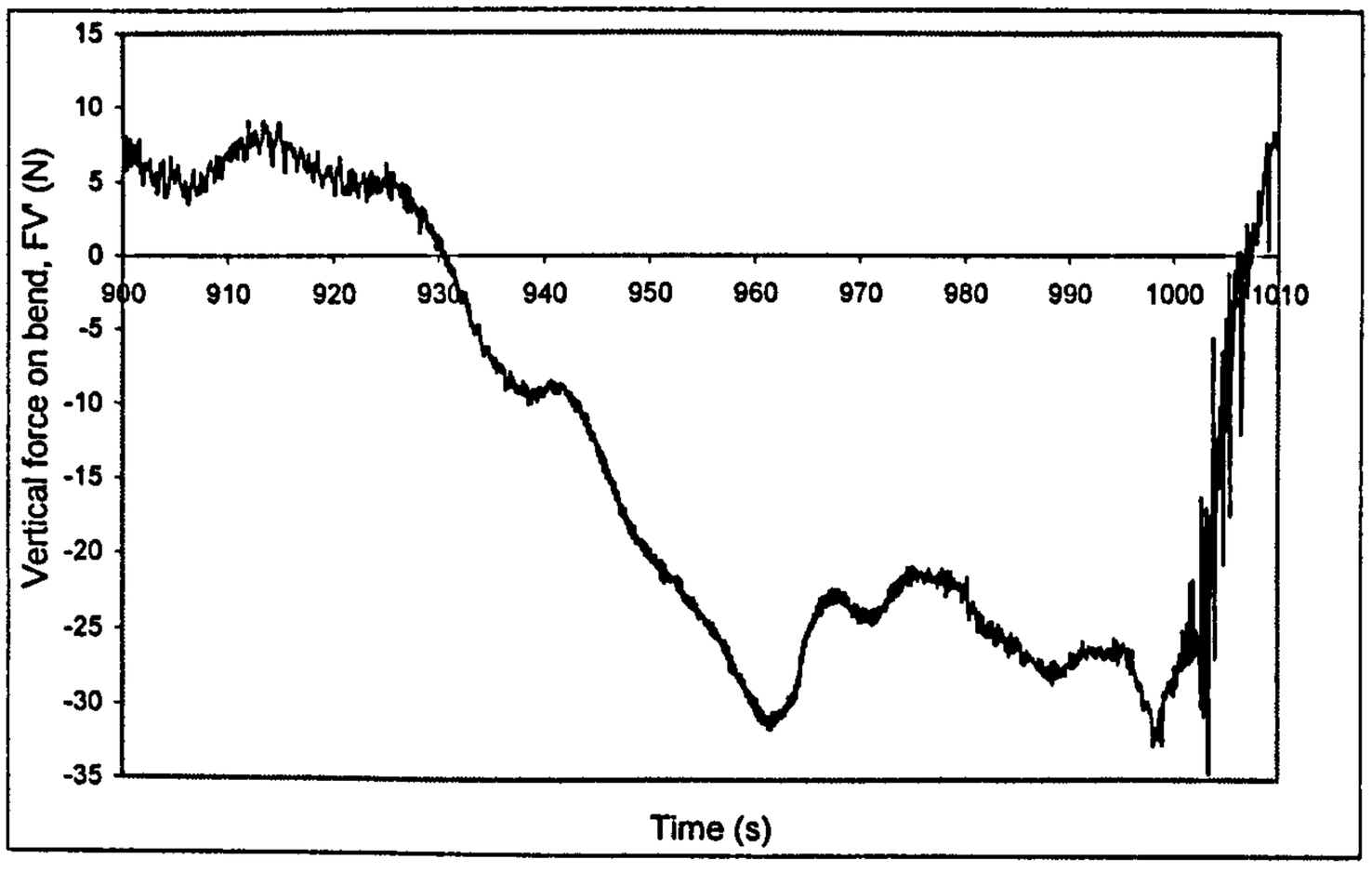

Figure E1.6 Severe slugging 1 traces [v_{SG}=0.32m/s, v_{SL}=0.19m/s]

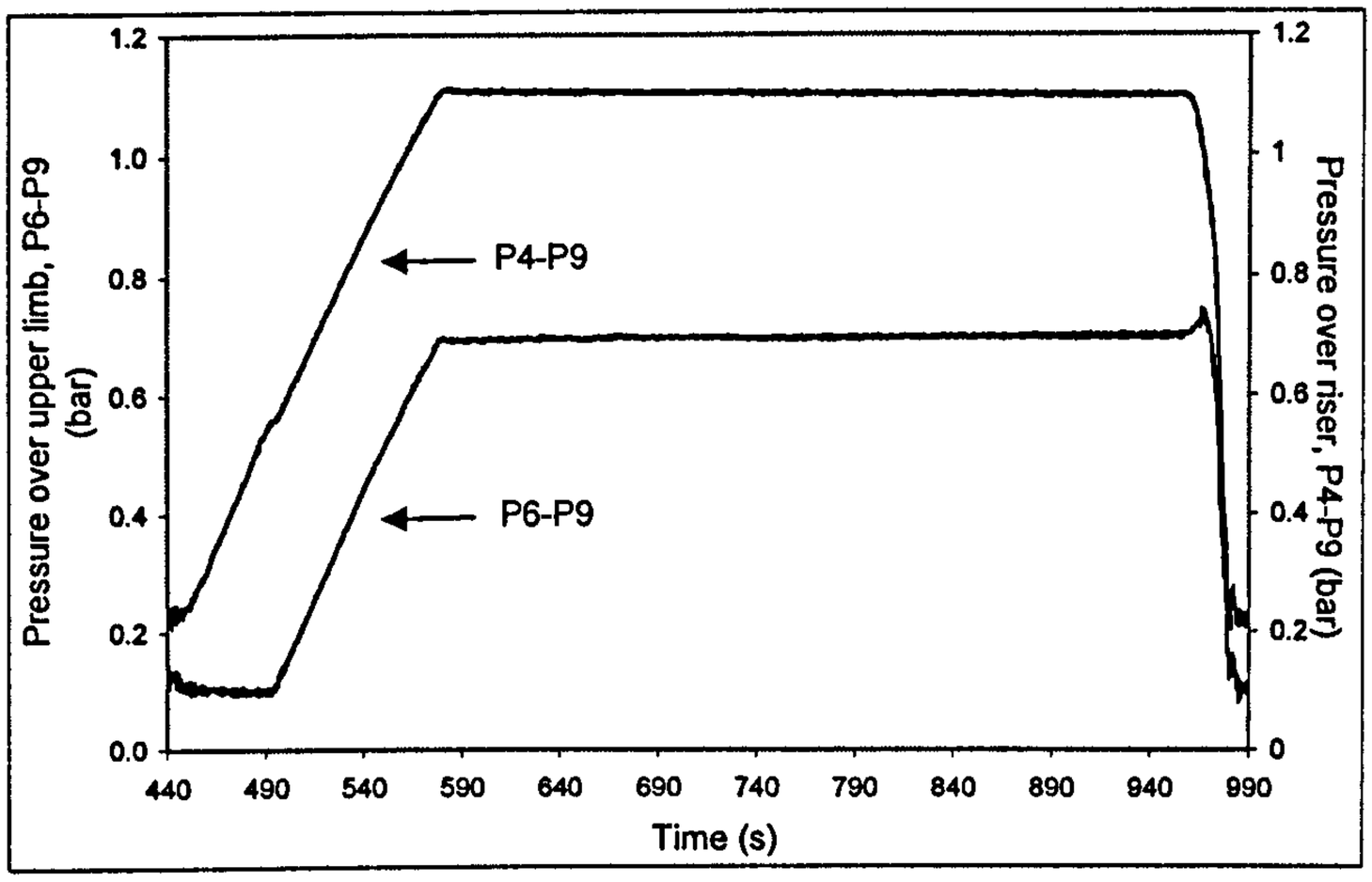

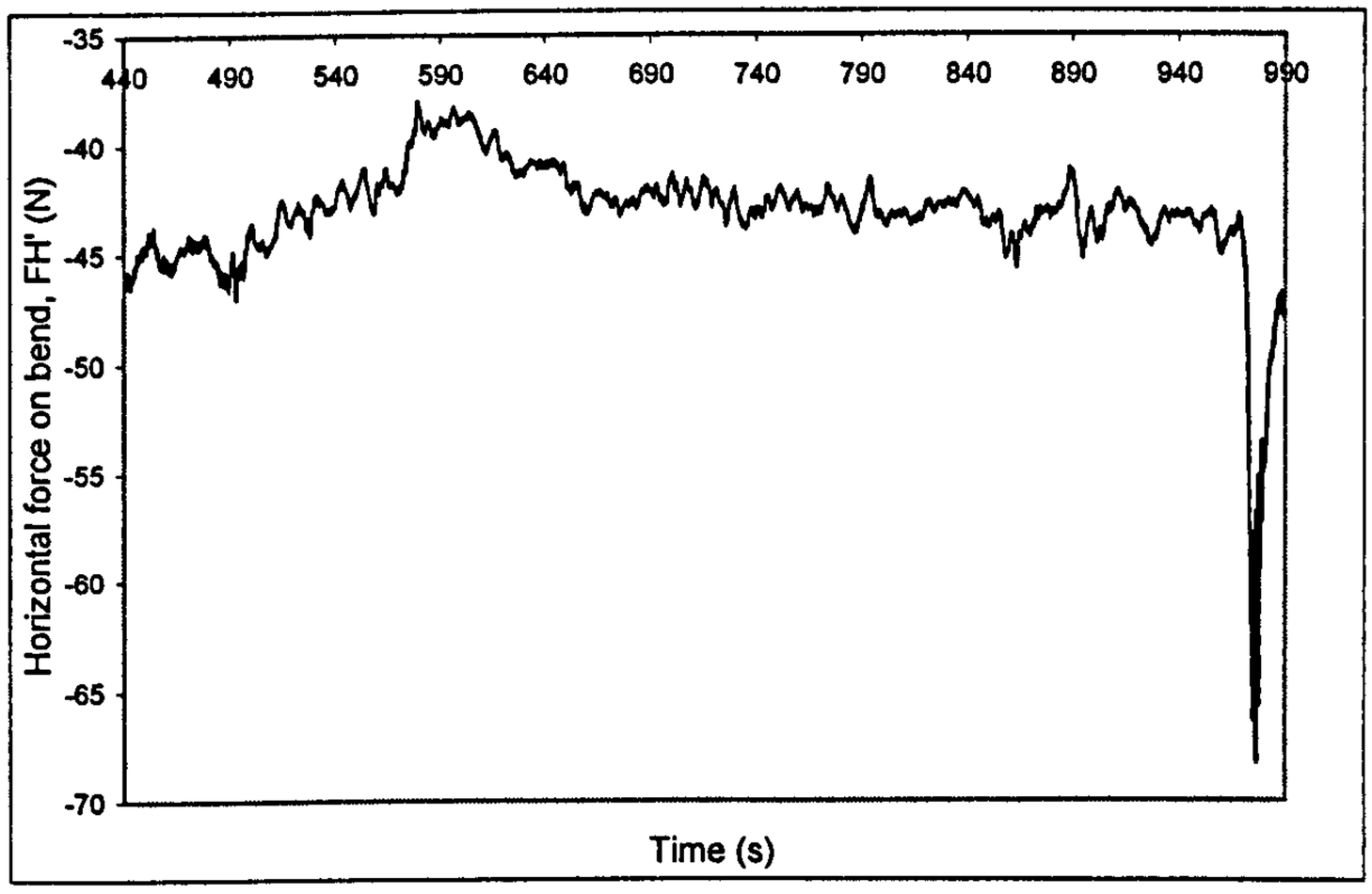

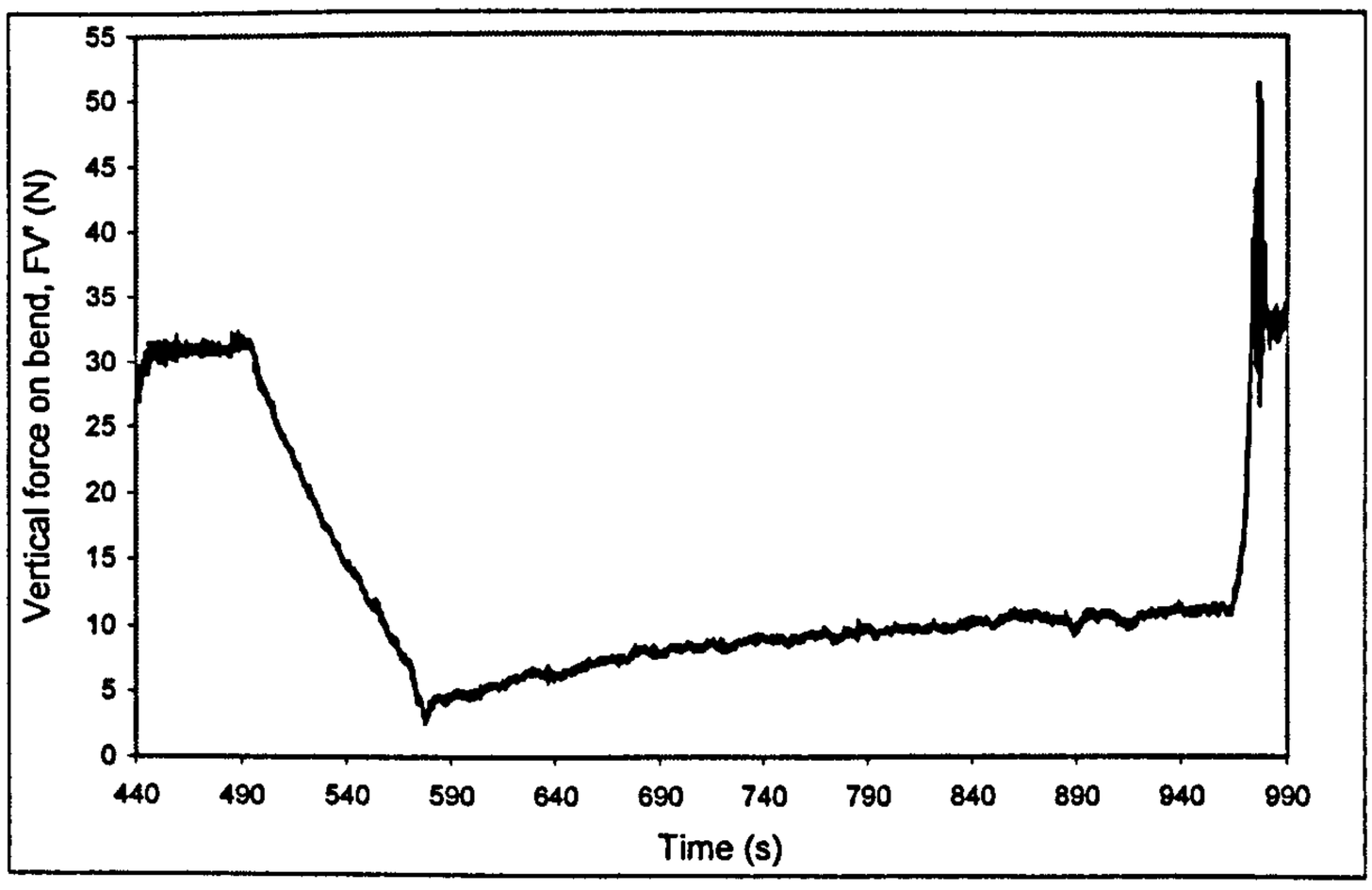

Figure E1.7 Severe slugging 1 traces [v_{SG}=0.07m/s, v_{SL}=0.10m/s]

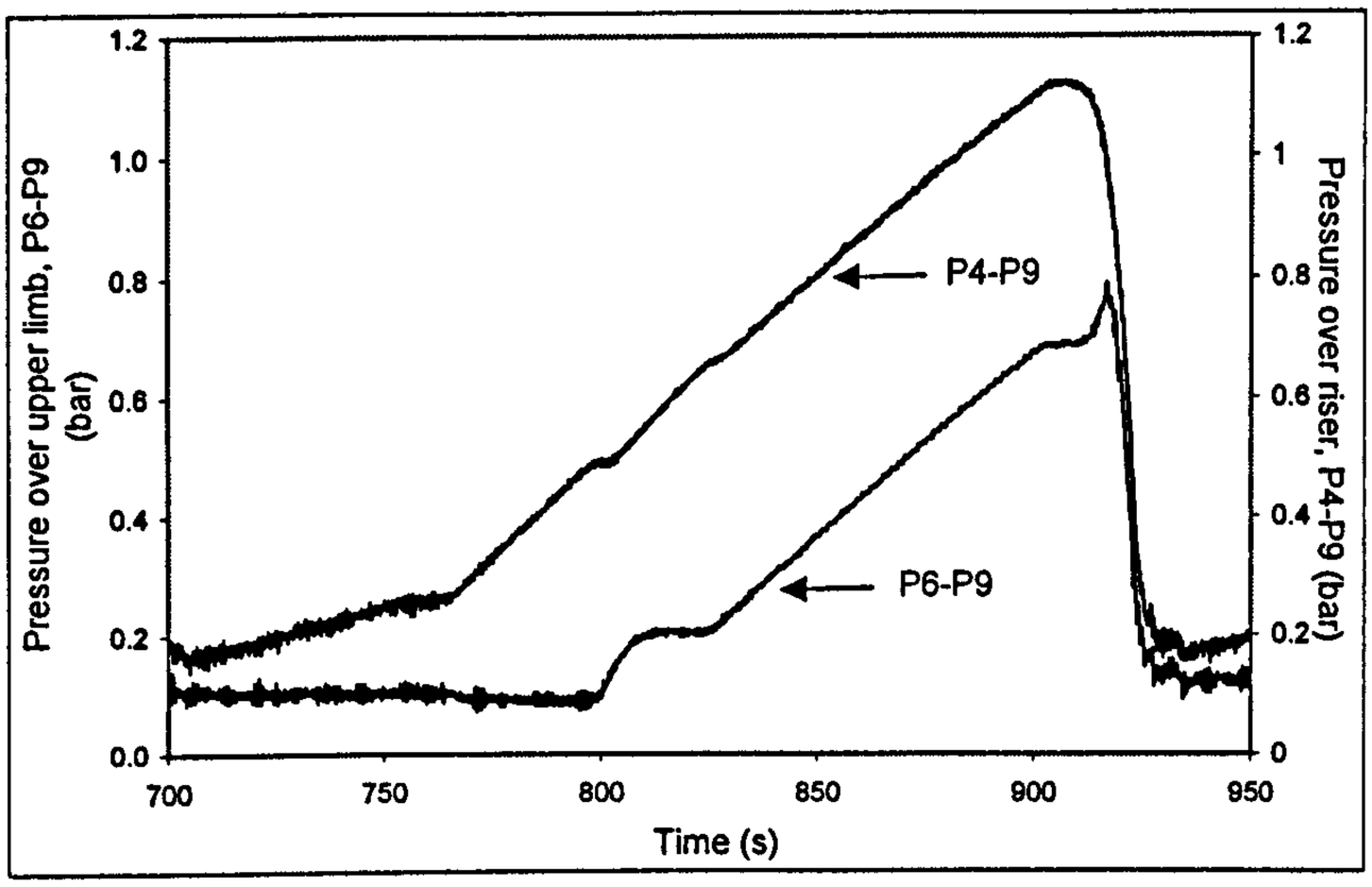

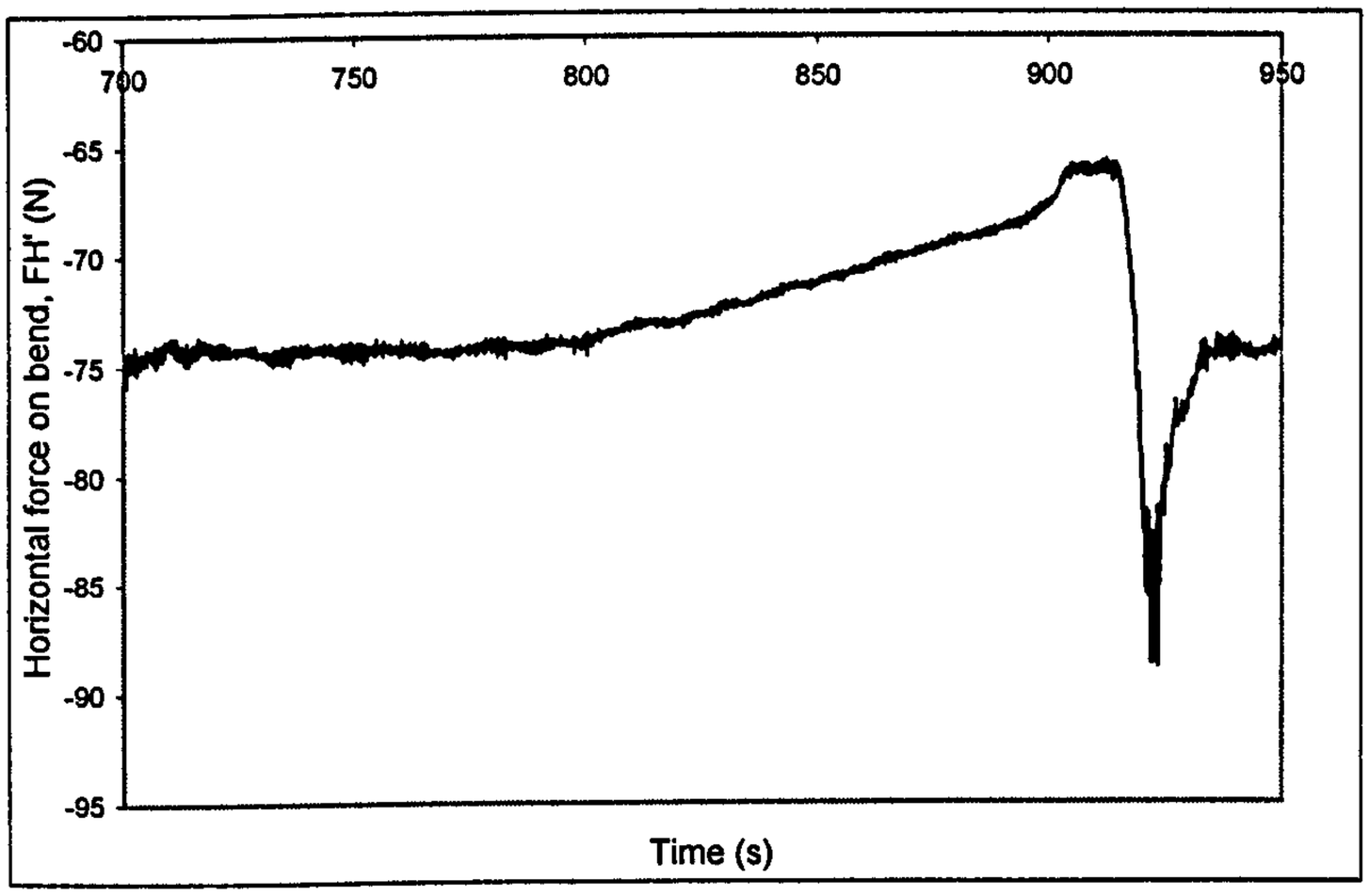

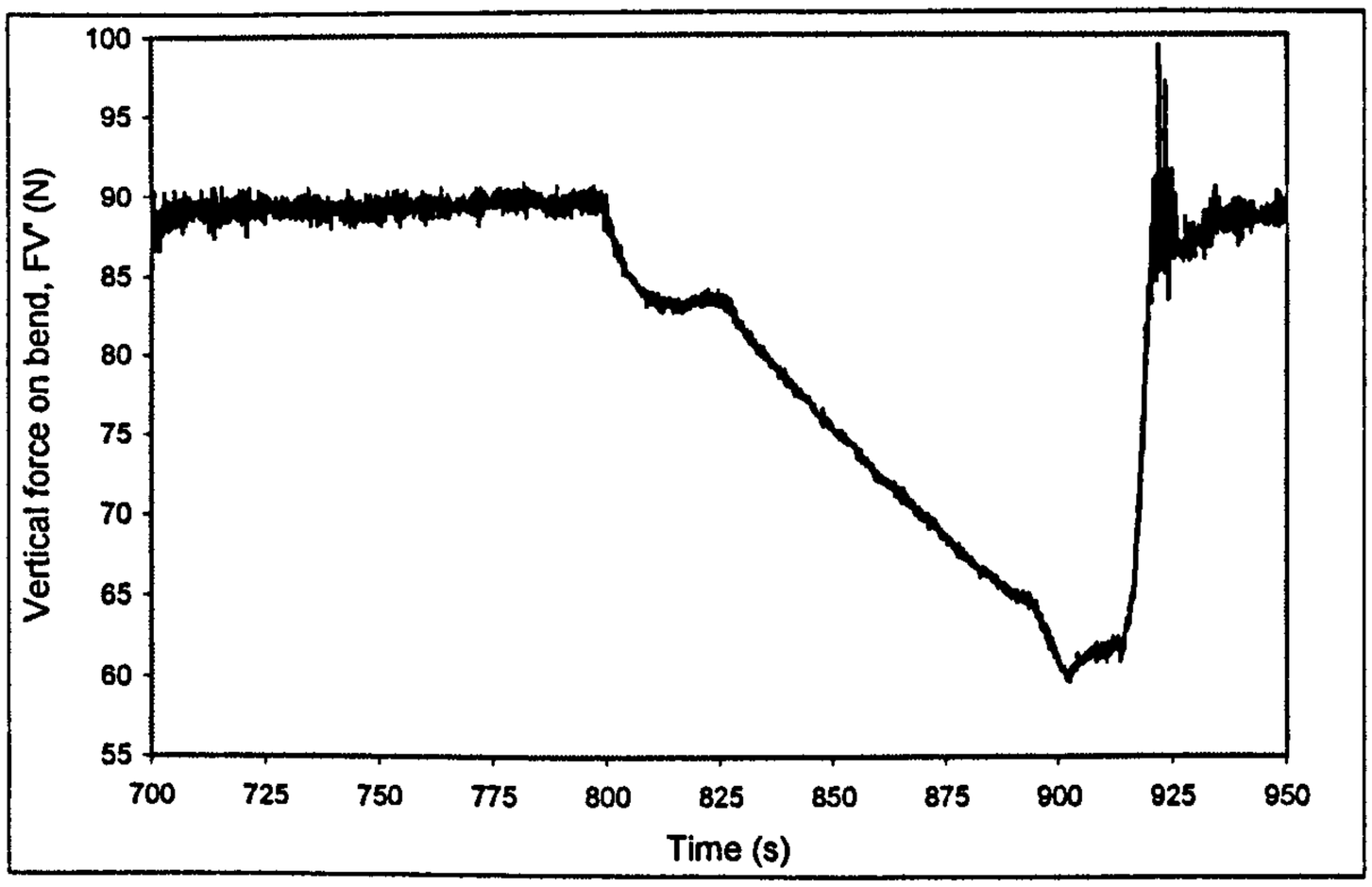

Figure E1.8 Severe slugging 1 traces [v_{SG}=0.26m/s, v_{SL}=0.06m/s]

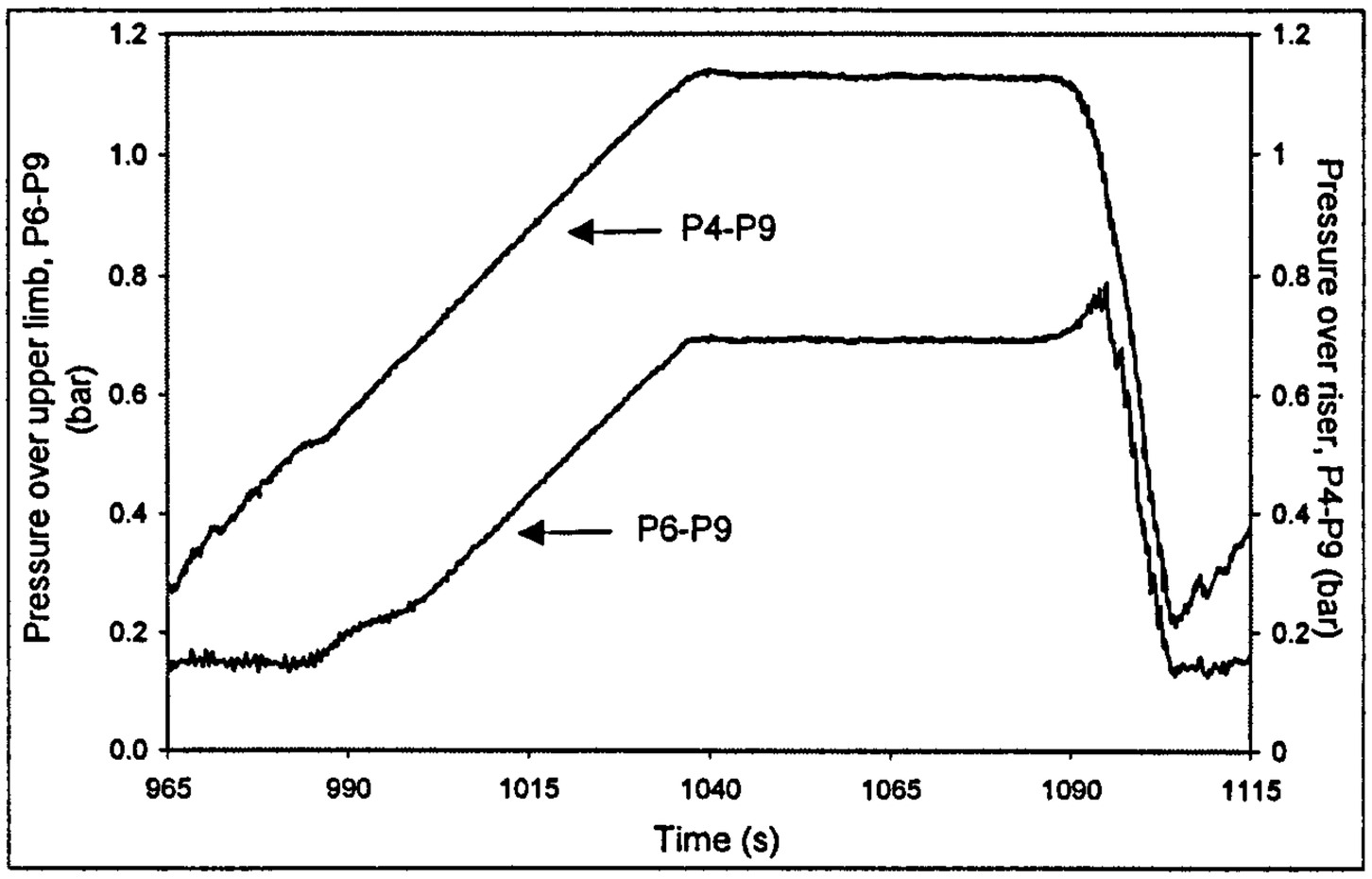

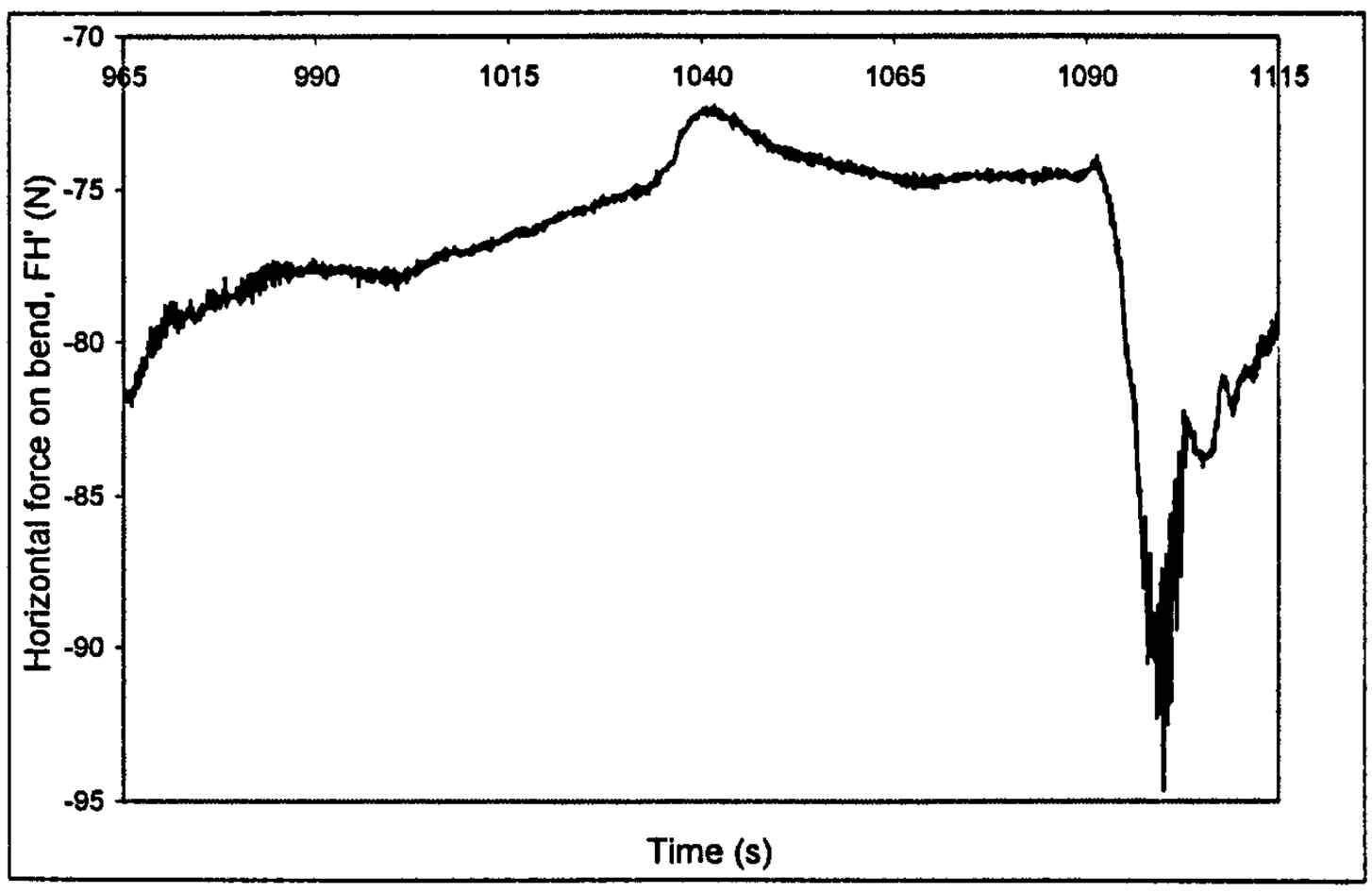

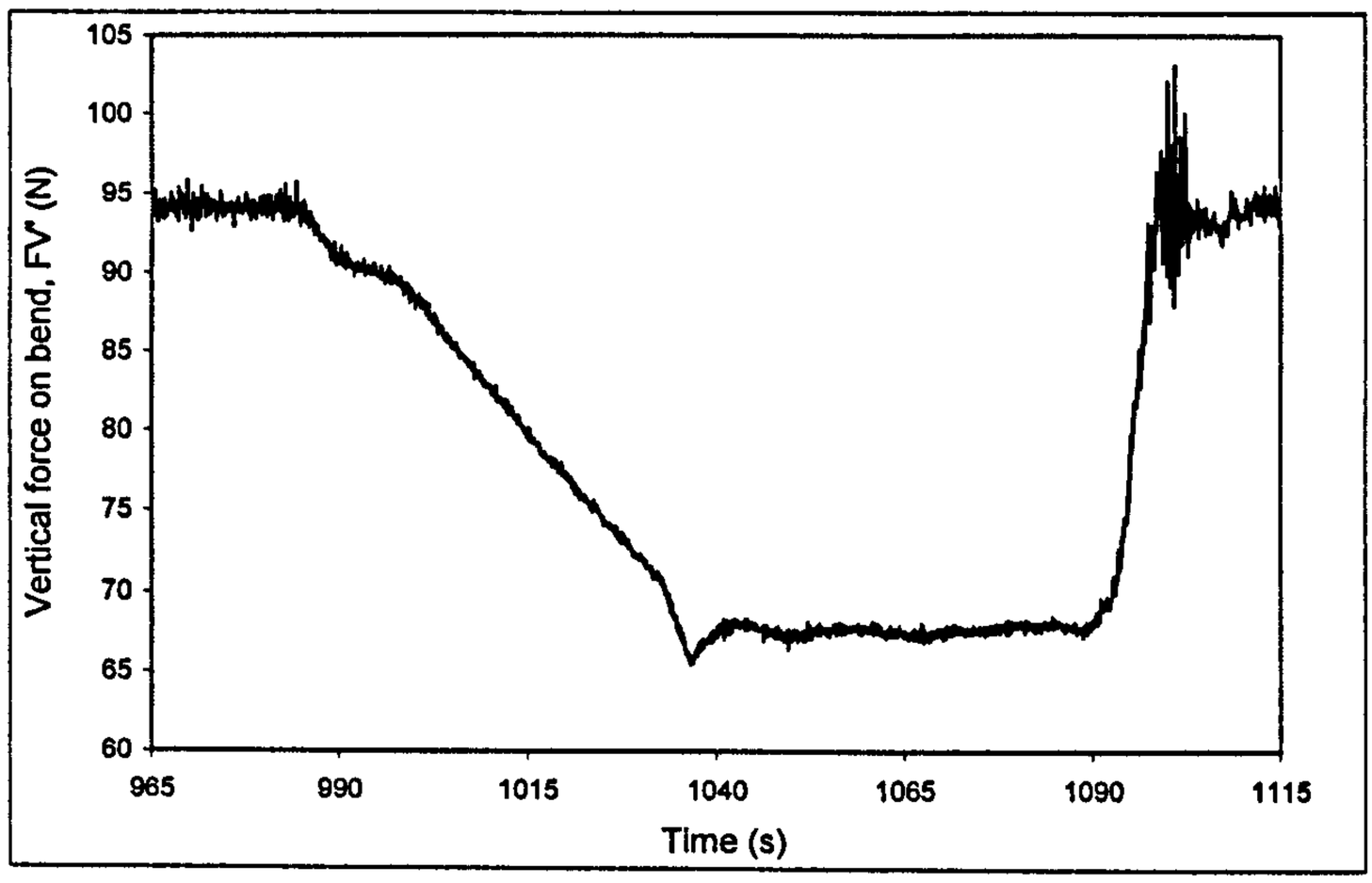

Figure E1.9 Severe slugging 1 traces [v_{SG}=0.18m/s, v_{SL}=0.19m/s]

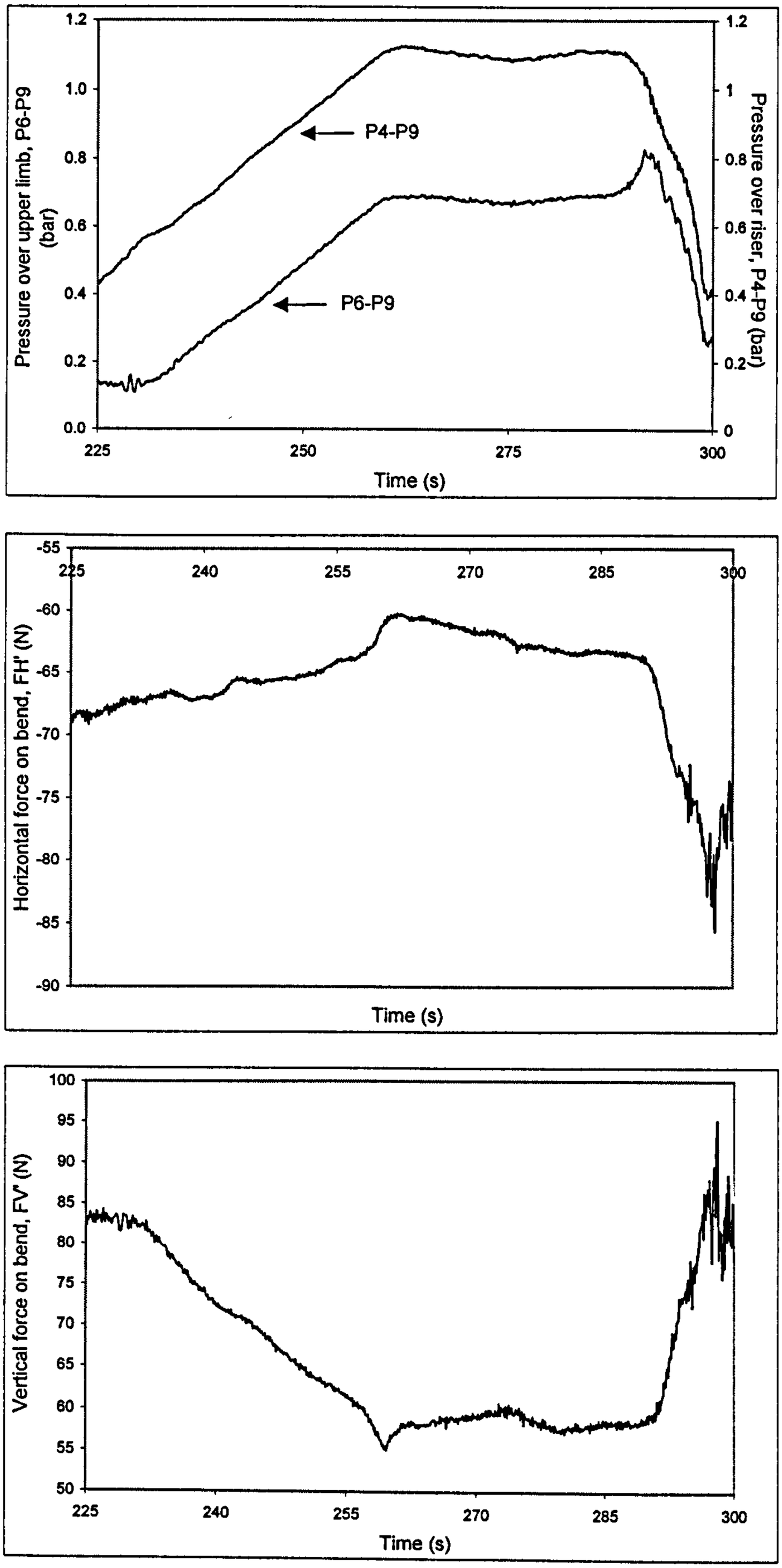

Figure E1.10 Severe slugging 1 traces [v_{SG}=0.31m/s, v_{SL}=0.31m/s]